Modelling Plate Kinematics in the Scotia Sea

Graeme Eagles

Submitted in accordance with the requirements for the degree of
Doctor of Philosophy.

The University of Leeds
School of Earth Sciences
September 2000

The candidate confirms that the work submitted is his own and that appropriate credit has been given where reference has been made to the work of others.

I must go down to the sea again

to the lonely sea and sky

I left my vest and socks there

I wonder if they're dry?

Spike Milligan, Return to Sorrento (3rd class)

THESIS CONTAINS CD/DVD

CONTAINS

PULLOUTS

Acknowledgements

I thank Roy Livermore and Derek Fairhead for setting up the project, and for their guidance and support: In particular, GETECH provided a workstation and Cambridge Paleomap Systems provided the *ATLAS* program. For double-CASE funding I must thank NERC, BAS, and BG plc. Adrian Nankivell gave permission and advice to implement his reconstruction programs. Likewise did Bob Parker (UCSD) for his Fourier terrain correction technique. Steve Cande (also UCSD) provided the confidence ellipse in Figure 4.14. Sidney Mello of Leeds directed me to the inverse magnetization code, and Fernando Martínez advised on its implementation. I thank Peter Morris (BAS), unofficial 'third supervisor', for magnetic and bathymetric grid data, and for 3 months work digitising analogue seismics. Andy Jackson (Leeds) gave much-needed advice on quantitative geoscience, and criticised early drafts of the thesis. Joe Cann and Graham Stuart (Leeds) recommended transfer to PhD, and Joe was a great source of encouragement. For computer-related help I thank Stuart Borthwick and Nick Barber (Leeds), and Pete Lens, Jim Summers, and others in computer support at BAS. This thesis is typeset using LaTeX and many of the figures were produced with the *GMT* programs, all running on a portable computer. This was made more portable by the gift of a car from Keith Stevens (Royal Holloway). I thank all on the JR39b cruise leg in February–March 1999, where I found out that, although fascinating, the Scotia Sea is cold and wet like the one at home in Clacton.

On a less specific basis here I thank staff and postgraduates at Leeds, particularly Steve Hall, Dan Raymer, Alex Brisbourne, Aoife O'Mongain, Shafkit Abdullah, Steve Gibbons, Trevor King, Susannah Bruce, James Wookey, Andy Carter, Nick Teanby, Mike Bourne, Sid Mello, Maxine Zaidman, Sarah Gleeson, Rob Newton, Andy Jackson, Cindy Ebinger, Roger Clark, Clare Buckee, Lawrence Amy, Omar Al-Jaiidi, Clare Davies, Chris Peel, Mike Kendall, Tine Thomas, Art Jonkers and Tara Fawdington, and outside of the office Mark, Darren, Cecely, Richard and MJ. At BAS I acknowledge Alex Cunningham, Nigel Bruguier, Rob Larter, Phil Jones, Steve Moreton, John Howe, Julie Ferris, Lieve Vanneste, Bryan Storey, Mike Thomson, Ed King and Tony Bell. The libraries' staff at Leeds, BAS and Royal Holloway are duly thanked here. Special thanks, for accommodation, and more importantly, friendship whilst in Cambridge, go to Deborah and Keith Clements.

More thanks go to Bernard Spilsbury, for starting me off in geology, and to Mary Fowler at Royal Holloway, for inspiring me as a geophysicist. My close friends Dave, Dan, Graeme, Andy G., Neil and Steve have kept me amused with endless diversions, for which I am (usually) grateful. For, well, everything, I give love and thanks to my parents, their spouses, and my sister Suzy. To Grandad, who won't hold this thesis now: 'dead right's good enough'. Finally, to Louise, for being so much more than can be written, my love, gratitude and promise: your turn now.

Abstract

Modelling Plate Kinematics in the Scotia Sea

A new model of plate kinematics in the Scotia Sea region is presented in which continental crustal blocks and the signatures of seafloor spreading are defined semi-automatically using gravity and total field magnetic anomalies and some of their residuals, transformations and derivatives. This study is the first of the region to integrate gridded magnetic and gravity data in order to make reconstructions, and one of the first anywhere to make full use of gridded magnetic data in an inverse procedure. The context provided by the quantitative reconstructions allows qualitative assessment of visually-derived reconstructions of small movements in the region.

The Scotia Sea floor consists of three large oceanic magnetic provinces: the west, central and east Scotia seas, and four smaller sub-basins, all enclosed within the elevated submarine and emergent Scotia Arc. The Scotia Arc consists of Mesozoic continental and Cenozoic island-arc fragments. Only the east Scotia Sea remains active; the west and central parts are the products of extinct spreading centres.

West Scotia sea spreading is reasonably well described by tectonic flowlines expressed in satellite free-air gravity anomalies and magnetic reversal isochrons in total field anomalies. These data are combined in an inversion to reconstruct the west Scotia Sea's margins between its inception at chron C8 ($\sim$ 26.5 Ma) and extinction at chron C3a ($\sim$ 6 Ma). The results suggest strongly, and for the first time, that the west Scotia Sea formed as a small ocean basin whose passive margins were Tierra del Fuego and the central Scotia Sea, and not as a back-arc basin in the strict sense. During its growth the kinematics of the west Scotia Sea's margins approximated those of the South American and Antarctic plates. The small kinematic differences are suggested to be due to convergence at the 'proto-South Sandwich–Discovery' subduction zone, to the east of the central Scotia Sea, and to dextral strike-slip (pre-C6 ($\sim$ 20 Ma)) and oblique convergence (post-C6) at the North Scotia Ridge, the Mesozoic northern arm of the Scotia Arc.

The most widely-accepted interpretations of the central Scotia Sea hold that it is a back-arc basin, but model flowlines about published reconstruction poles in the region show that instead it could have originated by accretion to the South American plate at the ancestral South American–Antarctic Ridge in the Weddell Sea, later to move eastwards as the eastern passive margin to the west Scotia Sea. Magnetic reversal anomalies in the central Scotia Sea are consistent with its accretion in this way during the Cretaceous, probably between chrons M4 and M20 ($\sim$ 126–149 Ma). All of this material was hitherto thought to have been destroyed completely by subduction at the ancestors of the South Sandwich subduction zone. The central Scotia Sea is thus also re-assigned in the model to have an oceanic, rather than back-arc basin, origin. Hence, the bulk of the Scotia Sea floor formed as a consequence of the predictable movements of major plates following the break-up of Gondwana, with back-arc basins in the strict sense only forming small sub-basins until the inception of the east Scotia Sea at or soon after C5c. The development of this much larger, oceanic, back-arc basin occurred following a change in the direction of relative motion at the West Scotia and South American–Antarctic Ridges at C6. This new model of Scotia Sea kinematics, presented as a series of reconstructions of total field and Bouguer anomalies, is the first to be both self-consistent and consistent within the context of known major plate motions.

The new interpretation of the central Scotia Sea is at odds with previous reconstructions which place South Georgia in the heart of a reconstructed compact connection between Tierra del Fuego and the Antarctic Peninsula. The altered position of South Georgia, south of Maurice Ewing Bank (Falkland Plateau) helps explain the puzzling provenance of its turbidites and suggests, as previous workers have done, that it may be appropriate to redefine the genesis of at least the eastern part of the Rocas Verdes Basin as an oceanic basin formed by accretion at a propagating rift, rather than (as before) a rare example of a back-arc basin formed behind an east-directed subduction zone.

Although the new model is self-consistent, it is not uniquely so for two of the small basins in the Scotia Sea (Protector and Dove Basins) whose age remains poorly defined.

It can be speculated that either or both of these basins may have opened deep-water gateways in the Drake Passage region prior to spreading in the west Scotia Sea, possibly in the Middle Eocene. A very tentative correlation between such events and initial cooling prior to the onset of Antarctic glaciation, via the cooling effect of establishing an efficient Antarctic Circumpolar Current, is suggested.

Contents

List of Figures

List of Tables

Chapter 1

Introduction and Review

Keywords Scotia Sea geology. Scotia Sea geophysics. Plate tectonic theory. Reconstruction techniques.

1.1 Introduction

Covering well over one percent of Earth's surface area, the Scotia Sea region is an important interchange in the Southern Ocean's tectonic, biological and oceanographic systems (Figure 1.1). Tectonically it constitutes a boundary between the Pacific and Atlantic spreading systems and between South America and Antarctica. The east Scotia Sea is the longest known example of back-arc extension by seafloor spreading (Barker, 1970), and possibly the simplest. The region is a long standing problem in Gondwana reconstructions in which the Antarctic Peninsula overlaps Tierra del Fuego, some 100 million years prior to the opening of the Scotia Sea (Smith and Hallam (1970), Figure 1.2). The initial position and subsequent dispersal of the Peninsula during the later Mesozoic and Cenozoic are largely unconstrained, but are thought to be intimately bound up with the history of the 'Weddellia' collage of microplates in West Antarctica (Grunow *et al*, 1987; 1991). In biogeography the Scotia Sea is the most recently established barrier to dispersal

of marsupial mammals (Woodburne and Zinsmeister, 1982; Case *et al*, 1988; post-60Ma) between South America and Antarctica, and the most recently established pathway for interchange between Pacific and Atlantic marine life (Beu *et al*, 1997), including vent-specific fauna (Tunnicliffe *et al*, 1998). Oceanographically the region is the final barrier to establishment of the Antarctic Circumpolar Current, which is influential in the global ocean as the dominant feature of Southern Ocean circulation and therefore a major contributor to late Neogene climate. A more controversial circulation, of Earth's mantle, is also hypothesised to exploit the gateway between thick continental lithosphere of South America and Antarctica which blocks outflow of asthenosphere beneath the shrinking Pacific Ocean to the growing Atlantic Ocean (Alvarez, 1982).

1.1.1 Aims of the thesis

An important theme in all these points of significance is the establishment and destruction of gateways and barriers by tectonics. The Antarctic region is dominated by microplate tectonics (Dalziel and Elliott, 1982; Martin, 1986; Mitchell *et al*, 1986; Maslanyj and Storey, 1990; Grunow *et al*, 1992; DiVenere *et al*, 1995; for example) with the potential for fine scale segregation, dispersal and vertical movements of crustal blocks as barriers. Thus the main aim of this thesis is to address the problem of the kinematic evolution of the region since separation of the Antarctic Peninsula and Tierra del Fuego. This provides a new framework within which the issues associated with the evolution of gateways and barriers can be addressed. A quantitative reconstruction technique—joint inversion of seafloor flowline and magnetic isochron data—is used for the extinct west Scotia Sea and Phoenix–Antarctic spreading systems. For the numerous smaller basins within the region non-quantitative reconstructions are made and assessed within the context of major plate motions. The modelling process gives some results which are pertinent to the earlier breakup of Gondwana, which will be explored briefly.

In this chapter, **Chapter 1**, a review of previous reconstructions of the region is given. The major-plate context, in which the region is set, is introduced. Brief reviews

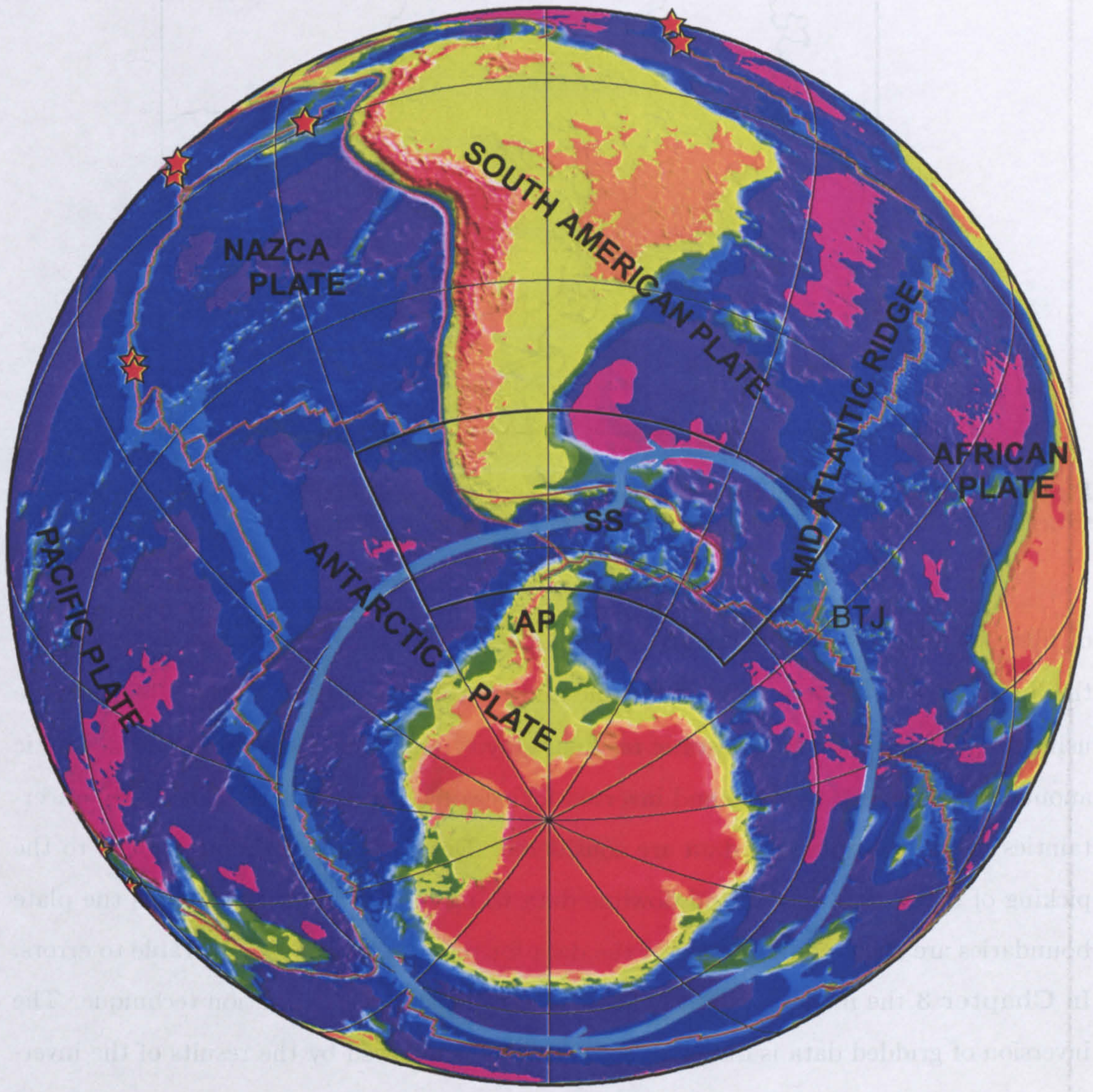

Figure 1.1: Location of the Scotia Sea (box). Red lines are active plate boundaries, stars the positions of hydrothermal vent sites from which vent-specific fauna have been collected (Tunnicliffe *et al*, 1998). Light blue line shows the approximate path of the Antarctic Circumpolar Current. SS: Scotia Sea; AP: Antarctic Peninsula; BTJ: Bouvet Triple Junction.

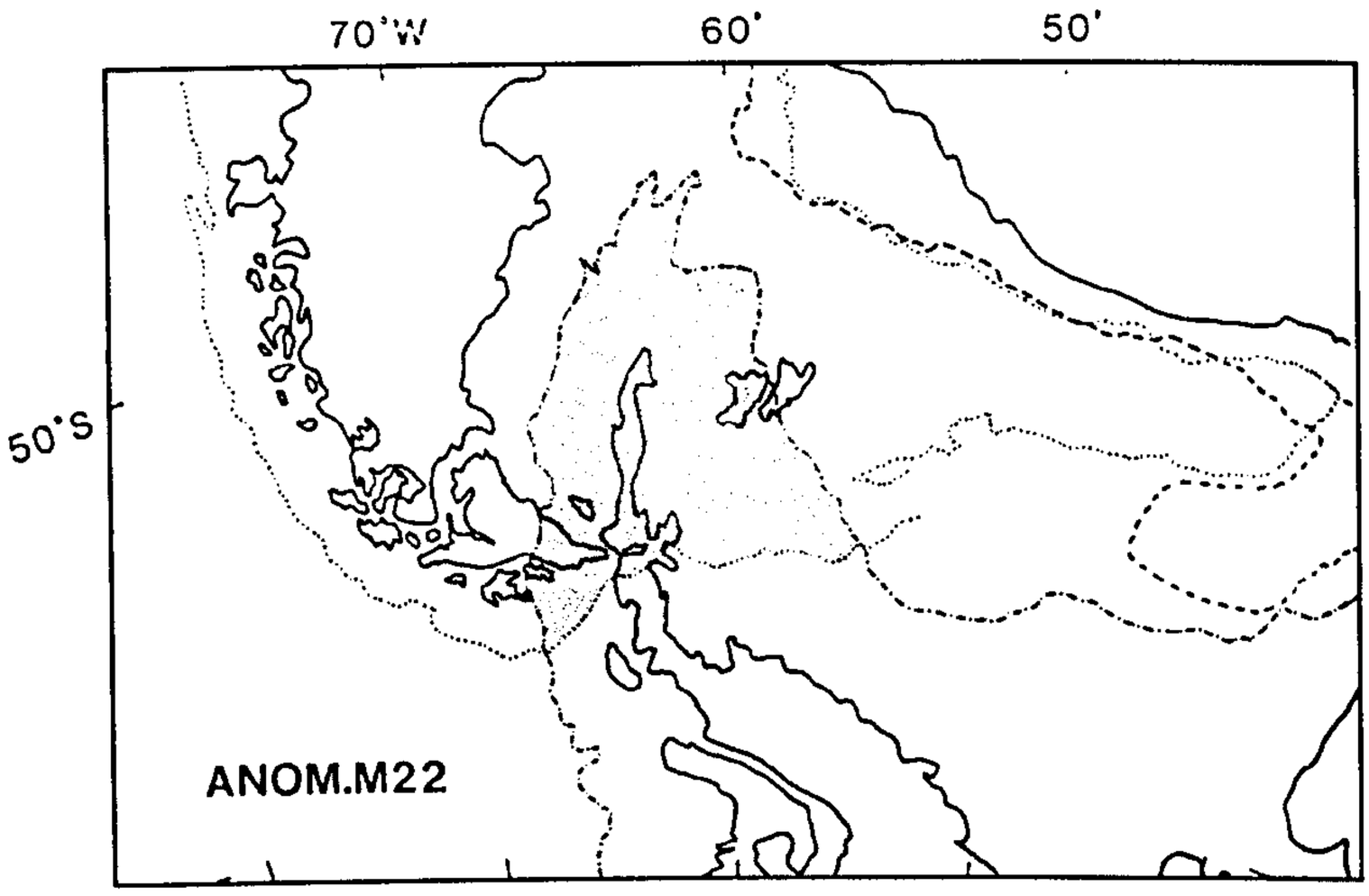

Figure 1.2: Overlap of the Antarctic Peninsula with southernmost South America in a reconstruction of Gondwana in the late Jurassic (from Lawver *et al* (1985)).

of plate tectonics and reconstruction techniques are given. In **Chapter 2** a model of the Scotia Sea as discrete units of oceanic and continental crust is set up. This is done using free-air, Bouguer and isostatic residual gravity anomalies, and total field magnetic anomalies reduced to the pole and inverted for oceanic magnetization. The likely uncertainties in these geophysical data are considered. Detailed consideration is given to the picking of magnetic isochron and flowline data to be used in joint inversion as the plate boundaries are short and inversion of the data for reconstructions is vulnerable to errors. In **Chapter 3** the model is subjected to the joint inverse reconstruction technique. The inversion of gridded data is discussed briefly. This is followed by the results of the inversions as applied to the region. In **Chapter 4** consideration is given to the opening of smaller basins and strike-slip movements of microplates in the Scotia Sea region: their age, extent, tectonic setting and reconstruction. Preference is given to conclusions which are consistent within the context of major plate motions and the reconstructions given by the previous chapter, but consideration is given to alternatives. **Chapter 5** consists of a

series of reconstructions of total field magnetic and Bouguer anomalies in the Scotia Sea region during the Cenozoic, and the possible plate boundaries they imply. In **Chapter 6** the history of the enigmatic central Scotia Sea is addressed in the context of the Cenozoic model and what is known of the history of seafloor spreading between Antarctica and South America. In the final chapter, **Chapter 7**, briefer discussions and speculations are given regarding the implications of the new model for the tectonics of the Shackleton Fracture Zone, and, more speculatively, for asthenosperic outflow. The implications of the new model of kinematics to paleo-circulation are explored. Two appendices contain further information on some of the techniques adopted in modelling. One enclosure provides larger versions of some figures, and data used for the quantitative reconstructions.

1.2 Plate tectonics

The possibility that continents might be reconstructed pre-dates all theories about their kinematic independence; Ortelius, Bacon, Placet, Lilienthal, von Humboldt and Snider-Pellegrini all comment, in the pre-uniformitarian age, on the similarities of mapped coastlines, the last of these publishing the first reconstruction (see Kearey and Vine (1996; p.1–2)). Only since the early twentieth century has evidence for this independence been weighty enough to drive serious efforts by reconstructionists. The endeavour found the possibility of analytical rigour with the advent of plate tectonic theory.

Continental drift

Non-catastrophic explanations of mobilism first appeared in the twentieth century explaining the distribution of old coastlines and young mountain chains (Taylor, 1910), igneous provinces, cratons, disrupted old fold belts, climate-thems, fossil fauna and flora (Wegener, 1924; du Toit, 1937) and apparent paleomagnetic polar wander (Runcorn, 1959; Creer, 1965). In this literature the past supercontinents Pangaea, Gondwana and Laurasia and the associated oceans Panthalassa and Tethys were first postulated and reconstructed. The theory of drifting continents ascended only slowly to orthodoxy because

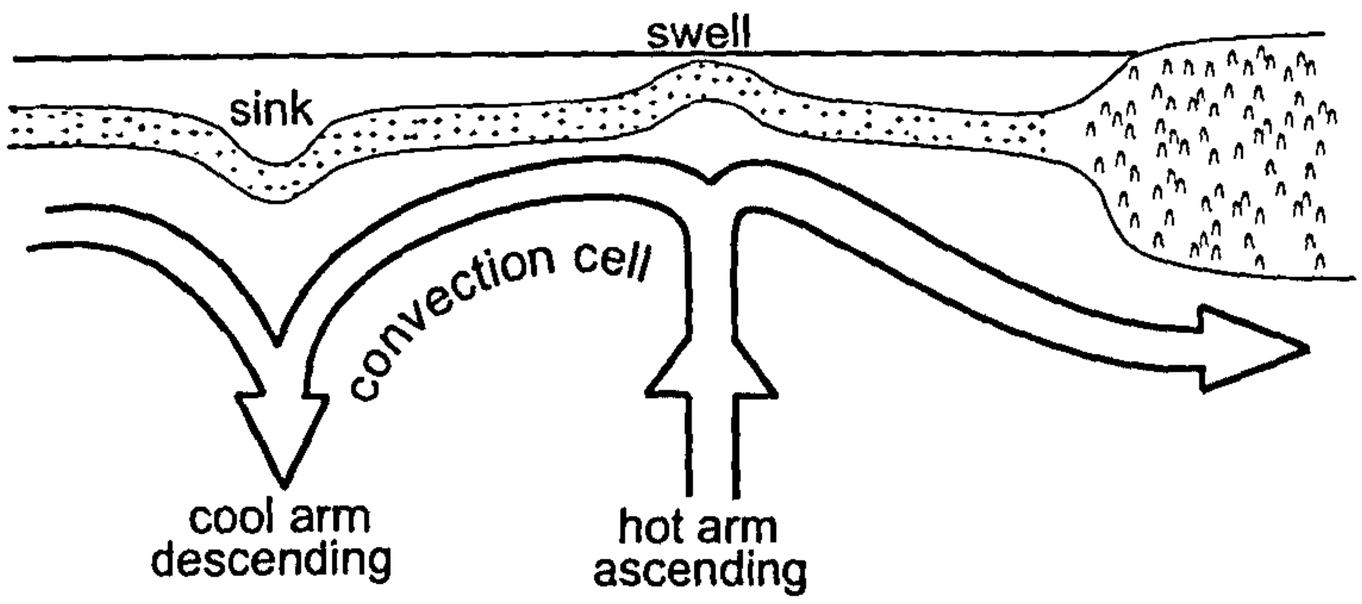

Figure 1.3: Cartoon representation of mantle convection as the driving force for continental drift, new figure after the theory of (Holmes, 1928).

mantle convection, the most believable of a number of proposed mechanisms (Figure 1.3; Holmes (1928)) could not completely produce the apparent continental motions.

Seafloor spreading

The seafloor spreading concept (Dietz, 1961; Hess, 1962) arose out of the initial stage of exploration of the deep oceans which began after the Second World War. The ocean basins were seen to be much younger than the continents (see Heezen (1962) and references in Vogt *et al* (1969)), with thinner crust (Talwani *et al* (1965) and summary in Oxburgh and Turcotte (1968)), and topographically dominated by a median volcanic ridge feature (Heezen, 1959; 1960; 1962; Heezen *et al*, 1959; for example). The role of the crust in mantle convection was developed, so that in the hypothesis hot convecting mantle ascends, then diverges laterally, moving the oceanic crust with it by basal drag and simultaneously filling the divergence (Figure 1.4). It is thrust down into the mantle at oceanic trenches by the cold arms of convection currents. The continents are entirely passive.

A prediction by Vine and Matthews (1963), accompanying widespread acceptance of the phenomenon of geomagnetic field reversal (Cox and Doell, 1962; Cox *et al*, 1963), provided a test of the hypothesis. As the reversing geomagnetic field is recorded by the thermo-remanent magnetization of ferromagnetic minerals in the new rocks continually

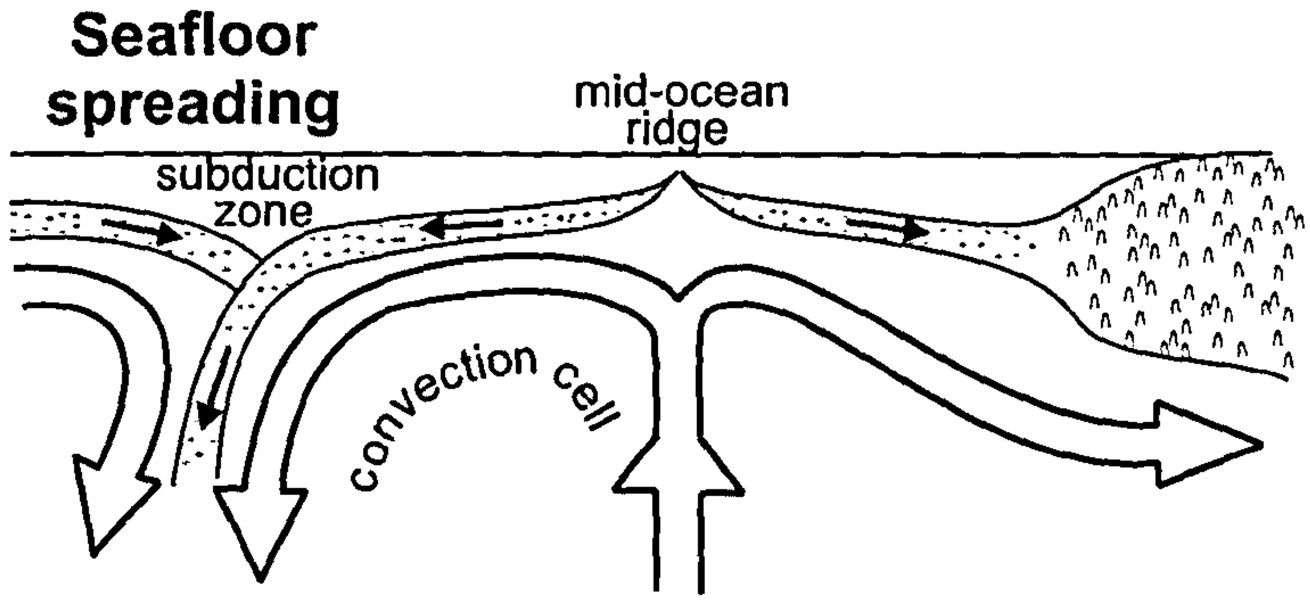

Figure 1.4: Cartoon representation of classical seafloor spreading, in which the oceanic lithosphere moves due to drag at its base by convection cells transporting heat away from Earth's interior.

forming in the volcanic divergence at the elongated mid-ocean ridge crests, a map of seafloor magnetization should show alternating strips of reverse and normally magnetized rocks. This was already well known from the northeast Pacific (Mason and Raff, 1961; Raff and Mason, 1961; Figure 1.5), and subsequently shown to be true for large areas of oceanic crust (Vine, 1966).

The problem of linkage between spreading centres and subduction zones was addressed by Wilson (1965) and by McKenzie and Parker (1967), Morgan (1968) and McKenzie and Morgan (1969), with the concept of transform faults (Figure 1.6). The transform fault hypothesis accounts for failings of previous ideas concerning the formation of long seafloor troughs which segment the median volcanic ridges (Menard, 1955). Transform faults passively accommodate relative motions about ridges and trenches rather than actively cutting them. Those which accommodate ridge offsets of less than 100–200 km often do this is by acting in a purely strike-slip sense: that is to say the motions of the opposing flanks of the fault are parallel to one another, to the transform fault itself, and to relative plate motions at it, but in opposite directions (Wilson, 1965). As a result of this process such transform faults leave a scar in older seafloor outside of the active region between ridge–transform intersections, called a fracture zone, which describes the past motion of the flanking plates at the ridge crest—a tectonic flowline. With the recognition of

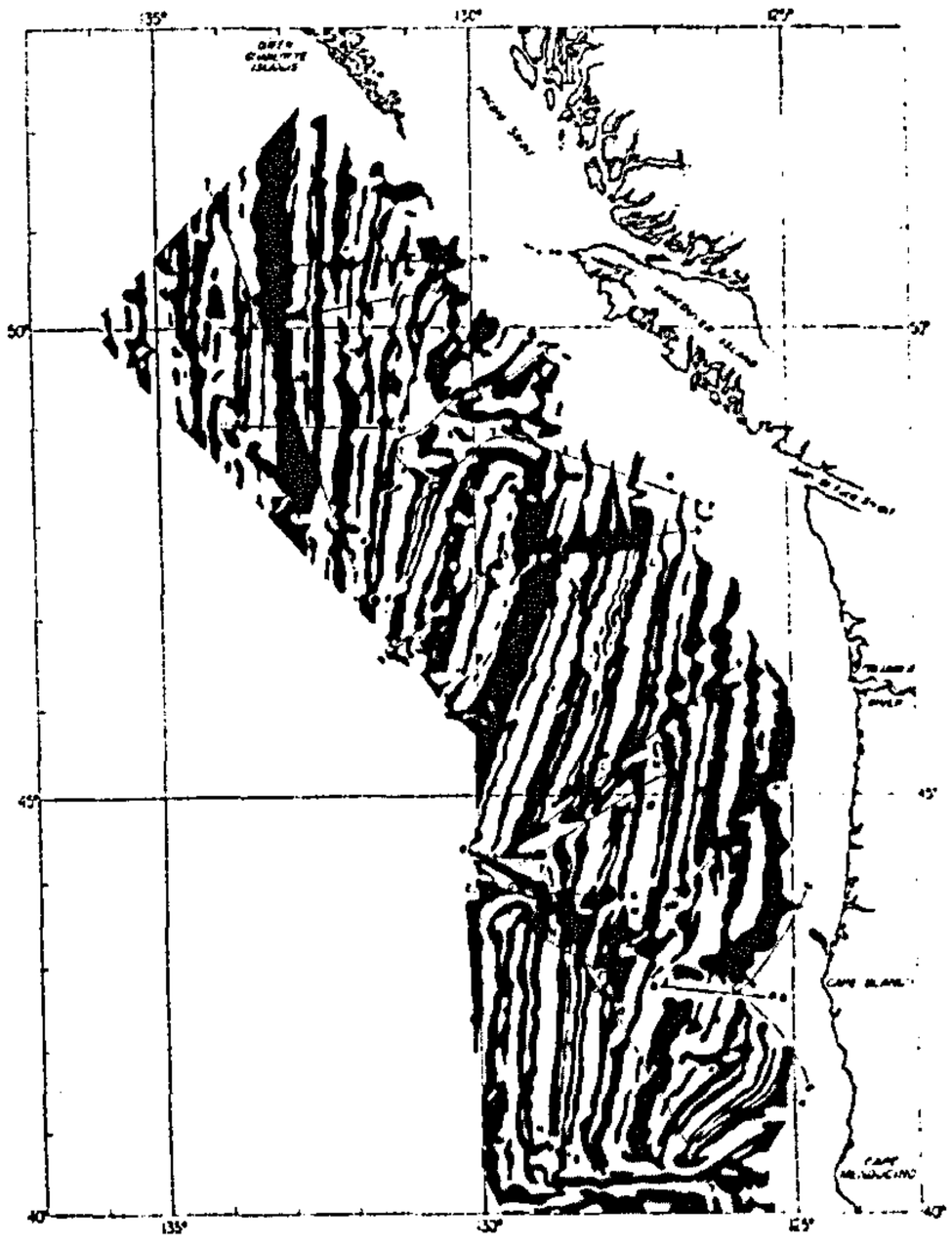

Figure 1.5: Magnetic reversal anomalies of the northeast Pacific Ocean, after Raff and Mason (1961). Their presence confirmed the prediction of Vine and Matthews (1963), which was a test of the seafloor spreading hypothesis, that such anomalies would be seen in accreted oceanic crust.

divergence and convergence in the continental lithosphere, as continental rifts and young mountain belts, the entire lithosphere was included in an essentially complete kinematic theory.

Plate tectonics

World seismicity, at first order, is consistent with the kinematic disposal of elastic (rigid) plates bounded by the linear mid ocean ridges, subduction zones and transform faults. Earthquakes cluster along these linear belts, having extensional source mechanisms at ridges and rifts, compressional mechanisms at trenches, and strike-slip at transform faults (Sykes, 1967; Isacks *et al*, 1968; Barazangi and Dorman, 1969). The first order distribution of volcanism is similarly consistent. In vertical section the rigid plates include all of the crust (oceanic or continental) and the uppermost mantle: together a rheologically distinct

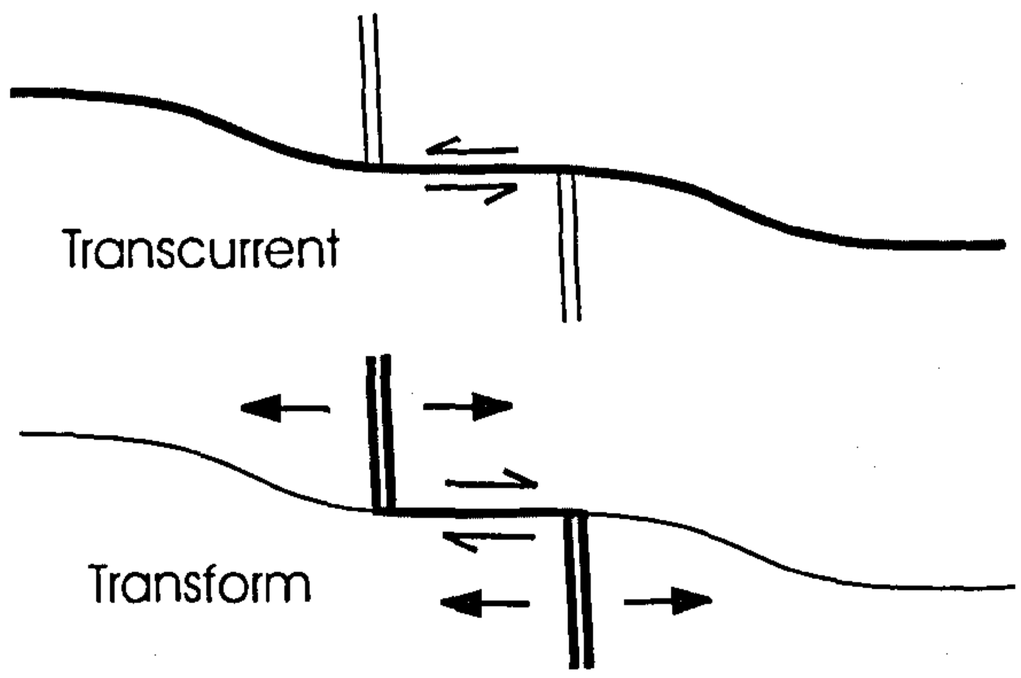

Figure 1.6: Transcurrent and transform faults. Active elements are shown as thick lines, passive elements as thinner ones. The entire length of a transcurrent fault is active: it offsets passive features in the sense (thin half-arrows) apparent by the step in the feature's strike. Transform faults are only active in the offset between active spreading centres. Relative motion (thick arrows) of the plates on opposing flanks of the active fault is opposite to the apparent sense of offset.

layer termed the lithosphere. Beneath the lithosphere a weak layer, characterised by slow convection, is called the asthenosphere. The plates are the basis of plate tectonic theory (Figure 1.7). It assumes that the plates do not deform internally, but only at their edges by accretion or subduction.

At subduction zones oceanic lithosphere sinks into the asthenospheric mantle due to its increased density resulting from thermal contraction. Within the sinking slabs increasing pressure induces minerals to change to more dense phases, which perpetuates subduction. The initial descent of slabs may be spontaneous, or forced, where oceanic lithosphere converges with less dense continental lithosphere. In this view of subduction the role of oceanic lithosphere in plate tectonics is not passive. Basal drag, of the plates by convection currents in the mantle, is not considered to be a strong enough driving force to give observed rates of plate motion. Instead the oceanic lithosphere is thought to form the upper layer of one length-scale of convection in the mantle. The vertical scale is not agreed on: it may be important enough to involve the whole mantle or just its upper 670 km (Loper, 1985; Christensen, 1985; for reviews). The weight of sinking slabs of oceanic lithosphere, the downgoing limbs of mantle convection cells, is calculated to

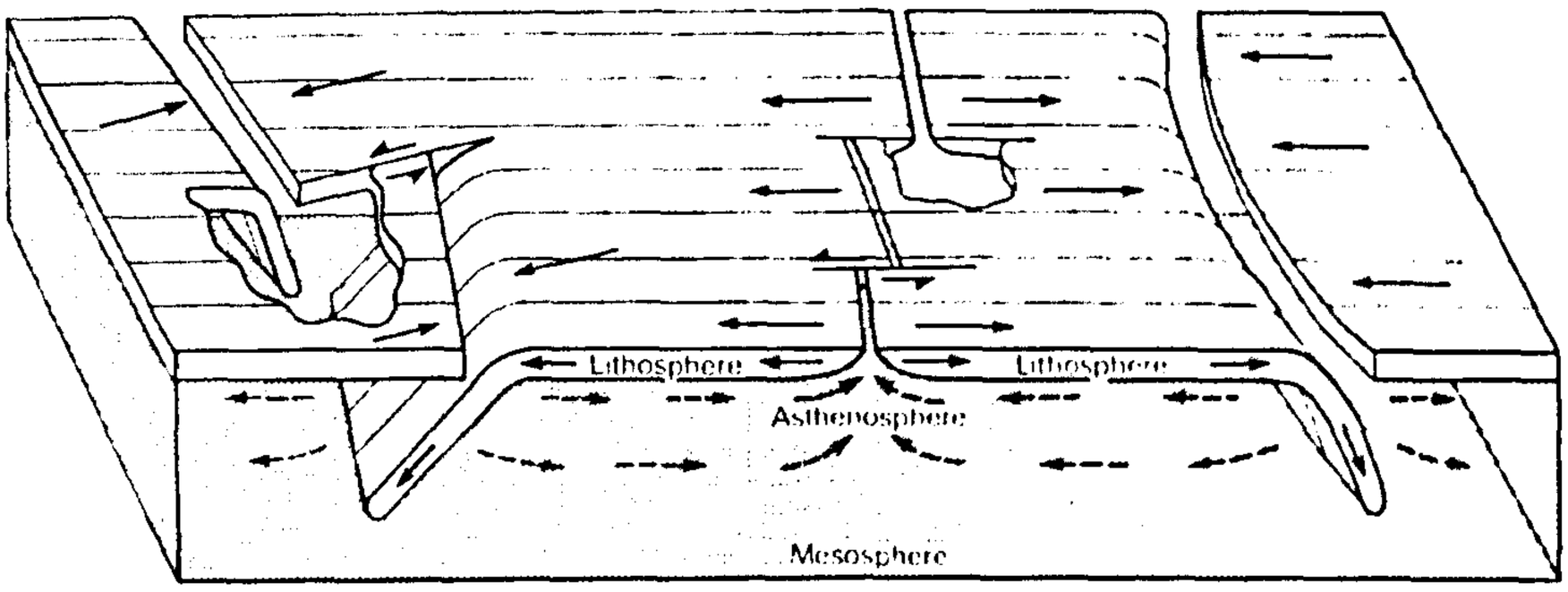

Figure 1.7: Plate tectonic model showing the role of subduction in plate movements and convection in the asthenosphere (after Isacks *et al* (1968)).

be the dominant force driving the plates—'slab pull' (Richter, 1973; Forsyth and Uyeda, 1975), although the driving force of plate tectonics remains a controversial subject.

New oceanic lithosphere is created at the mid oceanic ridge crests where plates diverge, probably as a consequence of slab pull forces. The opening gap between them is filled by asthenospheric material rising in response to decreased pressure at the elevated ridge crest. Decompression accompanying its rise allows the asthenosphere to melt partially. The melt products fill the gap as volcanic and intrusive mafic rocks, giving rise to a characteristic layered velocity structure in seismic profiles (Hill, 1957; Raitt, 1963). From top to bottom these layers are numbered 1 to 3 (Figure 1.8). The lavas of layer 2 are strongly magnetized and give rise to most of the magnetic anomaly recorded at the sea surface.

Back-arc basins

At subduction zones partial melting of the subducted slab gives rise to surface volcanism in an arc, usually about 150 km beyond the trench, on the overriding plate. Back-arc spreading, which is extension by seafloor spreading behind the arc as seen from the trench, is a special local consequence of subduction (Figure 1.9). Back-arc extension usually begins within the arc itself because it is hot and ductile (Tamaki, 1985). Extension may

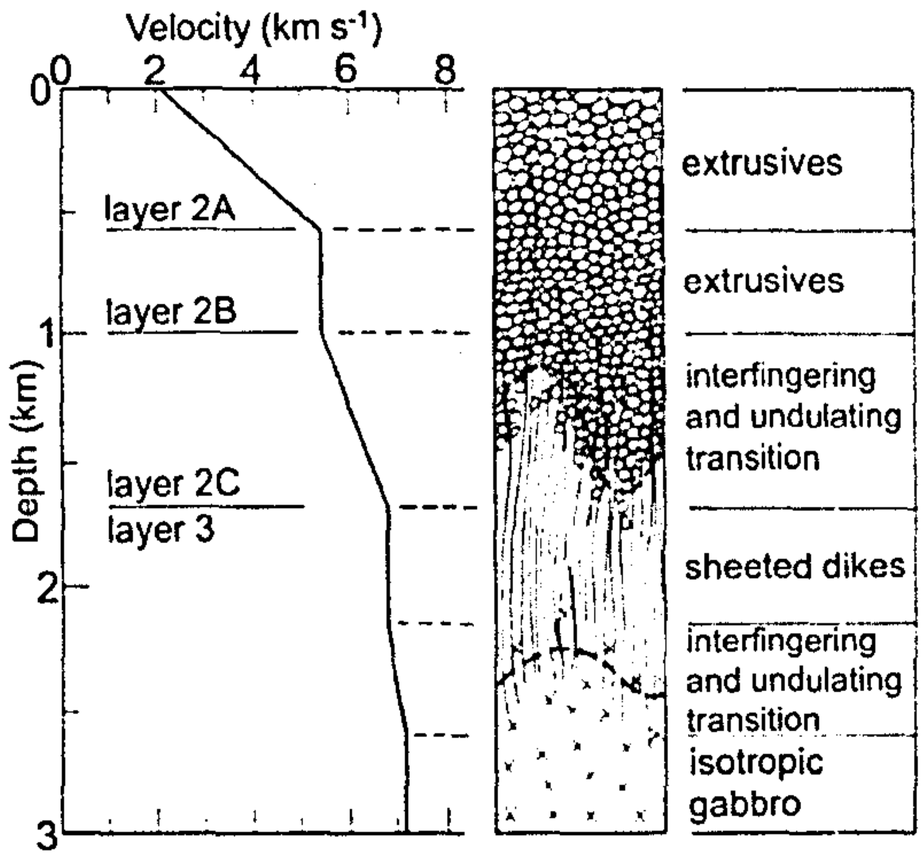

Figure 1.8: Summary of layers in 6.2 million-year-old oceanic crust near the East Pacific Rise defined by their seismic velocities and lithologies from DSDP borehole 504B (after Bratt and Purdy (1984)). Layer 1 (not shown) is a layer of abyssal sediments.

proceed to seafloor spreading, often after just a few million years, moving one half of the split arc away from the volcanic locus and giving rise to an inactive remnant arc. Within this general scheme there is much variability, and the stages of extension may overlap in time, so that it is no surprise that back-arc basins do not all show similar characteristics. The locus of extension may or may not be well defined (Barker, 1972; Hamburger and Isacks, 1988). The basin may or may not show a multiphase history (Karig, 1971). The basin may appear to have originated in either continental (Dalziel *et al*, 1974) or oceanic (Karig, 1971) lithosphere. This variability is the reason for the variety of causative mechanisms proposed for the development of back-arc basins. Back-arc extension has been proposed to be a consequence of partial melting in the upper part of the subducting slab and ensuing forcible diapirism (Karig, 1971). Packham and Falvey (1971) suggest that this diapirism is instead passive, in response to regional tension due to the seismic coupling at the trench and its rollback, or retreat, towards the downgoing plate, as the slab sinks vertically into the mantle (Chase, 1978; Dewey, 1980). Secondary convection induced in the asthenosphere by the descent of the slab is invoked as a means

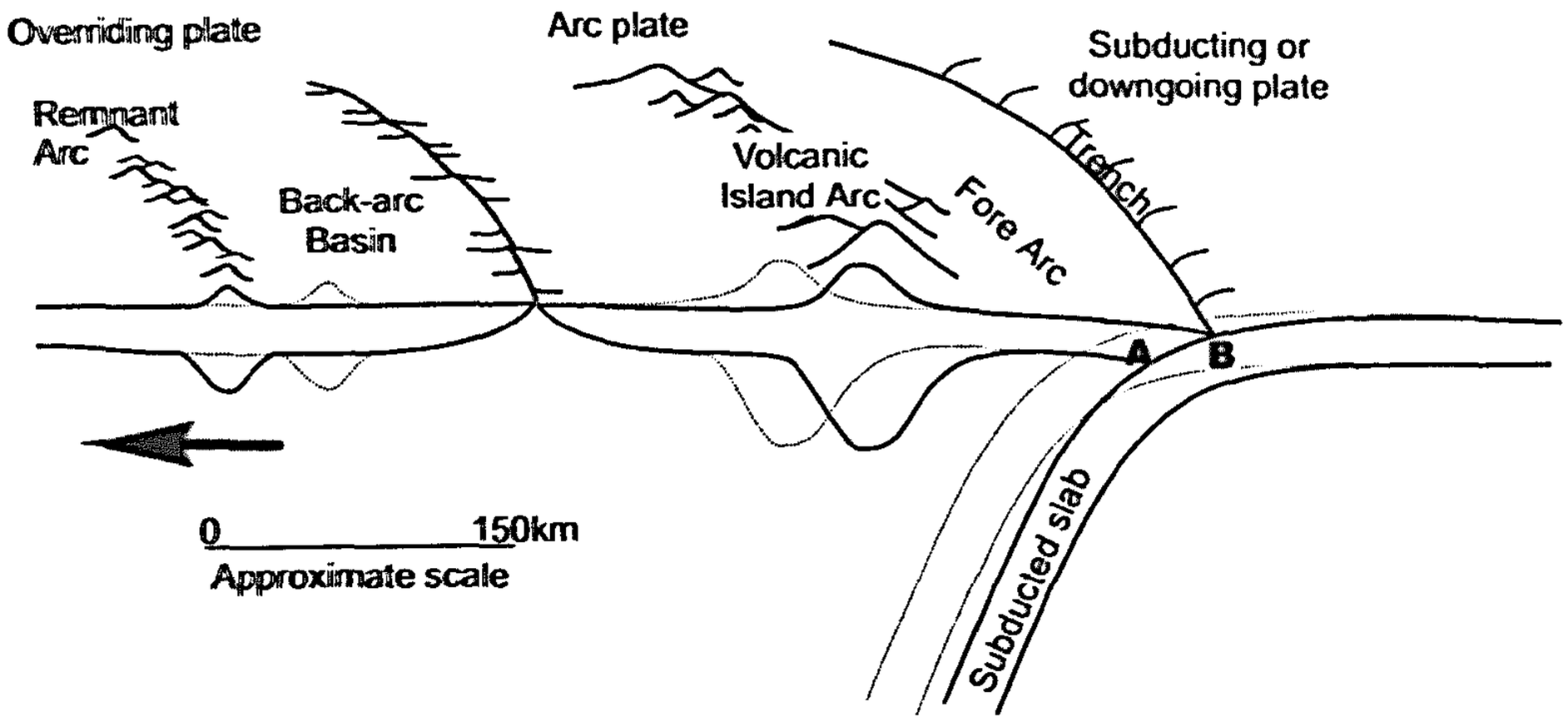

Figure 1.9: Features of a subduction zone with back-arc extension. Although the dynamics of back-arc extension are still not well understood, absolute retreat of the overriding plate (grey arrow) is thought to be important. To accommodate this retreat a back-arc basin develops in its wake. An accompanying phenomenon is trench rollback: the dotted lines show the disposition of the slab, arc, back-arc basin and remnant arc at a time when the trench was positioned at point **A**, whence it rolled back to point **B**.

by which decompression melting might give way to back-arc volcanism (Hsui and Toksöz, 1981; Jurdy and Stefanick, 1983). A jump of the subduction locus toward the downgoing plate has been suggested as a causative mechanism for back-arc basins opening in the Bering and Caribbean seas (Karig, 1974). Recent times have seen a consensus forming around the importance of a situation where the overriding plate's absolute motion (in a fixed reference frame: usually tied to the surface expression of mantle hotspots) is away from the subduction hinge (Chase, 1978; Dewey, 1980), which can be moving or fixed with respect to the mantle. The accompaniment of trench rollback seems important but there is some debate regarding whether it is a cause or a consequence of back-arc spreading.

1.3 Two plate reconstruction techniques

Many different techniques have been used to produce tectonic reconstructions. The simplest reunite geological markers from continental crust on a flat map (Wegener, 1924; du Toit, 1937), or by using transparent spheres (Carey, 1958). Single fits like these are made visually and their significance is difficult to assess. With the advent of plate tectonics and marine geophysics, visual fits of very large data sets representing magnetic isochrons and fracture zones in the oceans allow reconstructions other than at closure (Cande *et al*, 1988; Nürnberg and Müller, 1991; Reeves and Sahu, 1999).

Automated fitting using mathematical methods gives results which can be reproduced and their significance assessed by formal statistical means. Two classes of methods, grid searches and iterative inversion, attempt to minimise a 'misfit' quantity for a model which fits the data as closely as possible. Each can be subdivided by the features fitted and by how quantification is achieved, although all make use of some sense of least-squares fitting.

1.3.1 Euler poles

The most common means of describing the movements of plates is by the use of Euler's fixed point theorem. On a sphere, or a spherical Earth, movement of one point with respect to another can be described by a rotation of a given number of degrees about a pole (an 'Euler pole') at a certain latitude and longitude. The trajectory of the moving point is a small circle about that pole. At the pole itself there is no relative motion between points. By convention anticlockwise rotation about a pole is given a positive value. In practice poles and circles are often handled as vectors, and rotations as matrices, in the mathematics of spherical geometry, which is summarised in Appendix A.

Different types of poles describe different types of rotations in plate tectonics (Figure 1.10). Instantaneous poles describe the true relative motion between plates at an

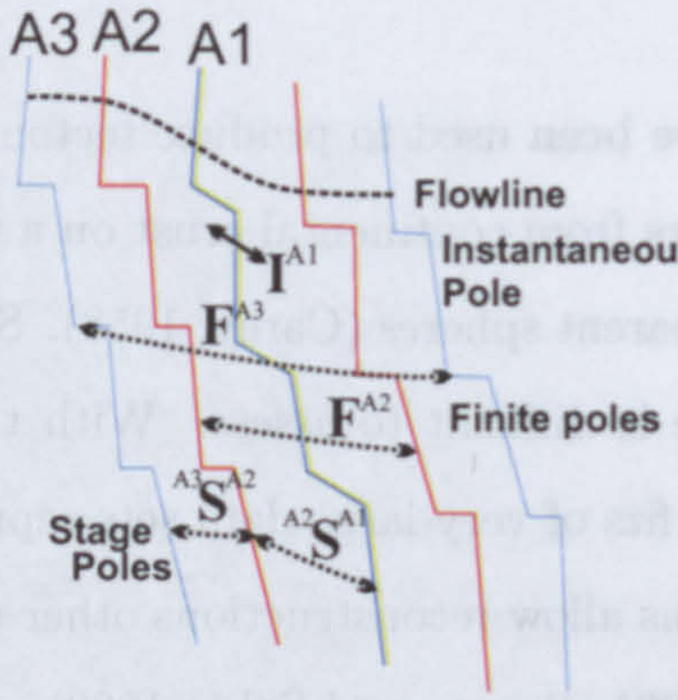

Figure 1.10: Instantaneous, finite and stage poles, for describing motion which has given rise to three isochrons labelled A1 (green, at ridge crest), A2 (red) and A3 (blue). $\mathbf{I}^{A1}$ describes the motion at chron A1 only. $\mathbf{F}^{A3}$ is a rotation which reunites the conjugate A3 isochrons. A sequence of stage poles $^{A3}\mathbf{S}^{A2}$, $^{A2}\mathbf{S}^{A1}$ more closely resembles actual motion in the A3–A1 period, shown by the tectonic flowline (top).

instant in time, usually the present. Finite poles describe a single rotation between one time and another: they do not necessarily describe the plates' actual paths within that time bracket. Reconstruction poles are finite poles for a given time and the present. Stage poles describe motion which is assumed to have been constant, for one plate only, between two times: say 40 Ma and 20 Ma. Subject to the assumption of constant spreading, a sequence of stage poles therefore more closely describes the plates' actual paths—a tectonic flowline of plate motion. If the latter time is the present then the stage pole is the same as the reconstruction pole for the earlier time, but with half the rotation angle. Stage poles for two plates sharing a boundary are separated by the finite rotation between those plates for the younger end of the stage.

1.3.2 Grid search techniques

In techniques of this kind a set of test pole parameters (*e.g.* latitude, longitude of Euler pole, rotation angle) juxtaposes a set of conjugate features. A definition of 'misfit' is used to generate residuals which are used to quantify the juxtaposition by some test criterion.

A minimum test criterion is searched for in a grid in parameter space around the pole. The procedure is repeated about the new pole, if necessary with reduced grid spacing, for a solution that satisfies some predetermined limit.

The first quantitative reconstruction (Bullard *et al*, 1965) reunites the 500 fathom bathymetric contours bounding the Atlantic Ocean. Points on one contour are rotated to the conjugate contour. Residuals are the points' displacements from the contour measured on a small circle about the test pole. The mean square of all residuals is minimised by grid searching, giving total-reconstruction poles in the North and South Atlantic oceans.

McKenzie and Sclater (1971) rotate magnetic isochron data and minimize the area enclosed by the rotated and conjugate isochrons. Hellinger (1981), after early studies (Morgan, 1968; Le Pichon *et al*, 1973) highlighted the importance of fracture zones, includes them with isochrons to define staircase-like figures for reconstruction. This method has seen extensive use ever since, see for instance Stock and Molnar (1983); Chang (1987); Wilson (1993) and Kirkwood *et al* (1999).

Engebretson *et al* (1984) develop a grid search technique for data from single plates, which is applied in the Pacific Ocean. Points of fracture zone–isochron intersection are fitted progressively along each fracture zone. Residuals are the angular distance between rotated and target intersections, weighted by the number of residuals supplied from each point, so that all rotating intersections can have equal influence. The test criterion is the sum of squared residuals.

1.3.3 Iterative inversion techniques

Iterative inversion similarly begins with a set of residuals from a test rotation. Partial derivatives describe how small changes in the pole parameters affect a test criterion. Expressing this description as a least squares problem allows changes to the pole parameters to be found which reduce the test criterion. Iterations of this process approach a solution which minimises the test criterion as much as possible.

Pilger (1978) uses fracture zone and isochron data jointly. Residuals are defined with respect to great circles through the two nearest points on the target figure. Partial derivatives are used in a non-linear iterative inversion for solution poles which minimise the sum of squared residuals. Nishimura *et al* (1984) alter the method of residual generation so a linear least-squares approximation can be made. Only fracture zone–isochron intersection data are used. This method also admits pseudofault–isochron intersection data, which are similarly produced by a symmetrical process—ridge propagation.

Shaw (1987) uses continuous fracture zone traces from satellite altimeter data to constrain the continuity of plate motion as tectonic flowlines. Residuals are defined with respect to target flowlines, composed of small circle segments about the test poles, grown outwards from ridge–transform intersections. The fracture zone itself is not used as a target in the knowledge that, for finite length transform faults, fitting conjugate fracture zones involves small errors not due to the pole parameters. Shaw and Cande (1990) combine this technique with the use of isochron data. Residuals are defined separately for each data type: for magnetic data as angular distance between the rotating point and a point on a target great circle defined by the data describing the conjugate isochron. For fracture zone residuals the flowline of Shaw (1987) is used. To ensure all data are treated equally each set is normalised before the method proceeds to a linearised least squares inversion. This technique is the basis of that of Nankivell (1997a) used in Chapter 3, where it is outlined. A fuller treatment of Nankivell's (1997a) technique can be found in Appendix A .

1.4 Regional synthesis

The Scotia Sea is named after the *S.Y. Scotia* which brought the first, Scottish, oceanographic expedition to the region in 1902-3. It is enclosed by the Scotia Arc, consisting of islands and submarine highs extending east from Tierra del Fuego via South Georgia to the South Sandwich Islands and then west through the South Orkney Islands to

the Antarctic Peninsula (Figure 1.11). The Scotia Arc has long been postulated as the location of a disrupted link between the Andes and the 'Antarctandes' of the Antarctic Peninsula (Barrow, 1830-1; Arctowski, 1895; Suess, 1909; Matthews, 1959; Hawkes, 1962; Wilson, 1966). The idea of a compact connection is so strongly founded in this literature that many later reconstructions take its existence as given—an end-point for the reconstruction to achieve rather than a consequence to be proved (Barker and Griffiths, 1972; Dalziel and Elliott, 1973; Barker and Burrell, 1977; King and Barker, 1988; Barker *et al*, 1991). The region was sparsely charted during the first half of the twentieth century, and organised marine geophysical exploration began in the late 1950s by the University of Birmingham in collaboration with the British Antarctic Survey (BAS), whose ships are annual visitors to the region. The region is also the subject of scientific visits by ships of other national surveys, institutions and programs.

1.4.1 Islands and Submarine Highs

Northern area

The onshore geology of the northern part of the Scotia Arc is shown in Figures 1.12 and 1.13. Stratigraphically, Tierra del Fuego is simply a continuation of the Andean margin of South America, bent through nearly ninety degrees to form the southern end of the 'Patagonian orocline' (Carey, 1958) which strikes west-northwest. Bending was probably complete prior to opening of the Scotia Sea (Cunningham, 1993), although paleomagnetic constraint for this dating is not complete (Cunningham, 1993; Cunningham *et al*, 1995). The origin of the orocline is not well understood—it could possibly have been due to glancing collisions between Tierra del Fuego and the Antarctic Peninsula as the two separated about a nearby Euler pole (Livermore and Woollett, 1993), or may simply be the original shape of the tectono-magmatic belt.

The orocline exposes three major lithotectonic provinces (Dalziel and Elliott, 1971; 1973; Tectonic map of the Scotia arc, 1985) also striking west-northwest. At the Pacific margin a mainly Late Cretaceous calc-alkaline batholith with Cenozoic additions and an

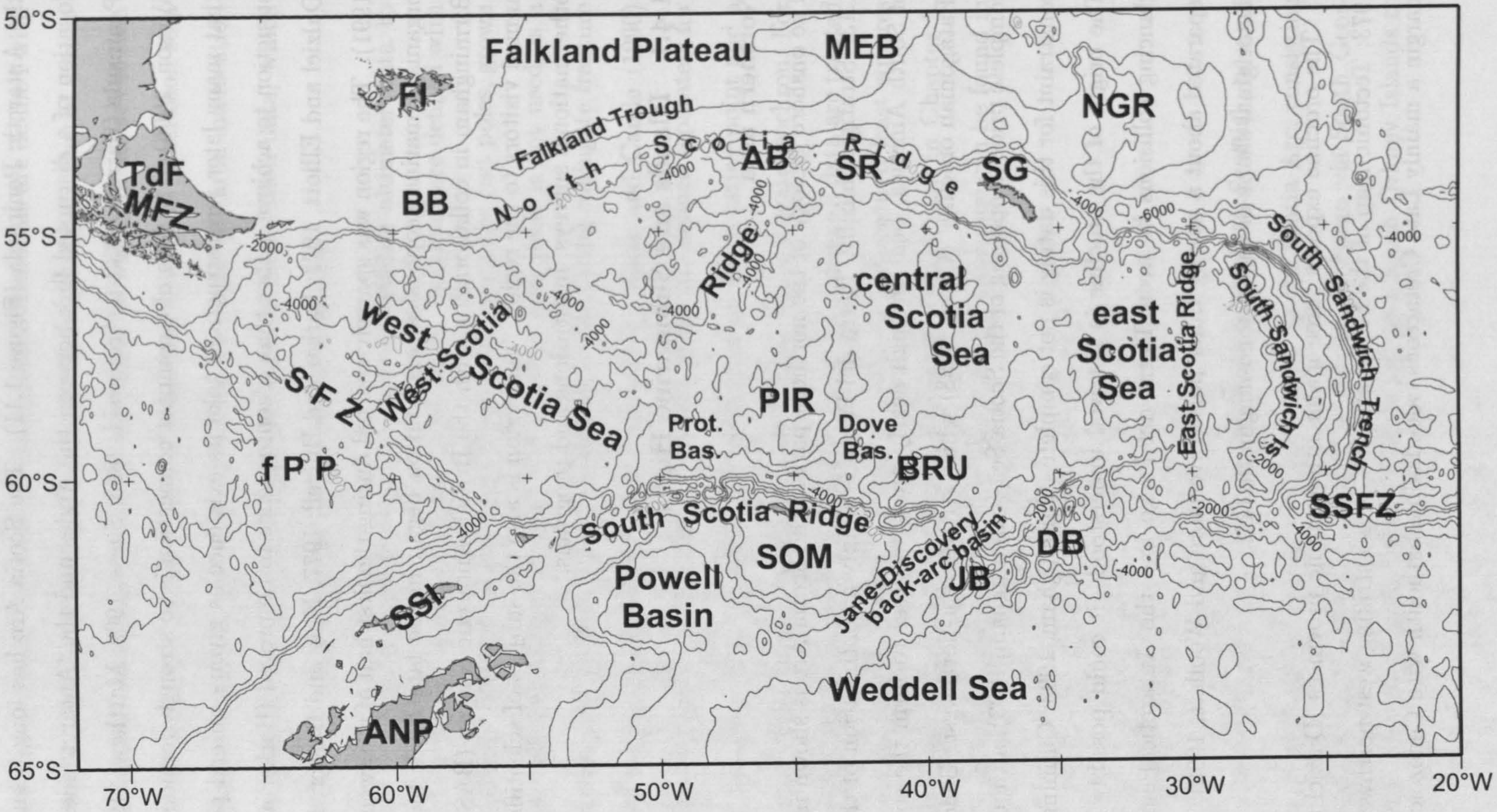

Figure 1.11: Bathymetric contour map of the Scotia Sea. Contour interval 1000m. AB: Aurora Bank, ANP: Antarctic Peninsula, BB: Burdwood Bank, BRU: Bruce Bank, DB: Discovery Bank, Dove Bas.: Dove Basin, fPP: former Phoenix plate, JB: Jane Bank, MEB: Maurice Ewing Bank, MFZ: Magallanes fault zone, NGR: Northeast Georgia Rise, PIR: Pirie Bank, Prot. Bas.: Protector Basin, SFZ: Shackleton Fracture Zone, SG: South Georgia, SOM: South Orkney Microcontinent, SR: Shag Rocks, SSFZ: South Sandwich Fracture Zone, SSI: South Shetland Islands, TdF: Tierra del Fuego. The region of ocean bisected by the Shackleton Fracture Zone is referred to as Drake Passage.

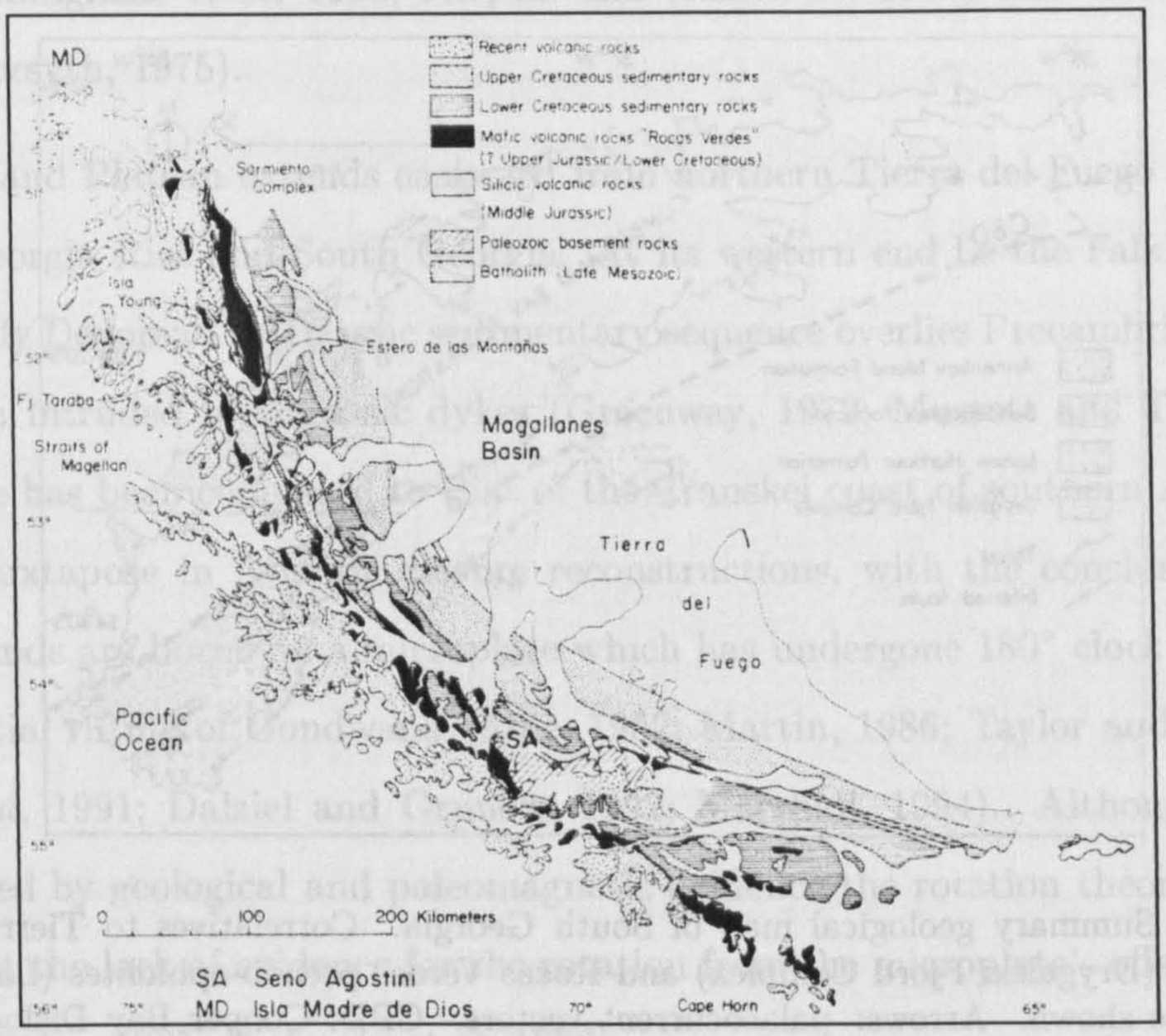

Figure 1.12: Summary geological map of Tierra del Fuego showing the curved arc, pseudo-ophiolite (Rocas Verdes) and other terranes. From Dalziel (1982).

accretionary prism at its seaward face represents the exhumed roots of a volcanic arc above the southern Chile Trench (Suárez and Pettigrew, 1976). Immediately to the north and east lies a discontinuous belt of lensate mafic igneous bodies, consisting of massive and layered gabbros intruded by sheeted dyke complexes, all overlain by a landward dipping marine extrusive sequence with sediments. Although a peridotitic layer is not proved the bodies are taken as an ophiolite sequence representing the floor of a late Jurassic to early Cretaceous, possibly back-arc, basin—the 'Rocas Verdes Basin' (Katz, 1973; Dalziel *et al*, 1974; 1975; Alabaster and Storey, 1990; Stern *et al*, 1992; Mukasa and Dalziel, 1996). Opening of the Rocas Verdes Basin was concurrent with the initial rifting of the southernmost Atlantic between South America and Africa, and a later increase in the spreading rate of the southern Atlantic coincides with the closure and shortening of the Rocas Verdes Basin in mid-Cretaceous regional convergence (Dalziel *et al*, 1974; Bruhn

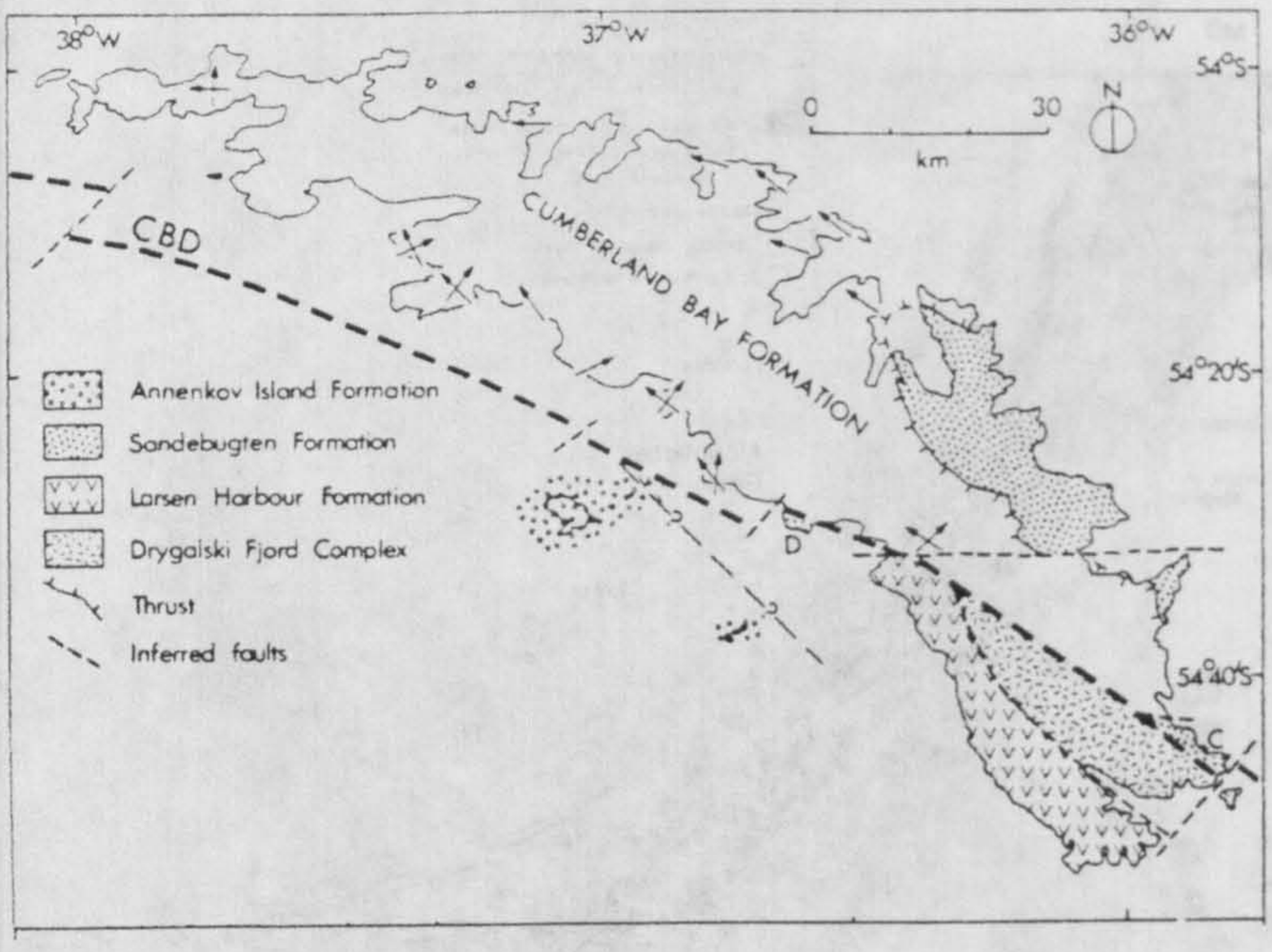

Figure 1.13: Summary geological map of South Georgia. Correlatives to Tierra del Fuego's Serie Tobifera (Drygalski Fjord Complex) and Rocas Verdes pseudo-ophiolites (Larsen Harbour Formation) are shown. Arrows: palaeocurrent vectors. CBD: Cooper Bay Dislocation. From Storey and Macdonald (1984).

and Dalziel, 1977).

The arc and pseudo-ophiolite terranes of Tierra del Fuego presumably terminate at its rifted eastern margin. Further north and east still, on inferred Paleozoic basement, lies a thick (locally $>$ 2000m) volcaniclastic sequence (the 'Serie Tobifera') which is overlain by marine sands and later black shales, all of Jurassic age (Biddle *et al*, 1986; Pittion and Gouadain, 1992) and thought to represent extended continental crust at the margins of the Rocas Verdes Basin (Dalziel *et al*, 1974). Overlying the Jurassic sequence is a thick Cretaceous–Cenozoic sedimentary sequence interpreted as the fill of an extra-cordilleran foreland basin active since the Albian-Cenomanian (Biddle *et al*, 1986). This is referred to as the Magallanes (or Magellan, or Austral) basin and is not specifically related to the Rocas Verdes Basin. Tierra del Fuego is cut, parallel to the cordillera, by numerous presently-sinistral strike-slip faults, which display evidence for a long history of movement: transpressional in the Paleogene ($\sim$ 65–23 Ma), transtensional in the Neogene ($\sim$post

23 Ma) (Cunningham *et al*, 1995; Klepeis and Austin Jr, 1997) and latterly, sinistral strike-slip (Forsyth, 1975).

The Falkland Plateau extends eastward from northern Tierra del Fuego as far as the Northeast Georgia Rise and South Georgia. At its western end lie the Falkland Islands, where an Early Devonian to Triassic sedimentary sequence overlies Precambrian basement and has been intruded by Jurassic dykes (Greenway, 1972; Mussett and Taylor, 1994). The sequence has been compared to that of the Transkei coast of southern Africa, where the islands juxtapose in Atlantic closure reconstructions, with the conclusion that the Falkland Islands are borne on a microplate which has undergone 180° clockwise rotation since the initial rifting of Gondwana (Adie, 1952; Martin, 1986; Taylor and Shaw, 1989; Grunow *et al*, 1991; Dalziel and Grunow, 1992; Marshall, 1994). Although seemingly well-supported by geological and paleomagnetic evidence the rotation theory has critics, who highlight the lack of evidence for the rotation from the microplate's offshore margins (Platt and Philip, 1995; Richards *et al*, 1996).

The Falkland Islands are surrounded by sedimentary basins. The North Falkland Basin lies to the north of the islands. Separating the islands from Tierra del Fuego is the Malvinas Basin, which gives way via the South Falkland Basin, between the islands and Burdwood Bank, to the Falkland Plateau Basin to the east of the islands. At the eastern end of the Falkland Plateau Basin lies Maurice Ewing Bank, which, on the basis of drilling results, bears a Jurassic–Cretaceous sequence overlying Precambrian basement (Barker *et al*, 1977). The Falkland Plateau Basin is thought to consist of thinned continental crust (Ewing *et al*, 1971; Ludwig and Rabinowitz, 1982a; Lorenzo and Mutter, 1988), or possibly oceanic crust (Marshall, 1994; Barker, 1999), with a thick sedimentary overburden (Lorenzo and Mutter, 1988; Richards *et al*, 1996). Initial extension in the basin preceded the separation of South America and Africa in the Early Cretaceous. The exact timing is not well constrained but may have been as early as Permo-Triassic times (Lorenzo and Mutter, 1988; Marshall, 1994; Richards *et al*, 1996). The South Falkland and Malvinas basins may have a similar history to the Falkland Plateau Basin but their

southern margins are modified to form the Cenozoic transpressional strike-slip boundary between the west Scotia Sea and the Falkland Plateau–Tierra del Fuego (Richards *et al*, 1996). Because of their timing, extension in all the Falkland Plateau's basins is interpreted to be related to the initial break-up of Gondwana.

To the south of the Falkland Plateau, and separated from it by the Falkland Trough which consists of thinned continental or thick oceanic crust (Ewing *et al*, 1971; Ludwig *et al*, 1978; Lorenzo and Mutter, 1988), lies the North Scotia Ridge which is exposed at Black Rocks, Shag Rocks and South Georgia. All these exposures show that the core of the ridge consists of a deformed Mesozoic sequence, which dredging results suggest is exposed on the summit of the ridge at Burdwood Bank (Macfadyen, 1933) and Shag Rocks (Tyrrell, 1945). Seismic refraction, reflection and gravity models suggest that the northern side of the ridge has accreted onto this core during the Cenozoic (Ludwig *et al*, 1968; 1978; Ludwig and Rabinowitz, 1982b; Ludwig, 1983; Cunningham *et al*, 1998; Cunningham, 1998). This accretion is attributed by Ludwig *et al* (1978) and Cunningham *et al* (1998) to northward propagation of the ridge in the west Scotia Sea, which ceased spreading at around 6 Ma. Cunningham *et al* (1998) contend that convergence at the North Scotia Ridge has ceased except in the area just north of Burdwood Bank.

On South Georgia an upper Jurassic to lower Cretaceous sedimentary sequence is exposed, similar to that drilled on Maurice Ewing Bank. The island is cut by a major northwest trending shear zone, called the Cooper Bay Dislocation, which has a poorly understood kinematic history including strike-slip and reverse movements (Tanner and Macdonald, 1982; Storey, 1983; Macdonald *et al*, 1987). In addition, the southeast extremity of the island includes an igneous complex of similar age and petrology to the Rocas Verdes Basin sequence, called the Larsen Harbour Complex, and a volcaniclastic sequence similar to the Serie Tobifera, the Drygalski Fjord Complex (Dalziel *et al*, 1975; De Wit, 1977; Storey *et al*, 1977; Storey and Mair, 1982; Mukasa and Dalziel, 1996). Correlatives to the Patagonian batholith and sedimentary fill of the back-arc basin are also

contended for South Georgia (see Macdonald *et al* (1987) for review). The geological similarities between South Georgia and Tierra del Fuego prompted regional reconstructions in which South Georgia is situated immediately south of Burdwood Bank in Jurassic and Cretaceous times (Section 1.5.1). Geochemical data from the igneous complexes suggest the basin on South Georgia may not have been a true back-arc basin, however, instead it may have occupied an oceanic transtensional setting like the modern Gulf of California (Alabaster and Storey, 1990). The complexes are thought to have been spared destruction during closure of the parental basin by concentration of strain along the Cooper Bay Dislocation (Macdonald *et al*, 1987). The northern margin of the South Georgia block probably accreted early in the Cenozoic, but apparently accretion there has ceased (Cunningham *et al*, 1998).

South Sandwich Islands

The South Sandwich Islands lie approximately 100 km west of the South Sandwich Trench which reaches a maximum depth in excess of 8 km and is associated with a well defined Benioff-Wadati seismic zone. Subduction of oceanic lithosphere of the South American plate is ongoing beneath the islands. In all, eleven islands are emergent, several of which have been active since their discovery. In addition numerous volcanic shoals are known from the arc. Geochemical classification of samples recovered from the islands and dredged submarine scarps ascribes them a young age (0.7–4 Ma; Baker (1978)) and island-arc–back-arc origin. There is no documented evidence from exposure or geochemical analyses for any other crustal component to the islands.

Southern area

Dredging of Discovery Bank suggests that it was, at least in part, ancestral to the South Sandwich Arc, with subaerial or shallow marine components (Barker *et al*, 1982). Together with Jane Bank it is postulated to have been deactivated by collisions of the ancestral South American–Antarctic ridge-crest with the trench to their southeast. Barker *et al* (1982; 1984) envisaged long ridge segments colliding to deactivate the arcs in single large episodes, but Hamilton (1989) suggests a modified scenario where collision (and

maybe therefore deactivation) were more piecemeal. A possible northern limit to the arc is defined from an isolated high presently in the South Sandwich forearc discussed by Livermore *et al* (1994) and Barker (1995). This high has been dredged, yielding hydrothermally altered basalts and andesites dated at 29–35 Ma, suggesting it is older than the present east Scotia Sea back-arc spreading. The presence of this feature puts the northern limit of the Discovery–Jane ('proto-South Sandwich') arc at $\sim$ 56°S (present coordinates) at about the time of opening of the west Scotia Sea.

Cored micropaleontological evidence from Bruce Bank suggests it was more elevated in the Middle Eocene than presently. The core recovered no volcaniclastic or igneous material, but did yield derived fossils of Cretaceous age which are not thought to have been transported very far, suggesting that Bruce Bank may be a fragment of continental origin (Toker *et al*, 1991; Mao and Mohr, 1995). A suite of Eocene alkali basalts recovered from the southwestern margin of Powell Basin may be related to its opening and development (Barber *et al*, 1991). A single dredge sample of quartz-rich cataclasite is documented from the Shackleton Fracture Zone (Burrell, 1983), suggesting it may entrain pods of continental lithologies. The South Orkney Islands and Antarctic Peninsula are geologically similar to the northern area, with a Paleozoic–Mesozoic arc–fore-arc sequence exposed at a structurally higher level (Smellie and Clarkson (1975); Dalziel (1984); Tectonic map of the Scotia arc, 1985; Meneilly and Storey (1986)). However there is no known evidence for a basin analagous to the Rocas Verdes Basin. The group of islands around Elephant Island and Clarence Island, further west, is yet a further continuation of the subduction-related sequence (De Wit *et al*, 1977; Dalziel, 1984; Trouw *et al*, 1991; 2000), which continues through the South Shetland Islands and Antarctic Peninsula.

1.4.2 Deep Marine Areas

West Scotia Sea

Marine magnetic anomaly sequences in the west Scotia Sea, symmetrical about the axial West Scotia Ridge, show that active seafloor spreading occurred there in the period

between 26 Ma and 6 Ma (Barker and Burrell, 1977; Burrell, 1983; Tectonic map of the Scotia arc, 1985; Livermore *et al*, 1994). Barker (1995) contends on the basis of previous work (Barker and Burrell, 1977) that the west Scotia Sea is 'back-arc in the broad sense'—part of a multiphase back-arc basin represented by the whole Scotia Sea. A break in oceanic basement slope at about 100 km from the West Scotia Ridge is consistent with a slowdown in spreading rates at or near 17 Ma (Livermore *et al*, 1994). The West Scotia Ridge is distinct bathymetrically and gravimetrically and is dextrally offset six times by transform and non-transform offsets. The west Scotia Sea margin with Tierra del Fuego is steep and abrupt, with seismic evidence for block faulting suggesting it is a rifted margin (Maldonado *et al*, 1993). Parts of the northern margin are bathymetrically steep and probably dominated by strike-slip faults. At the eastern margins of the spreading system are areas of oceanic crust: the central Scotia Sea and Protector Basin. The nature of the interfaces is indistinct. The southern margin is at the steep northern edge of the South Scotia Ridge near Elephant Island, and probably has a strike-slip dominated origin. This gives way further west to the Shackleton Fracture Zone, a bathymetrically distinct compound ridge–trough feature with a complicated trace. Strike-slip tectonics dominate the Shackleton Fracture Zone, but other components of strain are likely to be accommodated.

Central Scotia Sea

The central Scotia Sea lies immediately to the east of the west Scotia Sea. There is no bathymetric or gravimetric ridge expression, but a sequence of magnetic reversal anomalies is present. Hill and Barker (1980) interpret these to represent back-arc spreading in a north–south direction between 20 Ma and 6 Ma, or between 33 Ma and 23.5 Ma, favouring the former interval. This interpretation is the pre-eminent view of the development of the central Scotia Sea, but not without criticism and alternatives. De Wit (1977) builds a case that the central Scotia Sea is an extension of the Rocas Verdes Basin that escaped mid-Cretaceous inversion. Livermore *et al* (1994) suggest alternative views, that the central Scotia Sea may be a crustal allochthon or the result of disorganized back-arc spreading (Lawver and Hawkins, 1978; Tamaki, 1985).

East Scotia Sea

The east Scotia Sea lies immediately to the east of the central Scotia Sea and to the southeast of South Georgia. Its boundary with each is not distinct. Early studies of magnetic reversal anomaly profiles suggested that it probably began spreading near to 8 Ma and continues to the present, and later work puts initiation at or before 15 Ma (Barker, 1972; Livermore *et al*, 1994; Barker, 1995). The axial ridge is evident in bathymetric and gravimetric data, and is segmented into at least nine axial valleys with mostly sinistral offsets. The ridge terminates at an east–west arm of the South Sandwich Trench in the north and at the South Sandwich Arc in the south. Thus is defined the modern Sandwich plate, which overrides the South American plate at the subduction zone. At the western edges of the east Scotia Sea there is no obvious remnant arc to the South Sandwich Arc.

Small basins

Powell basin separates the South Orkney Microcontinent from the Antarctic Peninsula, it is thought to have opened in the late Oligocene and early Miocene (King and Barker, 1988; King *et al*, 1997; Lawver *et al*, 1994; Eagles and Livermore, 1999). Protector Basin intervenes between the southern parts of the west and central Scotia Seas. Hill and Barker (1980) determine that it opened between 17 Ma and 11 Ma. The deep-water gap between Jane and Discovery Banks and the South Orkney Microcontinent and Bruce Bank is interpreted as a back-arc basin, termed Jane Basin, which is thought to have opened in response to subduction of South American lithosphere beneath the microcontinent, possibly between 32 Ma and 25 Ma (Lawver *et al*, 1991). Dove basin (Hill, 1978; Burrell, 1983) intervenes between Bruce Bank and Pirie Bank, little is known about its development.

Southeast Pacific

To the southwest of the Shackleton Fracture Zone an extinct oceanic spreading system is present. It formed by accretion at the now extinct Phoenix ridge (Barker, 1982; Larter and Barker, 1991; Livermore *et al*, 2000). Upon extinction of the ridge at magnetic chron C2a ($\sim$ 3.3 Ma) the Phoenix plate on its southeastern flank fused to the Antarctic plate

on its northwestern flank. The Phoenix plate had been subducting beneath the western margin of the Antarctic Peninsula, and upon deactivation of spreading, the slab continued to sink and the trench to roll back. The result was net extension behind (landward of) the trench which is manifest as a young back-arc basin in Bransfield Strait. Lawver *et al* (1995) reverse the causality, suggesting that opening of the back-arc Bransfield Strait drives ongoing subduction at the South Shetland Trench, which is aseismic.

Weddell Sea

Southeast of Jane and Discovery Banks, east of the Antarctic Peninsula and north of the Dronning-Maud Land–Berkner Island coast of East Antarctica the Weddell Sea formed by the relative movement of South America away from East Antarctica between the Early Cretaceous and about 20 Ma. Only the southern flank of the system exists in its entirety now as much of the northern flank has been subducted at the South Sandwich Trench and its presumed predecessors. East of the Scotia Sea relative motion between South America and Antarctica is taken up by spreading at the South-American–Antarctic ridge, which joins the Mid Atlantic Ridge and Southwest Indian Ridge at the Bouvet triple junction 1400 km east of the South Sandwich Trench.

1.5 Plate kinematics in the Scotia Sea

The present-day kinematics of the Scotia Sea region has been addressed by Forsyth (1975) and Pelayo and Wiens (1989). The modern Scotia Sea consists of two main plates, the western, Scotia plate and eastern, Sandwich plate. Their mutual boundary is the East Scotia Ridge. The Sandwich plate advances behind the retreating South Sandwich Trench, which is joined to the East Scotia Ridge by an east–west trough at its northern end and by less obvious means at the south, at about 55 mma^{-1} (Pelayo and Wiens, 1989). Minor sinistral movements are known along the north and south Scotia Ridges, which define the northern and southern margins of the Scotia plate, from earthquake focal mechanisms (Pelayo and Wiens, 1989), accommodating the slow east-northeast relative movement

between South America and Antarctica. The Scotia plate intervenes between these two major plates. Slow advance of the South Shetland microplate behind the South Shetland Trench is accommodated by opening of Bransfield Strait.

1.5.1 Reconstructions of the Scotia Sea

Reconstructions of the Scotia Sea intending to show its development from a region of connection between South America and the Antarctic Peninsula have been given by Dalziel and Elliott (1971); Barker and Griffiths (1972); Barker and Burrell (1977); De Wit (1977); Hill (1978); Hill and Barker (1980); Barker and Hill (1981); Burrell (1983); Dalziel (1983); Barker *et al* (1984); Garrett *et al* (1986); King and Barker (1988); Hamilton (1989); Barker *et al* (1991); Diraison *et al* (2000) and others.

The first published reconstruction is that of Dalziel and Elliott (1971), based on litho-tectonic division of the region from outcrop geology extrapolated offshore (Figure 1.14). They assume a compact, linear connection between Tierra del Fuego and the Antarctic Peninsula existed in the latest Mesozoic. South Georgia and the Shag Rocks part of the North Scotia Ridge were positioned at the Pacific side of this connection, which subsequently deformed by oroclinal bending in Patagonia and the Antarctic Peninsula. South Georgia and Shag rocks dispersed from the interior of the bent region after the early Cenozoic.

A linear connection is not assumed in the next reconstruction attempt, of Barker and Griffiths (1972); Figure 1.15, which attempts to reconstruct simultaneously sedimentary basins, shallow basement, and 'intense magnetic zones' prior to 'lower Tertiary fragmentation' of an assumed compact cusp. The Shackleton Fracture Zone is used as a tectonic flowline for closure of the west Scotia Sea. It is not clear which modern regions some of the fragments in the closure reconstruction represent. A number of 'random relative motions' are applied on an *ad hoc* basis to produce the final fit. The admission is made that a number of other reconstructions are possible, but that all imply the existence of a

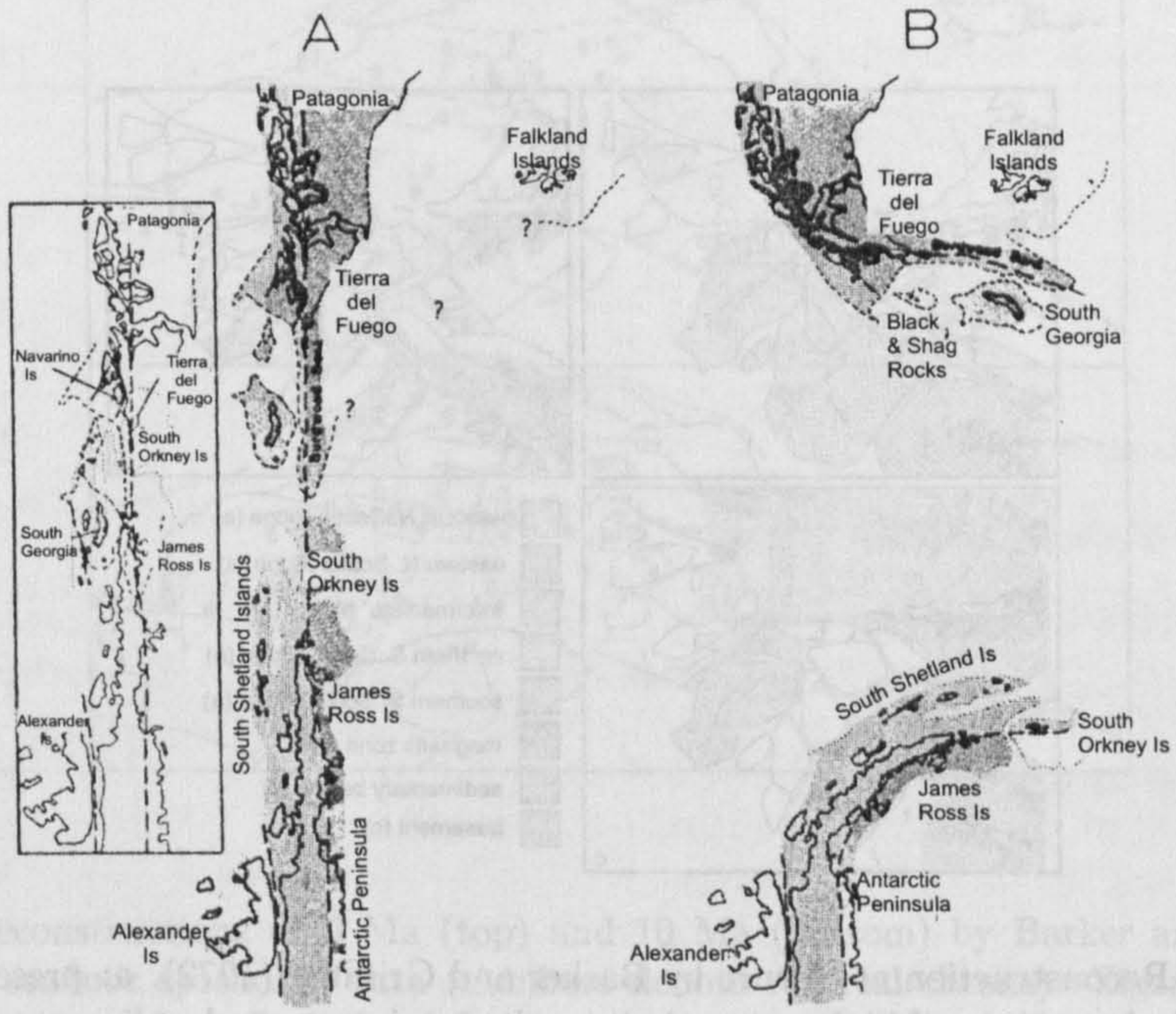

Figure 1.14: Reconstruction by Dalziel and Elliott (1971). A: Mesozoic, as a linear margin beneath which Panthalassa is being subducted. B: early Tertiary, after initial opening in the west Scotia Sea. Labels redrawn.

compact cuspate connection prior to development of the region.

No such compact cusp is reconstructed, however, by aligning the earliest seafloor spreading anomalies (chron C8) from the west Scotia Sea manually on a polar stereographic projection, as done by Barker and Burrell (1977; Figure 1.16). The existence of an assumed compact cusp is nonetheless maintained, and its disassembly is attributed to movements preceding C8. Very similar reconstructions, based on a least-squares fit of magnetic anomaly data and using similar assumptions, are given by Burrell (1983) (see also Section 3.1). In both, again, the Shackleton Fracture Zone is used as a tectonic flowline, defining the effective southwestern boundary of the west Scotia Sea. However it is also suggested to entrain a pair of sliver-shaped continental fragments pared off the southern edge of Tierra del Fuego.

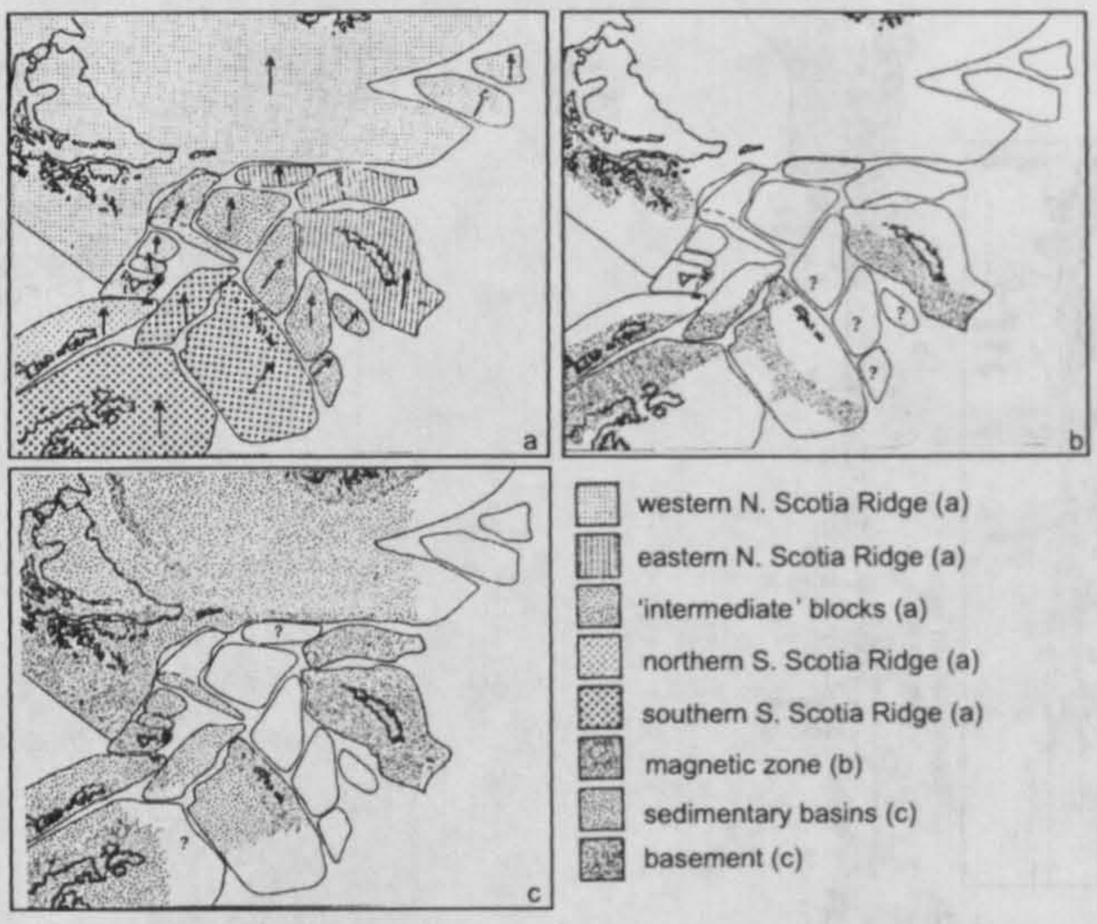

Figure 1.15: Reconstruction at closure by Barker and Griffiths (1972). a: present-day magnetic north (arrows). b: regions of high magnetic intensity. c: interpreted sedimentary basins. Labels redrawn.

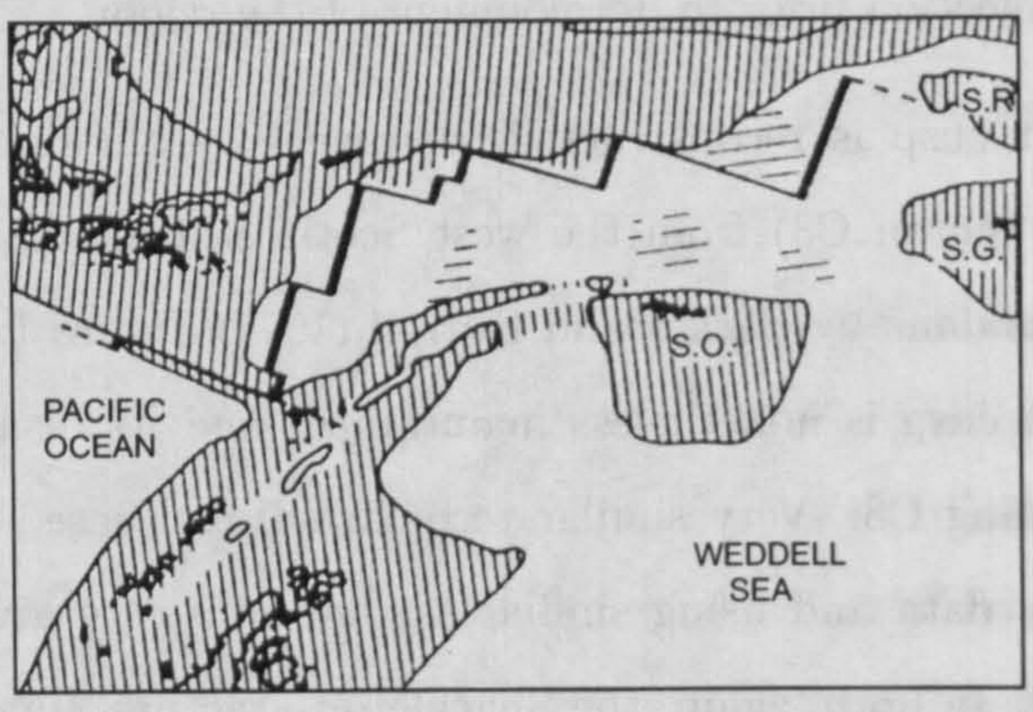

Figure 1.16: Reconstruction at C8 by Barker and Burrell (1977). Close-hatching: continental crust, loose hatching: 'unusually elevated oceanic crust' (including Pirie and Bruce banks), SO: South Orkney Islands, SG: South Georgia, SR: Shag Rocks. Labels redrawn.

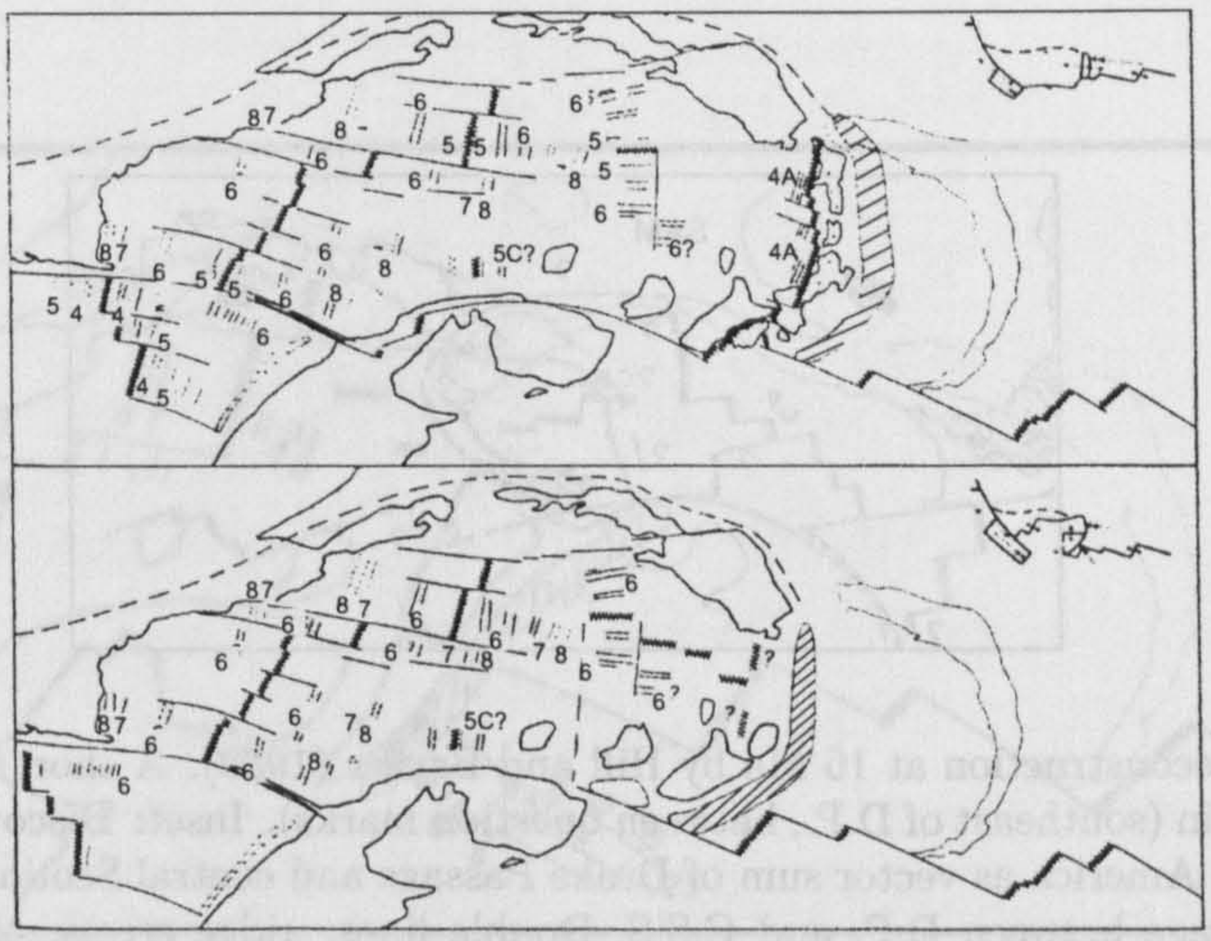

Figure 1.17: Reconstructions at 5 Ma (top) and 10 Ma (bottom) by Barker and Hill (1981) by visual fits of seafloor spreading data (numbers denote reversal chrons). Zigzag lines: ridge crests, plain lines: transform faults and fracture zones, enclosed hatched regions: trenches at subduction zones. Modern South Sandwich Trench is shown as faint enclosed contour on each. Insets: summary plate boundaries. Labels redrawn.

The 5 Ma, 10 Ma and 16 Ma (~C3, C5, C5c) reconstructions of Hill and Barker (1980) and Barker and Hill (1981) have their origins in the work of Hill (1978), and are concerned with exposition of the interpreted back-arc opening of the central Scotia Sea and its tortuous linkage with the west Scotia Sea and east Scotia Sea systems with which, the studies maintain, it is partially contemporaneous (Figures 1.17 and 1.18). The approach makes fits of seafloor spreading anomalies at the reconstruction times using pieces of paper cut from Mercator projections.

Barker *et al* (1984) provide a 20 Ma reconstruction (Figure 1.19) in the light of their ideas concerning the history of subduction in the northern Weddell Sea and the influence of ridge-crest–trench collisions on a back-arc basin with multiple spreading loci in the west, central and east Scotia Seas. Hamilton (1989) presents reconstructions of the proximal effects of these collisions, and concludes that there is little evidence to support the notion

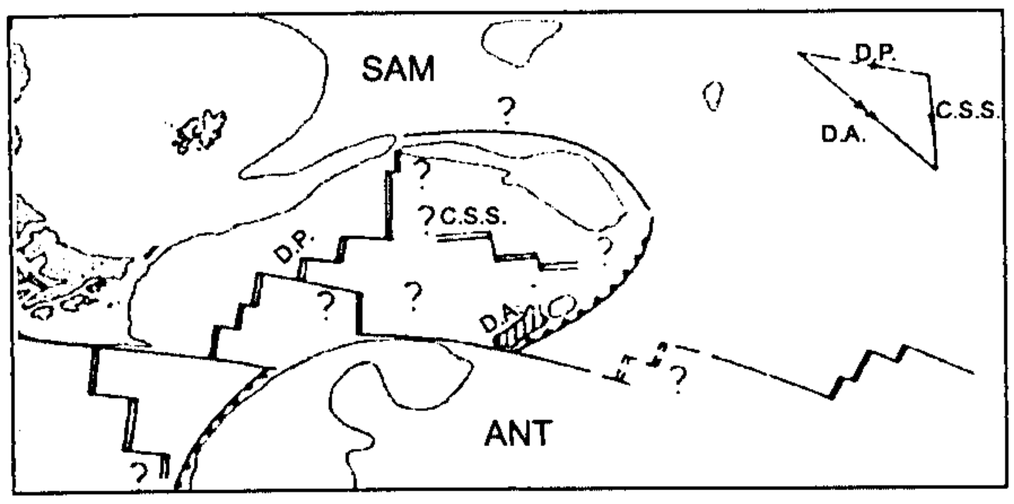

Figure 1.18: Reconstruction at 16 Ma by Hill and Barker (1980). A short ridge is shown active in Protector Basin (southeast of D.P., between question marks). Inset: Discovery Arc motion with respect to South America as vector sum of Drake Passage and central Scotia Sea spreading. Note problematic linkage between D.P. and C.S.S. Double lines: ridge crests, plain lines: transform faults, barbed lines: subduction zones (barbs on overriding plate). SAM: South American plate, ANT: Antarctic plate, D.P.: Drake Passage, C.S.S.: central Scotia Sea, D.A.: the Discovery Arc. Labels redrawn.

of ridge-crest–trench collisions having observable effects in the west and central Scotia Sea. The attempt to reconstruct at 30 Ma (Barker *et al*, 1991; Figure 1.20) by fitting the earliest reversal anomalies of the central and west Scotia Seas sets the scene just following the initial disruption of a cuspate connection as envisaged by Barker and Burrell (1977).

South Georgia is situated at the eastern end of a deep water corridor, whose opening is attributed to unspecified 'earlier events' for which no evidence is extant. The existence of a compact cusp is an explicit constraint on the 40 Ma reconstruction of King and Barker (1988) (Figure 1.21), which is presented again as the precursor to the 30 Ma reconstruction by Barker *et al* (1991). Both the 30 Ma and 40 Ma reconstructions feature apparently unconstrained rotations and unexplained changes in the shapes of crustal blocks. All these reconstructions are shown yet again, and the multi-local back-arc basin hypothesis is made explicit, by Barker (1995). A Middle Eocene ($\sim$ 45 Ma) reconstruction is presented by Toker *et al* (1991). Like the 40 Ma reconstruction of King and Barker (1988) it features subduction beneath Burdwood Bank which is wrapped tightly around South Georgia by some unexplained means.

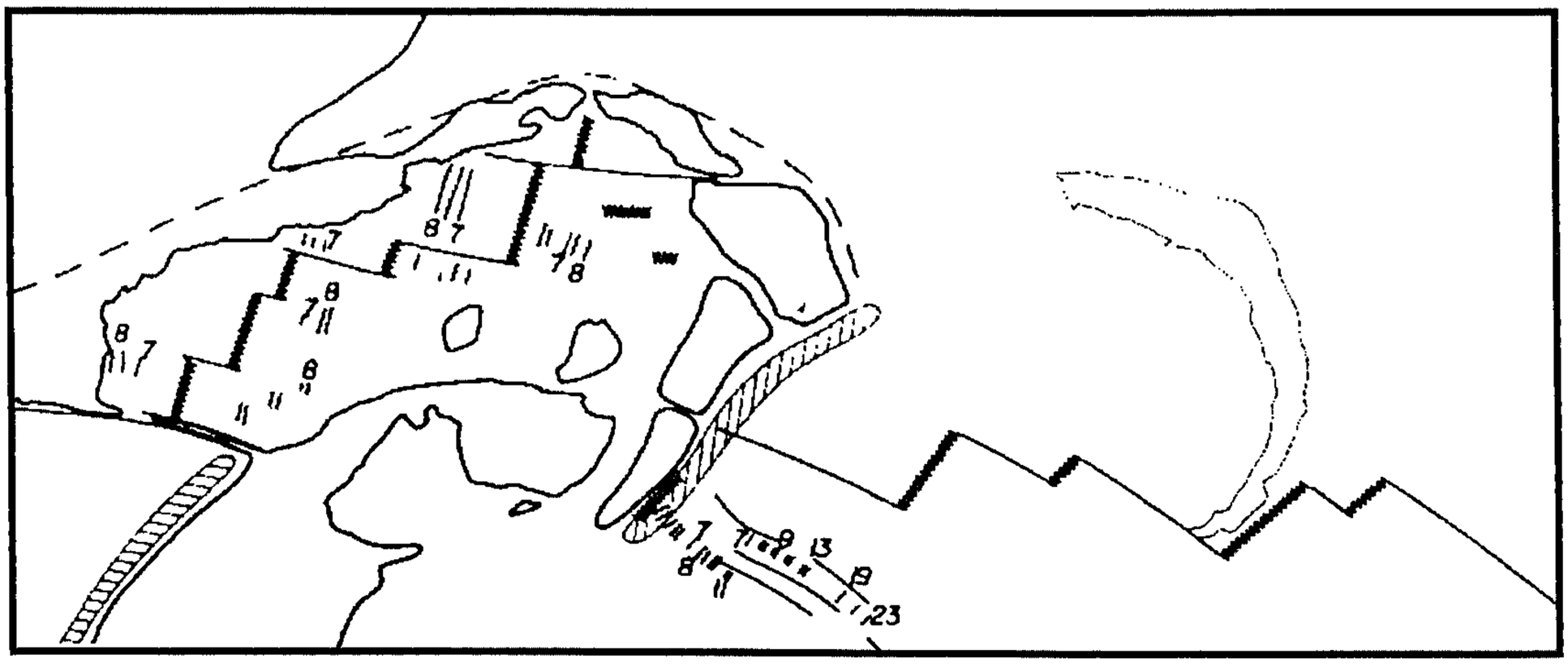

Figure 1.19: Reconstruction at 20 Ma by Barker *et al* (1984). Use has been made of seafloor spreading anomalies in the west and central parts of the Scotia Sea.

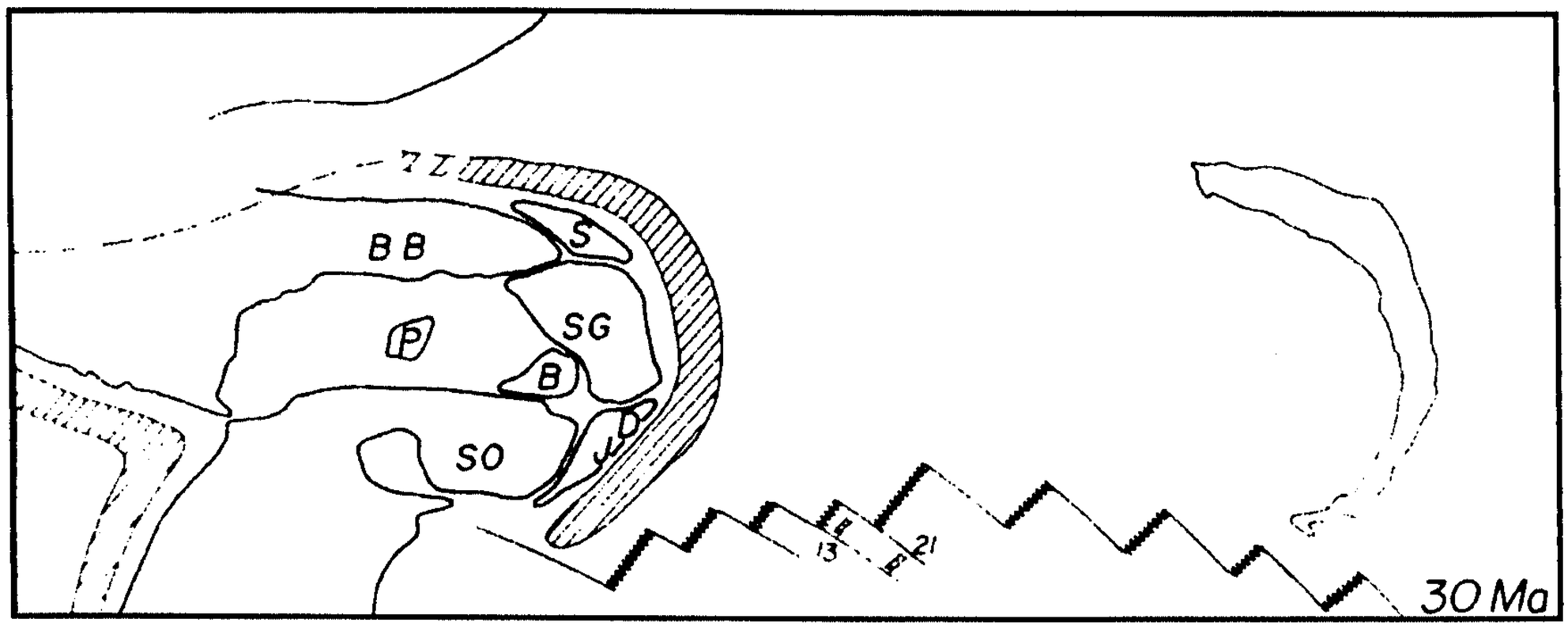

Figure 1.20: Reconstruction at 30 Ma by Barker *et al* (1991). Despite use of seafloor spreading data in central and west Scotia Seas there are unconstrained rotations and unexplained changes in the shapes of crustal blocks. BB: Burdwood Bank, S: Shag Rocks, SG: South Georgia, D: Discovery Bank, J: Jane Bank, B: Bruce Bank, P: Pirie Bank, SO: South Orkney microcontinent.

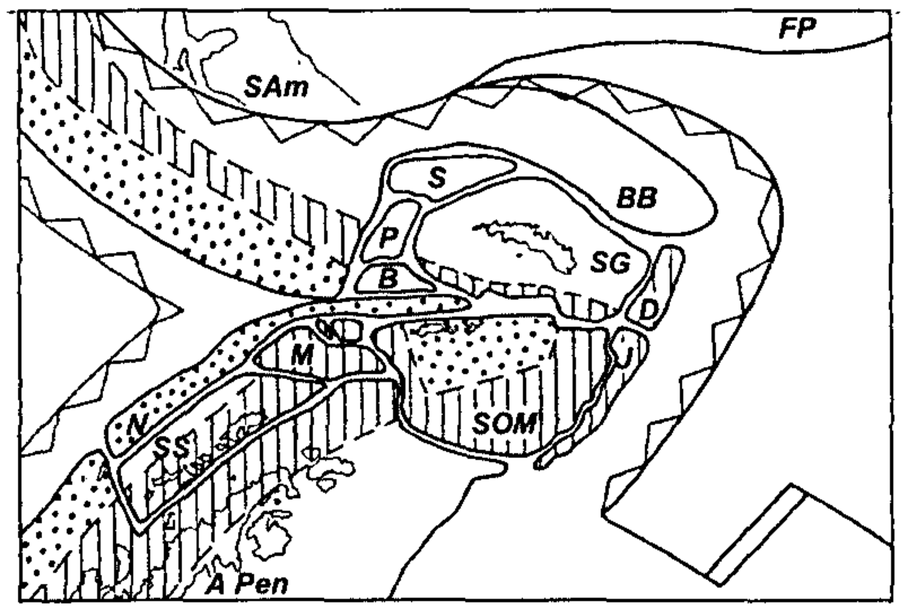

Figure 1.21: Reconstruction at closure (~ 40 Ma) by King and Barker (1988). Hatched areas: interpreted magmatic arcs, spots: fore-arc areas. Labels as Figure 1.20, except SOM: South Orkney Microcontinent, SAm: South America, APen: Antarctic Peninsula, FP: Falkland Plateau, N: northern part of South Scotia Ridge, M: southern part of South Scotia Ridge, SS: South Shetland Islands.

Dalziel (1983) reviews cuspate reconstructions and favours a modification with the Antarctic Peninsula rotated more than ninety degrees anticlockwise about a pole in the cusp. This produces an extension to the Patagonian batholith through the juxtaposed southern South Orkney Microcontinent and South Georgia block (Figure 1.22). Subsequent characterization of the Weddell Sea's spreading history is not consistent with the large rotation required of the Antarctic Peninsula. A similar rotation is evident in the reconstruction of De Wit (1977); Figure 1.23, whose novelty is the continuation of the Rocas Verdes Basin into the central Scotia Sea, its opening being responsible for the folding of a linear connection to a cuspate one. Its subsequent dispersal from within the cusp is a result of the action of the West Scotia Ridge.

The reconstruction of Garrett *et al* (1986) is an attempt to produce a continuous belt of magnetic anomalies through a closed Scotia Sea region (Figure 1.24). A straight anomaly is reconstructed through the South Scotia Ridge and South Orkney Microcontinent quite simply, as is another straight anomaly through Tierra del Fuego and southern South Georgia. The two are connected into a cuspate form at 65 Ma via a similar anomaly on Discovery Bank using a simple translation with no relative close-pole rotation between

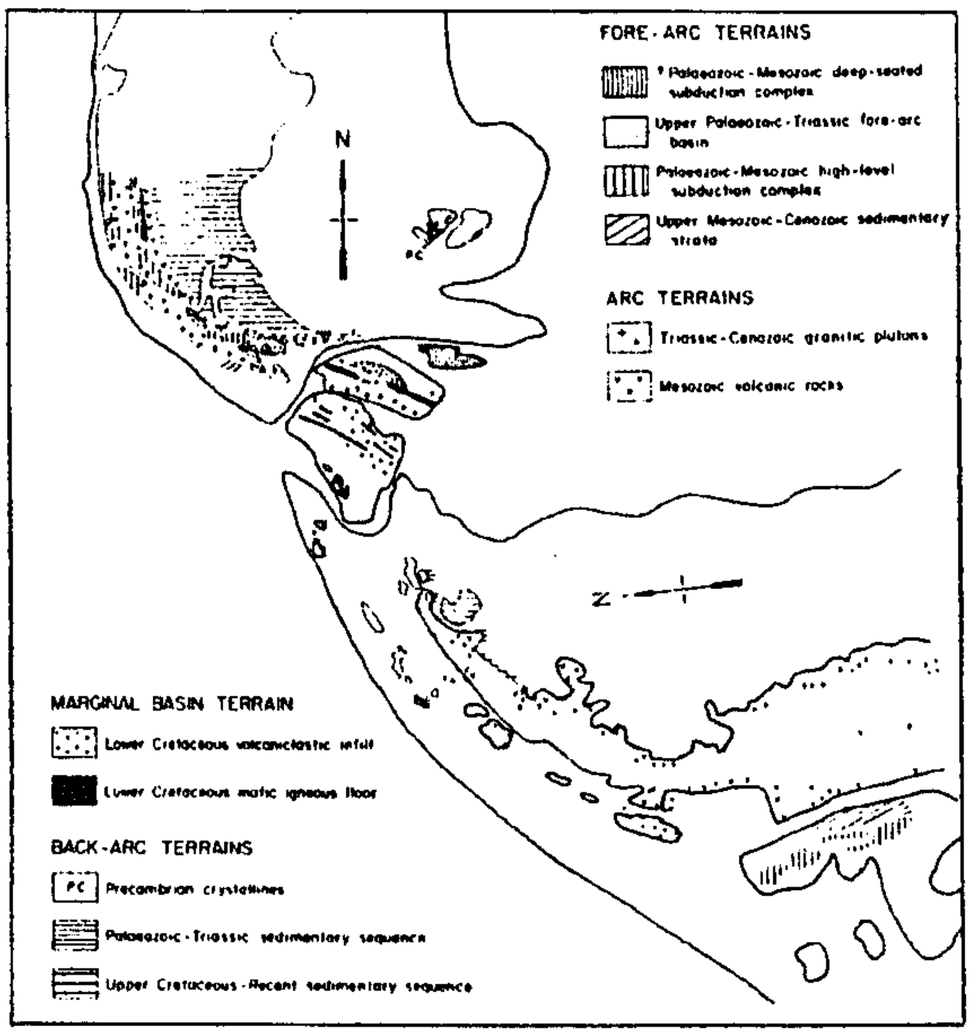

Figure 1.22: Reconstruction prior to Scotia Sea development, from Dalziel (1983), presented in response to perceived problems with cuspate reconstructions. It need not represent the Scotia Sea immediately prior to its formation.

the two linear anomalies. To progress from this situation to the C8 reconstruction of Barker and Burrell (1977) implies northeast directed convergence between the southern and northern limbs of the cusp in the period 65–30 Ma.

1.6 Gondwana tectonics

The history of dispersal of the constituents of the former supercontinent Gondwana, which now form the southern hemisphere continents, is important to the study of the Scotia Sea's evolution because it is within this context that the Scotia Sea grew. In particular, the Scotia Sea is set within the boundary between South America and Antarctica. The development of the Southern Ocean in the breakup of Gondwana is summarised by Lawver *et al* (1992), Figure 1.25. Initial separation of eastern and western Gondwana occurred at chron M22 (about 150 Ma) between the Mozambique Basin and Dronning-Maud Land

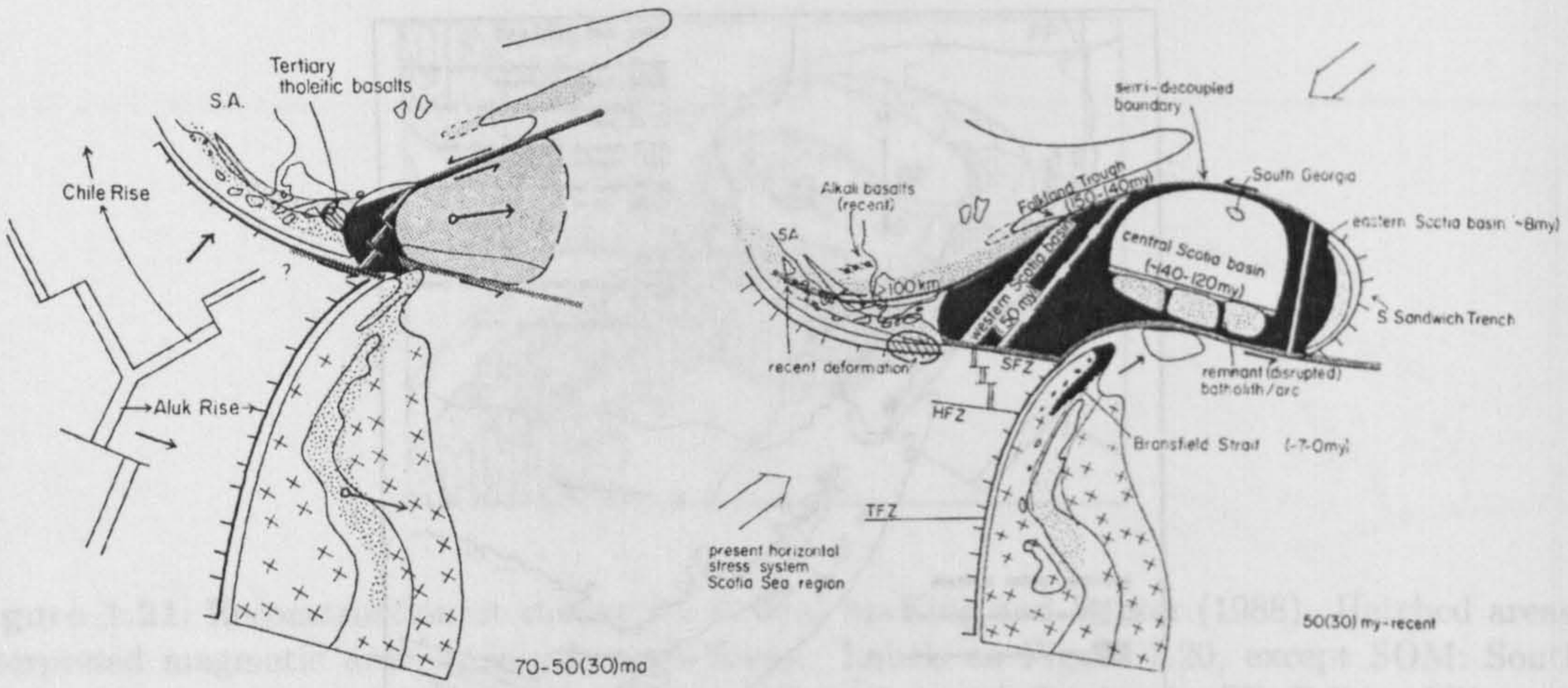

Figure 1.23: Reconstructions at 70–50 Ma (left) and post-50 Ma (right) by De Wit (1977). Central Scotia Sea is the wide eastern end of Rocas Verdes Basin, with remnant arc in south (Pirie and Bruce banks). Falkland Trough interpreted as a related, older, back-arc basin exposed on South Georgia. Double lines: ridges, lines with ticks: trenches (ticks on downgoing plate), dark shading: Cenozoic ocean crust, loose stipple: arc, close stipple: back-arc, SA: South America, SFZ: Shackleton Fracture Zone, HFZ: Hero Fracture Zone, TFZ: Tharp Fracture Zone.

(East Antarctica) (Bergh, 1977; Simpson *et al*, 1979). Further breakup, of West Gondwana, between South America and Africa began in the southern Atlantic Ocean before M12 (135 Ma). Mesozoic seafloor spreading anomalies are identified from the Falkland Plateau, Agulhas Basin, Argentine Basin, Natal Basin and Cape Basin (Larson and Ladd, 1973; Rabinowitz, 1976; du Plessis, 1977; Rabinowitz and LaBrecque, 1979; Martin *et al*, 1982). The South American–African system is well constrained by a long series of studies, to have been a relatively stable episode with only small changes in opening direction and rate giving rise to significant ridge jumps in the southern part of the ocean (Barker, 1979; for example). By the time of the opening of the Scotia Sea, however, spreading was a simple steady affair. Spreading between South America and Antarctica is much less well studied. Pioneer work on the present-day tectonics of the region (Forsyth, 1975; Lawver and Dick, 1983) confirmed the complex nature of the boundary within the Scotia Sea. East of the South Sandwich Trench, relative motion is divergent and the boundary is accretionary—the South American–Antarctic Ridge. Research by Barker and Jahn (1980)

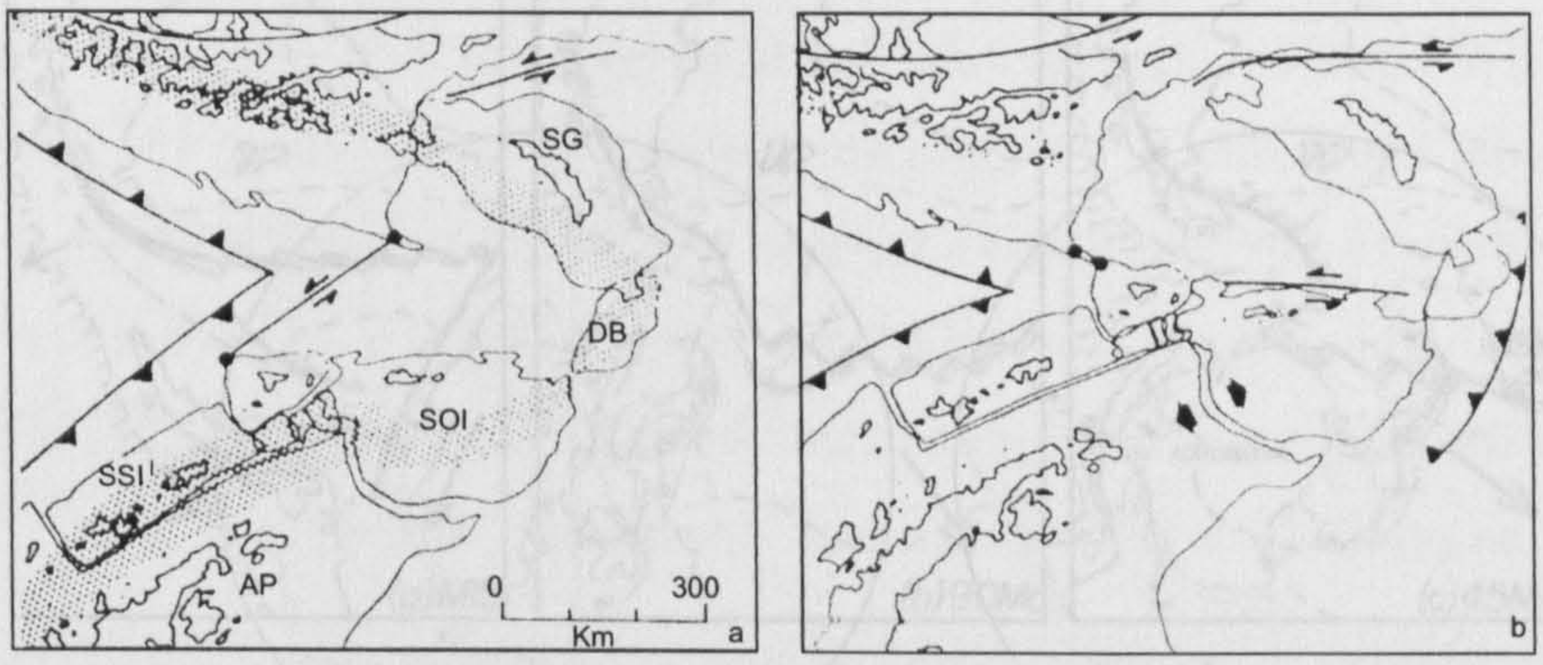

Figure 1.24: Reconstructions by Garrett *et al* (1986). b: at 30 Ma, after hypothesised regional convergence had disrupted continuous magnetic arc terrane (stipple) since 65 Ma: as shown in (a). AP: Antarctic Peninsula, SSI: South Shetland Islands, SOI: South Orkney Islands, DB: Discovery Bank, SG: South Georgia.

and LaBrecque and Barker (1981) concludes that the Weddell Sea probably formed by the action of this ridge, but that the ridge itself had been subducted along with much of the northern (South American) flank of the system at the South Sandwich Trench or its ancestors. Barker and Lawver (1988) combine data from the South American–Antarctic Ridge and Indian Ocean with a set of reconstruction poles for the South Atlantic (Cande *et al*, 1988) to produce reconstruction poles for the ridge back to C21 ($\sim$ 50 Ma). A change in the direction of spreading at C6 ($\sim$ 20 Ma) is hypothesised to have caused reorganisation of the ridge–transform geometry and the creation of two long-offset transforms—the Bullard and South Sandwich fracture zones. Later work by Livermore and Woollett (1993) and Livermore and Hunter (1996) using fracture zone traces in the Weddell Sea cemented the view that its most likely origin is seafloor spreading due to the relative motion of South America and East Antarctica. Livermore and Woollett (1993) show that the latter part of South American–Antarctic spreading in the Weddell Sea, including and during the period up to the development of the Scotia Sea, is a steady affair with no drastic changes in spreading direction or rate. Prior to this time, however, a series of changes in spreading direction give rise to a spectacular 'herring bone' pattern of flowlines in the

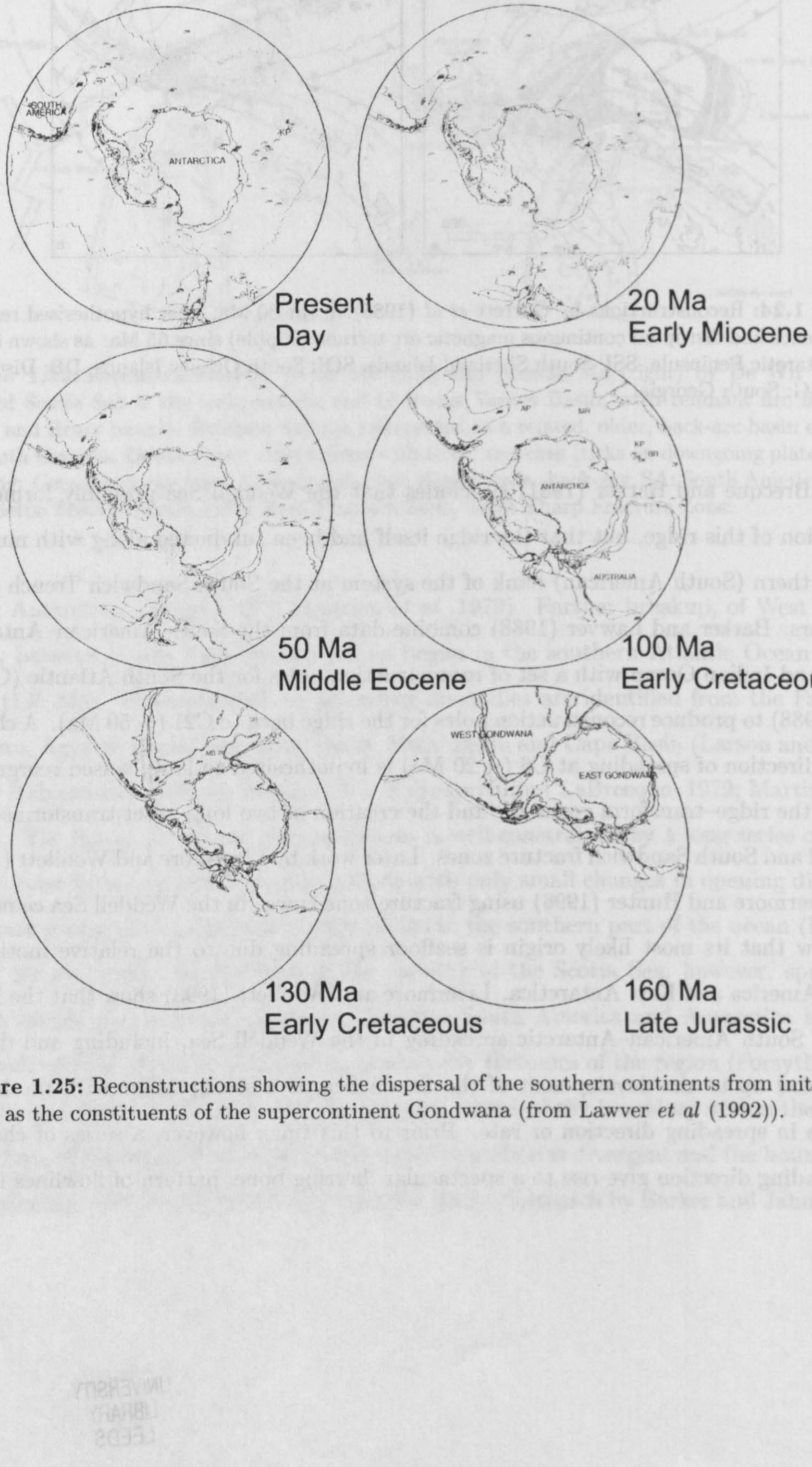

Figure 1.25: Reconstructions showing the dispersal of the southern continents from initial positions as the constituents of the supercontinent Gondwana (from Lawver *et al* (1992)).

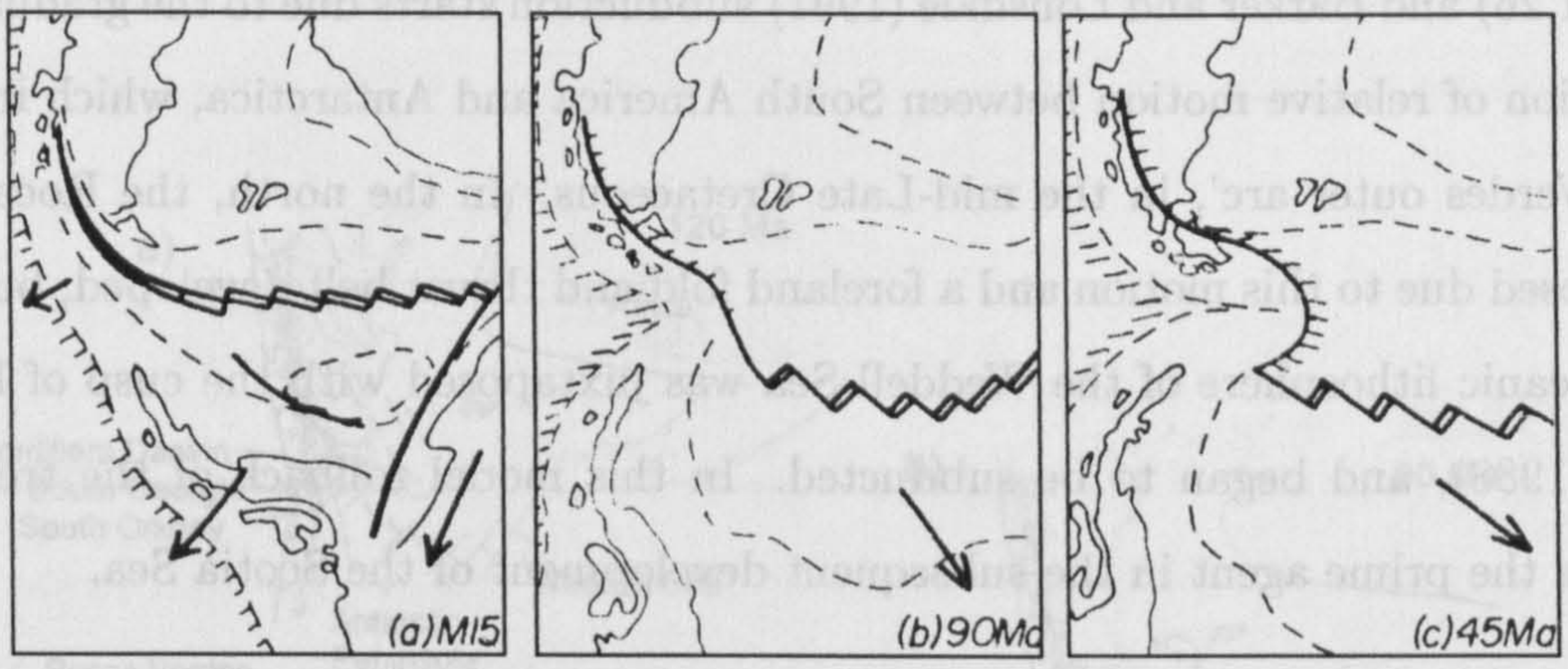

Figure 1.26: Cartoon by Barker *et al* (1991) showing how the changing direction of relative motion of Antarctic Peninsula with respect to South America (from M15 ($\sim$ 139.5 Ma) to 45 Ma) could result in subduction at an east facing trench. Mechanisms for inversion of the Rocas Verdes Basin and development of the Magallanes fold and thrust belt are corollaries. Lines with ticks: convergent margins (ticks on underthrusting plate), double lines: ridges, single lines: transform faults.

Mesozoic and early–middle Cenozoic Weddell Sea floor (Haxby, 1988; McAdoo and Marks, 1992; Livermore and Hunter, 1996). Dating of the break up preceding this is hampered by poor definition in the early magnetic reversal anomaly sequence in the southernmost Weddell Sea, and the lack of a definite conjugate margin. The anomaly identifications of Livermore and Hunter (1996) differ in their sequence from those of Barker and Jahn (1980); LaBrecque and Barker (1981) and LaBrecque *et al* (1989), but all suggest break up just before 165 Ma.

Work attempting to link the Weddell Sea and Scotia Sea histories using reconstructions usually assumes that Weddell Sea spreading was simply connected to the Rocas Verdes Basin, but escaped inversion that shortened it (Dott, Jr *et al*, 1982; Barker *et al*, 1991; Diraison *et al*, 2000). With the destruction of the Rocas Verdes Basin and most of one flank of the South American–Antarctic system, no evidence remains to test this type of hypothesis directly. Perhaps the biggest question remaining in studies of the Weddell Sea is the timing of the onset, and the extent of, subduction of the northern limb of the ancestral South American–Antarctic Ridge. In cartoons shown by Barker *et al* (1991)

(Figure 1.26) and Barker and Lonsdale (1991) subduction starts due to the gradual change in direction of relative motion between South America and Antarctica, which included a 'Rocas Verdes outer arc', in the mid-Late Cretaceous. In the north, the Rocas Verdes Basin closed due to this motion and a foreland fold and thrust belt developed, but further south oceanic lithosphere of the Weddell Sea was juxtaposed with the cusp of King and Barker (1988), and began to be subducted. In this model rollback of the trench thus formed is the prime agent in the subsequent development of the Scotia Sea.

The cartoons of Diraison *et al* (2000) (Figure 1.27) show a similar initial story for the Weddell Sea–Rocas Verdes Basin, but subduction of the Mesozoic Weddell Sea crust is not shown at all. Instead the South Sandwich Trench appears between 50 Ma and 30 Ma, presumably as a response to the opening of the west Scotia Sea, although this is not made explicit.

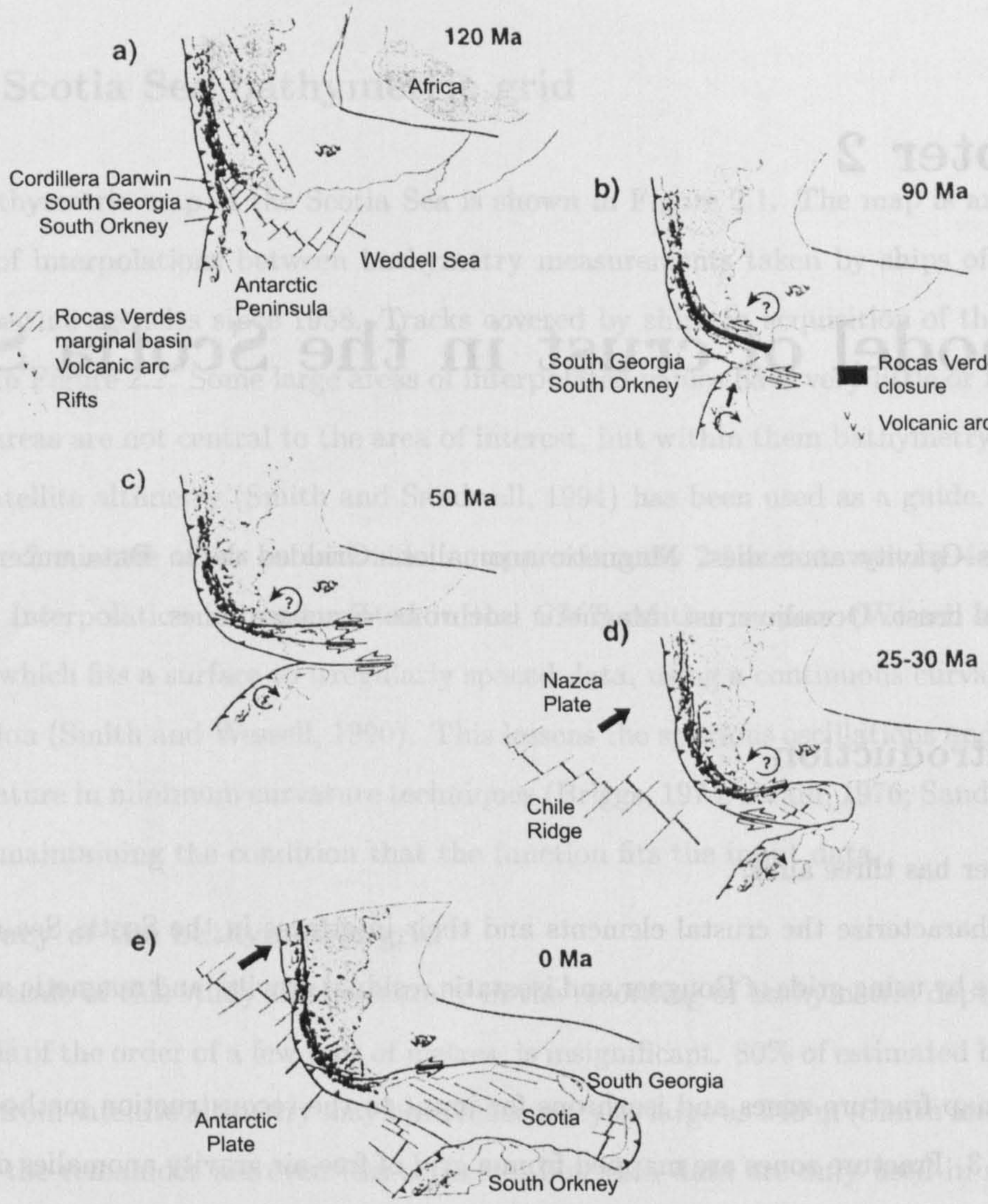

Figure 1.27: Reconstructions by Diraison *et al* (2000) to show the development of the Scotia Sea region since the mid Mesozoic. Note continuity between the Rocas Verdes Basin and Weddell Sea. Development of the South Sandwich Trench occurs only at 25–30 Ma when the west Scotia Sea opens. Circular arrows: oroclinal bending, barbed lines: subduction zones (barbs on overriding plate), thick single lines: spreading centres, thin single lines: transform faults (sense of motion shown by half-arrows) and fracture zones. Labels redrawn.

Chapter 2

A model of crust in the Scotia Sea

Keywords Gravity anomalies. Magnetic anomalies. Gridded data. Data uncertainty. Continental crust. Oceanic crust. Magnetic isochrons. Fracture zones.

2.1 Introduction

This chapter has three aims:

1) To characterize the crustal elements and their interfaces in the Scotia Sea region. This is done by using grids of Bouguer and isostatic residual gravity, and magnetic anomalies.

2) To map fracture zones and isochrons for input to the reconstruction method used in Chapter 3. Fracture zones are mapped from a grid of free-air gravity anomalies derived from satellite altimetry (Smith and Sandwell, 1995). A map of magnetic reversal isochrons is made using magnetic anomaly profiles and a grid of modelled seafloor magnetization.

3) To identify evidence for past plate tectonic regimes on the continental parts of the Scotia Sea. The geology of continental crust, which is buoyant and long-lived, is complicated by its involvement in multiple plate tectonic regimes which may leave evidence as magnetic batholiths, dyke swarms, sedimentary basins, or major faults, for instance.

Grids of bathymetry, free-air, Bouguer and isostatic residual gravity anomalies and reduced to the pole total field anomalies are used to infer the presence of such features.

2.2 Scotia Sea bathymetric grid

The bathymetric map of the Scotia Sea is shown in Figure 2.1. The map is an image of a grid of interpolations between bathymetry measurements taken by ships of BAS and other marine agencies since 1958. Tracks covered by ships in acquisition of the data are shown in Figure 2.2. Some large areas of interpolated values have very little or no control. These areas are not central to the area of interest, but within them bathymetry predicted from satellite altimetry (Smith and Sandwell, 1994) has been used as a guide. Grid cells measure 2 minutes of arc on each side, or approximately 2 km east–west by 4 km north–south. Interpolation is implemented in the *GMT* routine *surface* (Wessell and Smith, 1991), which fits a surface to irregularly spaced data, using a continuous curvature spline in tension (Smith and Wessell, 1990). This lessens the spurious oscillations and inflexions that feature in minimum curvature techniques (Briggs, 1974; Swain, 1976; Sandwell, 1987) whilst maintaining the condition that the function fits the input data.

Accuracy of the bathymetric grid

At the scale of this study the inaccuracy in the recording of bathymetric depth by ships, which is of the order of a few tens of metres, is insignificant. 80% of estimated bathymetry values from satellite altimetry may have inaccuracy as large as 240 m (Smith and Sandwell, 1994), the remainder are even less accurate, but such data are only used in non-critical areas. Elsewhere the most serious problem is navigational uncertainty which can occur at kilometres-scale. Navigational uncertainty contributes to cross-over errors which must be corrected for (Johnson, 1971; Smith, 1993). The largest cross-over errors ($\sim$ 200–500 m) are due to problems in data reduction and digitising (Smith, 1993). By 1993, inter-cruise cross-over errors in the Scotia Sea had median values of 0–25 m, and 100 m or more in the Weddell Sea and eastern Falkland Plateau (figure 10 of Smith (1993)). These

Era	Likely Navigation	Uncertainty at ~ 50°S			Length in Figure 2.2
		km	°latitude	°longitude	
pre-1975	Celestial	15	~ 0.13	~ 0.26	~ 176000 km
1972–78 (BAS)	Transit satellite	10(4?)	~ 0.04	~ 0.08	~ 175000 km
1975–1980	Transit satellite	10	~ 0.09	~ 0.18	~ 96000 km
1980–85	Transit & partial GPS	5	~ 0.04	~ 0.08	~ 46500 km
post-1985	Full GPS	2.5	~ 0.02	~ 0.04	~ 203000 km

Table 2.1: Likely navigational uncertainties for marine bathymetric data acquisition in the Scotia Sea, by era. No data are duplicated between the pre-1975 and 1975–80 eras and the 1972-78 (BAS) era.

values are consistent with navigational uncertainty being the main cause of uncertainty in bathymetric data. With later satellite-fixed and swath bathymetry data (Livermore *et al*, 1997; Cunningham *et al*, 1998; Livermore *et al*, 2000; for example) these median values are likely to have lessened.

A general value for uncertainty in bathymetric grid data

BAS marine operations in the Scotia Sea in the era 1972–1978 used Transit satellite navigation, for which Hill and Barker (1980) contend navigational uncertainty of 4 km. Implicit in the discussion of Kirkwood *et al* (1999) is that this figure might be put more conservatively at 10 km. Navigational uncertainty for bathymetric data acquisition is summarised in Table 2.1.

Figure 2.2 shows the distribution of likely navigational uncertainty in data contributing to the grid. Most of the Scotia Sea is well served by satellite fixed data whereas the peripheries of the region tend to have seen infrequent visits by poorly fixed passage. Average navigational uncertainty per line-kilometre of data (modern cruises typically use more frequent sampling rates than older cruises) is 7.2 km admitting values from Hill and Barker (1980), or 8.7 km assuming the estimations of Kirkwood *et al* (1999) to apply to BAS data in the 1972–78 period. No weighting is imposed to favour newer data in

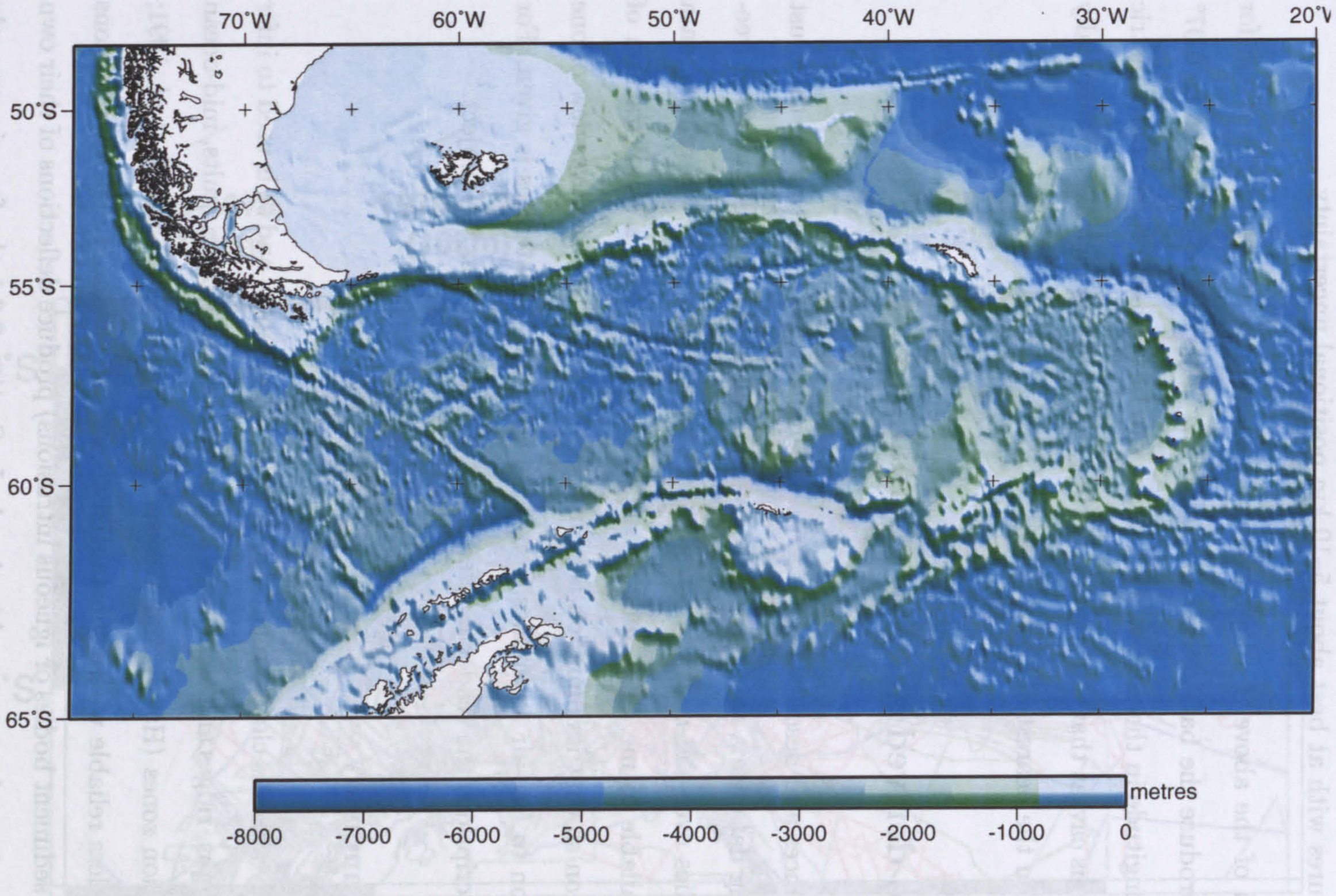

Figure 2.1: Mercator projection of the bathymetric grid from ship-track and selected satellite data, produced by Peter Morris of BAS. Ship tracks used are shown in Figure 2.2. Artificial illumination is from the northeast. A larger version of this figure can be found inside the back cover of the thesis.

interpolation. The bathymetry derived from satellite altimetry of Smith and Sandwell (1994) locates features with at best about 5–10 km positional uncertainty.

Considering all of the above, I adopt average navigational uncertainty of 8 km for the data used to produce the bathymetry in Figure 2.2. This can be expressed as 0.07° latitude or 0.14° longitude in the region. This figure can be extended to the bathymetric grid, with the obvious caveat that uncertainty in the gridded values increases dramatically with separation from the nearest ship track.

2.3 Satellite derived gravity anomalies

This section introduces and describes the gravity anomalies used in setting up the crust model. The starting data are a subset of a widely-available grid of satellite-derived free-air gravity anomalies over the marine parts of the Scotia Sea region. No gravity data over land were available to me. The missing area over land is only a small fraction of the Scotia Sea region so that its omission is of little importance. A brief overview of one method of reduction to free-air anomalies from data collected by satellites is given. For more complete descriptions the reader is referred to the literature on the subject.

2.3.1 Free-air anomaly

The free-air anomaly at sea is closely related to seafloor topography, and so is used to infer the presence of troughs, ridges and trenches at fracture zones, transform faults, mid-ocean ridges and subduction zones (Haxby and Weissel, 1986; Shaw, 1987; Marks *et al*, 1991; for example). It is less reliable where substantial geologically-induced density variations (for example thick sediment bodies or igneous intrusions) produce deflections of their own which are superposed on the topographic signal. In Section 2.6.1 the free-air anomaly grid in the Scotia Sea region is presented and used to inform the crust model.

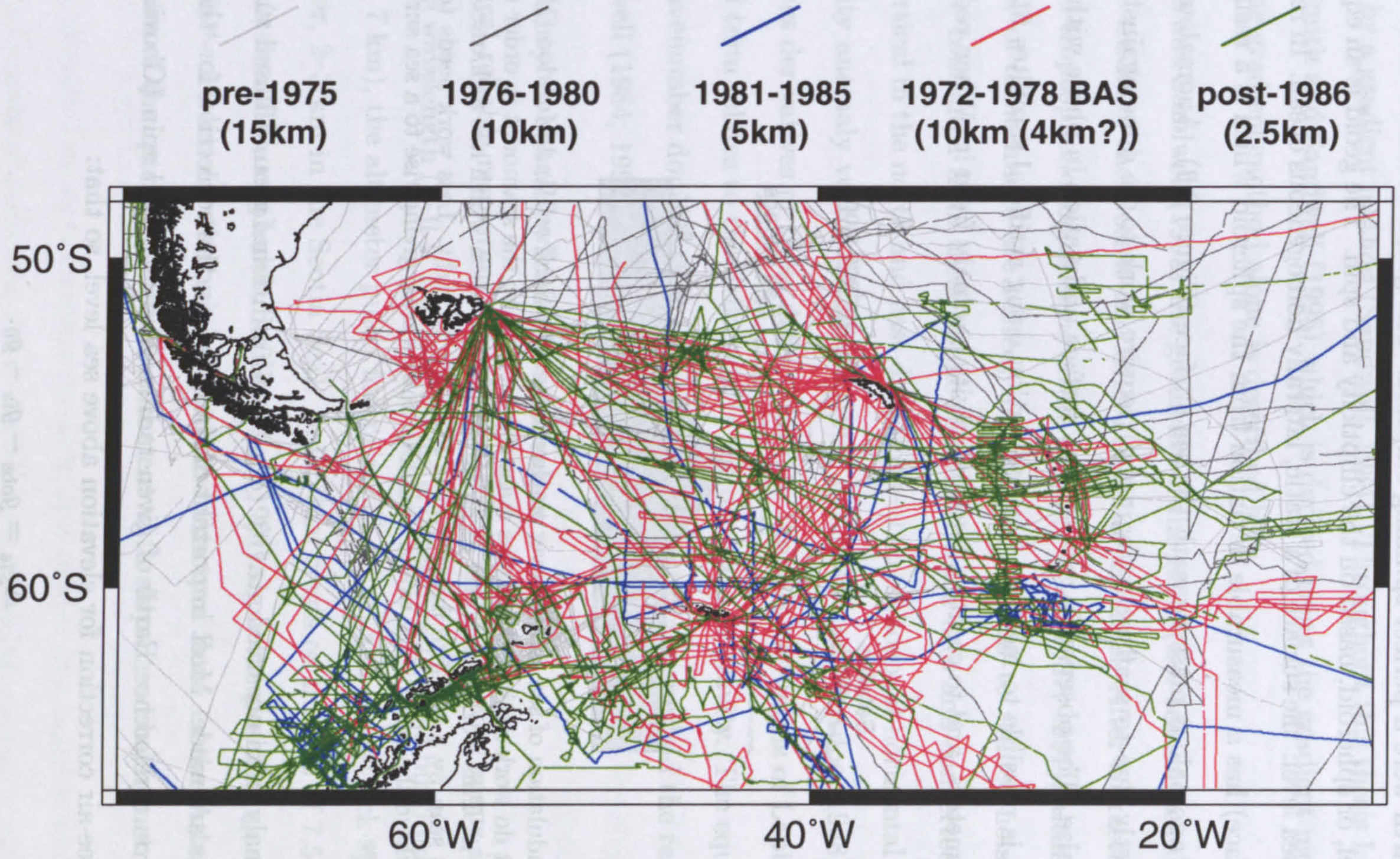

Figure 2.2: Mercator projection of ship tracks used to construct the bathymetric grid in Figure 2.1. The distribution of data by era is shown by the different colours of ship tracks. Key shows the eras and, in brackets, corresponding navigational uncertainties for different groups of the data as discussed in Table 2.1.

Free-air anomalies from satellite altimetry

Assume the Earth were a perfect spinning ellipsoid. The geoid would be described by a reference model, or spheroid, based on the ellipticity and spin. The geoid is an equipotential surface at sea level: the surface of a static, laterally homogeneous ocean. In reality the geoid (sea surface) has a measurable deviation from the spheroid which is a result of the distribution of anomalous mass beneath the sea surface (Figure 2.3). Anomalous masses (which are mostly due to seafloor topography) require work to be done against the potentials they raise. The observable result is sea surface undulation in phase with seafloor topography. It is possible to measure the undulation using artificial satellites fitted with microwave altimeters, and to create a free-air gravity anomaly from it. When reducing to

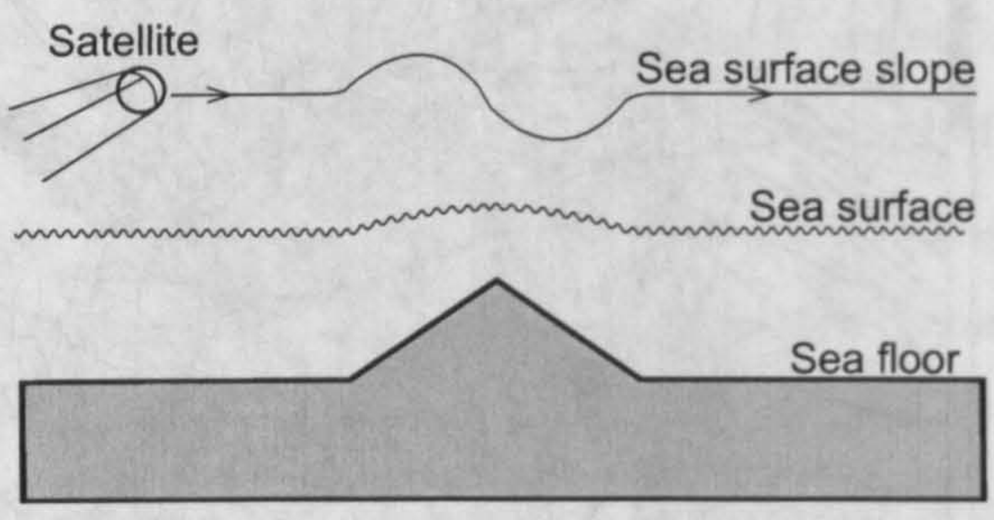

Figure 2.3: Undulation of sea surface over a seamount, after Sandwell and McAdoo (1988). The sea surface must do work against the excess mass represented by the seamount in order to assume a potential over it. This work is manifest as an upwards undulation which has a characteristic sea surface slope as seen by a satellite flying over it from left to right. Less work needs to be done over a trench, where the sea surface would undulate downwards, giving rise to a sea surface slope of opposite phase.

a free-air anomaly from observed gravity (g_{obs}) in a traditional ground-based survey several corrections are made. Most important of these are g_0; the correction for 'theoretical' gravity based on a reference Earth of given radius, ellipticity and spin (Chovitz, 1981), and g_{fa}; the free-air correction for elevation above sea level, so that:

$$\Delta g_{\text{fa}} = g_{\text{obs}} - g_{\text{fa}} - g_0. \tag{2.1}$$

The altimeter approach is a direct inversion for the free-air anomaly however, so that g_{fa} and g_0 are implicitly accounted for.

There are two approaches to reducing the raw altimeter data to a gravity anomaly: by direct conversion from geoid height (Rapp, 1983; Haxby *et al*, 1983; Fairhead *et al*, 1998) or by a gradient method (Sandwell, 1984). Throughout this thesis I use the free-air grid of Smith and Sandwell (1995) which is derived using the gradient method. For this reason the gradient method alone is described here.

Smith and Sandwell (1995) use gradients of the geoid (*i.e.* sea surface slope) measured along the tracks of the Geosat and ERS-1 satellite missions. After corrections for orbital, tidal, and tropospheric-ionospheric errors (Cheney *et al*, 1987; 1991), altimeter data from a number of orbit tracks are edited, binned, and stacked to reduce noise. Sea surface slopes are computed from these spline-smoothed track arcs and converted to deflections of the vertical in the north and east directions—two orthogonal horizontal components of the gravity anomaly vector (Sandwell, 1984; Sandwell and McAdoo, 1988). The method substitutes derivatives of these deflections into the first two terms of Laplace's equation; the third term relates to the deflection in the direction of gravity. The equation is solved in the wavenumber domain. For a rigorous treatment of the method the reader is referred to Sandwell (1984; 1992).

Uncertainty in satellite free-air anomalies

The typical reliable resolution offered by satellite free-air gravity maps is about 15 km minimum wavelength ($\sim 0.1°$ latitude). This is determined by the bin duration (1 second, or about 7 km), the altimeter pulse 'footprint' (2–9 km) and cross-track spacing (3–5 km at equator, 2–3 km in the Scotia Sea). Individual crests or troughs of 7.5 km dimension across axis should be resolvable. Müller *et al* (1991) show the positioning error of satellite passage is $\sim \pm 5$ km for the axis of the Kane Fracture Zone in the Atlantic Ocean, by comparison of the satellite geoid measurement with ship-based bathymetry.

2.3.2 Bouguer anomaly

The Bouguer anomaly is most strongly influenced by the varying thickness and density of the crust, the variable mass due to which is compensated for by mass variations at depth: a phenomenon known as isostasy. It is positive over oceanic crust due to its greater density compared to continental crust, and more importantly to the high density antiroot which isostatically compensates for the negative topography. The thick, anomalously low density root beneath continental crust, which compensates its greater elevation and lower density, gives rise to negative Bouguer anomalies. The Bouguer anomaly, then, can be useful to identify and delineate differing areas of isostatic compensation, which, at first order, correspond to regions of continental and oceanic crust. For the Scotia Sea this is done in Section 2.6.2.

Reduction to a Bouguer anomaly

To determine the Bouguer anomaly the gravity effects of topography and bathymetry are removed from the free air anomaly. The Bouguer anomaly is nearly always the objective of land based gravity surveys, but is less often wanted for surveys exclusively in oceanic crust, within which density contrasts are subtle. Reducing a free-air anomaly (Δg_{fa}) to a Bouguer anomaly (Δg_{boug}) requires two corrections. The first is for the column of anomalous material (air or water) between the reference plane (usually sea level) and the land surface or seafloor; this is called the slab correction, or water-depth correction, g_{slab}. The second correction is for the gravity effect of the relief of the surface surrounding the observation; the terrain correction g_{terr}, so that

$$\Delta g_{\text{boug}} = \Delta g_{\text{fa}} - g_{\text{slab}} - g_{\text{terr}}. \tag{2.2}$$

Slab correction

The slab correction (g_{slab} and Figure 2.4) is the gravity effect of an infinitely extensive flat slab of uniform density difference ρ and thickness h (elevation between the reference plane and the seafloor or land surface):

$$g_{\text{slab}} = 2\pi \mathsf{G} \rho h, \tag{2.3}$$

where G is the universal gravitational constant. For this work I use two slab corrections:

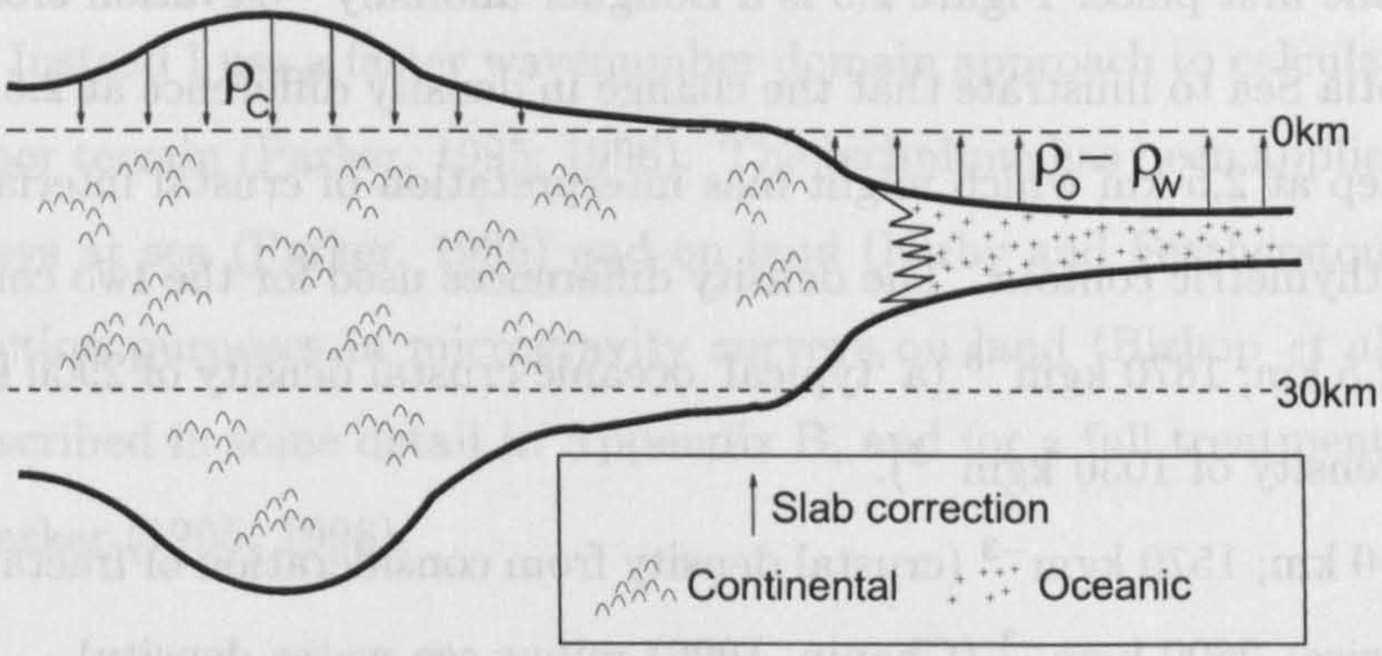

Figure 2.4: Slab correction for reduction to a Bouguer anomaly. Slab thickness at each observation point over the ocean equals the water depth, over land it equals topographic height. Slab has infinite horizontal extent and density defined as density difference between crustal rocks (ρ_c continental, ρ_o oceanic) and sea water (ρ_w), or air. The sign changes for corrections above and below the 0 km reference plane. No Bouguer anomaly over land areas has been calculated in this thesis.

one each for bathymetry deeper and shallower than 2.5 km. The intention is to use suitable density differences for regions which approximate continental and oceanic crust. The 2.5 km criterion envelopes most oceanic crust because it is the global average depth of the youngest oceanic crust. Oceanic crust subsides with time (Trehu, 1975; Parsons and Sclater, 1977), so it is unlikely that large areas of normal oceanic crust lie shallower than 2.5 km. In the Scotia Sea this assumption is consistent with the following: (i) the majority of spreading centres are extinct and subsided; (ii) the active East Scotia Ridge crest at 3–4 km is anomalously deep; (iii) no oceanic large igneous provinces are positively identified in the Scotia Sea (Coffin and Eldholm, 1992). A result of this is that any areas of extended, subsided continental crust below 2.5 km are given a correction several times larger than continental crust shallower than 2.5 km. The effect of this is less dramatic than at first seems since extended continental crust is likely to be denser than unextended continental crust due to intrusion and underplating of mafic igneous rocks during stretching (Cox, 1980; McKenzie, 1984; White and McKenzie, 1989; Brodie and White, 1994).

The effect of varying the slab correction is much less than that of applying a slab correction in the first place. Figure 2.5 is a Bouguer anomaly—elevation cross plot of the northwest Scotia Sea to illustrate that the change in density difference at 2.5 km does not introduce a step at 2.5 km which might bias interpretation of crustal interfaces to follow the 2.5 km bathymetric contour. The density differences used for the two corrections are:

1. Below 2.5 km; 1870 kgm^{-3} (a 'typical' oceanic crustal density of 2900 kgm^{-3} minus ocean water density of 1030 kgm^{-3}).

2. 2.5 km–0 km; 1570 kgm^{-3} (crustal density from consideration of fractal topography in South America: 2600 kgm^{-3} (Chapin, 1996) minus sea water density).

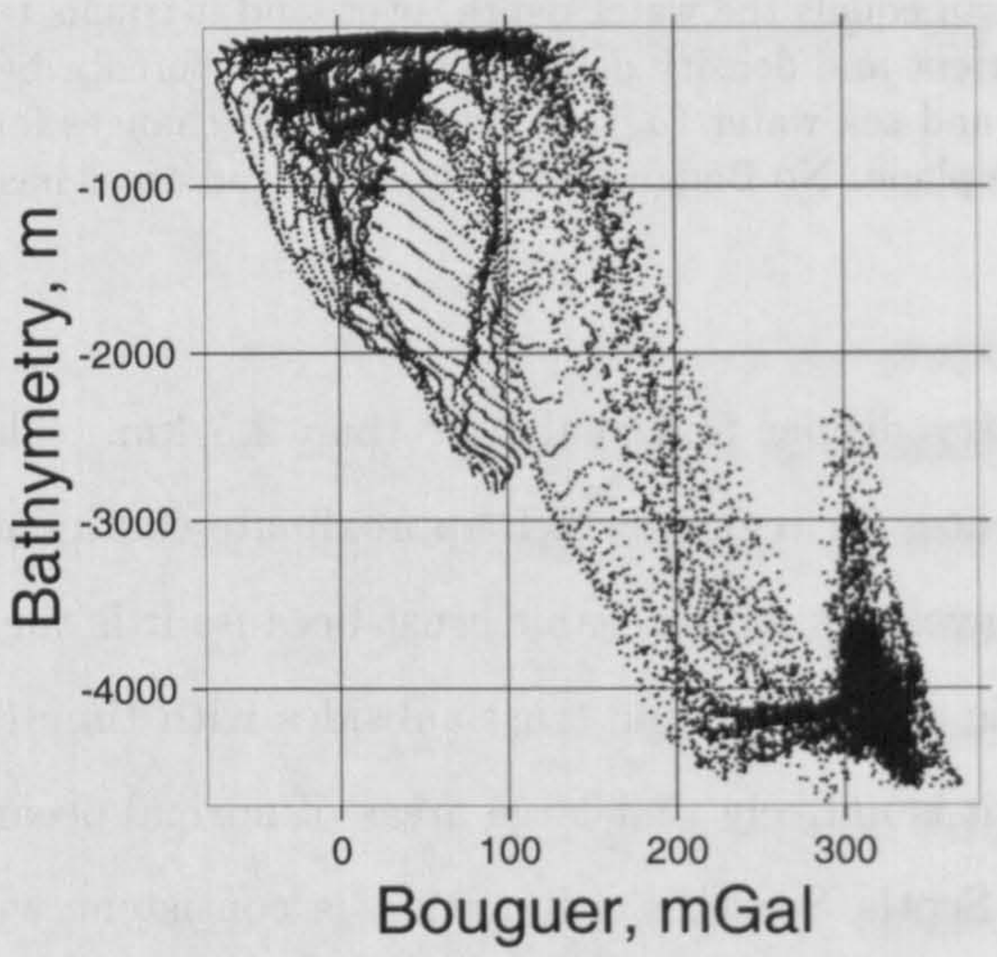

Figure 2.5: Bouguer–elevation cross plot for the northwest Scotia Sea and Scotia Arc. Note the strong correlation of Bouguer gravity with bathymetry. The use of different slab corrections for water depths greater than and less than 2500m does not introduce an artefact in the Bouguer anomaly along the position of the 2500m submarine contour which, if it existed, might bias interpretation of the continent–ocean boundary. The individual trends in the plot have probably carried through from the ship tracks used to make the bathymetric grid.

Terrain correction

The terrain correction is of smaller size than the slab correction, and is of most importance in areas of large topographic gradients. The terrain correction process I use is different

to the traditional approach (Plouff, 1977; Spielman and Ponce, 1984; for example), which involves laborious calculations of the gravity effect of volumes concentric about the observation point. Instead I use a faster wavenumber domain approach to calculate the gravity effect of seafloor terrain (Parker, 1995; 1996). The technique has been applied successfully to large surveys at sea (Parker, 1996) and on land (Kirby and Featherstone, 1999), and for void detection purposes in microgravity surveys on land (Bishop *et al*, 1997). The method is described in some detail in Appendix B, and for a full treatment the reader is referred to Parker (1995; 1996).

2.3.3 Isostatic residual anomaly

A further gravity correction, the isostatic correction (g_{iso} and Figure 2.6), aims to remove the long wavelength components of observed gravity due to deep masses compensating topographic loads. The result is the isostatic residual anomaly (Δg_{iso}):

$$\Delta g_{\text{iso}} = \Delta g_{\text{boug}} - g_{\text{iso}}. \tag{2.4}$$

Because gravity anomalies due to compensating masses in the mantle are removed, the isostatic residual anomaly gives information regarding the distribution of anomalous mass above an adopted compensation depth: *i.e.* within the crust or lithosphere. In fact some mantle anomalies probably remain as the mantle is likely to contain inhomogeneities unrelated to its role in compensation (McKenzie *et al*, 1980; Bowin, 1983; Hartley *et al*, 1996; for example). However these should have long wavelength, given the source depth. With this reasoning shorter wavelengths in the isostatic residual anomaly can be attributed mainly to upper crustal density sources.

Isostatic correction

A model is needed to predict the shape of compensating masses, given the distribution of the topographic loads. Models may consider pure Airy-type isostasy (the compensating blocks are vertical-sided and the crust has no strength between them) or a crust of finite strength governed by an effective elastic thickness. In places models can be informed by

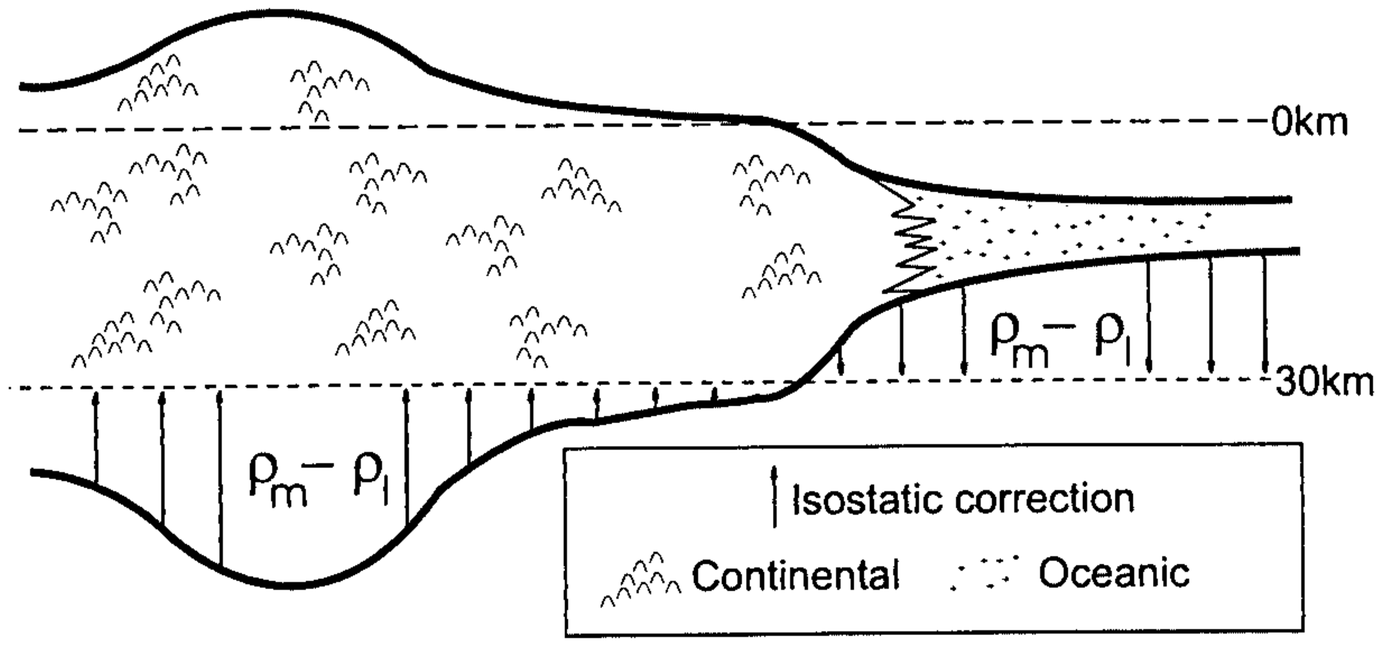

Figure 2.6: The isostatic correction is similar to the slab correction, but of opposite sign. It is shown here before upward continuation to the 0 km reference plane. The thickness of the slab representing the compensating mass at the observation point is calculated using assumed Airy-type isostatic compensation of the topographic load, with respect to a reference depth of 30 km, assumed to represent the thickness of crust at sea level. The density of the slab is the density difference between rocks of the mantle (ρ_m) and of the lower crust (ρ_l). Note the sign of the isostatic correction changes for the compensation surface above and below the 30 km reference depth.

seismic experiments. All models provide very similar isostatic corrections given the depth and equality of compensating mass in each (Simpson *et al*, 1986).

I assume simple Airy-type isostasy, balancing crustal masses about a 30 km compensation depth for crust at sea level, to predict the topography of the crust-mantle boundary. A density contrast of 430 kgm^{-3} at the boundary is used. The gravity effect of compensating masses is calculated using an implementation of the method of Parker (1973) in the *GMT* routine *grdfft*. This is a method of calculating the anomaly due to a distribution of density (or magnetization) on a flat surface by use of the Fast Fourier Transform. Upward continuation of the anomaly by 30 km, also with *grdfft*, gives the correction at sea level to remove from the Bouguer anomaly.

2.4 Magnetic anomalies and some transforms

This section introduces and describes the total field anomaly, its transformation by reduction to the pole, and inversion for oceanic crustal magnetization. A brief description of how magnetic anomalies are defined and measured is given, but for textbook treatments the reader is referred to Dobrin and Savit (1988); Fowler (1990) and Blakely (1995).

2.4.1 Total field anomaly

The compilation of total field anomalies recorded by ships in the Scotia Sea region is shown in Figure 2.7. The illuminated function is produced by the same continuous curvature spline technique as was the bathymetric grid described in Section 2.2. The grid cell size is also the same. The ship track data interpolated for the surface are shown in Figure 2.8, which also shows their likely navigational uncertainty. No weighting has been applied to account for the varying vintages of data used.

The total field anomaly

The total field anomaly, ΔT, is a residual magnetic field intensity after removal of the theoretical magnetic field intensity, F, and the time-variant part of the ambient field, F_{TV}, from the observed total magnetic intensity, T_{obs}:

$$\Delta T = T_{\mathrm{obs}} - F - F_{\mathrm{TV}}. \tag{2.5}$$

The theoretical value F comes from a mathematical model (Langel, 1992; for example) which describes the magnitude of the geomagnetic field at the Earth's surface. The geomagnetic field originates in Earth's liquid iron outer core, and is probably due to its convection possessing a self-exciting dynamo-like property (Elsasser, 1956a;b; Carrigan and Gubbins, 1979). F_{TV} has its sources in interactions of atmosphere with ionosphere, and of the sun and moon with the ionosphere. It varies on many time scales.

Most of the remainder of the recorded field (about 1%) has its source in the crust above the intersection of the geotherm with the Curie temperatures of the common crustal

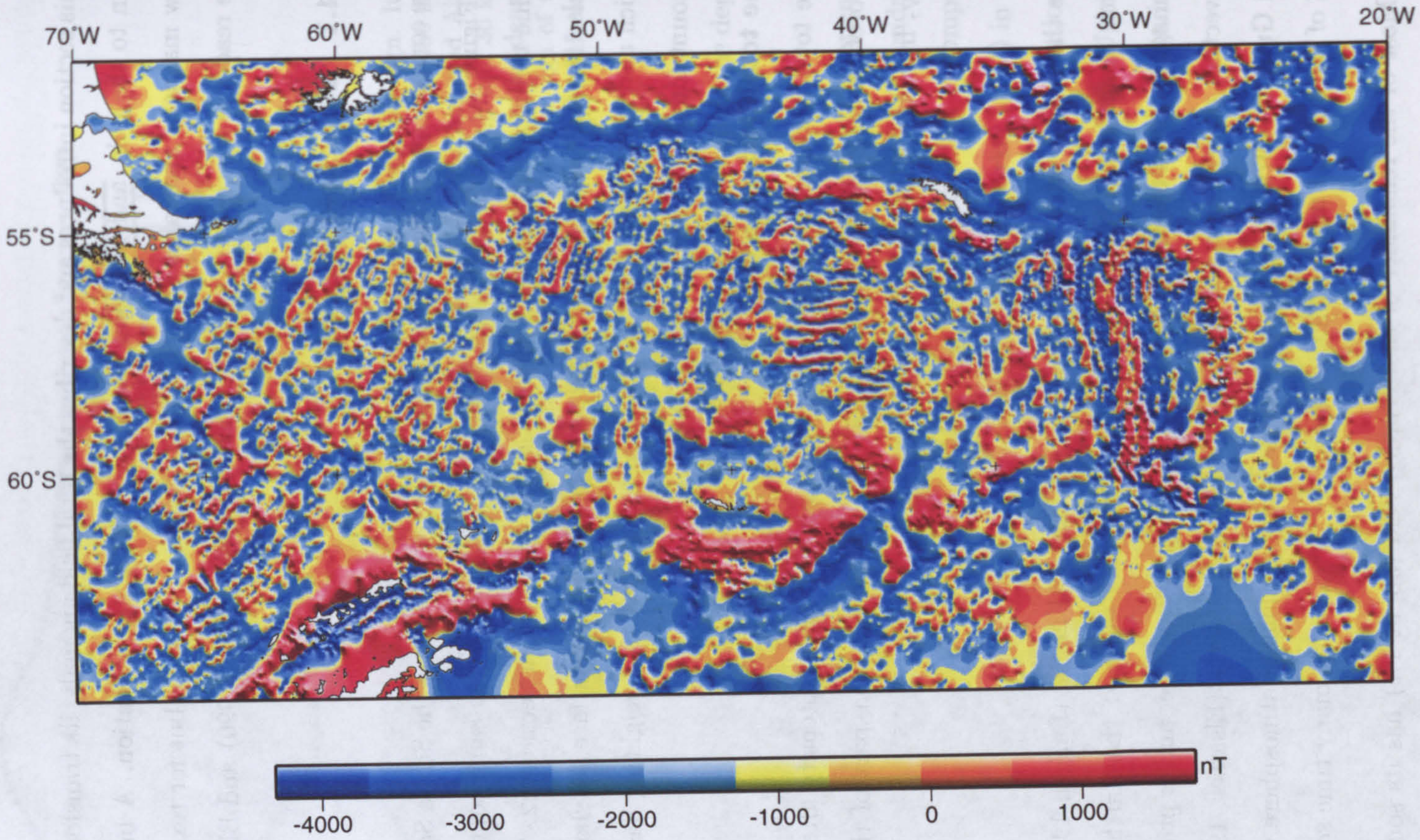

Figure 2.7: Mercator projection of the total field anomaly grid supplied by Peter Morris of BAS. Due to the lack of recordings at a base-station in the region the time-variant field has been removed by a visual inspection of profile data. Levelling by shifts and tilts has been performed. The ship track data used are shown in Figure 2.8. Illumination is from the northeast. A larger version of this figure can be found inside the back cover of the thesis.

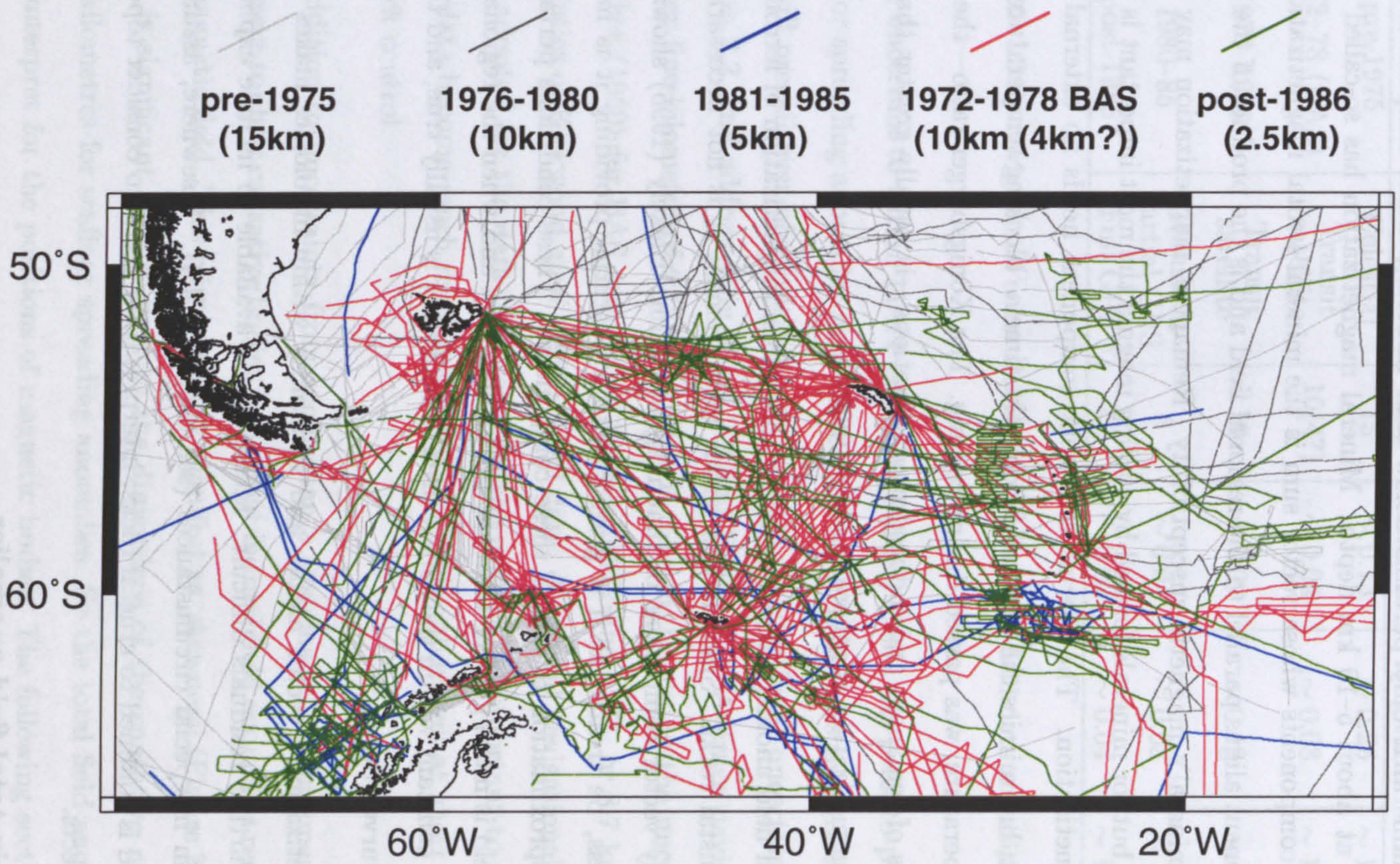

Figure 2.8: Mercator projection of ship tracks taken in acquisition of the total field anomaly grid. The distribution of data by era is shown by the different colours of ship tracks, relative lengths of acquisition are given in Table 2.2. Key shows the eras defined by colours, and their corresponding navigational uncertainty, as discussed in Table 2.2

ferromagnetic minerals. Ferromagnetism will not be addressed here: it is enough to know that for each mineral it only pertains below that mineral's Curie temperature, which is usually met at about 5–10 km depth. Mineral magnetization has so-called induced and remanent components whose vector sum is the mineral's total magnetization. The induced component aligns parallel to the regional field and is the product of the regional field and the mineral's magnetic susceptibility. Remanent magnetization may arise in different ways, but for minerals formed by cooling magma the most important is thermo-remanent magnetization. The thermo-remanent component needs no external field in order to persist, but mimics the regional field at the time a 'blocking temperature', below the Curie temperature, was passed during cooling. The Königsberger ratio—the ratio of the magnitudes of remanent and induced magnetizations—is usually greater than unity, as remanent magnetization is generally the stronger.

So the total field anomaly arises from the anomalous magnetization of ferromagnetic minerals in crustal rocks. Since it is a scalar measurement it is not necessarily a description of any vector component of that magnetization. Blakely (1995) shows that it can, nonetheless, be treated as if it gives rise to a potential providing it is harmonic, and a good approximation to one of these components. These conditions pertain when the ambient field is much greater than the perturbing field and when the regional field is approximately constant within the survey area. The former is usually true, and the latter is a point for survey design.

The magnetization's vector nature and variability within lithologies makes the task of producing further residuals difficult. Methods are available to include explicitly the effect of terrain in special circumstances (see Section 2.4.4). Elsewhere, assuming the perturbing field is confined to crustal rocks, interpretation needs to consider topographic and terrain effects.

Uncertainty in total field anomalies

Most of the total field anomaly data used in this study were collected by proton magnetometers towed behind ships. Anomalies recorded in the Scotia Sea between 1972 and

Era	Likely Navigation	Uncertainty at ~ 50°S			Length in Figure 2.8
		km	°latitude	°longitude	
pre-1975	Celestial	15	~ 0.13	~ 0.26	~ 128000 km
1972–78 (BAS)	Transit satellite	10(4?)	~ 0.04	~ 0.08	~ 168000 km
1975–1980	Transit satellite	10	~ 0.09	~ 0.18	~ 59000 km
1980–85	Transit & partial GPS	5	~ 0.04	~ 0.08	~ 30000 km
post-1985	Full GPS	2.5	~ 0.02	~ 0.04	~ 153000 km

Table 2.2: Likely navigational uncertainties for marine total-field data acquisition in the Scotia Sea.

1978 are uncertain to within 11 nT (Hill and Barker, 1980). As peak-to-peak amplitudes of seafloor spreading anomalies may exceed 500 nT it is obvious that navigational uncertainty will prevail over observational uncertainty. Navigational uncertainty is discussed in Section 2.2, and addressed in Table 2.2 and Figure 2.8. Average navigational uncertainty per line-kilometre of total field data is 6.7 km, assuming the uncertainty of Hill and Barker (1980) for BAS acquisition between 1972 and 1978, or 8.7 km applying the uncertainties of Kirkwood *et al* (1999) to all data. A general navigational uncertainty of 8 km is adopted for the data used to make the grid. It is important to remember that gridded data become much more uncertain than this value even at short distances from ship track control.

In addition to uncertainty from acquisition a systematic misplacement of anomalies with respect to their causative bodies is inherent in total field anomalies recorded in an inclined magnetic field. This misplacement, manifest as 'skewness' (Figure 2.9) in magnetic profiles, is significant with respect to the dimensions of the causative magnetization—several kilometres for seafloor spreading anomalies. So the total field anomaly is unsuitable to interpret for the positions of magnetic bodies. The following sections detail how to remove much of the skewness so that in effect only navigational uncertainties remain.

2.4.2 Reduction to the pole

Reduction to the pole is a treatment of total field anomalies which aims to remove their skewness (Baranov and Naudy, 1964; Bhattacharyya, 1965). Skewness comes from the contribution to an anomaly's phase of the inclination of a ferromagnetic body's magnetization, which is a vector quantity. Inclined magnetization is the result of the dipole-like core field which is inclined everywhere but the magnetic equator. At the magnetic poles the field aligns vertically with respect to the surface. A smaller 'anomalous' skewness (Cande, 1976; Roest *et al*, 1992) may be present due to other effects which are not well understood.

Skewness gives rise to appreciable systematic misplacement of the anomaly with respect to the underlying source: the skewed anomaly will not align with all the causative body's edges, and has a large negative component to the main part of the anomaly (Figure 2.9). Reduction to the pole deskews anomalies by changing the inducing field to a vertical orientation, as if the source body were situated at one of the magnetic poles. The transformed anomaly's induced component is centred over the perturbing body and is monopolar. Remanent magnetization may continue to supply a dipole component to the anomaly as most methods assume that the anomaly is completely induced. However if the latitude of the body at the time of formation and the present latitude are similar much of the skewness supplied by remanent magnetization will also be removed. A treatment of one means of performing reduction to the pole is given in Appendix B.

The reduced to the pole grid was produced by transforming total field anomalies using *Geosoft* software. To address the large changes in the inducing geomagnetic field in the Scotia Sea region I perform the transformation on a set of five degree by five degree tiles, overlapping by one degree at the edges to enable smoothing between tiles.

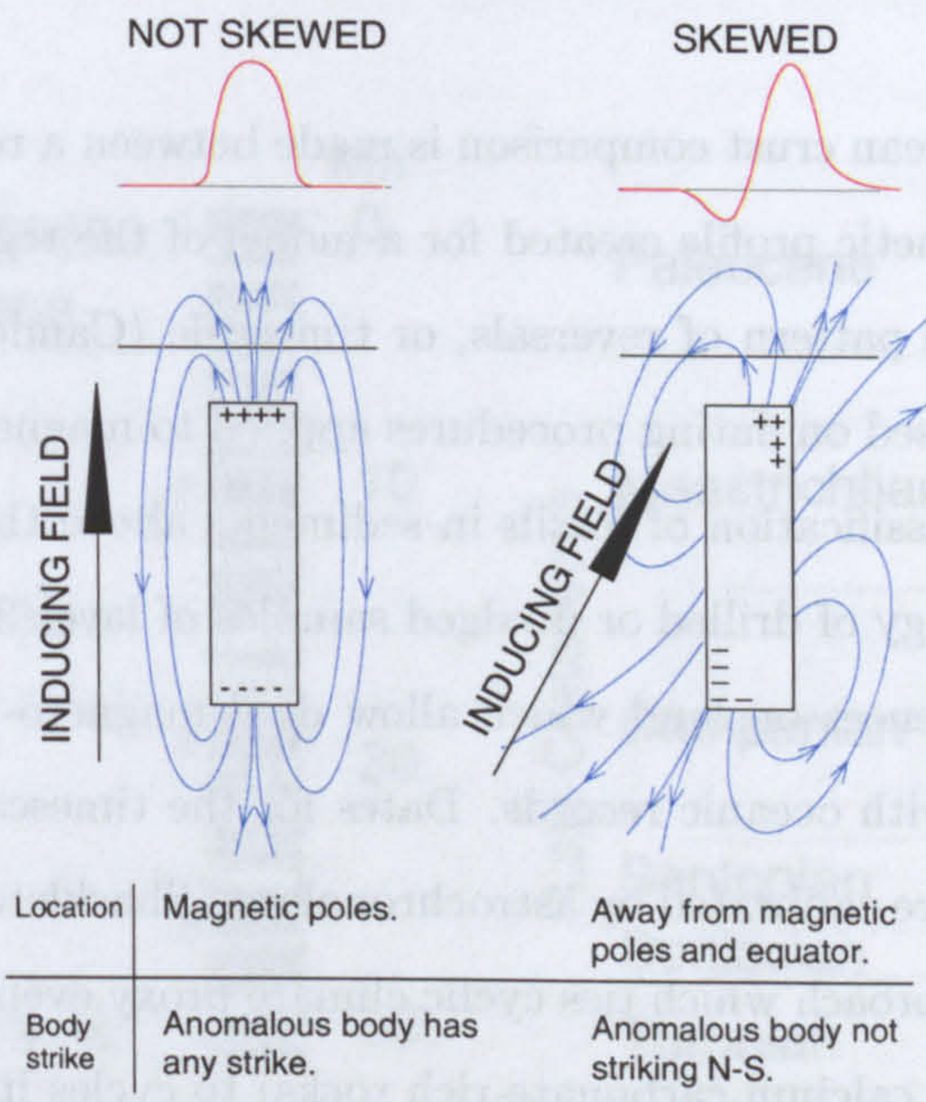

Figure 2.9: For identical dyke-like magnetic bodies, the total field anomaly depends on the direction of the inducing field and the body's strike. At the magnetic poles the inducing field is aligned vertically and the total field anomaly is monopolar and centred over the dyke. Elsewhere the dipole component induced gives rise to 'skewness' in the total field anomaly.

2.4.3 Block models

The importance to plate tectonics of reversals of the geomagnetic field is reviewed in Section 1.2. The present north geographic pole is in fact a south magnetic pole as it attracts the north seeking needles of compasses, but the anomaly field from rocks world-wide exhibits multiple synchronous reversals over geological time, at apparently random intervals. The reversal mechanism is not well understood but is thought to be related to the instability of the core dynamo (Gubbins, 1987). Relative to the duration of periods of constant polarity (chrons) the time taken for a reversal to occur is geologically instantaneous (about 10 thousand years). Dates from rocks characterized by a known reversal sequence can be applied everywhere the sequence is identified. The magnetic reversal record provides a basis for dating and measuring the plate movements that create the

ocean basins.

To assess the age of ocean crust comparison is made between a real magnetic anomaly profile over it and a synthetic profile created for a model of the region. The synthetic is created using a published pattern of reversals, or timescale (Cande and Kent, 1995; for example; Figure 2.10), based on dating procedures applied to magnetic rocks. Dating can be by biostratigraphic classification of fossils in sediments above the magnetic layer 2 of seafloor, by radiochronology of drilled or dredged samples of layer 2 itself, or by comparison with geological sequences on land which allow dual magneto- and biostratigraphic analysis for comparison with oceanic records. Dates for the timescale used in this study (Cande and Kent, 1995) are calibrated by astrochronology (Shackleton *et al*, 1990; Hilgen, 1991; for example), an approach which ties cyclic climate proxy events (for example cyclic deposition of sapropels or calcium carbonate-rich rocks) to cycles in Earth's orbit, which are precisely known. These dates are then applied to magnetic reversal sequences via biostratigraphic markers.

Source model for synthetics in the Scotia Sea

Synthetic profiles are created for a source model of rectangular sectioned prisms having infinite length in the direction of anomaly strike. Just two components of the induced field (horizontal, perpendicular to the length of the blocks, and vertical) need be considered. The third component is confined to the block itself (Figure 2.11). Parameters describe the magnetic susceptibility and thickness of the layer, whose upper surface is the sea floor. Each block's magnetization is allowed to reverse according to the reversal timescale and user-defined spreading rates which also determine block width. The source, thus described, is magnetized by a model field at its present latitude and longitude (induced component), and latitude at the time of block formation (remanent component). Asymmetric accretion and ridge jumps can also be modelled. An implementation of this technique, in the Fortran program *magbath*, was supplied by BAS.

The field due to the model is determined as components in the vertical and spreading

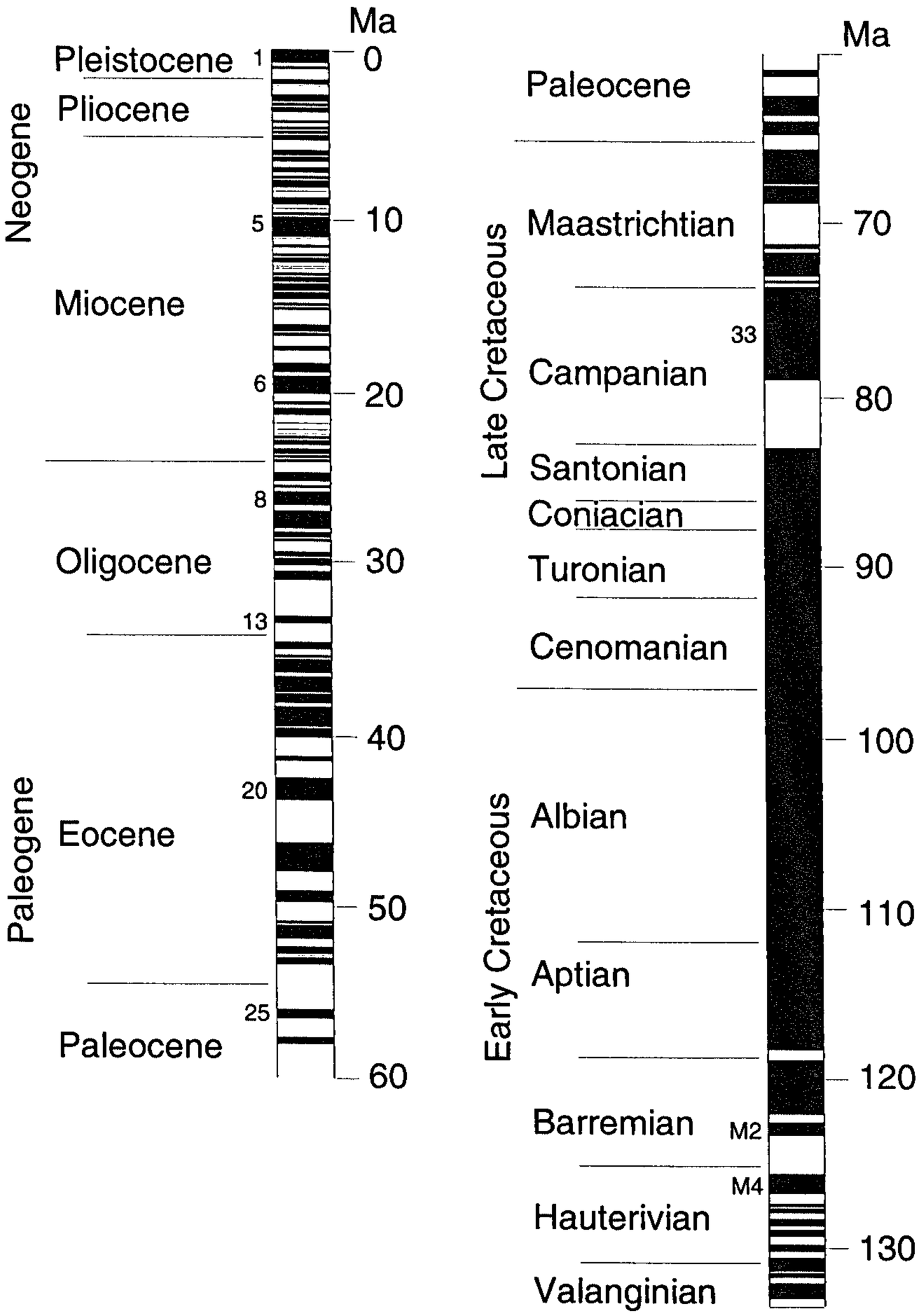

Figure 2.10: Part of the magnetic anomaly reversal timescale of Cande and Kent (1995) between 0 Ma and 133 Ma (Early Cretaceous to Present day). Ages on the right of the columns, on the left are the names of some major chronostratigraphic divisions, and (small numbers) selected reversal anomaly numbers.

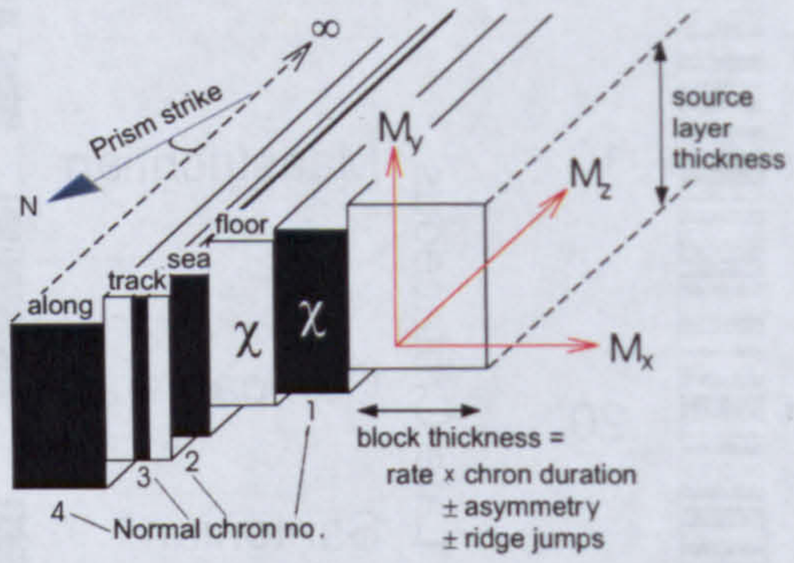

Figure 2.11: The block model scheme by which synthetic magnetic anomaly profiles are generated. Three components characterize magnetization in the model blocks, which have infinite length along strike. Only two (M_x and M_y) need be considered as M_z is confined within the infinite dimension of the model. The magnetization (χ) is given a constant value but allowed to change sign according to whether a normally- (black) or reverse-magnetized (white) block is being modelled. Blocks have a constant thickness and their upper surface is constrained to coincide with the bathymetric surface.

directions which are added to the local reference field to determine a resultant. This resultant field's magnitude is taken from the reference field's magnitude to give a synthetic total field anomaly due to the model magnetization. Some synthetics modelled for the Scotia Sea region are presented in Section 2.6.4. They are generated by *magbath*, embedded in a shell script **model_it** written to perform data pre-processing and display, using some *GMT* programs and the *UNIX* utility *awk*.

2.4.4 Seafloor magnetization

The convolution of anomalies due to terrain can be mitigated for by determination of rock magnetization, a scalar quantity which therefore shows no skewness or spherical divergence (*i.e.* it does not vary with the observer's distance). Magnetization distributions can be forward modelled (Whitmarsh and Miles, 1995; for example) or inverted for assuming

an appropriate source model. A source model appropriate to oceanic crust formed by seafloor spreading is used here in an inversion for a grid of seafloor magnetization. This grid is used in Section 2.6.5 to pick edges of magnetic isochrons for use in Chapter 3.

Modelling seafloor magnetization

An inverse Fourier procedure for determining rock magnetization from a two dimensional source model is described by Parker and Huestis (1974). The source model is similar to that used for making synthetic profiles: a constant thickness layer whose upper surface is the seafloor, in which layer the magnetization is constant but allowed to reverse. The method is extended to deal with three dimensional sources by Macdonald *et al* (1980), an approach which is described in Appendix B.

I use an implementation of the inverse technique for three-dimensional anomalies in a Fortran program *inv3d* (Martínez *et al*, 1995; Smith *et al*, 1999; Taylor *et al*, 1999) which works for sea-surface as well as deep-tow total field anomalies. I embed *inv3d* in a *GMT-awk* shell script, **mgz_grd**, along with two short Fortran data handling programs, in order to pre-process and filter the input and display the results. In order for the inversion to succeed, which is inherently unstable as it is in effect a downward continuation (Appendix B), the input bathymetric grid is masked to 2500 m depth for all areas shallower than 2500 m. In addition total field anomalies are band-pass filtered between 6 km and 50 km, with cosine taper to 3 km and 100 km. A source layer thickness of 1 km is used. Model magnetizations typically reproduce the input total field anomaly with root-mean-square differences of less than 10 nT.

For ship-track total field anomalies I use a similar implementation, *inv2d*, embedded in a shell script **mgz_prof**. As with the three-dimensional implementation a 1 km thick source layer is used, but it is necessary sometimes to use a different filter width to achieve convergence.

2.5 Other data

In addition to potential field data, numerous other data exist in and out of the literature as a result of the prolonged period of exploration in the Scotia Sea region. In particular, at BAS, a large volume of seismic reflection data is held which has never been published. Where necessary, this is used to inform models set up in the course of the thesis.

2.6 Scotia Sea model of crust

2.6.1 Free-air anomaly grid

The free-air anomaly from satellite altimetry is shown in Figure 2.12. The dominant topographic signature can be appreciated by comparing it with the bathymetric grid of Figure 2.1. Most prominent are the elongated, deep low anomalies associated with the trenches at the South Sandwich and South Shetland subduction zones, and with the active strike-slip boundaries north of the North Scotia and South Scotia ridges. The highs of the ridges themselves and the South Sandwich Islands are clearly visible as are the spreading centres of the west Scotia Sea, east Scotia Sea, and the former Phoenix spreading centre. Another prominent class of anomalies is the fracture zone troughs caused by the action of transform faults and other features offsetting segments of the West Scotia and Phoenix Ridges. The anomaly fabric created by the presence of slow-rate spreading centres and their offsets is striking in these areas. No such fabric is evident in the central Scotia Sea.

In the west Scotia Sea the median ridge anomaly is segmented into seven parts by transform and non-transform offsets. From southwest to northeast these are referred to as W1—W7, and can be considered parental to spreading segments similarly numbered.

Segments W1 to W4 are bounded to the southwest by the Shackleton Fracture Zone and northeast by the Quest Fracture Zone. Segmentation between these fracture zones is by non-transform offsets. The offsets in magnetic anomalies they produce were named, by

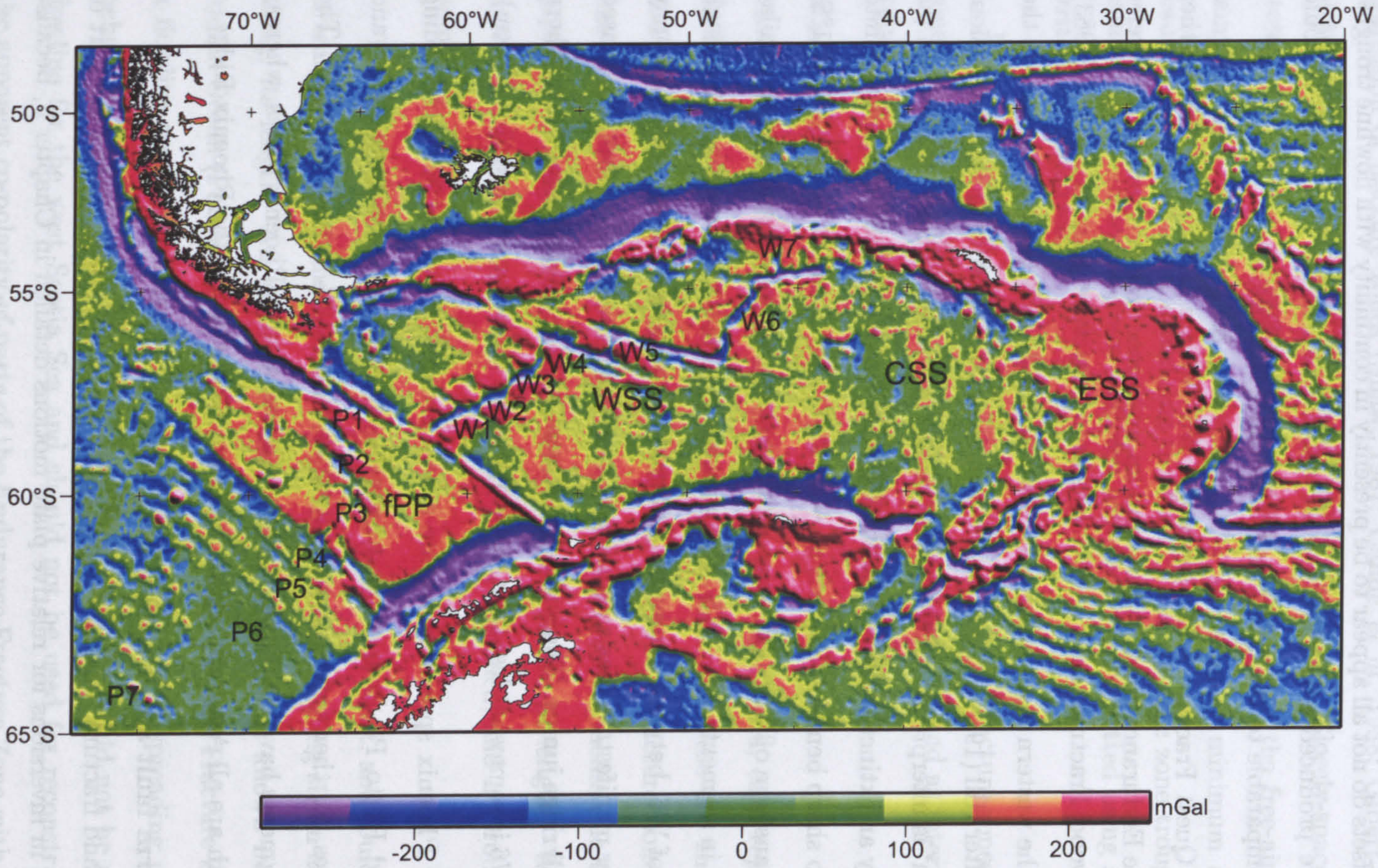

Figure 2.12: Mercator projection of the satellite derived free air gravity anomaly in the Scotia Sea region (Smith and Sandwell, 1995). Illumination from northeast. W1–W7: segments of the spreading system in the west Scotia Sea (WSS), P1–P7: segments of the spreading system that created the former Phoenix plate (fPP), which is now only comprised of the east flanks of P1–P3, after subduction of the ridge crest in P4–P7 (and further south). The central Scotia Sea (CSS) shows little similarity to the spreading fabric of these two systems, or to the east Scotia Sea (ESS). A larger version of this figure can be found inside the back cover of the thesis.

Burrell (1983), the Beagle, Terror and Fram fracture zones, from southwest to northeast. Although these offsets do not all appear to be presently in continuity with flowline troughs, all appear to have produced lengths of free air anomaly lineations that adopt tectonic flowline trends comparable to the Quest and Endurance fracture zones.

North of the Quest Fracture Zone, segments W5–W7 are bounded by two further fracture zones, the Endurance fracture zone and an un-named fracture zone which I refer to as the 'Burdwood Fracture Zone'. The Burdwood fracture zone of Burrell (1983) strictly refers to the western fossil offset only. Burrell (1983) calls the eastern feature the 'Scotia trough' (after Hill (1978)). I will not be using this term in order to avoid confusion: the 'Scotia trough' is interpreted by Hill (1978) as a triple-junction trace rather than (as here) a scar left by an extinct transform fault. Segment W6 appears to be segmented into three parts by two sharp bends in the axis at $\sim$ 48.1°W, 56.0°S and at $\sim$ 47.1°W, 55.1°S, possibly at non-transform offsets. The axial anomaly strike between these bends is similar ($\sim$N45°E) to that in segments W1—W5. The presence of a short fracture zone-like trough on the east flank of W6, between anomalies C6b and C8, suggests this segmentation may have had an earlier manifestation as a significant age offset, which might have been erased by successive small ridge jumps. The width of segment W7 ($\sim$ 600 km), and the northern part of segment W6 is somewhat less than the widths of all the other segments ($\sim$ 770 km).

In the former Phoenix spreading regime a well ordered system of seven spreading segments, labelled P1 to P7 from north to south, are offset by transform faults and their fracture zones. Further segments, not shown in Figure 2.12, exist south of P7. The northern three segments have crust of both Antarctic and former-Phoenix plates, whereas those further south are all Antarctic plate, following subduction of the Phoenix Ridge.

Picking transform fault and fracture zone troughs

Transform faults and fracture zones are important in the crust model. They form part of the data set used in inversions for relative plate motions detailed in Chapter 3, because many transform faults act purely by displacement along their strike to accommodate strain between separating plates, later to become fossilized as fracture zones: they are therefore

tectonic flowlines of plate motion. Free-air anomaly troughs, which are a systematic expression of fracture zones (Shaw, 1987; Cande *et al*, 1988; Gibert *et al*, 1989), are picked using the method of Nankivell (1997a) as follows. Closely-spaced sets of profiles cross perpendicular to fracture zone troughs, along which the free-air anomaly grid is sampled, and an automated procedure picks an anomaly minimum along each. The resulting line of minima, describing the floor of the fracture zone trough, can be edited using an X-Windows program - *xfzpick*, and the data formatted using *split_fzpicks*, both written by Nankivell.

Using this process I produce a set of picks of all likely fracture zones, or part fracture zones, representing flowlines which are as long as possible and as internally consistent a data set as possible, without compromising their continuity.

West Scotia Sea

Three main fracture zones are picked in the west Scotia Sea, each represented on both flanks of the West Scotia Ridge. From south to north these are the Quest Fracture Zone, the Endurance Fracture Zone, and the Burdwood Fracture Zone. The Quest and Endurance Fracture zones have been split into shorter segments due to the presence of gaps in the fracture zone troughs which exceed 50 km in length. Within these gaps, continuity of the fracture zone trace can not be assumed, and no trough is available to be picked.

The Endurance Fracture Zone has a long (~250 km) offset, and could have been active in transpression or transtension at some time, accommodating strain across, rather than along, its length. An example of this kind of behaviour is known from the southwest Indian Ocean (Patriat *et al*, 1985), where the Prince Edward Fracture Zone fails to adopt a flowline trend consistent with predicted changes in the spreading direction. If such behaviour were the case, the Endurance Fracture Zone would not be a reliable tectonic flowline for the west Scotia Sea and should not be used for reconstructions. However the apparent co-polarity of parts of the Endurance Fracture Zone with the neighbouring, shorter-offset ($\sim$ 100 km), Quest Fracture Zone postpones its exclusion. A similar caveat

applies to sections of the Quest and Endurance fracture zones aged between anomalies C5c and C5. With the possibility of spreading in the Protector Basin during this interval (Hill and Barker, 1980) and possible presence of a triple junction at its northern margin involving either fracture zone as transform faults, data from between C5 and C5c were included in the data set with caution.

In addition numerous shorter troughs are picked. This is done under an assumption that flowline traces can be created at stationary non-transform offsets (Schouten and White, 1980). Data from features like this are desirable for the inverse procedure described in the next chapter. Picking must be undertaken with caution because without connection to an extant transform or non-transform offset, a feature's flowline nature can not be taken for granted. With this in mind the following criteria are used to select features in this class:

1. Presence within the west Scotia Sea spreading system (essential).
2. Apparent co-polarity with known fracture zone lengths in the west Scotia Sea (essential).
3. Length exceeding 30 km (essential given resolution of satellite gravity anomalies).
4. Apparent offset of magnetic anomalies (where magnetic grid resolution allows).
5. Existence of a conjugate feature (desirable).
6. Presence in other (*e.g.* bathymetry, seismic) data (desirable).

Phoenix system

In the Phoenix spreading regime a set of nine fracture zones (four are expressed on both Antarctic and Phoenix plates, the remainder are Antarctic plate features) are picked. Transform faults are typically less than 100 km in length, and magnetic isochron offsets for the region where the Phoenix plate has been subducted show that offsets here were similar. Fracture zone troughs show no significant breaks in continuity.

Pivoting subduction (which is thought to be the result of the greater slab pull force where the subducting crust is older, (Menard, 1978)) has acted within segment P4, meaning that it is possible that either of the fracture zone traces at its boundaries could have

been distorted. Some care is taken when picking data describing those fracture zones, although they appear not to have been distorted as their strikes do not deviate significantly from the strikes of the set of fracture zones in the Phoenix system.

The tectonic flowline data picked in the west Scotia Sea and Phoenix system are shown in the introductions to the inversions of Chapter 3 (Sections 3.4.1, 3.4.2, 3.4.3 and 3.4.5).

Shackleton Fracture Zone

The Shackleton Fracture Zone is not included in either the west Scotia Sea or Phoenix system pick sets. The Shackleton Fracture Zone is part of the modern sinistral transpressional plate boundary between the Scotia and Antarctic plates. The extinct Phoenix spreading system to its southwest is the result of relative motion between the Antarctic and former Phoenix plates but, in the west Scotia Sea to its northeast, a different plate pair was active. As a result this feature is of no use as a passive recorder of plate motion in either system. Exclusion of the Shackleton Fracture Zone from the reconstruction process is a crucial difference between this study and all previous Scotia Sea reconstructions, in which the assumption of its importance as a tectonic flowline for motion between the Antarctic Peninsula and Tierra del Fuego is a keystone (Barker and Burrell, 1977; Burrell, 1983; Cunningham *et al*, 1995).

2.6.2 Bouguer anomaly grid

The Bouguer anomaly grid for the Scotia Sea region is shown in Figure 2.13. Most striking is the strong anticorrelation with long-wavelength topography, which is the result of no account being made for compensating masses in the mantle. On this basis the following fragment groups are of likely thickened crust:

1. Offshore Tierra del Fuego and the North Scotia Ridge as far east as 49°W.
2. The South Sandwich Arc, Herdman Bank, Discovery and Jane Banks (possibly extending north along 36.5°W as far as 57.3°S), a complex of highs around Herdman and Discovery Banks, and an isolated relative high in the South Sandwich forearc centred on

58.6°S, 25.3°W

3. The Antarctic Peninsula, South Shetland Islands, South Scotia Ridge and South Orkney Microcontinent.

4. Bruce Bank, Pirie Bank and the high centred on 51°W, 58.5°S at the western margin of Protector Basin (here named the Terror block, after the nearby magnetic-anomaly offset of Burrell (1983)).

5. South Georgia and Shag Rocks.

6. The Falkland Islands and Falkland Plateau as far east as Maurice Ewing Bank, the Northeast Georgia Rise.

Small areas of oceanic crust are interpreted from strongly positive anomalies in Drake Passage, the west Scotia Sea, east Scotia Sea, Powell Basin, Protector Basin and Dove Basin. In addition, as would be expected, the Weddell Sea and Atlantic and southeast Pacific oceans also show strong positive Bouguer anomalies.

Large areas of intermediate anomalies are identifiable. Often these intervene between the interpreted areas of continental and oceanic crust, they represent a transition between the two. Examples are the eastern margins of Tierra del Fuego and Burdwood Bank and the opposing Antarctic Peninsula and South Orkney Microcontinent margins of Powell Basin. Elsewhere areas of intermediate anomalies are less easy to interpret; in the central Scotia Sea and the eastern Falkland Plateau.

I use the total horizontal derivative of the Bouguer anomaly $\left(\Delta g^{\mathrm{THD}}_{\mathrm{boug}}\right)$ to pick prominent edges in the Bouguer anomaly grid. The intention is to draw outlines around regions, or blocks, of continental crust at whose boundary with oceanic crust $\Delta g^{\mathrm{THD}}_{\mathrm{boug}}$ assumes a maximum. This depends on two assumptions:

1) The density difference between continental crust and oceanic crust is greater than 100-km-scale rock-density differences within either, and

2) The transition occurs over a short enough horizontal distance for the density contrast to be manifest as a steep gradient in the Bouguer anomaly.

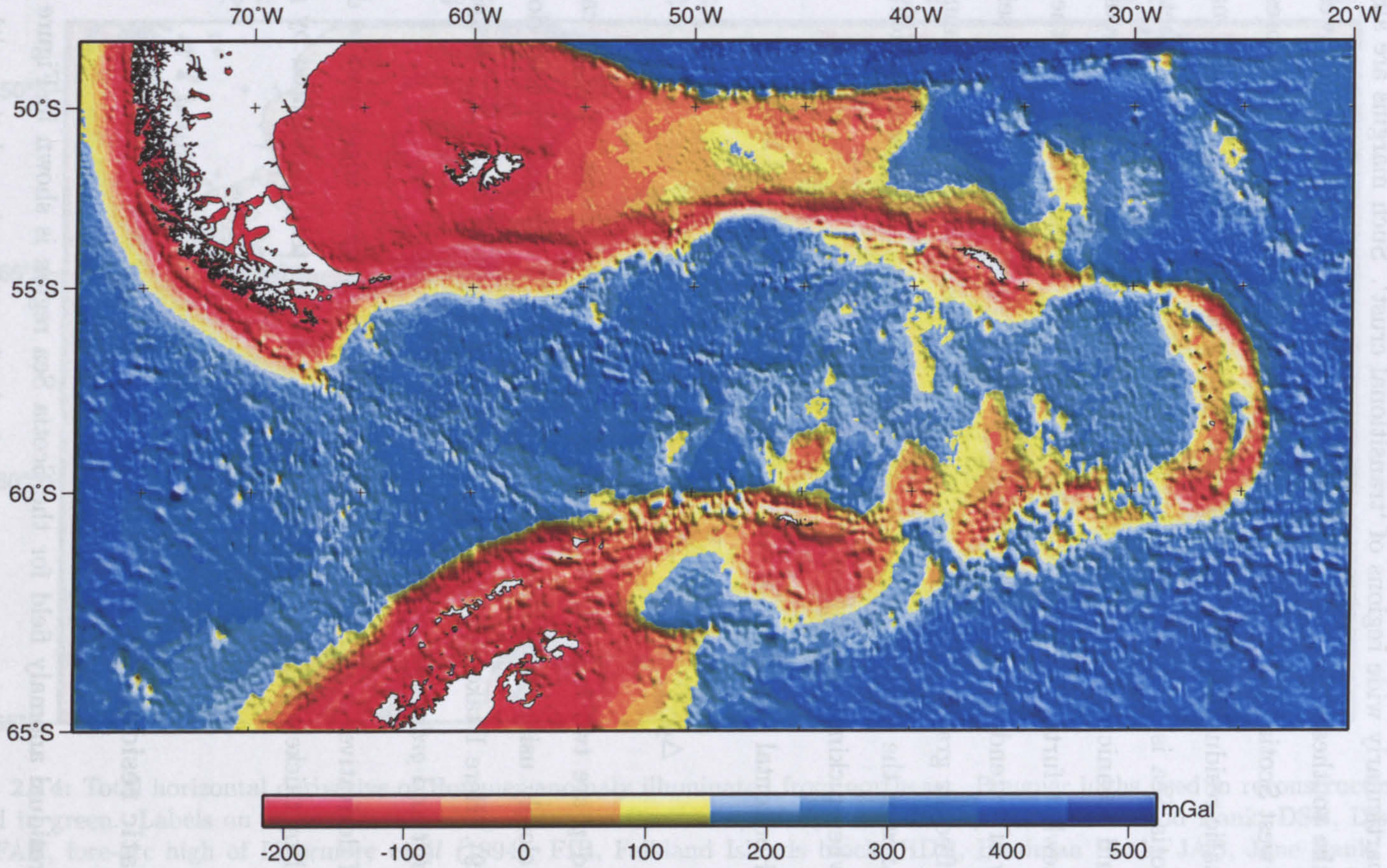

Figure 2.13: Mercator projection of the complete Bouguer anomaly over the Scotia Sea region, illuminated from the northeast. The sense of the colour scale is reversed so that red denotes negative anomalies and blue denotes positive ones. A larger version of this figure can be found inside the back cover of the thesis.

The first assumption is quite reasonable, but the second might be invalid for stretched margins with particularly wide regions of 'transitional crust'. Such margins are already identified: at the southeastern margin of the Falkland Islands block, the northwestern margins of the west Scotia Sea, and the opposing margins of Powell Basin. The presence of relative isostatic residual highs at the Falkland Islands block and northwestern margin of the west Scotia Sea is used as an indication of proximity to the boundary between 'transitional' and oceanic crust, the boundary of continental crust taken at a maximum in $\Delta g^{\mathrm{THD}}_{\mathrm{boug}}$ somewhat further landward of this anomaly. In Powell Basin I use the seaward boundary of 'extended continental crust', derived by King *et al* (1997) from seismic reflection and free-air gravity anomalies as a guide to choosing a suitable maximum in $\Delta g^{\mathrm{THD}}_{\mathrm{boug}}$. The axes of the deep trenches and troughs also all exhibit maxima which have been avoided when picking block edges.

The Total Horizontal Derivative of the Bouguer anomaly is defined here by

$$\Delta g^{\mathrm{THD}}_{\mathrm{boug}} = \sqrt{\left(\frac{\partial \Delta g_{\mathrm{boug}}}{\partial x}\right)^2 + \left(\frac{\partial \Delta g_{\mathrm{boug}}}{\partial y}\right)^2}, \tag{2.6}$$

in which x and y are two mutually orthogonal horizontal directions. $\Delta g^{\mathrm{THD}}_{\mathrm{boug}}$ can be approximated closely using finite-differences, or computed in the wavenumber domain (Pedersen, 1989). Here I take the wavenumber domain approach for $\Delta g^{\mathrm{THD}}_{\mathrm{boug}}$, using the *GMT* tools *grdfft* and *grdmath*.

The grid of derivatives is shown in Figure 2.14, with prominent edges used to define the continental or thickened crustal blocks mentioned in the text highlighted by green outlines.

2.6.3 Isostatic residual anomaly grid

The isostatic residual anomaly field for the Scotia Sea region is shown in Figure 2.15. The big difference from the Bouguer anomaly is the loss of anticorrelation with long-wavelength topography. As a result, at long wavelengths the isostatic residual anomaly

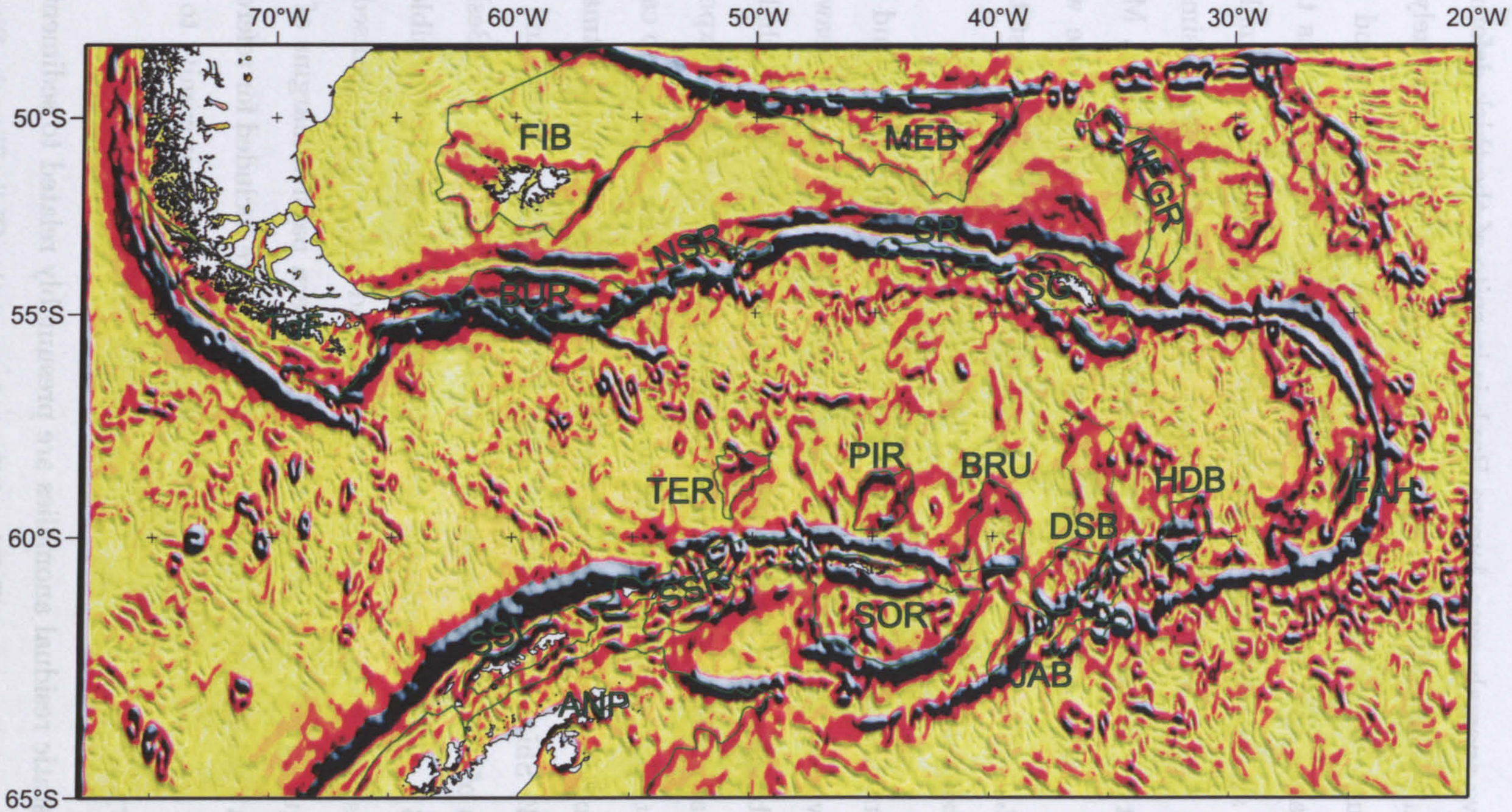

Figure 2.14: Total horizontal derivative of Bouguer anomaly illuminated from northeast. Bouguer highs used in reconstructions are outlined in green. Labels on or near each: ANP, Antarctic Peninsula; BRU, Bruce Bank; BUR, Burdwood Bank; DSB, Discovery Bank; FAH, fore-arc high of Livermore *et al* (1994); FIB, Falkland Islands block; HDB, Herdman Bank; JAB, Jane Bank; MEB, Maurice Ewing Bank; NEGR, Northeast Georgia Rise; NSR, North Scotia Ridge east of Burdwood Bank; PIR, Pirie Bank; SG, South Georgia microcontinent; SOR, South Orkney Microcontinent; SR, Shag Rocks block; SSI, South Shetland Islands; SSR, South Scotia Ridge; TdF, Tierra del Fuego; TER, Terror block. Dotted green lines: possible northern extension to Discovery Bank and, in the far northeast, the Islas Orcadas Rise.

resembles the free air anomaly but at shorter wavelengths there are significant differences.

The prominent positive anomaly over Aurora Bank is in spite of the thick deformed sediment pile there (Cunningham, 1998), so the basement beneath this pile is likely to be of oceanic crust. Southernmost Discovery Bank, Pirie and Bruce Banks, and the Terror block all show sharp-edged negative anomalies whose prominence suggests that each of these features is at least partially supported within the crust. The anomalies' similarity to those of the South Orkney Microcontinent suggests that all have a similar crustal nature: old, essentially continental, blocks which have undergone extension. More attenuated highs can be seen along the northwest and southeast margins of the west Scotia Sea. Their setting, landward of the older edge of C8, and character suggest that these anomalies are representative of stretched, thermally subsided crust.

Isostatic residual anomalies at passive margins are discussed by Rabinowitz and LaBrecque (1977) who show that a common feature is a narrow relative high just seaward of the continent—ocean boundary. This is hypothesised as due to anomalously shallow injection of oceanic crustal material at the earliest stages of seafloor spreading. Exposed dense, non-volcanic, mantle peridotite at the continent–ocean boundary could also cause such an anomaly. Such exposures are known at the Iberian passive margin (Whitmarsh *et al*, 1993; ODP Leg 149 Shipboard Scientific Party, 1993; Dean *et al*, 2000) and are a feature of some models of continental break-up (Boillot *et al*, 1995; Brun and Beslier, 1996; Pickup *et al*, 1996). Relative isostatic residual highs of this type are visible in the gridded anomaly presented here, southeast of the Falkland Islands as recognised by Rabinowitz and LaBrecque (1977), and also at the northwestern passive margins of the west Scotia Sea off Tierra del Fuego and Burdwood Bank. They are included for reference on Figure 2.15, although they are not used as unequivocal evidence for proximity to the continent–ocean boundary.

Strongly negative isostatic residual anomalies are presumably related to sedimentary accumulations in the South Orkney and Falkland Troughs and the Chile Trench. Similar anomalies are present at the deep South Sandwich and South Shetland trenches—although

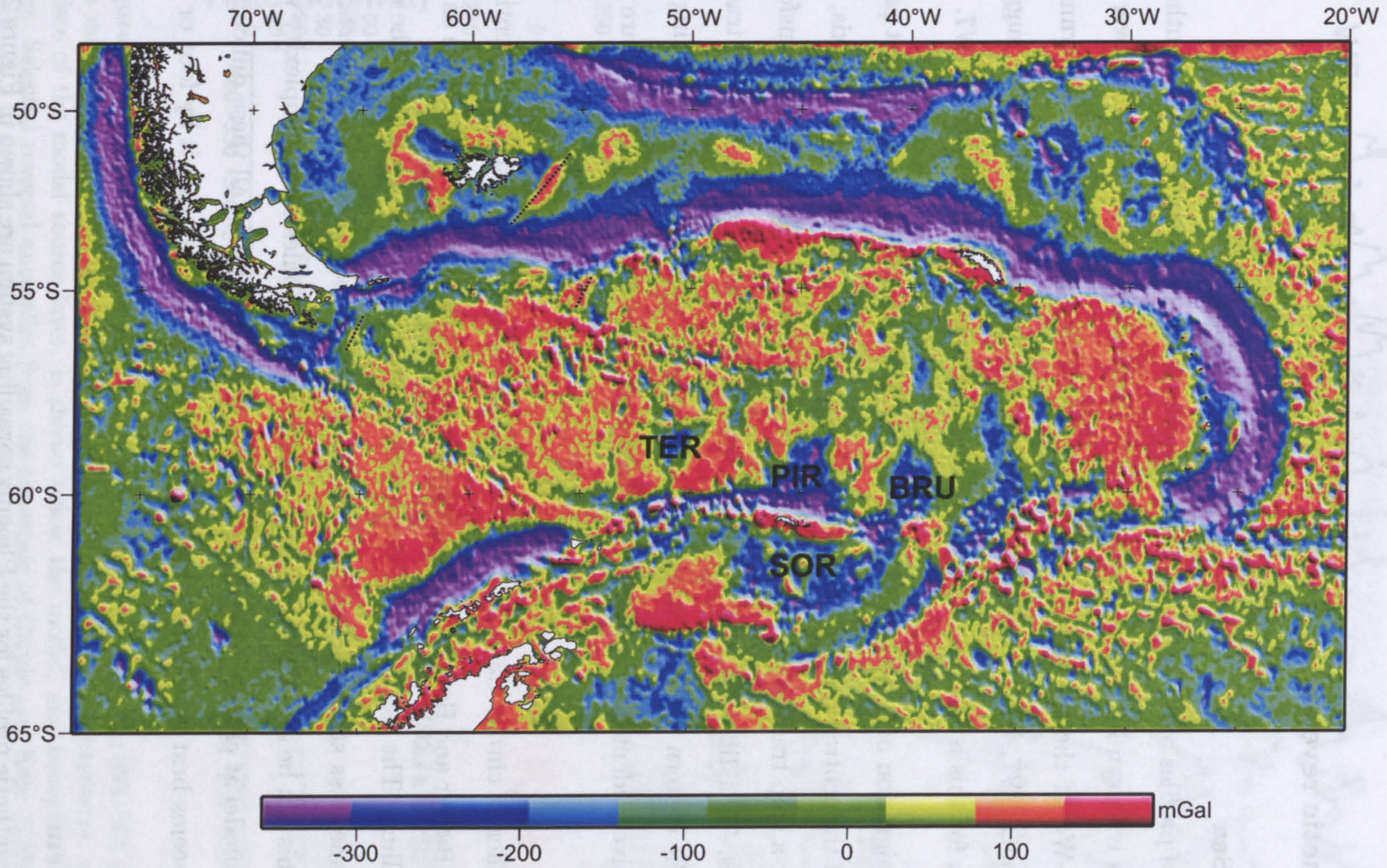

Figure 2.15: Mercator projection of the isostatic residual anomaly over the Scotia Sea region. TER (Terror block), PIR (Pirie Bank), BRU (Bruce Bank) and SOR (South Orkney Microcontinent), mentioned in the text, are labelled. Dotted black lines are the axes of relative highs seaward of continent–ocean boundaries (Rabinowitz and LaBrecque, 1977), where expressed.

neither is sediment-filled.

2.6.4 Magnetic reversal models

West Scotia Sea

A selected set of profiles recorded by ship passage over the west Scotia Sea, with synthetic reversal models is shown in Figures 2.16 and 2.17. Profiles come from modelling over six segments, W1–W6 of the spreading centre in the west Scotia Sea. The northernmost spreading segment, W7, has proved difficult to model. Livermore *et al* (1994) suggest that the reason for this is likely to be significant ridge-jumping tectonics within W7.

Apparent migration of non-transform offsets has made modelling for the oldest parts of W1–W4 and the central and northern parts of W6 difficult. Further from the axis, the possibility that a ship track may cross the track of one of these migrating non-transform offsets increases. This difficulty is compounded by a lack of suitably oriented ship tracks, especially on the eastern limb of the system. As a result, some anomalies preceding C6 are only tentatively identified using assumed symmetry about the ridge axis, or are left unidentified.

The anomalies at chrons C5, C5c, C6, C6b, C7 and C8 (Table 2.3) are well identified in the profiles (Barker and Burrell, 1977; Livermore *et al*, 1994) and so were chosen as the basis for modelling. The west flank of the system is often very well modelled. The east flank is sometimes less straightforward: even when ancient offsets are almost certainly not crossed. This can be seen in W6 where a number of the profiles show complexity with respect to the model at chrons prior to C6 or C6b. Notwithstanding all these difficulties, the east flank seems best matched by an asymmetrical model favouring it by four or five percent.

Phoenix system

Recorded and synthetic profiles for the Phoenix spreading system are shown in Figure 2.18, for eight spreading segments (P1 to P8, north to south; Figure 2.12). The five southern

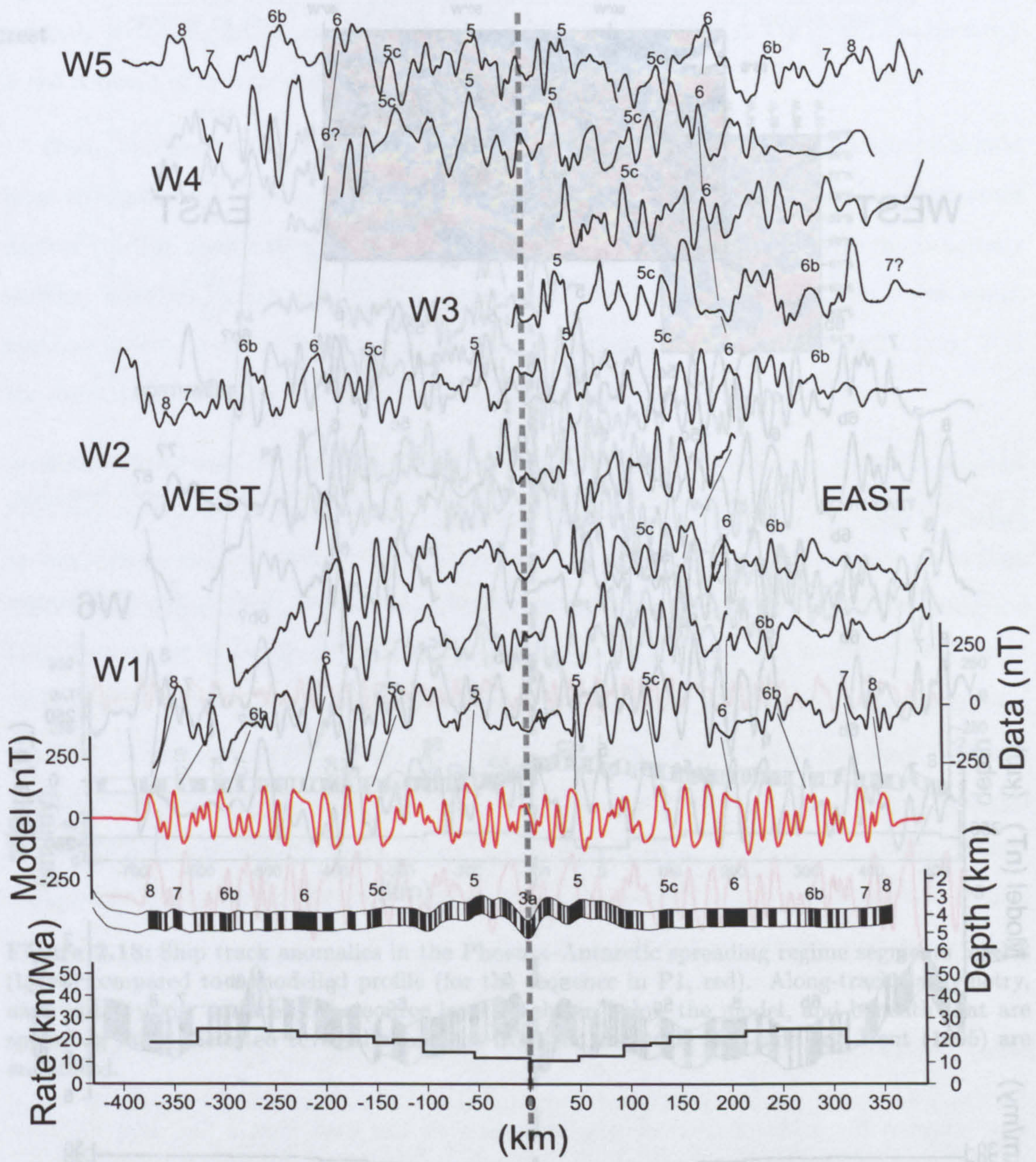

Figure 2.16: Ship track anomalies in the west Scotia Sea segments W1–W5 (black) compared to a modelled profile (for the sequence in W2, red). Along-track bathymetry, used as the upper surface of the model source layer, is shown below the model, and beneath that are spreading rates. Selected reversal anomalies from the timescale of Cande and Kent (1995) are annotated. For location of ship tracks see the inset to Figure 2.17.

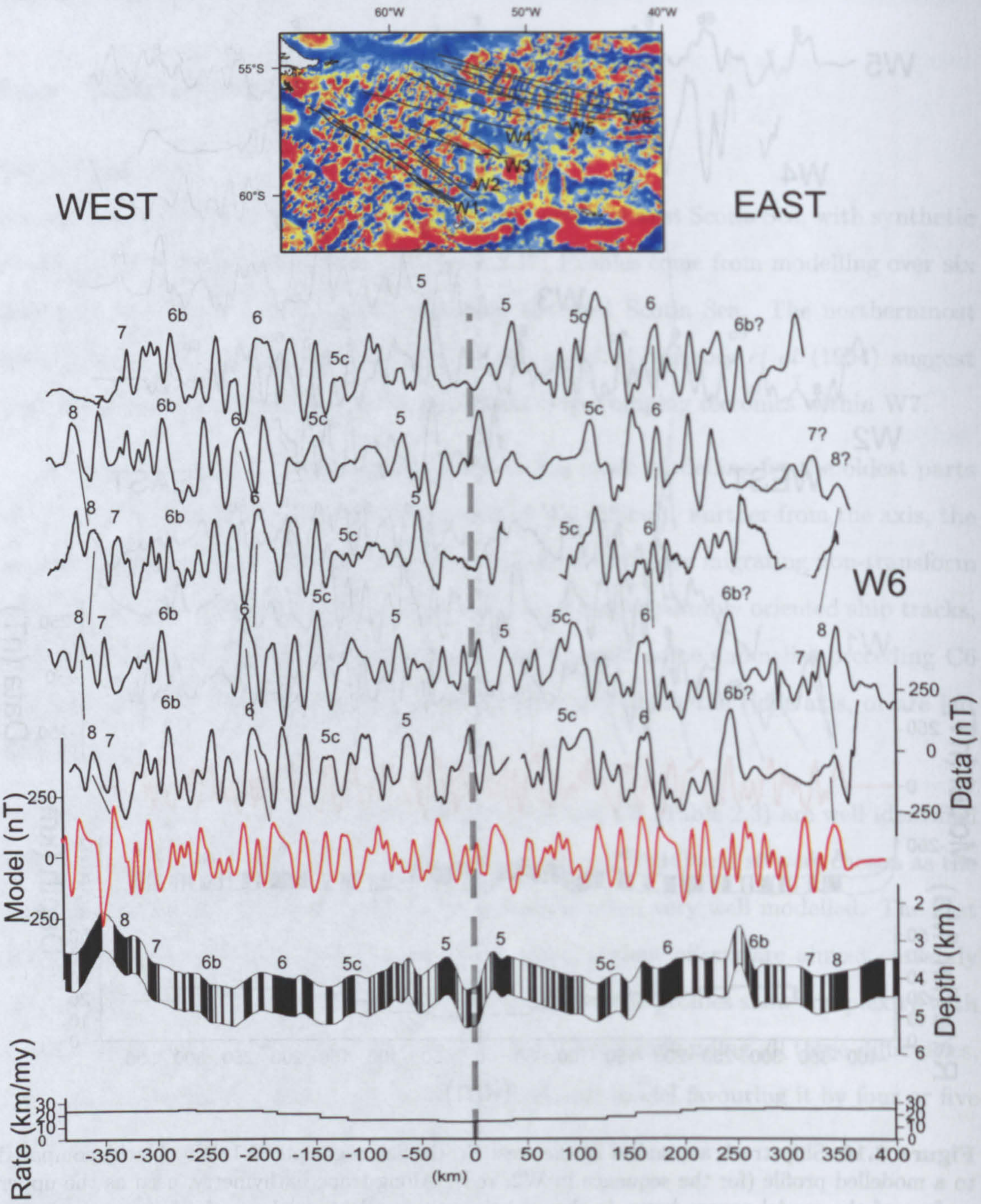

Figure 2.17: Ship track anomalies in the west Scotia Sea segment W6 (black) compared to a modelled profile for W6. Along-track bathymetry, used as the upper surface of the source layer, is shown below the model, and beneath that are spreading rates. Selected reversal anomalies from the timescale of Cande and Kent (1995) are annotated. Inset at top: location of ship tracks in this figure (segment W6) and Figure 2.16 (segments W1–W5).

segments are solely in crust of the Antarctic plate after subduction of the Phoenix ridge crest.

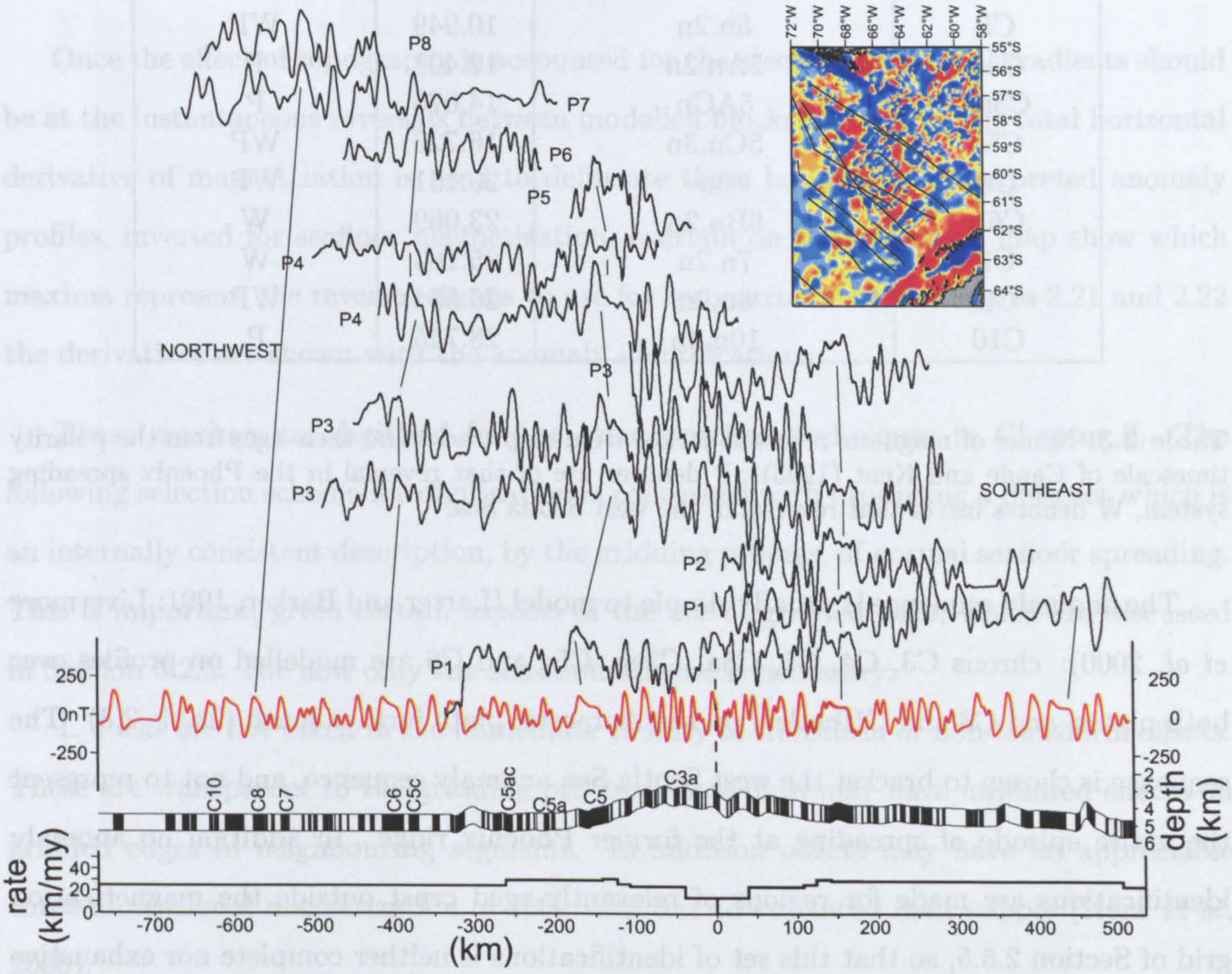

Figure 2.18: Ship track anomalies in the Phoenix–Antarctic spreading regime segments P1–P8 (black) compared to a modelled profile (for the sequence in P1, red). Along-track bathymetry, used as the upper surface of the source layer, is shown below the model, and beneath that are spreading rates. Selected reversal anomalies from the timescale of Cande and Kent (1995) are annotated.

Model chron	Cande and Kent (1995)	Age(Ma)	Used in system
C3	3n.4n	5.230	P
C4	4n.2n	8.072	P
C5	5n.2n	10.949	WP
C5a	5An.2n	12.401	P
C5ac	5ACn	14.076	P
C5c	5Cn.3n	16.726	WP
C6	6n	20.131	WP
C6b	6Bn.2n	23.069	W
C7	7n.2n	25.183	W
C8	8n.2n	26.554	WP
C10	10n.2n	28.745	P

Table 2.3: Names of magnetic reversals picked from ship tracks and their ages from the polarity timescale of Cande and Kent (1995). P denotes use of that reversal in the Phoenix spreading system, W denotes use of that reversal in the west Scotia Sea.

The anomaly sequence is usually simple to model (Larter and Barker, 1991; Livermore *et al*, 2000): chrons C3, C4, C5, C5a, C5ac, C5c and C6 are modelled on profiles over both plates, and C8 and C10 solely on the Antarctic plate further south (Table 2.3). The sequence is chosen to bracket the west Scotia Sea anomaly sequence, and not to represent the entire episode of spreading at the former Phoenix ridge. In addition no anomaly identifications are made for regions of relevantly-aged crust outside the magnetization grid of Section 2.6.5, so that this set of identifications is neither complete nor exhaustive with respect to spreading at the Phoenix ridge.

2.6.5 Seafloor magnetization grid

The inverted for grids of seafloor magnetization in the west Scotia Sea and Phoenix spreading region are shown in Figures 2.19 and 2.20. The transformation shows many of the seafloor spreading anomalies to be linear that appear more complicated as total field anomalies. This is to be expected as the inversion is intended to remove topographic effects. In addition the band-pass filter (applied to stabilise the inversion) will have removed some of the noise from other sources (*e.g.* gridding oscillations or noise from

acquisition). The inversion requires no *a priori* information explicitly regarding what the anomaly strike should be, and no directional filtering is applied at any stage; the linearity is not a result of over-zealous processing.

Once the effect of topography is accounted for the steepest horizontal gradients should be at the instantaneous reversals between modelled blocks of crust; so the total horizontal derivative of magnetization is used to delineate these boundaries. Interpreted anomaly profiles, inverted for seafloor magnetization, overlain on the derivative map show which maxima represent the reversal chrons to use for reconstructions. In Figures 2.21 and 2.22 the derivatives are shown with the anomaly identifications.

These maxima are digitized for the reconstruction techniques in Chapter 3. The following selection scheme for digitisation is concerned with producing a data set which is an internally consistent description, by the gridding process, of normal seafloor spreading. This is important, given certain aspects of the use of gridded data, which are discussed in Section 3.2.3. For now only the selection scheme is necessary:

1. Picks are not taken in the immediate vicinity of transform or non-transform offsets. These are transparent to the gridding process: some data may have unwanted effects on gridded edges in neighbouring segments. In addition offsets may have an appreciable three-dimensional magnetization of their own due to enhanced melt supply (Kent *et al*, 2000).

2. Picking is not undertaken further than 8 km (the likely uncertainty in ship track data) from ship track control.

3. No single edge or length of edge whose strike deviates from that of the set of edges in a segment is picked unless its conjugate deviates similarly. If such deviation is suspected to be a gridding artefact then edges with conjugates may also be discarded, depending on whether other data are available for the same chron.

4. Picks are made each 3-4 km along maxima so that no bias is introduced except to data from well defined, continuous, edges in the grid.

5. Three dimensional features such as seamounts (where identified) are not picked if

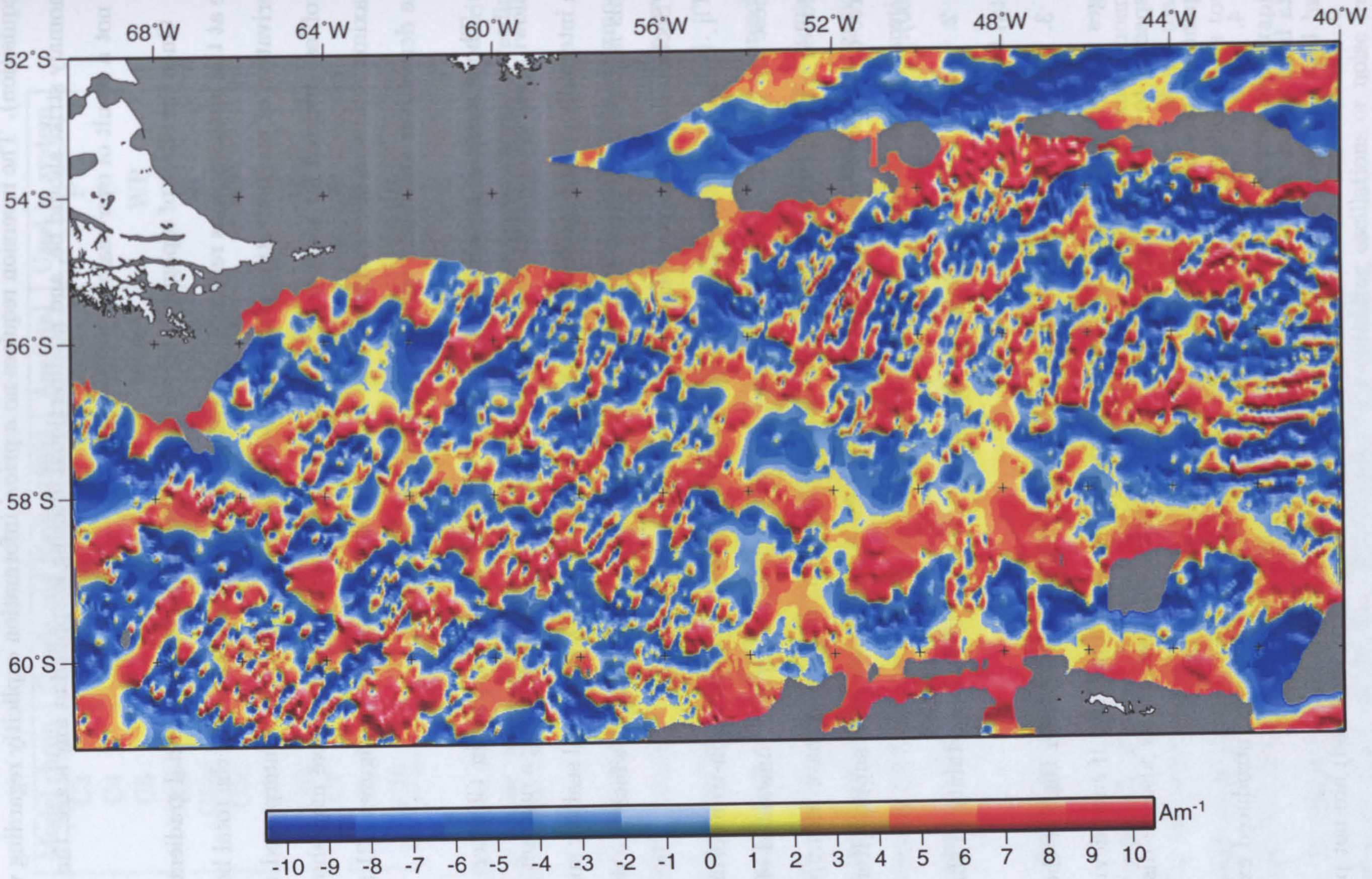

Figure 2.19: Mercator projection of the seafloor magnetization in the west Scotia Sea, modelled from total field anomalies in the presence of bathymetry. Grey areas: the 2500 m bathymetry mask.

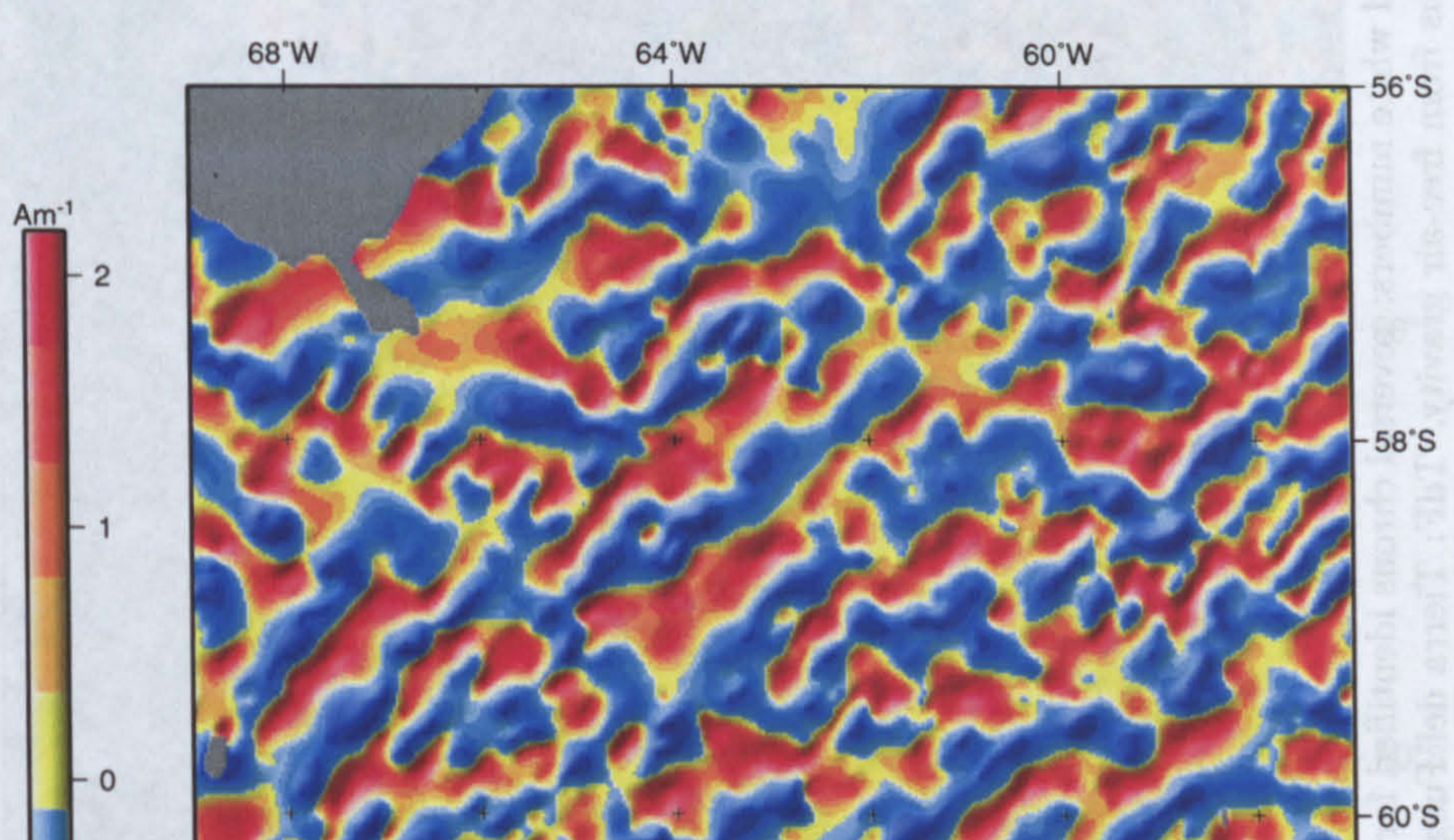

Figure 2.20: Mercator projection of the seafloor magnetization in some of the crust formed by the Phoenix spreading regime, modelled from total field anomalies in the presence of bathymetry. Grey areas: the 2500 m bathymetry mask.

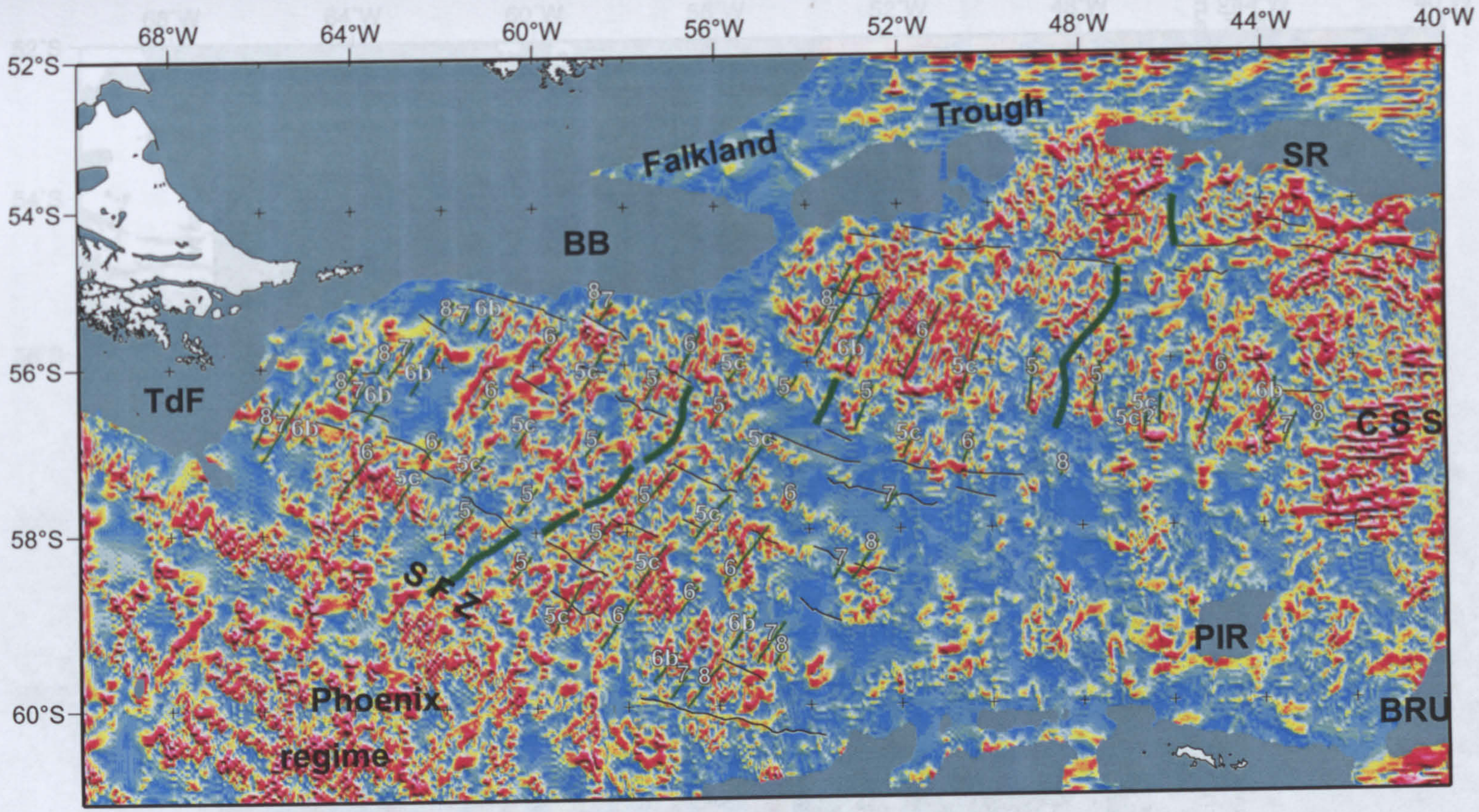

Figure 2.21: Mercator projection of the total horizontal derivative of modelled seafloor magnetization in the west Scotia Sea. Thin green lines and white numbers: reversal chrons identified for digitisation, thick green lines: ridge axis from free-air gravity, black lines: flowline troughs from free-air gravity. TdF: Tierra del Fuego, BB: Burdwood Bank, SR: Shag Rocks block, BRU: Bruce Bank, PIR: Pirie Bank, SFZ: Shackleton Fracture Zone, CSS: central Scotia Sea.

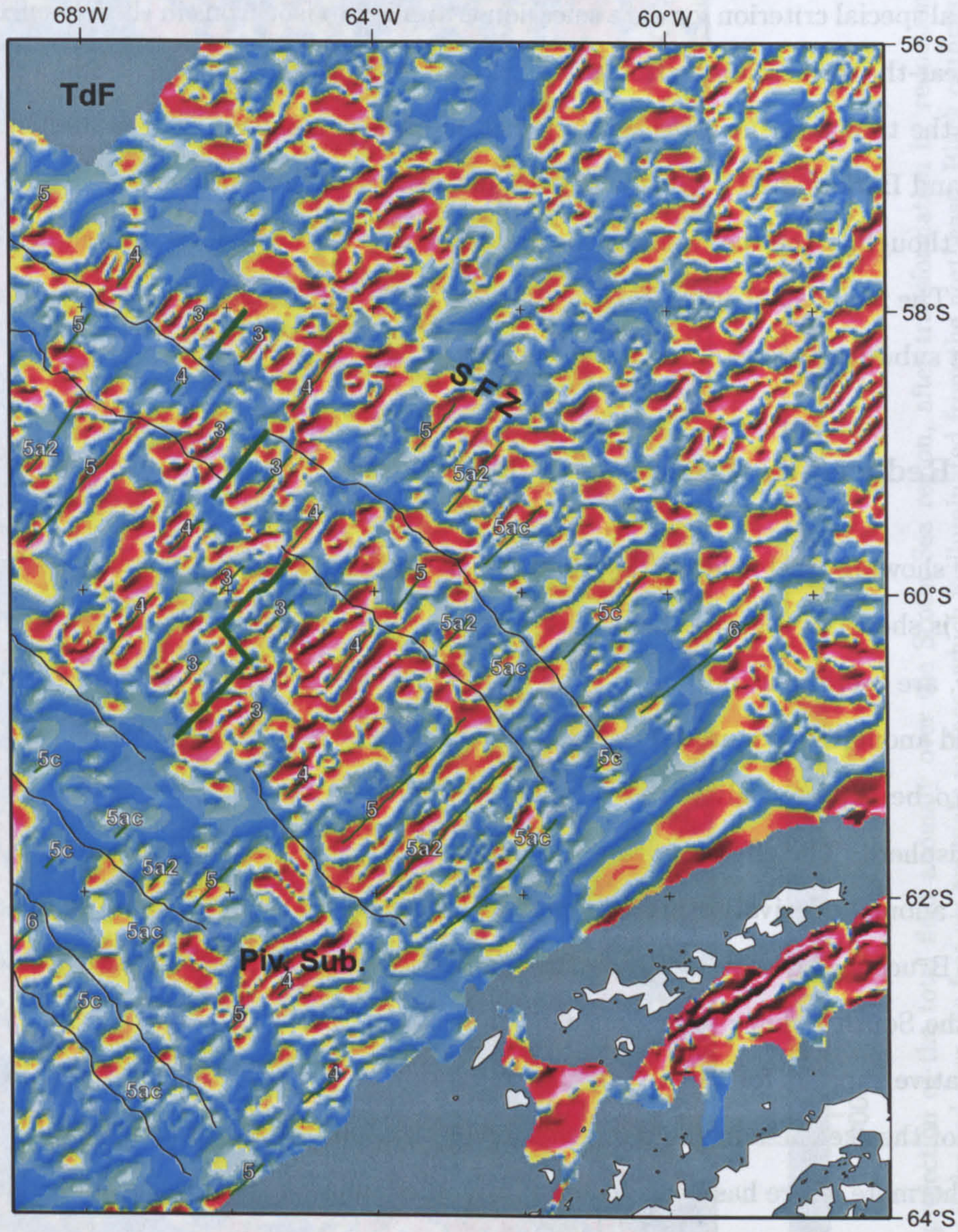

Figure 2.22: Mercator projection of the total horizontal derivative of modelled seafloor magnetization in the Phoenix spreading regime. Thin green lines and white numbers: reversal chrons identified for digitisation, thick green lines: ridge axis from free-air gravity, black lines: flowline troughs from free-air gravity, Piv. Sub.: area of pivoting subduction, SFZ: Shackleton Fracture Zone, TdF: Tierra del Fuego.

their modelled magnetization causes deviation to a chron edge.

A final special criterion for data selection is applied to isochrons in the Phoenix system. In P4, near the former subduction zone, gridded magnetization isochrons appear to bend towards the trench in the direction (northeast) of increasing age of the subducting plate (Larter and Barker, 1991). This is a consequence of pivoting subduction (Menard, 1978) which is thought to be the result of the greater slab pull force where the subducting crust is older. The fan-shaped accretion is a localised phenomenon, so data describing accretion behind a subduction zone pivot are discarded.

2.6.6 Reduced to the pole total field grid

The grid showing total field anomalies in the Scotia Sea region, de-skewed by reduction to the pole is shown in Figure 2.23. Areas of continental crust, as defined from the Bouguer anomaly, are overlain as outlines on the map to aid interpretation. Comparison with raw total field anomalies (Figure 2.7) reveals the phase effect of reduction to the pole is small. This is to be expected given the region's proximity to the magnetic pole in the southern hemisphere. The effect appears to align edges of some magnetic anomalies with the Bouguer anomaly derivative maxima picked in Section 2.6.2, for example at the southern edges of Bruce and Discovery Banks, the South Scotia Ridge, and the southeastern margins of the South Orkney Microcontinent and South Shetland Islands. This observation is qualitative support for the notion that reduction to the pole has succeeded in removal of some of the skewness in the remanent magnetization of the causative bodies, because, and furthermore, there has been no great latitudinal movement of these bodies since their formation.

Anomalies with established causes

Over continental areas the wide, linear, high-amplitude Pacific Margin Anomaly of the Antarctic Peninsula, and its continuation onto the South Shetland Islands, South Scotia Ridge and South Orkney Microcontinent is prominent. Where exposure is available this

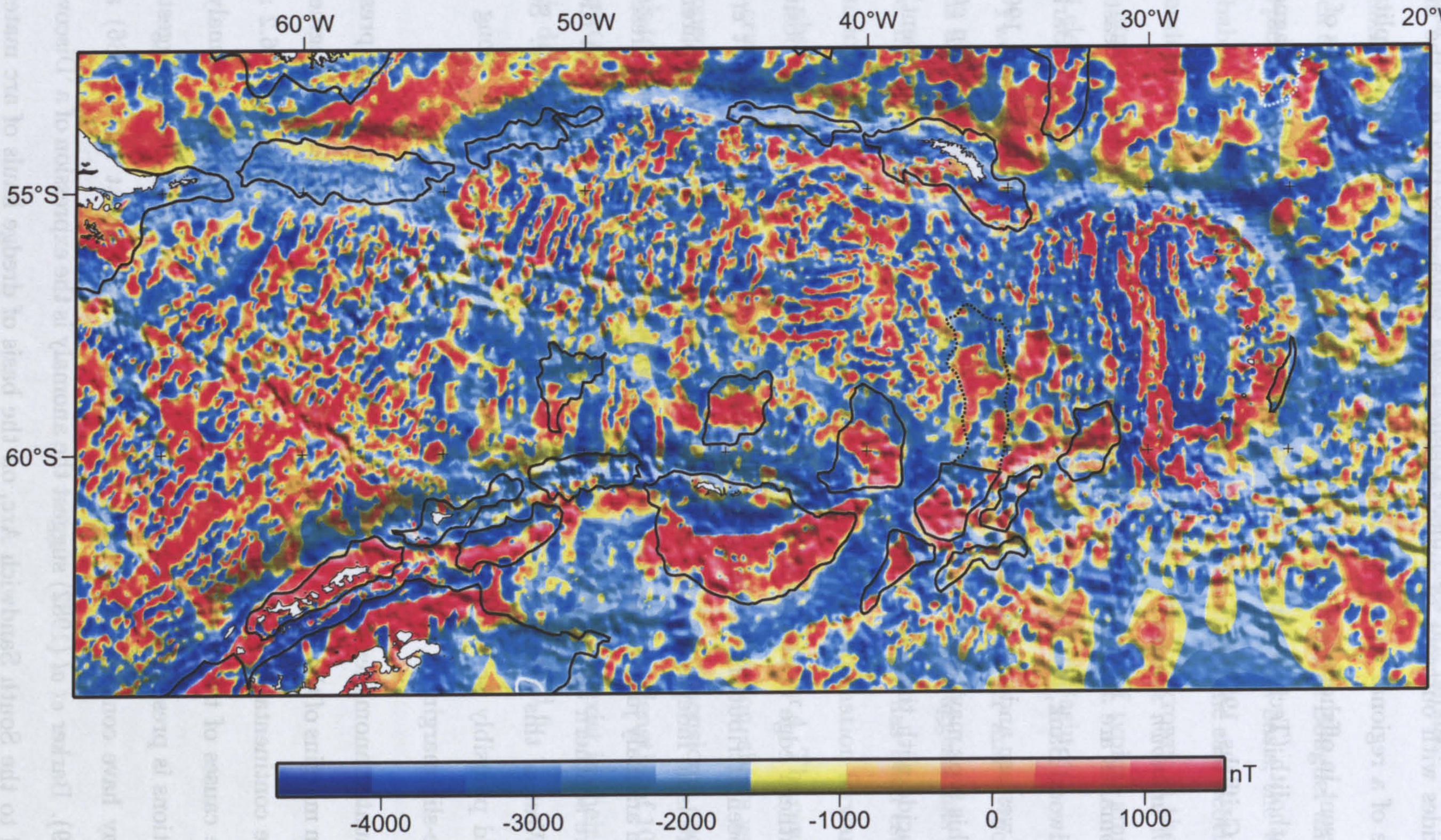

Figure 2.23: Mercator projection of the total field anomaly over the Scotia Sea region, after transformation by reduction to the pole. Anomalies shown as if draped over the free-air anomaly surface, which is illuminated from the northeast. Black outlines are the Bouguer anomaly highs of Section 2.6.2. Dotted outline: relative Bouguer high extending north from Discovery Bank.

anomaly coincides with outcrops of mafic igneous rocks, suggesting that it is the magnetic signature of a regional batholith (Leat *et al*, 1995). Another wide high-amplitude anomaly is present in offshore Tierra del Fuego, along strike from mapped outcrops of the Patagonian batholith (Tectonic map of the Scotia arc, 1985) which is strongly magnetic (Simpson and Griffiths, 1982).

Anomalies with unknown sources

Prominent anomalies are associated with the regions of transitional crust at the eastern margin of Burdwood Bank, the southeastern margin of the Falkland Islands Block (Barker, 1999), and the western and eastern margins of Powell Basin (Eagles and Livermore, 1999). Anomalies of this type may be related to volcanism during crustal stretching (Larsen *et al*, 1994) and coincide with the relative isostatic residual anomaly highs (where present) of Section 2.6.3.

At the southern edge of the South Georgia continental block a prominent positive anomaly has been attributed to a batholith (Simpson and Griffiths, 1982; Garrett *et al*, 1986), but there is no independent evidence for such a cause. This anomaly is apparently continued as an anomaly just to the south of the Shag Rocks block, completing its presence along the entire southern edge of the North Scotia Ridge east of the West Scotia Ridge axis in W7. West of this axis the North Scotia Ridge is not strongly magnetic. Such a pattern could plausibly be related to the presence or absence of volcanism along the northern strike-slip margins of the growing west Scotia Sea.

More attenuated anomalies all with similar ($\sim$ 80 km) width across strike are present on the southern margins of the Bruce and Pirie banks and the Terror block. The fragments are likely to be continental (Toker *et al*, 1991; Mao and Mohr, 1995; Sections 2.6.2 and 2.6.3), but the causes of the anomalies have never been speculated on. An anomaly of similar proportions is present over the wide southern part of Discovery Bank, suggesting that it too may have continental affinities, as speculated by Garrett *et al* (1986) and Hamilton (1989). Barker *et al* (1982) suggest the anomaly is the expression of a 'Discovery Arc', ancestral to the South Sandwich Arc, on the basis of dredge hauls of arc material

further to the northeast, where the anomaly itself does not persist.

Oceanic crust

Much of the region's oceanic crust, as defined by high positive Bouguer anomalies, shows a typical linear magnetic reversal anomaly character. On this basis, the west Scotia Sea probably includes the crust beneath Aurora Bank. Similarly, the east Scotia Sea probably extends from the South Sandwich Islands to 35°W, and is narrower in the south than in the north. Smaller areas showing reversal-type anomalies (of typical amplitude, width, and elongation) are evident in Protector Basin and in Dove Basin.

Two departures from the agreement between the Bouguer and reduced to the pole grids are apparent. Powell Basin, whose Bouguer anomaly suggests has an oceanic nature, has no apparent reversal anomalies. Its oceanic nature has been established using seismic reflection techniques (King *et al*, 1997), and an explanation forwarded to explain the absence of reversal anomalies, as will be outlined in Chapter 4. The central Scotia Sea, the crustal nature of which the Bouguer anomaly is equivocal on, shows very strongly developed east–west trending reversal anomalies. These two-dimensional anomalies, having peak-to-peak amplitudes typically exceeding 500 nT and wavelengths of 10–30 km, are almost certainly the result of seafloor spreading, but problems exist in their interpretation. This difficult area will be addressed further in Chapters 4 and 6.

Chapter 3

Reconstructions by joint inversion of isochrons and flowlines

Keywords Joint inversion. Isochrons. Flowlines. West Scotia Sea. Phoenix spreading system. Reconstruction poles.

3.1 Introduction

In this chapter I use an automated reconstruction technique for the margins of the spreading system in the west Scotia Sea and of the extinct Phoenix–Antarctic spreading system. Many plate tectonic reconstruction techniques rely on visual assessment of fits of reconstructed geological features and produce subjective results. Where enough good quality data can be amassed, mathematical techniques bring rigour and some objectivity to the endeavour.

Chapter 1 has shown how the Scotia Sea is a case in point where a number of visually-deduced fits are published within regional reconstructions. Because visual-fit reconstructions can not be assessed by formal uncertainties, different views of the formation of the Scotia Sea complex of basins have been able to co-exist in the literature. In particular,

reconstructions have presented the kinematics of the Scotia Sea plates:

1) As a multiphase back-arc region dominated by subduction dynamics (Barker *et al*, 1991; Barker, 1995),

2) As a complication of the South American–Antarctic plate boundary (Cunningham, 1993; Cunningham *et al*, 1995), and

3) because 1) and 2) are not necessarily mutually exclusive, as a hybrid system (Burrell, 1983).

In Chapter 2 I muster the data describing the west Scotia Sea and Phoenix–Antarctic seafloor spreading systems. Some of the magnetic data have been used previously for a mathematical analysis aimed at deriving plate tectonic reconstructions of the west Scotia Sea (Burrell, 1983), which closely resemble those published by Barker and Burrell (1977). Burrell's (1983) study suffers from unrealistic identification of flowlines by over-reliance on the use of sparse flowline magnetic profiles (Tectonic map of the Scotia arc, 1985), and, as in Barker and Burrell (1977) undue importance ascribed to the Shackleton Fracture Zone. The resulting reconstruction poles are poorly constrained (Figure 3.1) and the kinematic model unnecessarily complex. With gridded magnetic and satellite free-air gravity data, the opportunity arises for a more informed objective attempt at deriving reconstructions in the region. In this chapter I describe briefly the method used for two-plate reconstructions of the west Scotia and Phoenix systems. I present and discuss the data used, followed by the results of the method as applied to these data.

3.2 Two plate reconstructions in the Scotia Sea

Nankivell's (1997) iterative inverse method develops the joint inversion for isochron and flowline data of Shaw and Cande (1990). It defines magnetic residuals as displacements from a great circle rather than from a point on a circle (Figure 3.2). Residuals and partial derivatives for fracture zone data are also calculated in a simpler way. Inversion can be extended to three plate systems. Finally, the method allows use of data which have no

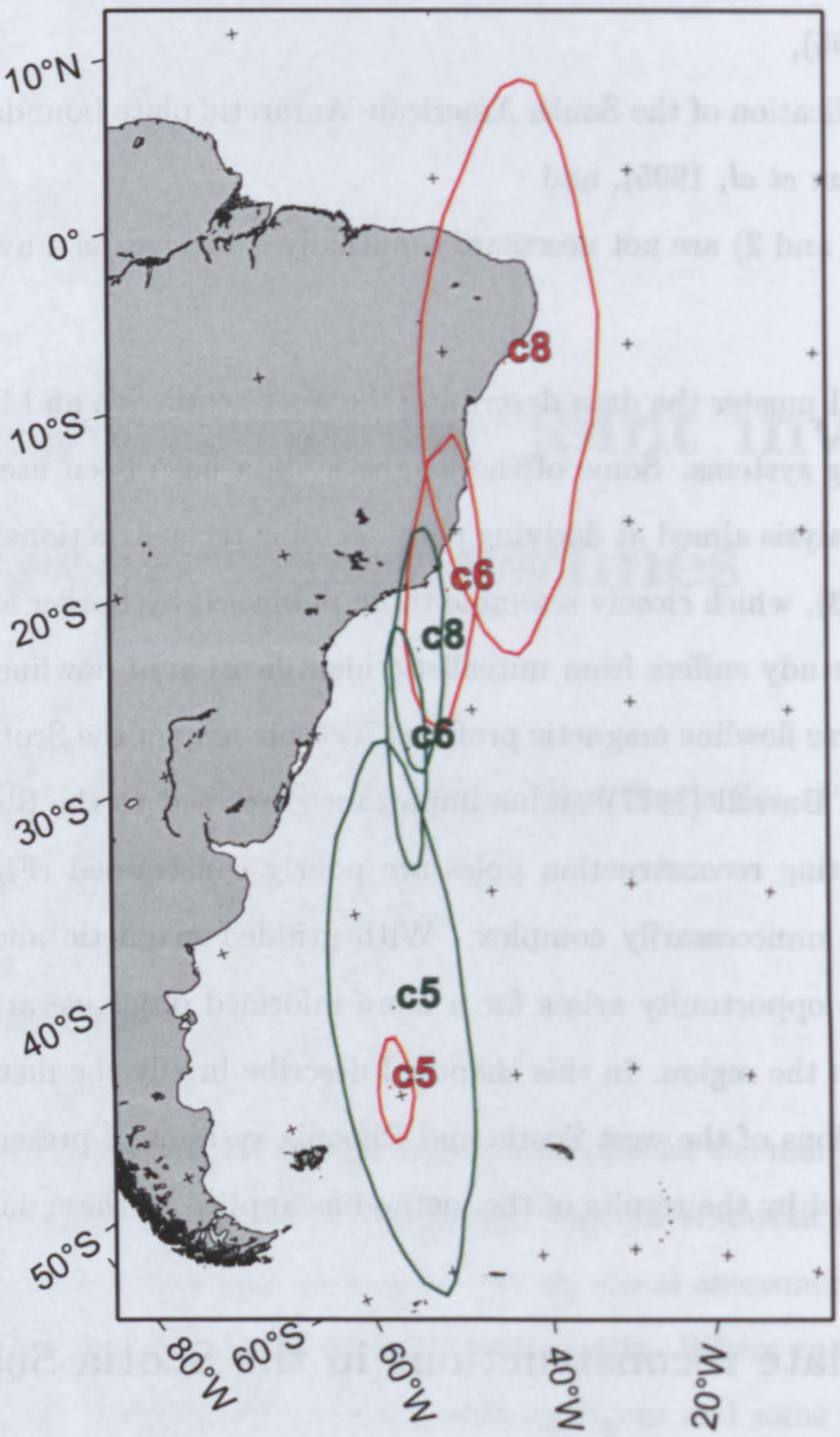

Figure 3.1: Reconstruction poles for the west Scotia Sea at anomalies C8, C6 and C5 derived from least-squares fitting of magnetic anomaly data (Burrell, 1983). A two plate (red) and three plate (green) model are presented. The ellipses (which have been digitised from a hand-drawn figure) are derived in a similar method to that used in this chapter, but define poles with low confidence due to the inadequate data set used and undue importance ascribed to the Shackleton Fracture Zone.

conjugate, for instance where data have been lost to subduction.

Here I deviate from Nankivell's method by using gridded model magnetization anomalies (Section 2.6.5) as opposed to picks from ship track profiles. This enables use of magnetic data from profiles which would be impractical to process for isochron picks due to their high angle to flowlines. A condensation of the description of the method for two-plate reconstructions, given in Nankivell (1997a) and Nankivell (1997b), follows. It is reproduced in greater detail in Appendix A.

3.2.1 Definition and calculation of residuals

A residual is the quantified difference between an observed datum and the model. It may take a positive or a negative value. Summation of the set of residuals gives a test criterion which the inverse method aims to minimise.

For magnetic isochron position data (picks) residuals are defined as the pick's displacement from the closest point on a target great circle (Figure 3.2). They are evaluated as the angular separation between the target great circle's pole and the rotated pick, minus ninety degrees. Target great circles are defined as the best fitting great circle to all picks in a 'target group' representing a single isochron in a single spreading segment. Data being rotated to target circles can be from the conjugate, or any non-conjugate, isochron on either ridge flank. Conjugate fitting is preferred because the solution is unaffected by spreading asymmetry or ridge jumps between conjugate isochrons. Non-conjugate fitting can not address asymmetric spreading using data from just one plate and may do so only incompletely with data from two plates.

For fracture zone picks residuals are defined as the pick's great circle distance from a model flowline. The flowline (Figure 3.3) is generated as a series of small circle segments about stage poles, calculated from the test finite poles, and emanating from a seed point. This seed point can be any isochron-intersection point along the flowline. A bad seed point could cause a systematic error in a flowline's residuals, so it is allowed to be perturbed

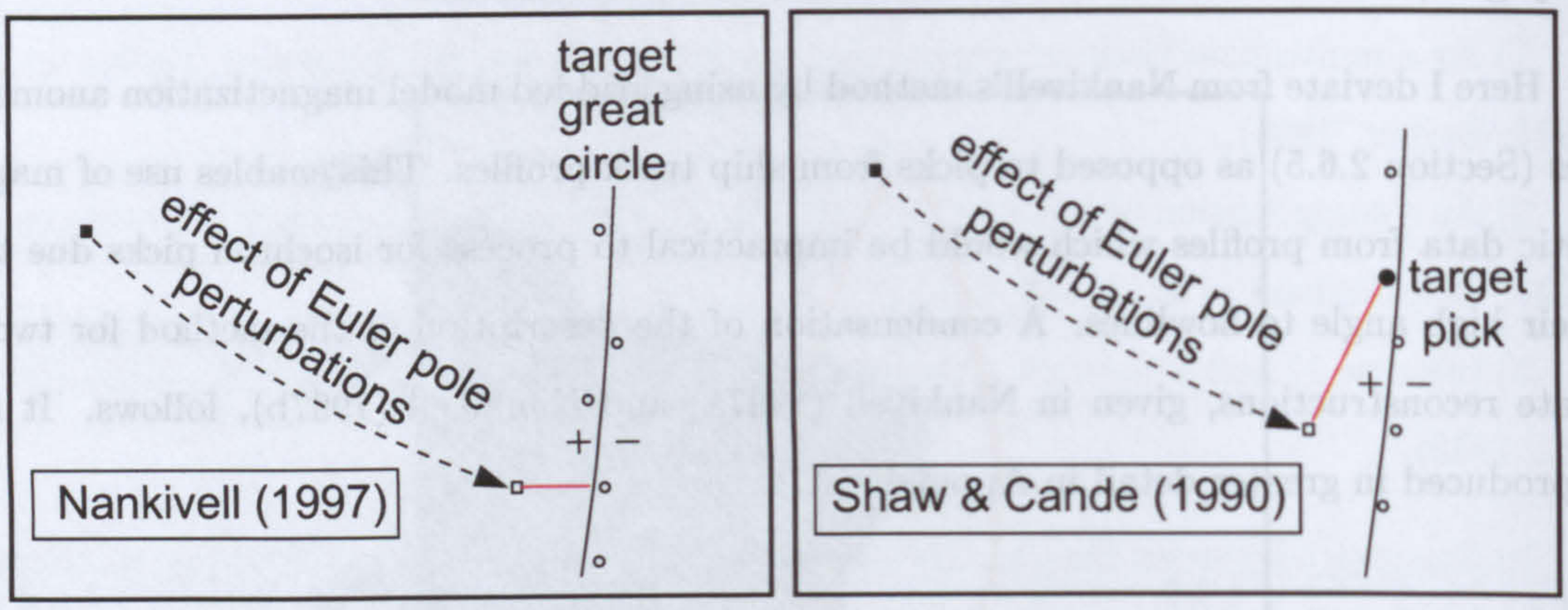

Figure 3.2: The definition of magnetic residuals used in the joint inversion scheme of Nankivell (1997a) as opposed to that used by Shaw and Cande (1990). Nankivell's method is more flexible in the case of a test rotation causing significant displacement of an isochron datum parallel to its target great circle. The rotating datum is shown by a square, the data used to define the target great circle are shown as circles.

slightly in order to minimize such error. Residuals are calculated as the angular difference between two small circles about the stage pole—one describing the flowline segment and the other containing the rotated pick. For picks of transform faults residuals are great circle displacements from the best fit small circle, about the test pole, to all the transform fault picks. This is evaluated as the difference between the colatitudes of the pick and the target small circle, using the current pole.

3.2.2 Partial derivatives, least squares and inversion

The method next takes partial derivatives of each residual with respect to perturbations to the Euler pole parameters (latitude λ, longitude ϕ, rotation angle θ). Each is a determination of how the residual would be changed by the perturbation to the next pole parameter.

Using a matrix of such partial derivatives, for all residuals with respect to all model

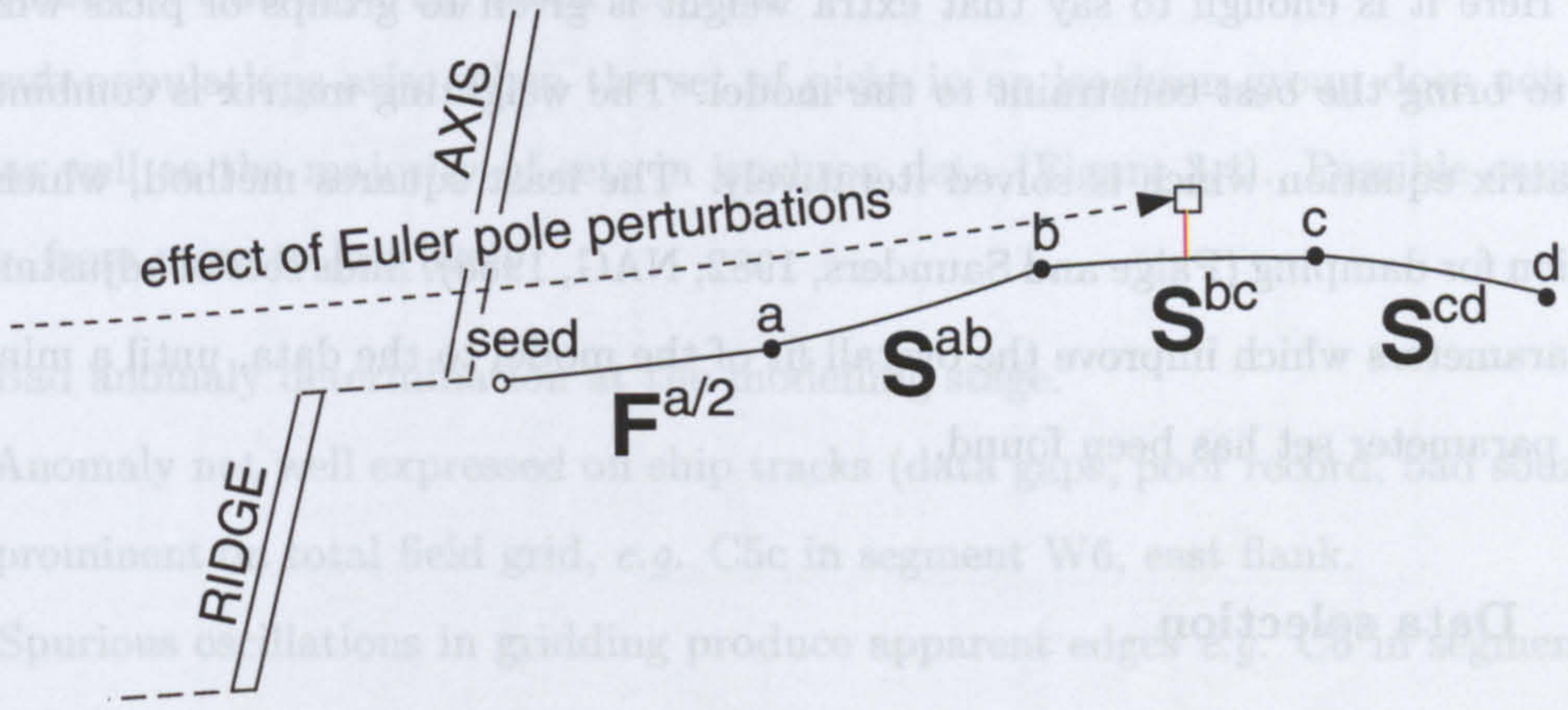

Figure 3.3: The definition of flowline residuals used in the joint inversion scheme of Nankivell (1997a). For the first flowline segment the small circle is about the first test reconstruction pole, and half a finite rotation in length. Subsequent sections are about stage poles calculated from the reconstruction poles; for instance $\mathbf{S}^{ab} = \mathbf{F}^{b/2}\mathbf{F}^{-a/2}$ (for notation see Appendix A).

pole parameters, a least squares procedure can determine changes to the model for minimising the set of residuals. The model parameters inverted for are a set of finite rotation poles each consisting of (λ, ϕ, θ). All residuals, from magnetic, fracture zone and transform fault data, and their sum, will equal zero for a perfect description of the observed data. The technique assumes that residuals generated by imperfect pole parameter sets differ only slightly from those generated by a perfect set in order to approximate a linear least-squares problem. The detail of the derivation of partial derivatives, and their incorporation into a working scheme by this assumption, is given in Appendix A.

Inversion

To combine all partial derivatives for the data sets (magnetics, fracture zones and transform faults), equally they are normalised by dividing each by its own uncertainty, the pick sets' standard deviations. A combined matrix of all these normalized partial derivatives and a normalised vector of residuals are incorporated into the inversion equation (Appendix A) to give a matrix equation which is used to perform the inversion.

Prior to inversion a weighting scheme is used to mitigate the effects of poor quality

data. Here it is enough to say that extra weight is given to groups of picks which are likely to bring the best constraint to the model. The weighting matrix is combined into the matrix equation which is solved iteratively. The least squares method, which has a provision for damping (Paige and Saunders, 1982; NAG, 1985), finds sets of adjustments to pole parameters which improve the overall fit of the model to the data, until a minimised stable parameter set has been found.

3.2.3 Data selection

Isochron data

The isochron data set inevitably contains outliers which can bias the reconstruction. To combat needless, and detrimental, inclusion of such compromised picks all data whose residuals exceed a cutoff criterion, Γ, are disregarded. A suitable value for Γ is chosen by looking at q-q (quantile-quantile) plots of the magnetic data (Shaw and Cande, 1990; Nankivell, 1997a; Kirkwood *et al*, 1999). A quantile $Q(p)$ is the value below which a fraction p, of data, lies. Given a hundred data each quantile is a percentile. The q-q analysis plots quantiles of the residuals against those of a Gaussian distribution with zero mean and standard deviation of one. Assuming the set of reliable residuals is normally distributed the q-q plot has gradient equal to the standard deviation of the residual set, and intercept equal to its mean value. The q-q plot deviates from a straight line where outliers become significant. Γ is a multiple of standard deviation chosen in order to ignore these outliers. The need to remove outliers is particularly important for reconstructions of the west Scotia Sea. Here the plate boundary is short and the influence of compromised data is potentially much higher than for a longer boundary.

When using gridded data normal distribution of errors can not be assumed for the residual set as a whole. As a result outliers occur as members of sub-populations. Broadly, two classes of sub-populations are evident from q-q analysis of isochron residuals. In the first class the mean residual differs from that of the main population. In the second class the standard deviation of the sub-population differs.

Sub-populations with differing mean residual

These sub-populations arise when the set of picks in an isochron group does not fit its target as well as the majority of sets in isochron data (Figure 3.4). Possible causes for this are, from more to less likely:

1. Bad anomaly determination at the modelling stage.

2. Anomaly not well expressed on ship tracks (data gaps, poor record, bad source) so is not prominent on total field grid, *e.g.* C5c in segment W6, east flank.

3. Spurious oscillations in gridding produce apparent edges *e.g.* C6 in segment W3, west flank.

4. Anomaly expression lost or suppressed by filter prior to magnetization inversion.

5. Picks belong in another spreading segment.

6. Large ridge jumps in segment.

7. Intra-plate deformation distorts anomalies (Wilson, 1993; Cunningham, 1993).

8. Anomalous skewness.

Some outlier populations originating from bad anomaly determinations are eliminated by reinterpretation of block models after early inversions. Problems of identification error must be present in inversions run on profile data alone but are not evident since they do not give rise to populations of residuals. By using data digitised from grids it proves possible to be able to address the worst of identification difficulties and salvage data. This is a further advantage in the use of isochron data from grids.

The remaining outlier populations seem most likely due to failure of the gridding or magnetization modelling processes to resolve isochron edges in regions of sparse or compromised data. This is a specific problem when using gridded isochron data. It imparts an *en echelon* segmentation to the q-q plot (Figure 3.4). In q-q analysis, *en echelon* sets with a mean differing by less than 8 km are not considered significant variance in the residual set, because they fall within the adopted navigational uncertainty. This uncertainty is a formal constraint on the accuracy of the inversion; removing such data does not have a beneficial effect on the solution.

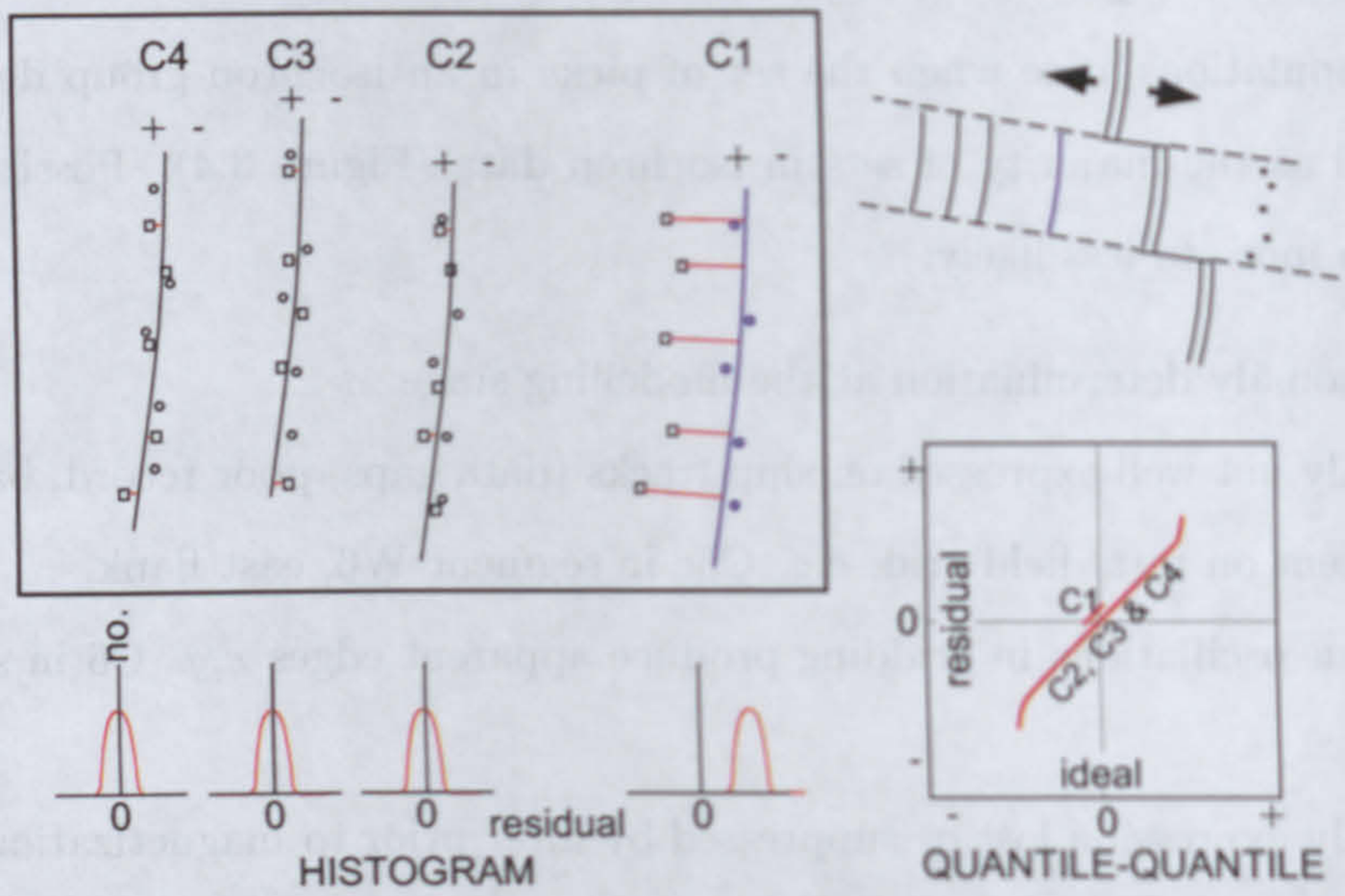

Figure 3.4: At top: the source of an outlier population having a different mean in an isochron (C1) fitting not as well as the rest of the isochrons (C2–C4) in the inversion. The same effect is achieved when the target data are used instead to generate residuals. Histograms for each isochron are shown at the bottom. The effect of the outlier population in a q-q analysis of the residuals—*en echelon* segmentation—is shown at bottom right.

Sub-populations with differing standard deviation

The most likely source of sub-populations with anomalous standard deviation is an isochron pick set and target great circle which are not co-polar, *i.e.* they have a different strike (Figure 3.5). The different standard deviations (steeper q-q gradients) give rise to a facetted q-q plot. It is difficult to envisage how single isochrons with unusual strike could be produced by seafloor spreading. These sub-populations are likely to arise out of the following, from more to less likely:

1. Gridding in the presence of sparse data or impertinent data.
2. Merging of a 'staircase' of anomalies and short non-transform offsets during gridding.
3. Off-axis volcanism distorting a pre-existing magnetization or anomaly.
4. Post-emplacement deformation of seafloor (Cunningham, 1993).

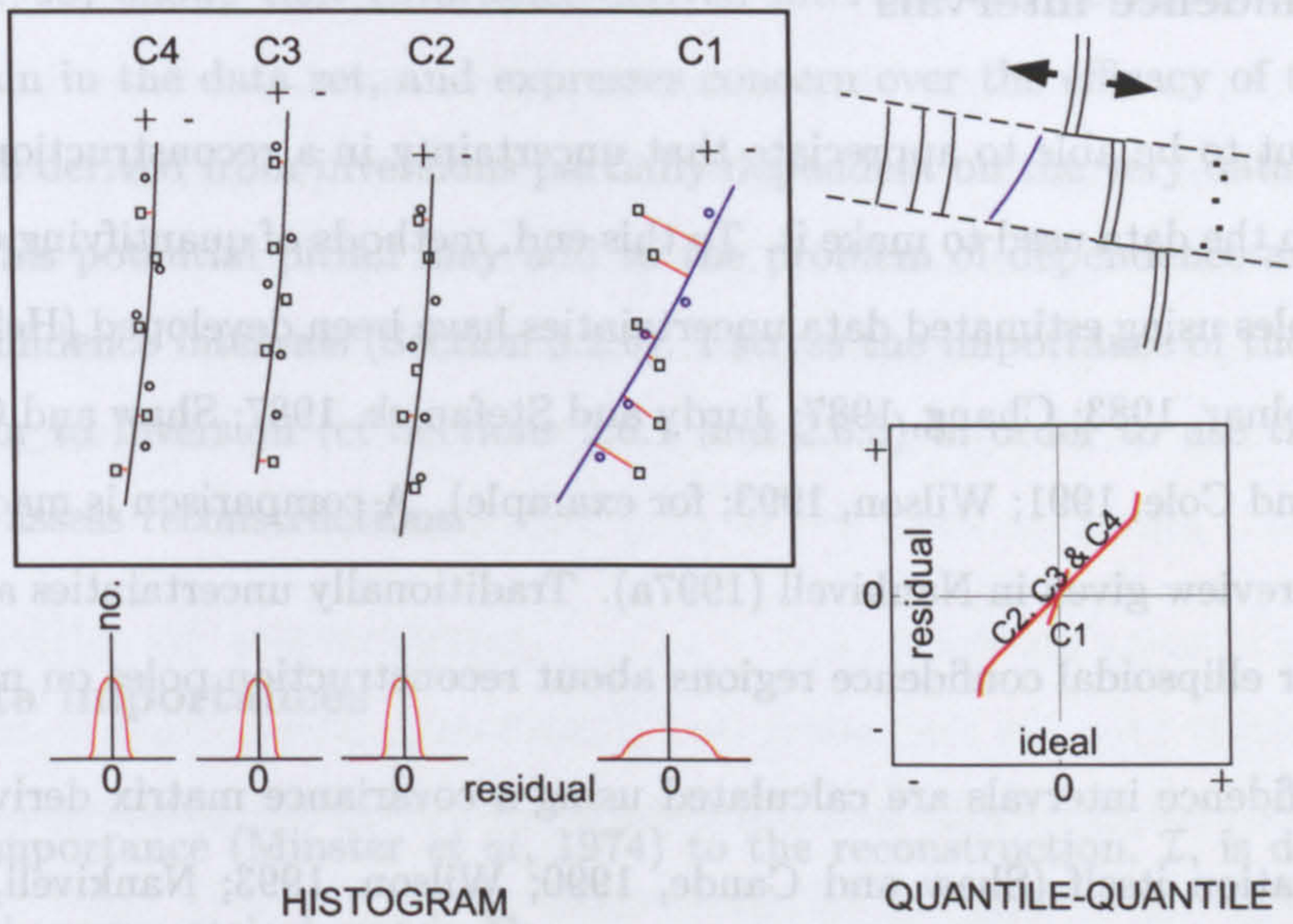

Figure 3.5: At top: the source of an outlier population having a different standard deviation in a target great circle (C1) not being co-polar with the rest of the targets (C2–C4) in the inversion. The same effect is achieved when the target data are used instead to generate residuals. Histograms for each isochron are shown at the bottom. The effect of the outlier population in a q-q analysis of the residuals—facetting—is shown at bottom right.

None of these is pertinent to the process of making reconstructions used here. Active selection against sub-populations with anomalous standard deviation is practised, although data which are compromised in this way are preferable to no data at all.

Fracture zone and transform fault data

Just two criteria were used for the selection of fracture zone and transform fault data: the presence of a trough exceeding 30 km length as part of an apparently co-polar set. As a result outliers are less inherent in these residuals, leading to larger Γ. The main difficulty lies with the possibility of a partial or complete fracture zone or transform fault locus not being representative of spreading. A scheme for consideration of each trough as a member of a set of troughs was described in Section 2.6.1, at the fracture zone picking stage. In q-q analysis any surviving trough not co-polar with the main set should give rise to facetting, allowing the offending feature to be discarded.

3.2.4 Confidence intervals

It is important to be able to appreciate that uncertainty in a reconstruction arises from uncertainty in the data used to make it. To this end, methods of quantifying uncertainties in solution poles using estimated data uncertainties have been developed (Hellinger, 1981; Stock and Molnar, 1983; Chang, 1987; Jurdy and Stefanick, 1987; Shaw and Cande, 1990; Richardson and Cole, 1991; Wilson, 1993; for example). A comparison is made by Wilson (1993) and a review given in Nankivell (1997a). Traditionally uncertainties are presented as elliptical or ellipsoidal confidence regions about reconstruction poles on maps.

Here, confidence intervals are calculated using a covariance matrix derived from the inversion equation itself (Shaw and Cande, 1990; Wilson, 1993; Nankivell, 1997a). A correlation matrix of partial derivatives:

$$\left[\hat{\mathbf{A}}^{\top}\hat{\mathbf{A}}\right]_{ij} = \frac{\partial\hat{\epsilon}_k}{\partial p_i}\frac{\partial\hat{\epsilon}_k}{\partial p_j} \tag{3.1}$$

relates changes in the normalised residuals ($\hat{\epsilon}$) to pole parameter perturbations (p). Its inverse is the covariance matrix

$$\mathbf{C} = \left[\hat{\mathbf{A}}^{\top}\hat{\mathbf{A}}\right]^{-1}. \tag{3.2}$$

By definition, for uncertain solutions, close-neighbour pole parameter sets do not cause large changes in residuals. The resulting low value of $\hat{\mathbf{A}}^{\top}\hat{\mathbf{A}}$ in that neighbourhood means a high value of $\mathbf{C}$. This shows how (assuming the problem function is linear in the region of the solution) the covariance matrix can relate uncertainties in the poles from uncertainties in the data.

The 3×3 submatrices for each individual pole can be extracted from the covariance matrix. The submatrices' eigenvectors represent the semimajor axes of their confidence ellipsoids in three dimensional parameter space, once their longitudinal (small circle) aspects have been converted to great circle distances. The ellipsoid's magnitude can be defined with χ^2 tables. Alternatively, assuming a fixed angle of rotation, 2×2 submatrices for each pole can similarly define a confidence ellipse for the pole's map position.

Wilson (1993) shows that covariance-derived intervals can be misleadingly small if outliers remain in the data set, and expresses concern over the efficacy of their removal with q-q plots derived from inversions partially dependent on the very data they seek to eliminate. This potential pitfall may add to the problem of dependence and underestimation of confidence intervals (Section 3.2.6). I stress the importance of thoughtful data selection prior to inversion (cf Sections 2.6.1 and 2.6.5) in order to use the covariance technique to assess reconstructions.

3.2.5 Data importances

A datum's importance (Minster *et al*, 1974) to the reconstruction, $\mathcal{I}$, is defined on the diagonal of the symmetrical matrix $\mathbf{P}$:

$$\mathbf{P} = \mathbf{A}(\mathbf{A}^\top\mathbf{A})^{-1}\mathbf{A}^\top \tag{3.3}$$

where $\mathbf{A}$ is the normalised and weighted partial derivative matrix. Hence, and since only the diagonal of $\mathbf{P}$ is needed, the importance of the i^{th} datum, $\mathcal{I}_i$, is defined at $\mathbf{A}_i$, the i^{th} row of $\mathbf{A}$:

$$\mathcal{I}_i = \mathbf{A}_i(\mathbf{A}^\top\mathbf{A})^{-1}\mathbf{A}_i{}^\top. \tag{3.4}$$

Each importance value is positive and measures how changes in the datum correlate with the stability of the reconstruction. Uncertainty in an important datum is strongly linked to uncertainty in reconstruction with respect to the linkage of less important data. It is therefore desirable that important data be confidently identified.

3.2.6 Use of gridded data

Use of gridded magnetic data has been unavoidable for inversions in this chapter. This is a significant departure in quantitative reconstruction techniques, and the issues associated with it have been approached piecemeal so far. A summary of those issues is given here, which is intended neither to be exhaustive nor rigorous.

Advantages of using gridded data

1. Allows use of all available ship track data, as a result:

a) highlights outliers in q-q analysis, as members of groups, and enables the possibility of reinterpreting those data;

b) the importance of the assumption of normal distribution of data is lessened as the number of data is much greater than the number of segments (Kirkwood *et al*, 1999).

2. Potentially eliminates error due to poor segment assignment.

Disadvantages of using gridded data

1. Unavoidably breaches the assumption of stochastic independence of data (*i.e.* that errors should not be predictable as members of a population (Kirkwood *et al*, 1999)). As a result of the greater numbers of correlated data:

a) calculated rotation uncertainties may be underestimated if the number of 'good' data greatly exceeds the number of features they describe, and

b) the calculated reconstruction poles may be susceptible to inappropriate 'bad' data introduced by the gridding process.

The selection criteria of Sections 2.6.1 and 2.6.5 are concerned with trying to make sure that dependence does not give rise to influential volumes of inappropriate data. It is to be hoped that further selection by q-q analysis is effective as a second line of defence. Whether or not dependence gives rise to underestimated rotation uncertainties in this chapter has not been tested. Such a test might be made either by using a different method to the covariance technique to calculate rotation uncertainties, or by altering the data set's volume and, somehow, its character so that it resembles data derived from profiles.

3.3 Data preparation and formatting

Some final editing may be desired before compiling all the input data in the formats used by the inversion suite. An interactive program by Nankivell—*xsortdata*—enables the full

data set to be viewed at once and, if necessary, edited. After this, magnetic data are pre-processed using the inversion-suite program *magprepro*, which formats them, calculates a starting set of target great circles, and calculates some of the parameters used for the weighting scheme. At this stage the instruction is given to undertake conjugate or non-conjugate fitting. Fracture zone and transform fault data are ready to use in the same format used by *xsortdata*.

3.4 Results of inversions

Results from inversions of the Scotia Sea region seafloor spreading data are presented in this section. I begin with results from the west Scotia Sea spreading centre, and explain why it is necessary to separate the data into two sets for more meaningful results to be obtained. Following this I present the results for the southern and northern parts of the west Scotia Sea system. Immediate implications are highlighted at this stage, but further discussion is reserved for a later chapter. Finally I present the results from the Phoenix-Antarctic spreading system.

Inversion Procedure

Uncertainty in input data is a formal constraint on the least squares procedure (Paige and Saunders, 1982; NAG, 1985). It is expressed as a single value, in essence the number of significant figures to which the data may be deemed reliable, for all data in the control file *inv.dat*. The 8 km navigational uncertainty (Section 2.4.1) is between the third and fourth significant figures for the Scotia Sea, formatted as latitude (-90–90°), longitude (-180–180°), as is the ±5 km uncertainty in satellite fixes of fracture zone troughs (Müller *et al*, 1991). I assume that all latitude–longitude data are accurate to three significant figures.

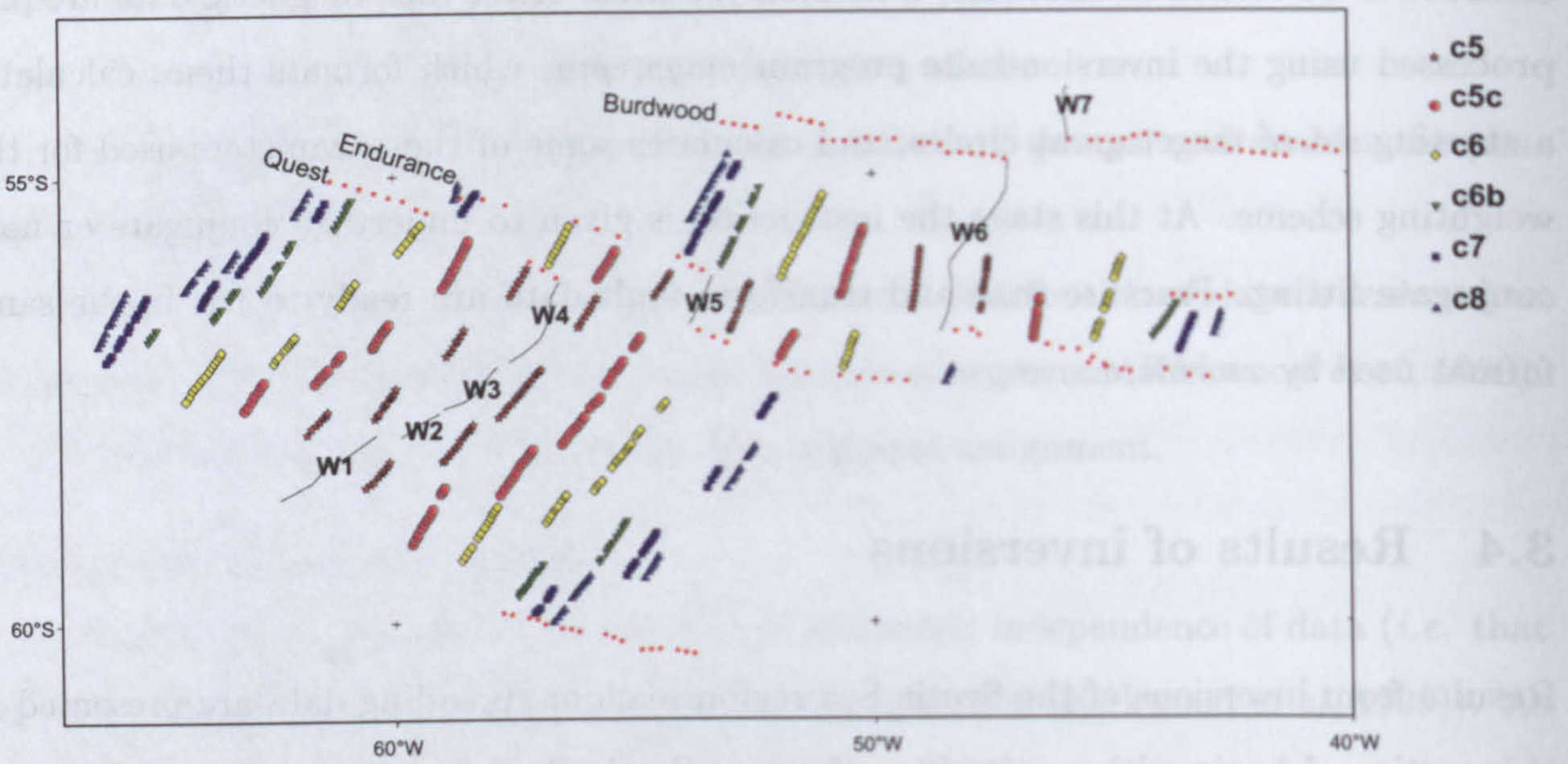

Figure 3.6: The data set used in inversion for reconstruction poles in the west Scotia Sea. Coloured symbols with black outlines locate picks of magnetic reversal anomalies. Smaller, unenclosed, red stars locate picks along tectonic flowlines. The West Scotia Ridge crest is shown by a black line.

3.4.1 West Scotia Sea - full data set

The full data set of magnetic and fracture zone data used in the entire west Scotia Sea is shown in Figure 3.6. Details of its acquisition are given in Chapter 2.

I apply the inversion procedure following Nankivell (1997a). Conjugate fitting is applied wherever possible. Where conjugate pairs are not identifiable this is due to absence of information on the grid as described in Sections 2.6.5 and 3.2.3. For these isochrons it is necessary to use non-conjugate fitting. In weighting, no simple overt bias towards any data set is applied. This inversion uses the three definite fracture zone traces: the Quest, Endurance and Burdwood Fracture Zones, and—in order to include flowline data from along the entire length of the West Scotia Ridge—the trough feature branching off the Shackleton Fracture Zone on the eastern flank. The cutoff criteria, Γ, are set to $\pm 5\sigma$ for the first ten iterations (this value results in the weighting subroutines being disregarded) in order to drive the solution quickly to a pole that satisfies the majority of the data. An

Chron	Age (Ma)	Latitude	Longitude	Angle	95% confidence ellipsoid, degrees			
					Axis 1	Axis 2	Axis 3	Azimuth
C5	10.95	68.35	-13.19	1.22	1.07	0.38	0.012	68.8
C5c	16.73	45.16	-10.36	2.51	7.44	0.42	0.010	68.4
C6	20.13	44.78	-26.05	3.71	2.46	0.20	0.008	75.7
C6b	23.07	52.28	-23.82	5.55	1.79	0.11	0.016	74.5
C7	25.18	53.38	-23.44	6.24	1.95	0.13	0.014	74.5
C8	26.55	53.28	-23.30	6.59	2.03	0.21	0.013	73.1

Table 3.1: Solution finite poles for the entire west Scotia Sea inversion; motion of west flank with respect to east flank. Axis 1 and Axis 2 describe variation in the position of the pole, and lie mostly within the surface of the globe. Axis 3 is for variation in the rotation angle. The azimuth is that of Axis 1. These parameters describe the 3D confidence ellipsoid, for completeness, but, following convention and for simplicity, only the 2D ellipses are shown in all the maps of reconstruction poles.

intermediate round of ten iterations with all $\Gamma = \pm 3\sigma$ (Nankivell, 1997b) maintains the influence of low-population regions in the data set. The final run, disregarding outliers by reducing Γ to $\pm 1\sigma$, continues until convergence (usually a few tens of iterations more). The starting pole set is a guess, to give a reasonable fit, by looking at the data. It is situated in the North Atlantic.

Solution poles for inversion with the whole west Scotia Sea data set are shown in Table 3.1 and Figure 3.7. Figure 3.7 also shows the solution poles of Nankivell (1997) for South America–Antarctica spreading from two-plate (South America and Antarctica) and unmodified three-plate (South America, Antarctica, Africa) inversions, and the solution poles from the rudimentary inversion on South American–Antarctic data of Barker and Lawver (1988) for which there are no confidence regions. Comparison of the west Scotia Sea poles with those for South America–Antarctica relative motion betrays a strong similarity between relative plate motion in the South American–Antarctic and the west Scotia Sea systems.

Figure 3.8 shows flowlines about solution poles to the data diverging significantly from the fracture zones in the northern part of the west Scotia Sea system, at the Burdwood

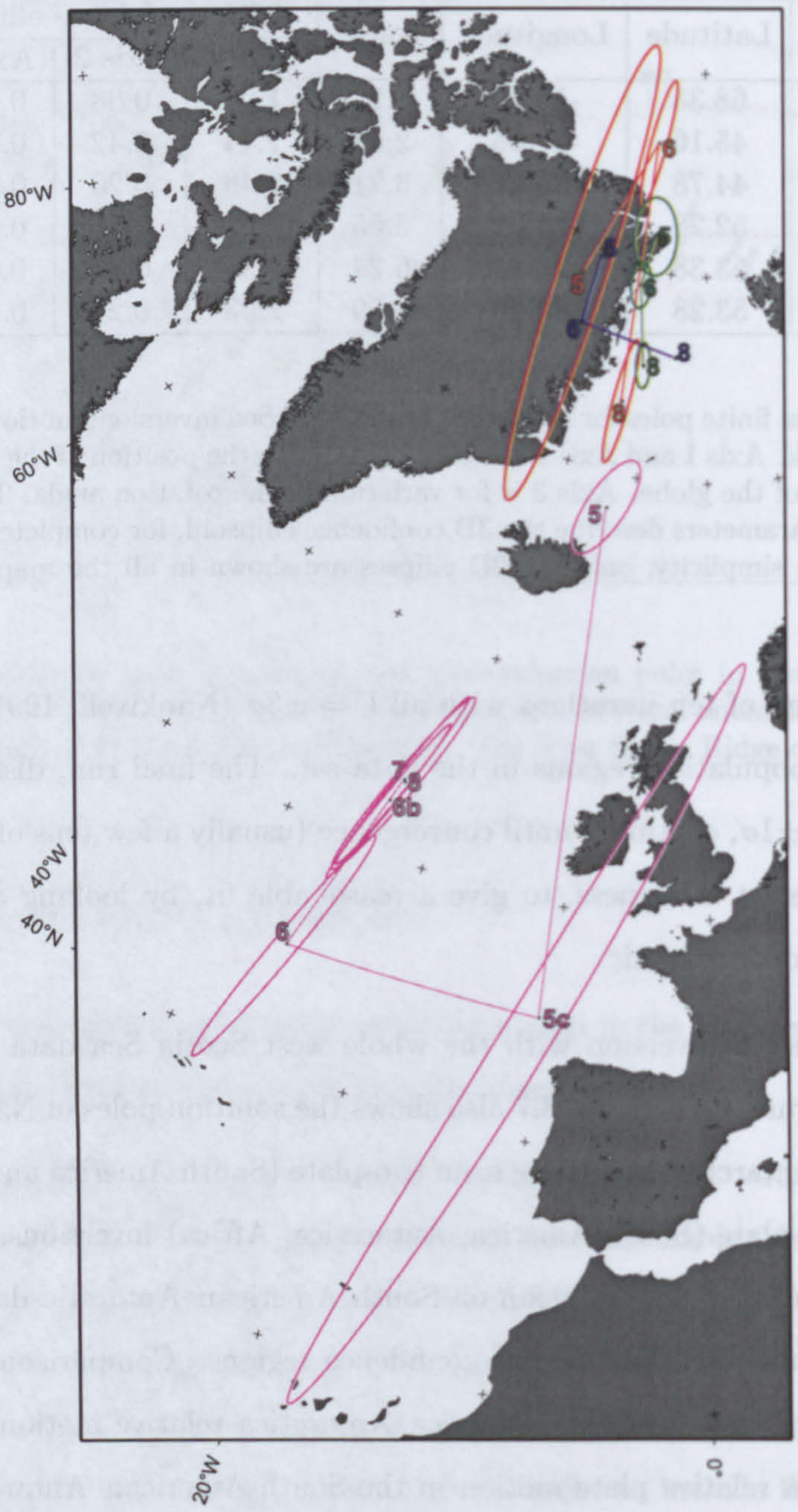

Figure 3.7: In pink: solution finite poles, and their 95% confidence ellipses for the entire west Scotia Sea inversion. The red and green sequences of ellipses are parts of the solutions of the two-plate and unmodified three-plate inversions of Nankivell (1997a), for relative movement between South America and Antarctica. The blue sequence is that of Barker and Lawver (1988), for which ellipses were not determined. Chron numbers for each given in appropriate colours.

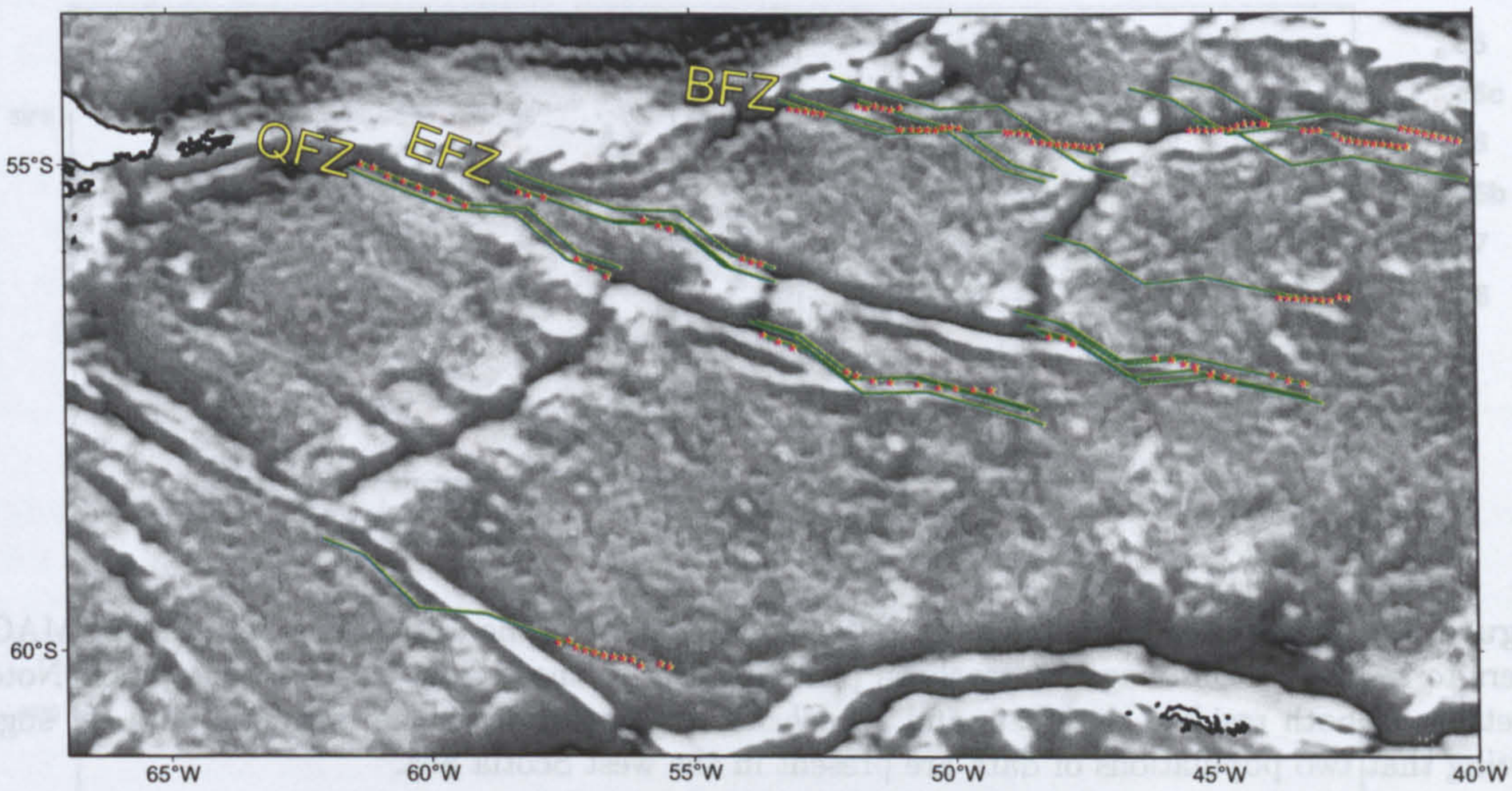

Figure 3.8: Model flowlines about the reconstruction poles from the entire west Scotia Sea inversion, in green, compared to fracture zone picks (red stars). Note the large inflexions which are not present in the data, and the poor fits to the Burdwood Fracture Zone (BFZ). EFZ: Endurance Fracture Zone, QFZ: Quest Fracture Zone.

Fracture Zone. Figure 3.9 shows q-q plots of the magnetic and fracture zone data sets used in the inversion. Facetting in both plots betrays the presence of two populations of data in the west Scotia Sea describing two seafloor spreading systems. Inspection of the residuals shows that the two populations broadly represent residuals from the northern and southern parts of the west Scotia Sea system, dissected by the Endurance Fracture Zone, or possibly the Quest Fracture Zone. The implication of this is that the northern and southern parts of the west Scotia Sea were not always co-polar.

In order to take account of this bi-polarity I split the west Scotia Sea data about the Endurance Fracture Zone and applied the inversion technique to the smaller data sets thus produced. The next two sections describe the results obtained from doing so.

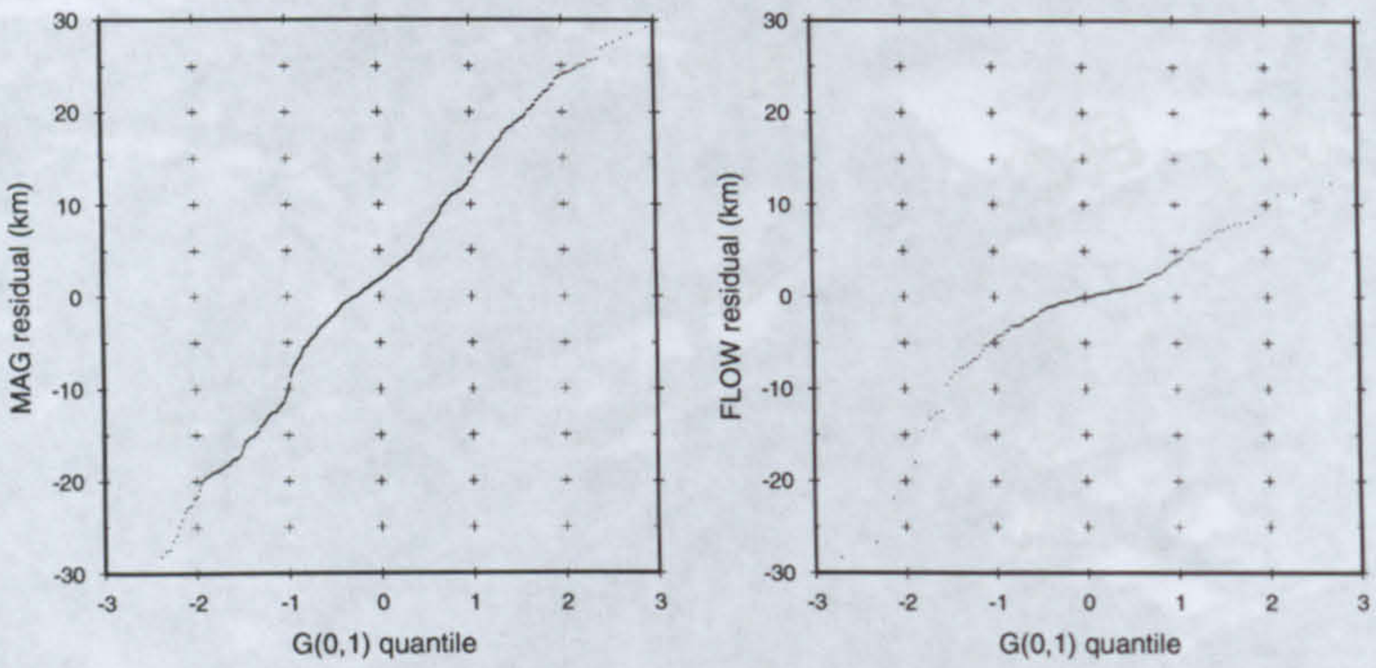

Figure 3.9: Quantile-quantile plots of residuals inverted for in the west Scotia Sea system. MAG refers to residuals from magnetic isochron picks, FLOW to those from fracture zone picks. Note facetting in both residual data sets and *en echelon* segmentation in the magnetic data set suggesting that two populations of data are present in the west Scotia Sea.

3.4.2 West Scotia Sea south of the Endurance Fracture Zone

The data sub-set for west Scotia Sea spreading south of the Endurance Fracture Zone is shown in Figure 3.10. The Endurance Fracture Zone itself is omitted on the grounds of a strong suspicion that its long offset accommodated differential strain between the northern and southern part of the west Scotia Sea. Initially, the inversion is performed using definite fracture zone traces only (*i.e.* the Quest Fracture Zone alone), prior to inclusion and reduction of the data set for shorter troughs not connected to offsets, to give the set shown in Figure 3.10. Solution poles produced using these data are given in Table 3.2 and Figure 3.11.

For most of the set of poles, within the bounds of the error ellipses, there can not be shown to be much difference from one chron to the next. The exceptions are jumps at C6 and C5 although the latter pole, being constrained only by a short length of fracture zone, could easily have been different. Given the possibility that error ellipses are underestimated by the use of gridded data I believe it wisest to conclude that the positions of the finite poles for the southern west Scotia Sea do not change much or at

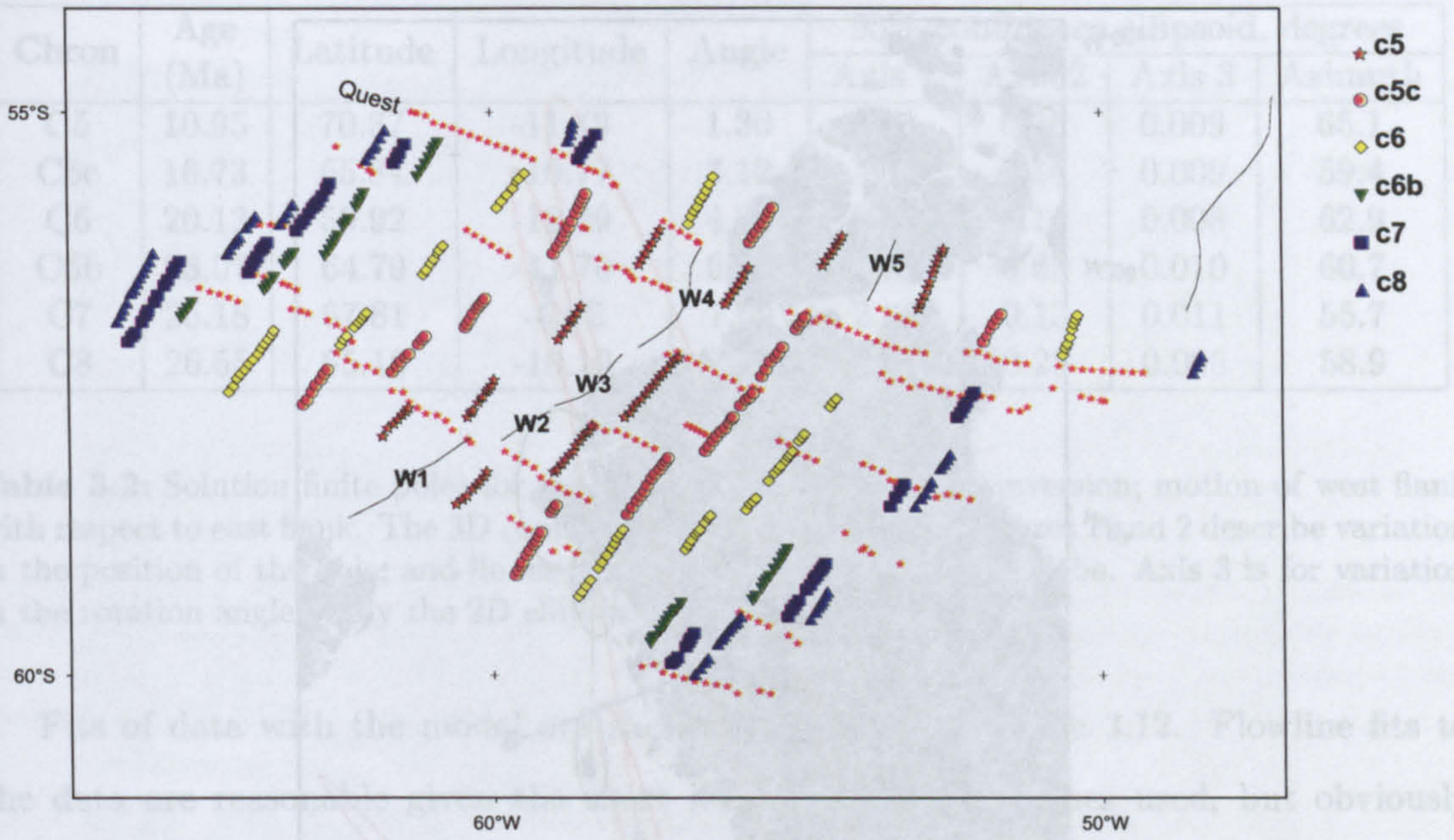

Figure 3.10: The data set used in inversion for reconstruction poles in the west Scotia Sea, south of the Endurance Fracture Zone. Symbols as for Figure 3.6.

all, except for a jump at C6. The group of poles, however, is displaced significantly south and east of the various groups of poles for the South American–Antarctic system. This displacement is by just a few degrees suggesting that the southern limb of the west Scotia Sea system was a close approximation to South American–Antarctic motion during its spreading. The clear separation of 95% confidence ellipses between the two systems nonetheless implies that some feature of the southern west Scotia Sea's margins decoupled it from South American–Antarctic relative motion. On the west flank relative motion is known from convergent deformation at Burdwood Bank and strike-slip movements on the Magallanes–Deseado fault zone in Tierra del Fuego, both presumed to have occurred in the post-C8 era. On the east flank the Antarctic plate can be reached via the South Sandwich Trench and South American-Antarctic Ridge, or through the small Protector, Dove and Jane basins. A final, more tortuous path is possible through Powell Basin and the Antarctic Peninsula.

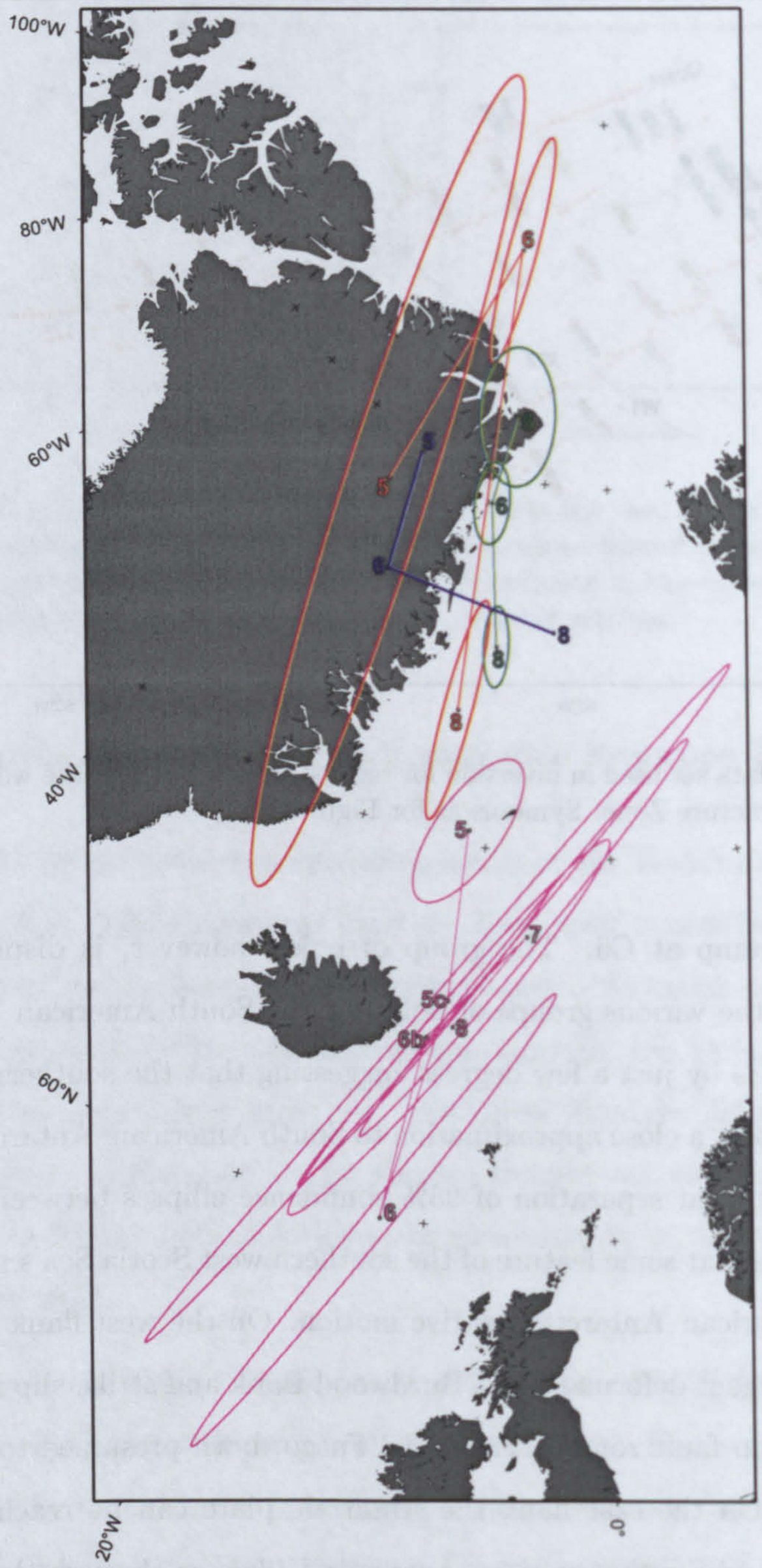

Figure 3.11: Solution finite poles, and their 95% confidence ellipses for the west Scotia Sea, south of the Endurance Fracture Zone, in pink. Red and green: two-plate and unmodified three-plate inversion results of Nankivell (1997a) for South America–Antarctica motion, blue: inversion of Barker and Lawver (1988) for which no confidence regions were determined. Chron numbers for each given in appropriate colours.

Chron	Age (Ma)	Latitude	Longitude	Angle	95% confidence ellipsoid, degrees			
					Axis 1	Axis 2	Axis 3	Azimuth
C5	10.95	70.37	-11.49	1.30	0.93	0.36	0.009	65.1
C5c	16.73	65.84	-10.77	3.12	4.84	0.14	0.009	59.4
C6	20.13	59.92	-12.29	4.26	3.08	0.14	0.008	62.9
C6b	23.07	64.79	-11.70	6.54	2.12	0.09	0.010	60.7
C7	25.18	67.81	-6.02	7.69	2.83	0.13	0.011	55.7
C8	26.55	65.18	-10.19	7.83	2.68	0.25	0.009	58.9

Table 3.2: Solution finite poles for the southern west Scotia Sea inversion; motion of west flank with respect to east flank. The 3D confidence ellipsoid is described: Axes 1 and 2 describe variation in the position of the pole, and lie mostly within the surface of the globe. Axis 3 is for variation in the rotation angle. Only the 2D ellipses are shown in Figure 3.11.

Fits of data with the model are shown graphically in Figure 3.12. Flowline fits to the data are reasonable given the short lengths of fracture zones used, but obviously more continuous fracture zone data would be useful. Importantly there is a good fit to the Quest Fracture Zone, the longest uninterrupted length of fracture zone and best constraint on continuous plate motion. A real kink in the Quest Fracture Zone correlates well with the changing reconstruction pole at C6. Data from the short trough features themselves are modelled well and consistently as parts of a set of flowlines. The feature branching off the Shackleton Fracture Zone on the eastern flank has been suggested in the past to be neotectonic, a readjustment of the modern Scotia—Antarctic plate boundary after extinction of the triple junction at the north end of Bransfield Strait (Klepeis and Lawver, 1996). I suggest here that it may have had an earlier (pre-C6b) manifestation as an age-offset producing a fracture zone. Magnetic data fits to their great circles are also good where available. The use of non-conjugate fits of C8, C7 and C6b anomalies in segments W3, W4 and W5 is shown.

Quantile-quantile plots for magnetic and fracture zone residuals are shown in Figure 3.13. Facetting of the magnetic plot suggests a number of edges with inconsistent strike are used in the inversion, probably coming from regions where the magnetic grid is not well constrained by ship track data (principally the east flank in W2–W4). A cutoff

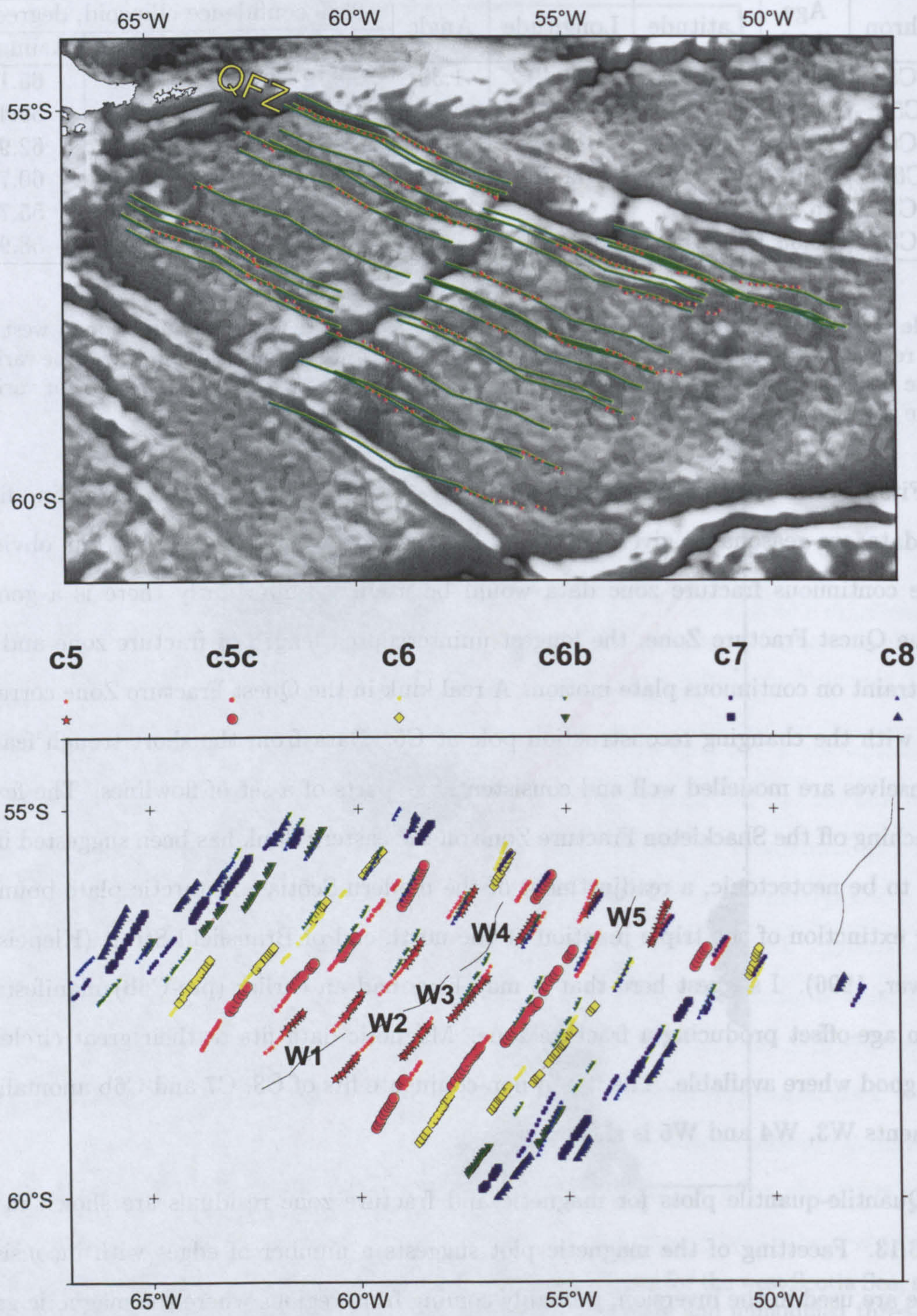

Figure 3.12: Fits of the model elements (great circles and synthetic flowlines) to the data used in the inversion for the west Scotia Sea south of the Endurance Fracture Zone. Flowlines (top, in green) are compared to fracture zone picks (red stars). Rotated magnetic anomalies (bottom, various small coloured symbols) are compared to their target great circles (larger coloured symbols and orange lines). QFZ: Quest Fracture Zone.

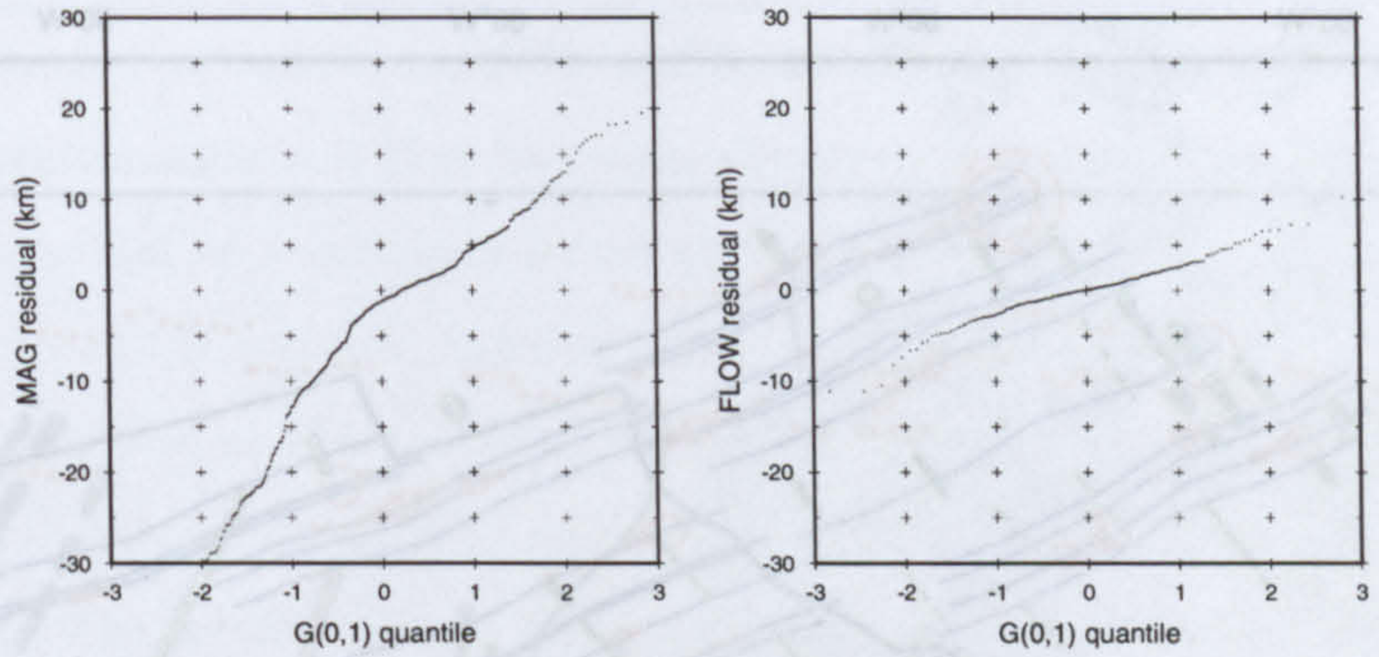

Figure 3.13: Quantile-quantile plots of residuals in the west Scotia Sea system, south of the Endurance Fracture Zone. MAG refers to residuals from magnetic isochron picks, FLOW to those from fracture zone picks. Facetting is eliminated from fracture zone data, but persists in the magnetic data.

criterion of $\pm 1\sigma$ is used in spite of this, as there are no alternative data. For flowline residuals cutoff at $\pm 1.0\sigma$ is also used and the data are clearly self consistent at this level.

Data importances are shown in Figure 3.14. A wide distribution of data has similar importances, which is good as it indicates that the influence of any remaining outliers will be quite small relative to the size of the data set. Encouragingly, the most important data are from the extremities of the fracture zones: the Quest Fracture Zone off Burdwood Bank and the short trough feature near Elephant Island. The Quest Fracture Zone is prominent and uncomplicated on the satellite gravity grid, inspiring a high level of confidence in its data. All magnetic picks have a roughly uniform level of importance, so that unfortunately some compromised data must have an influence on the solution. Because the compromised data are from the magnetic data set, the undue influence might be seen more strongly in the determined rotation angles than in the pole positions.

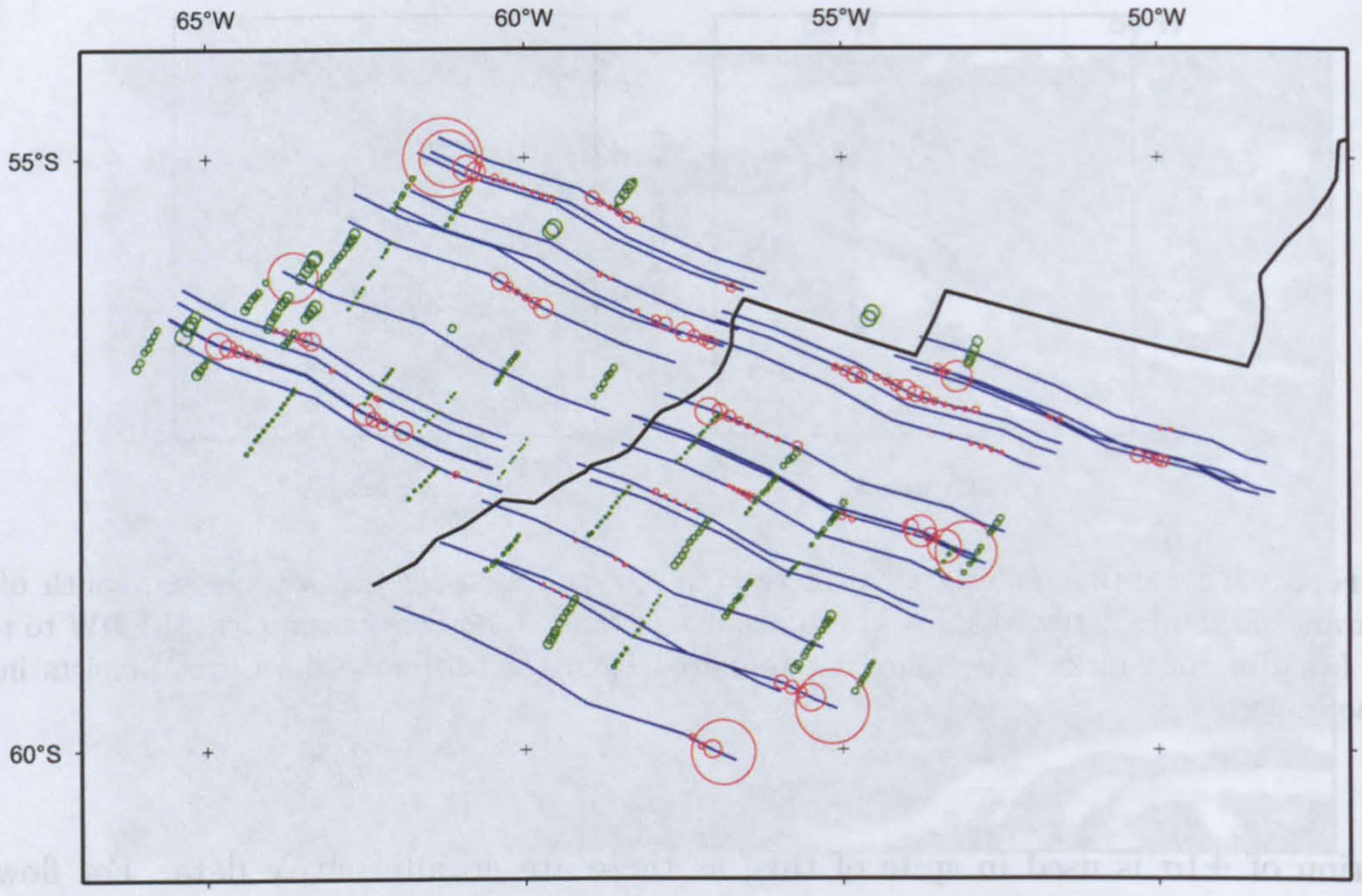

Figure 3.14: Relative importances of data to the solution poles inverted for in the west Scotia Sea system, south of the Endurance Fracture Zone. The size of each circle is proportional to the importance of the pick at its centre to the solution. Fracture zone picks have red circles, magnetic isochron ones green. Model flowlines are included, in blue, and the West Scotia Ridge crest, in black.

3.4.3 West Scotia Sea north of the Endurance Fracture Zone

The reduced data set used in inversion for west Scotia Sea reconstruction poles north of the Endurance Fracture Zone is shown in Figure 3.15.

Again, inversion was first done using only definite fracture zone traces in order to assess later the effect on the solution, and pertinence of, the short troughs picked as possible flowlines. Reconstruction poles are given in Table 3.3 and Figure 3.16.

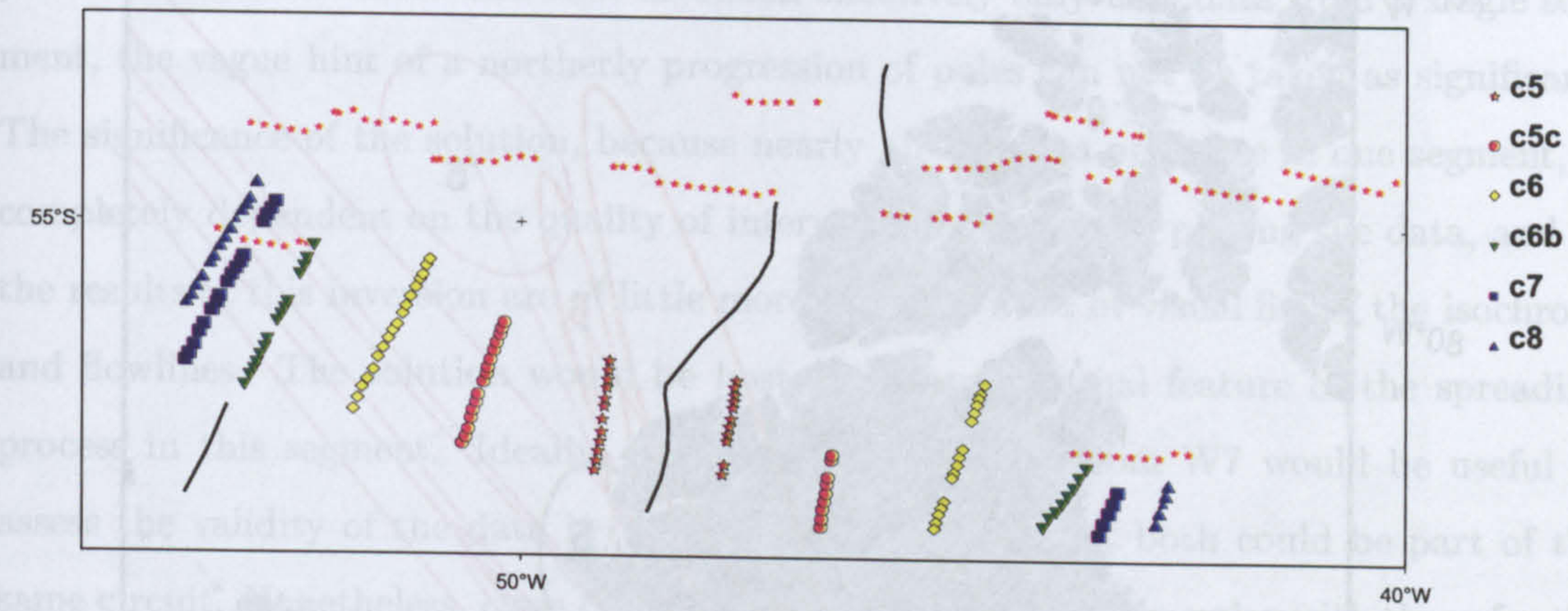

Figure 3.15: The data set used in inversion for reconstruction poles in the northern part of the west Scotia Sea. Symbols as for Figure 3.6.

Chron	Age (Ma)	Latitude	Longitude	Angle	95% confidence ellipsoid, degrees			
					Axis 1	Axis 2	Axis 3	Azimuth
C5	10.95	89.80	-17.25	1.44	1.00	0.64	0.002	71.4
C5c	16.73	80.32	-22.39	3.35	17.06	0.33	0.003	70.2
C6	20.13	74.39	-24.32	4.96	13.17	0.23	0.003	74.2
C6b	23.07	73.52	-22.52	6.76	4.25	0.13	0.005	72.3
C7	25.18	76.27	-18.07	8.13	2.79	0.11	0.003	67.2
C8	26.55	76.75	-15.80	8.83	7.05	0.20	0.005	65.4

Table 3.3: Solution finite poles for the northern west Scotia Sea inversion; motion of west flank with respect to east flank. The 3D confidence ellipsoid is described: Axes 1 and 2 describe variation in the position of the pole, and lie mostly within the surface of the globe. Axis 3 is for variation in the rotation angle. Only the 2D ellipses are shown in Figure 3.16.

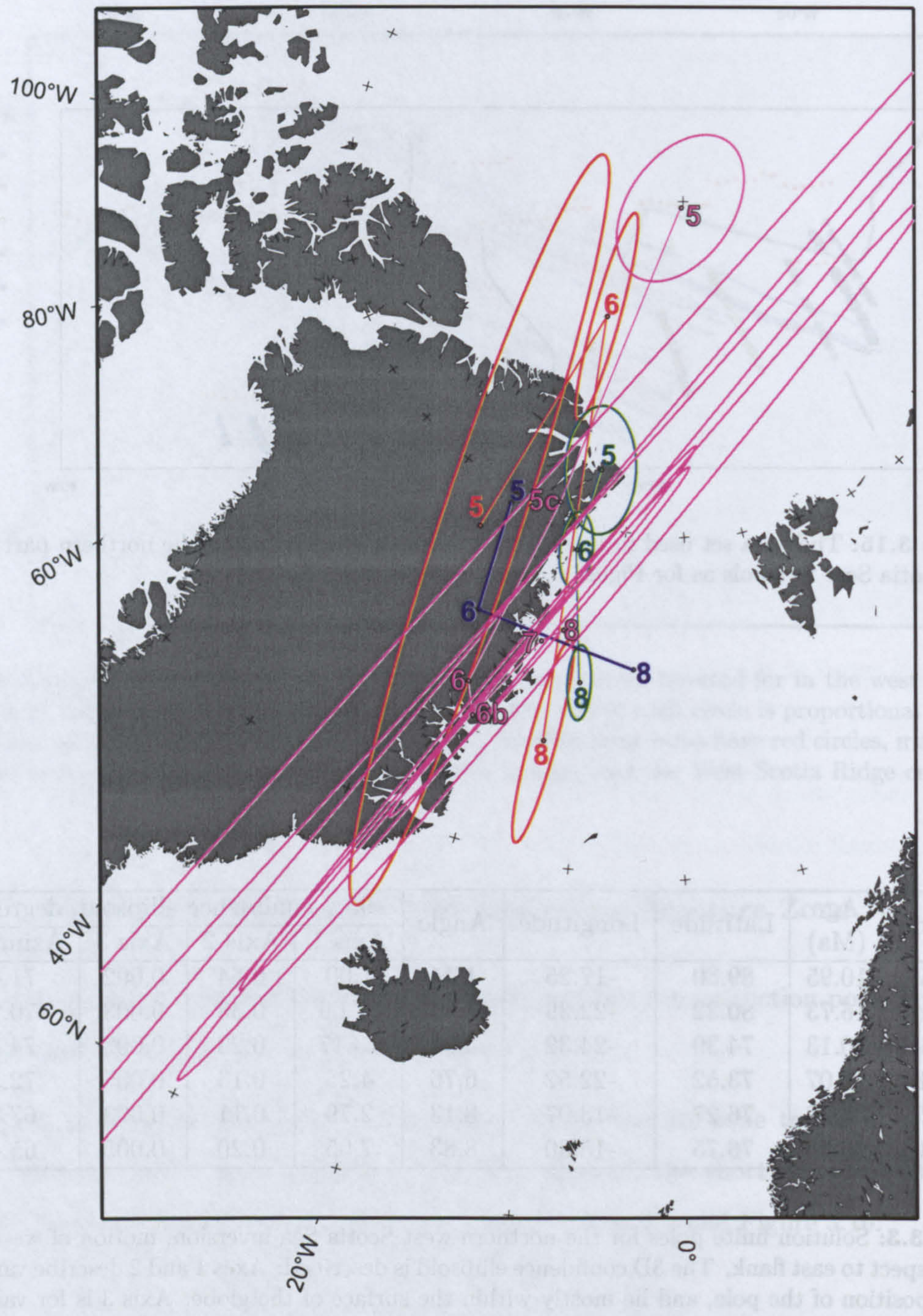

Figure 3.16: Solution poles and their 95% confidence ellipses for the west Scotia Sea system, north of the Endurance Fracture Zone, in pink. Red and green: two-plate and unmodified three-plate inversion results of Nankivell (1997a) for South America–Antarctica motion, blue: inversion of Barker and Lawver (1988) for which no confidence regions were determined. Chron numbers for each given in appropriate colours.

As was the case with the southern part of the system, progression in the sequence of poles is only hinted at outside the 95% confidence ellipses. Bearing in mind the ellipses' possible underestimation and that inversion effectively only uses data from a single segment, the vague hint of a northerly progression of poles can not be taken as significant. The significance of the solution, because nearly all the data originate in one segment, is completely dependent on the quality of interpretations made in picking the data, and so the results of this inversion are of little more use than a set of visual fits of the isochrons and flowlines. The solution would be hostage to any unusual feature of the spreading process in this segment. Ideally, magnetic isochron data from W7 would be useful to assess the validity of the data in W6, as it seems likely that both could be part of the same circuit. Nonetheless, close coincidence of the reconstruction poles with those for the southern part of the west Scotia Sea system and for South American–Antarctic relative motion gives cause for some satisfaction with the result.

Fits of data and model are shown graphically in Figure 3.17. The small set of flowlines is modelled reasonably well. This includes the prominent trough on the east flank, within W6, between chrons C8 and C6b, which has previously been suggested as a possible accretionary locus for the central Scotia Sea. Its model flowline tracks back to the ridge crest at the southerly bend and possible offset. Maybe the age-offset at this feature was reduced or eradicated at or soon after C6b: the reduction in the amount of offset might plausibly have been achieved by small, successive, ridge jumps below the resolution of magnetic reversal modelling in W6.

Quantile-quantile plots for fracture zone and magnetic residuals are shown in Figure 3.18. Data are consistent with the solution for flowline residuals within $\pm 1.0\sigma$. Again there are facets in the magnetic anomaly data set, in spite of which a $\pm 1.0\sigma$ cutoff criterion is used in the absence of alternative data. Inspection of the residuals, and of the magnetization anomaly grid, suggests that merging of 'staircase' anomalies by gridding on the east flank seems the most likely source of the deviant data.

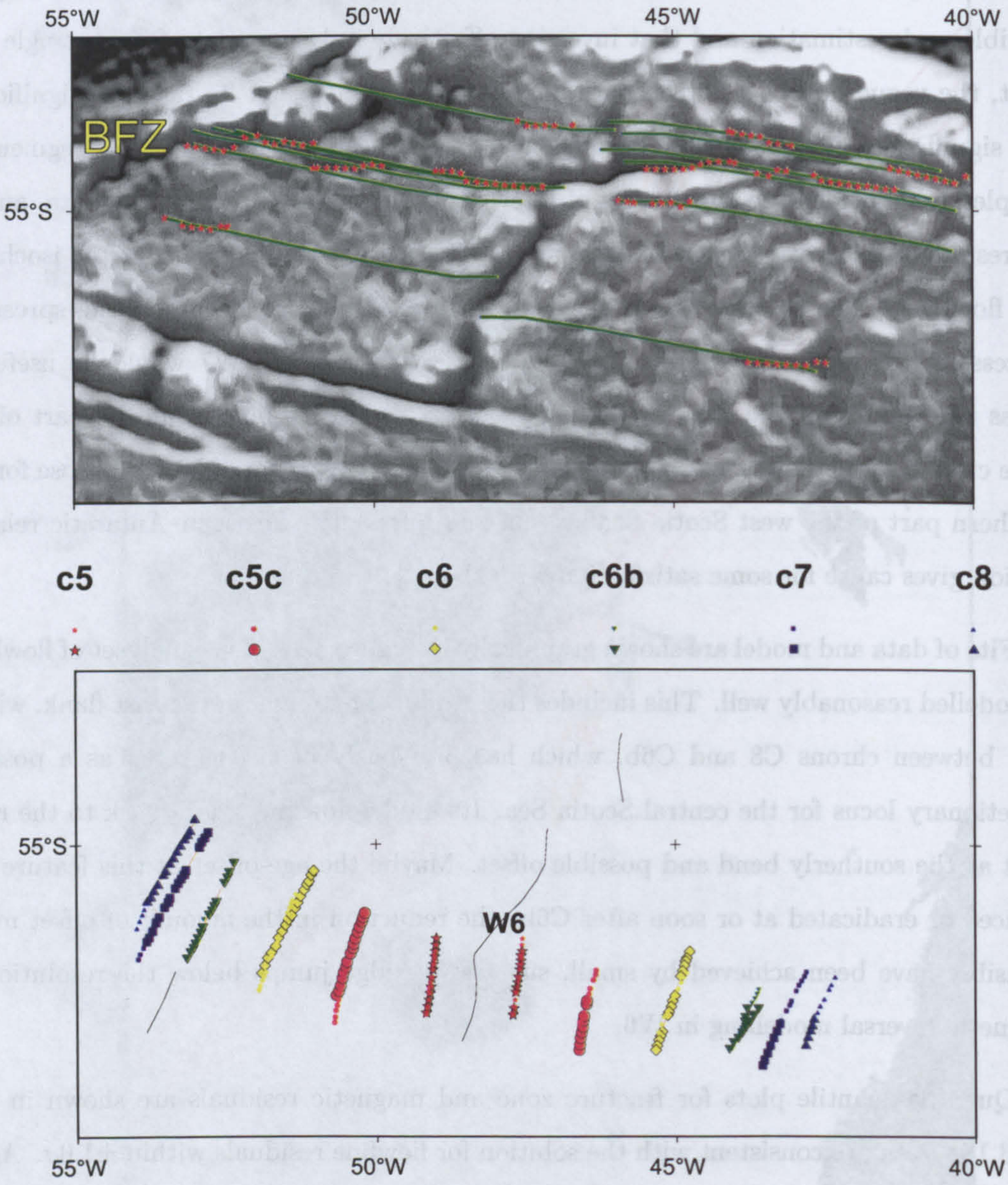

Figure 3.17: Fits of the model elements (great circles and synthetic flowlines) to the data used in the inversion for the west Scotia Sea north of the Endurance Fracture Zone. Flowlines, top, in green are compared to fracture zone picks (red). Rotated magnetic anomalies (bottom, various small coloured symbols) are compared to their target great circles (orange lines and larger coloured symbols). BFZ: Burdwood Fracture Zone.

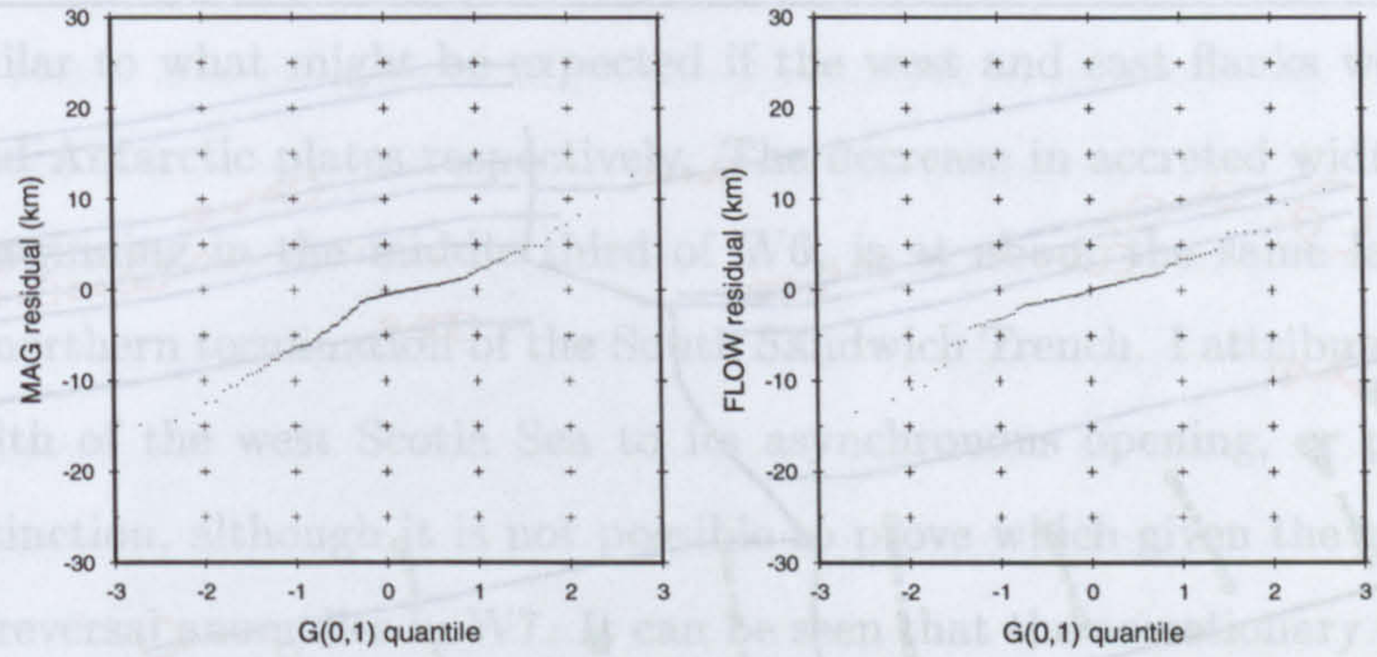

Figure 3.18: Quantile-quantile plots of residuals inverted for in the west Scotia Sea system, north of the Endurance Fracture Zone. MAG refers to residuals from magnetic isochron picks, FLOW to those from fracture zone picks. Facetting persists in the magnetic isochron data, where it forces the inclusion of many unsuitable data, but is unimportant in the fracture zone data.

Data importances to the reconstruction poles are shown by Figure 3.19. A wide distribution and great number of data are of similar importance to the solution suggesting that, unless the whole interpretation responsible for making the picks is flawed, the solution, such as it is, can be held with some confidence. The exception to this is the determined angles of rotation which depend more heavily on the compromised magnetic data.

3.4.4 Immediate implications

At the resolution allowed by available data within the west Scotia Sea system, there are only small differences in the positions of the reconstruction poles from what might be expected due to passive opening of the west Scotia Sea in response to relative motion between South America and Antarctica. Only the angles of rotation differ significantly, in the sense that more crust has been created than would be necessary if the passive margins of the west Scotia Sea were South America and Antarctica. The degree of coupling between the systems appears to have been strong enough for the west Scotia Sea to exhibit a change in spreading direction at C6, at which time a change also occurred in

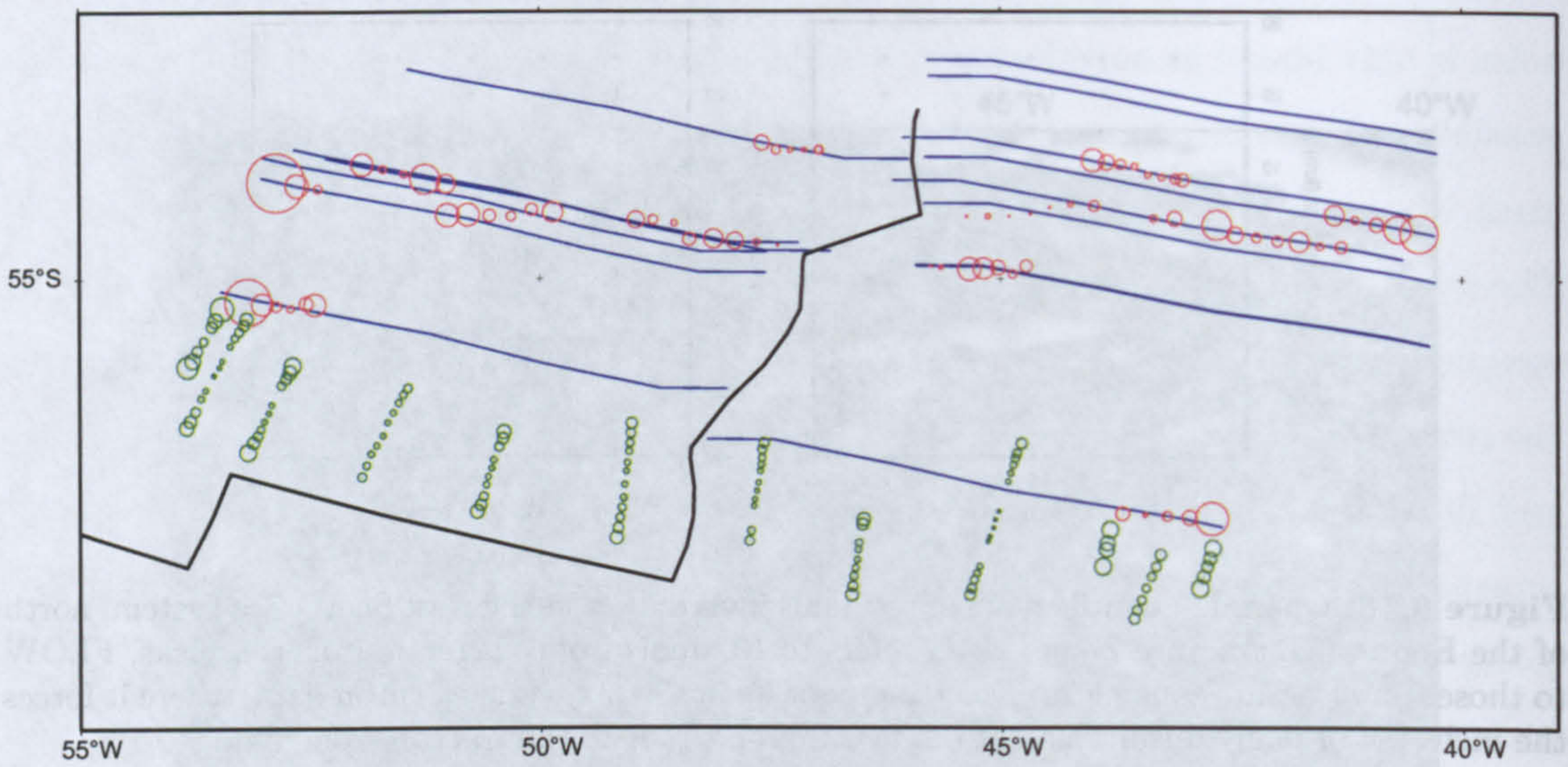

Figure 3.19: Importances of data in the west Scotia Sea system, to the results of the inverted for poles north of the Endurance Fracture Zone. Circles are proportional to the relative importance to the solution of fracture zone (red) and magnetic isochron (green) picks at their centres. Model flowlines are included, in blue, and the West Scotia Ridge crest, in black.

relative (Barker and Lawver, 1988; Nankivell, 1997a) and (since Antarctica was more-or-less fixed in an absolute sense) absolute motions of South America. Decoupling of the west Scotia Sea from the South American–Antarctic system might therefore be expected to occur largely on its 'Antarctic' eastern flank. The obvious location for this is the South Sandwich Trench.

The extra amount of accretion is significantly larger than the error that might be expected to have been introduced by the unavoidable use of inappropriate magnetic data in the inversions, visibly so on comparison of flowlines, as 'too much crust' in the west Scotia Sea (Figure 3.20). The extra accretion is noted by Hill and Barker (1980) and Barker (1995), and given as unequivocal evidence that the Scotia Sea is entirely back-arc in nature: that is, they relate it explicitly to the presence of the South Sandwich Trench. Figure 3.20 shows that the discrepancy is constant in W1–W5 but decreases northward

from the northern third of W6 so that in W7 the amount of crust produced is, coincidentally, similar to what might be expected if the west and east flanks were the South American and Antarctic plates respectively. The decrease in accreted width of the west Scotia Sea beginning in the middle third of W6, is at about the same latitude as the present-day northern termination of the South Sandwich Trench. I attribute this variable accreted width of the west Scotia Sea to its asynchronous opening, or possibly asynchronous extinction, although it is not possible to prove which given the garbled nature of magnetic reversal anomalies in W7. It can be seen that the accretionary discrepancy is reduced after C5c ($\sim$ 16.7 Ma), when South American–Antarctic and west Scotia relative motions become closely comparable. This correlates closely with estimates of the timing of the onset of spreading in the east Scotia Sea back-arc basin, at about 15 Ma.

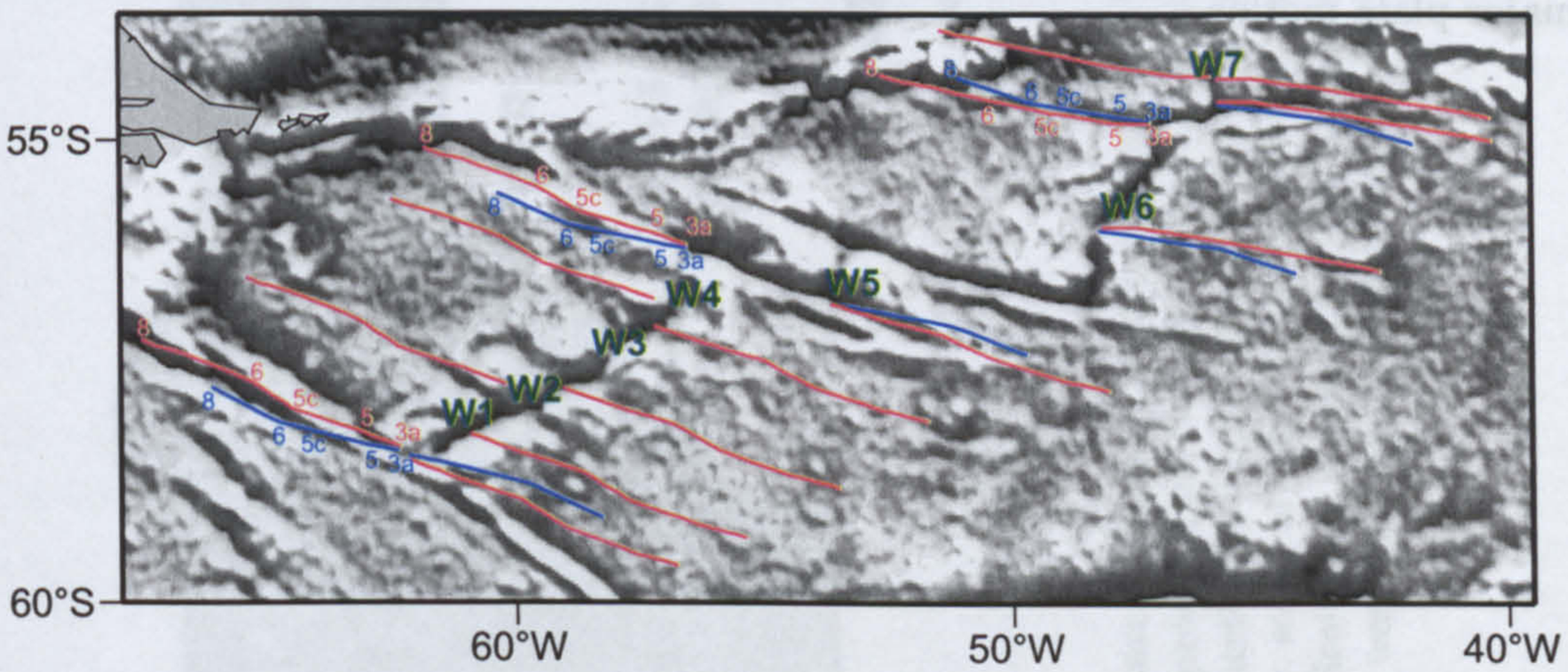

Figure 3.20: Comparison of model flowlines in the west Scotia Sea (red lines) and what might be expected there from spreading between South America and Antarctica during the same interval (blue lines). Small numbers indicate magnetic chrons. Most of the extra accretion in the west Scotia Sea occurs before C5c. In northern W6 and in W7 less crust is created than in W1–W5 and southern W6.

So there is a strong influence by major plate motions on spreading in the west Scotia Sea, and the enhanced accretion, over what might be expected from this influence, is apparently correlated in space with the presence on the east flank of the South Sandwich Trench and in time with the absence of back-arc extension in the east Scotia Sea. All

this suggests that subduction at the South Sandwich Trench has influenced the amount, but not greatly the azimuth, of seafloor spreading in the west Scotia Sea. I put forward an interpretation, (summarised in Figure 3.21) for the opening of the west Scotia Sea whereby its opening was due to the relative motion of southernmost South America away from a trench at the eastern edge of the Scotia Sea, which I refer to as the proto-South Sandwich–Discovery Trench. The trench therefore has to have had, between C8 and C6 (at least) a greater easterly component of motion relative to South America than has Antarctica. This can be attributed to its easterly rollback.

Although the trench had this relative easterly component of motion with respect to Antarctica, it still closely resembled it in a kinematic sense, as the absolute westerly motion of South America was much greater than both. Hence the strong apparent influence by major plate motion.

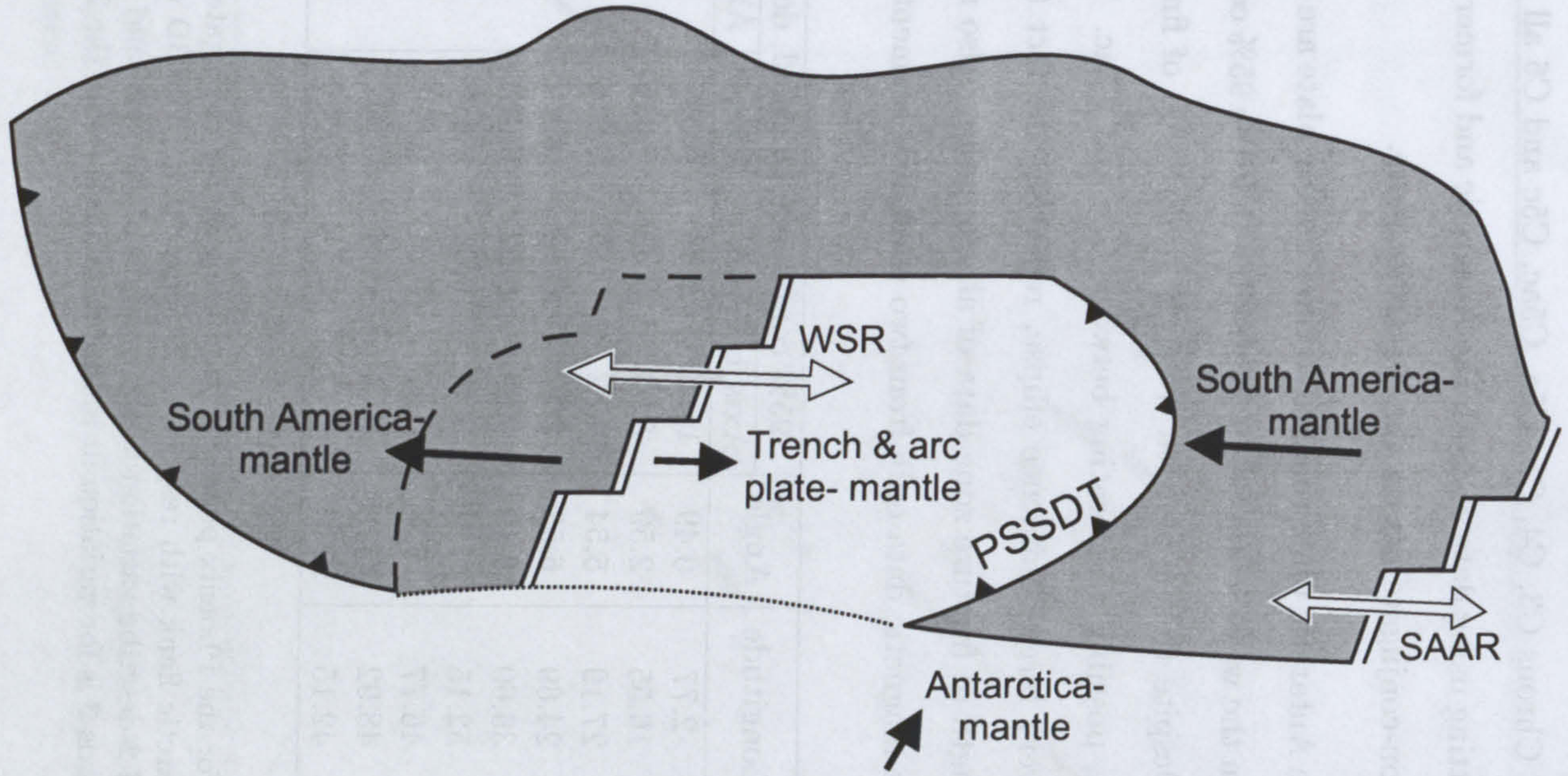

Figure 3.21: Simplified opening of the west Scotia Sea. Motion on North and South Scotia ridges and of Tierra del Fuego not shown: the South American plate is, to a first approximation, both overriding and subducting at the proto-South Sandwich–Discovery Trench (PSSDT). Easterly trench rollback is cancelled by South America's westerly motion so spreading continues at the South American–Antarctic Ridge (SAAR). Rollback is slow, so the arc plate has small easterly absolute motion, slightly larger than that of Antarctica by the rate of 'excess accretion' in the west Scotia Sea. Spreading at the West Scotia Ridge (WSR, white double arrow) closely resembles that at the SAAR since they share their west flank plate: South America, with fast westerly absolute motion, and each of their east flank plates has slow absolute motion.

3.4.5 Phoenix system

The full data set used in the inversion for relative motion of the Phoenix and Antarctic plates is shown in Figure 3.22. Chrons C3, C4, C5, C5a, C5ac, C5c and C6 all use both non-conjugate and conjugate fitting using data on both the Antarctic and former Phoenix plates. C8 and C10 use only non-conjugate fits on the Antarctic plate.

Reconstruction poles for the Antarctic plate relative to the Phoenix plate are shown in Figure 3.23 and Table 3.4. As in the west Scotia Sea it is possible that the 95% confidence ellipses are underestimated. Despite this, a smooth westerly progression of finite poles between C10 and C4 is shown, possibly accelerating between C5c and C5ac. The pole for C3 is contained within a very large confidence ellipse, reflecting the fact that it is constrained by the shortest length of fracture zone data of all the poles. Also note that the ellipses for C8 and C10 use magnetic data only from two spreading segments.

Chron	Age (Ma)	Latitude	Longitude	Angle	95% confidence ellipsoid, degrees			
					Axis 1	Axis 2	Axis 3	Azimuth
C3	5.23	47.38	-2.77	0.49	15.22	2.28	0.009	59.9
C4	8.07	73.61	16.55	2.59	5.03	0.39	0.016	30.3
C5	10.95	73.17	27.19	5.54	1.82	0.15	0.014	23.6
C5a	12.40	70.83	24.69	6.53	2.17	0.18	0.014	29.8
C5ac	14.08	73.01	36.60	9.19	0.88	0.12	0.014	15.8
C5c	16.73	75.50	52.15	14.16	0.49	0.06	0.018	6.1
C6	20.13	71.77	46.77	15.94	0.47	0.04	0.021	14.0
C8	26.55	71.65	48.92	23.04	0.71	0.04	0.032	12.5
C10	28.75	70.99	42.15	23.12	1.72	0.11	0.056	17.4

Table 3.4: Solution finite poles for the Phoenix plate inversion using mixed conjugate and non-conjugate fitting; motion of Antarctic flank with respect to Phoenix flank. The 3D confidence ellipsoid is described: Axes 1 and 2 describe variation in the position of the pole, and lie mostly within the surface of the globe. Axis 3 is for variation in the rotation angle. Only the 2D ellipses are shown in Figure 3.23.

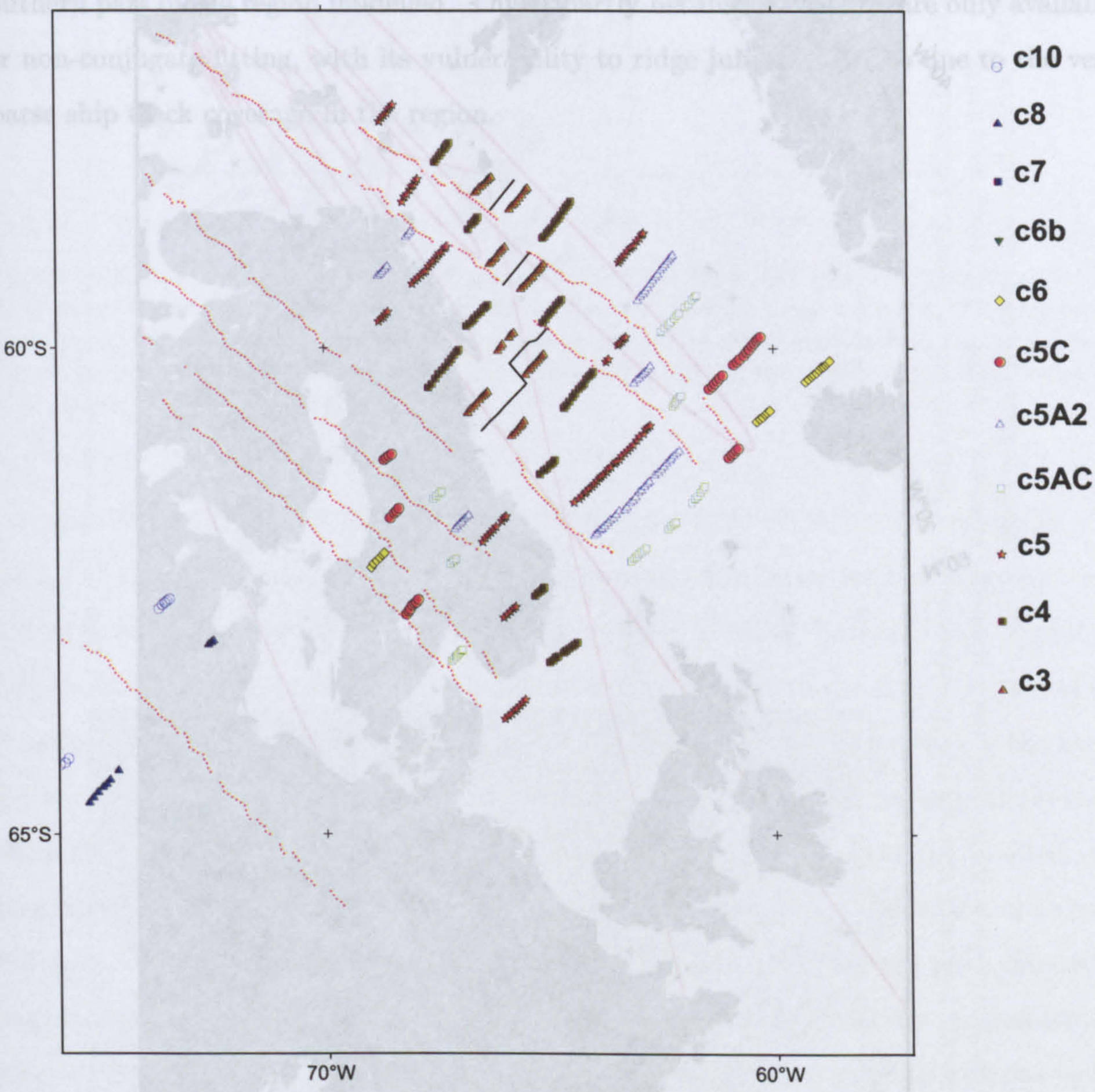

Figure 3.22: The data set used in inversion for reconstruction poles in the Phoenix spreading system. Small red stars locate fracture zone picks. Larger coloured symbols locate magnetic isochron picks.

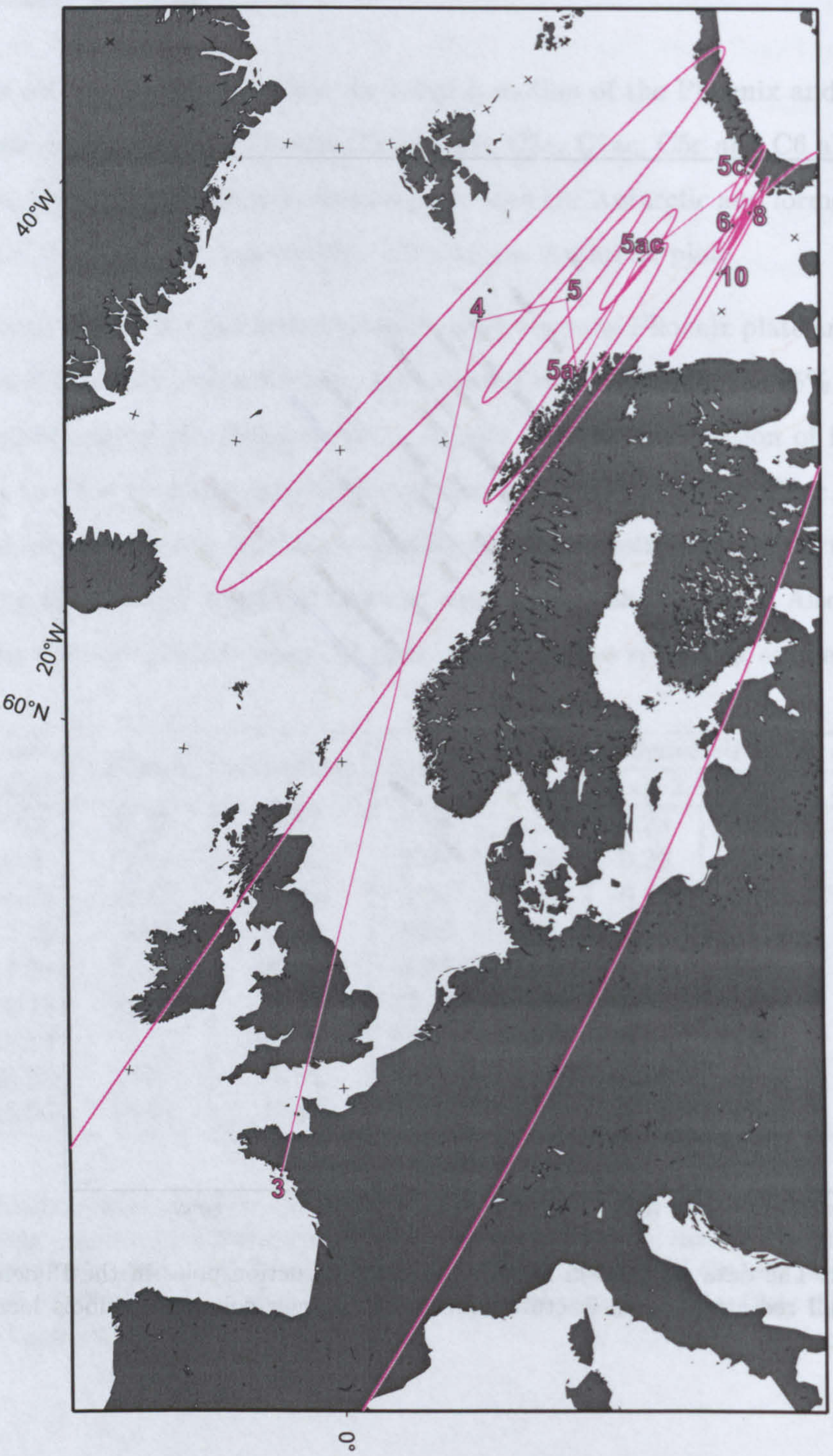

Figure 3.23: Solution finite poles, and their 95% confidence ellipses for the Phoenix spreading system between C10 and C3.

Model fits to the data are shown in Figure 3.24. Flowline fits to fracture zones are all very good—this is to be expected since there are no significant kinks in the fracture zones to model. Magnetic fits are similarly well made, magnetic errors are largest for the southern part of the region modelled. This is partly because these data are only available for non-conjugate fitting, with its vulnerability to ridge jumps, and also due to the very sparse ship track coverage in the region.

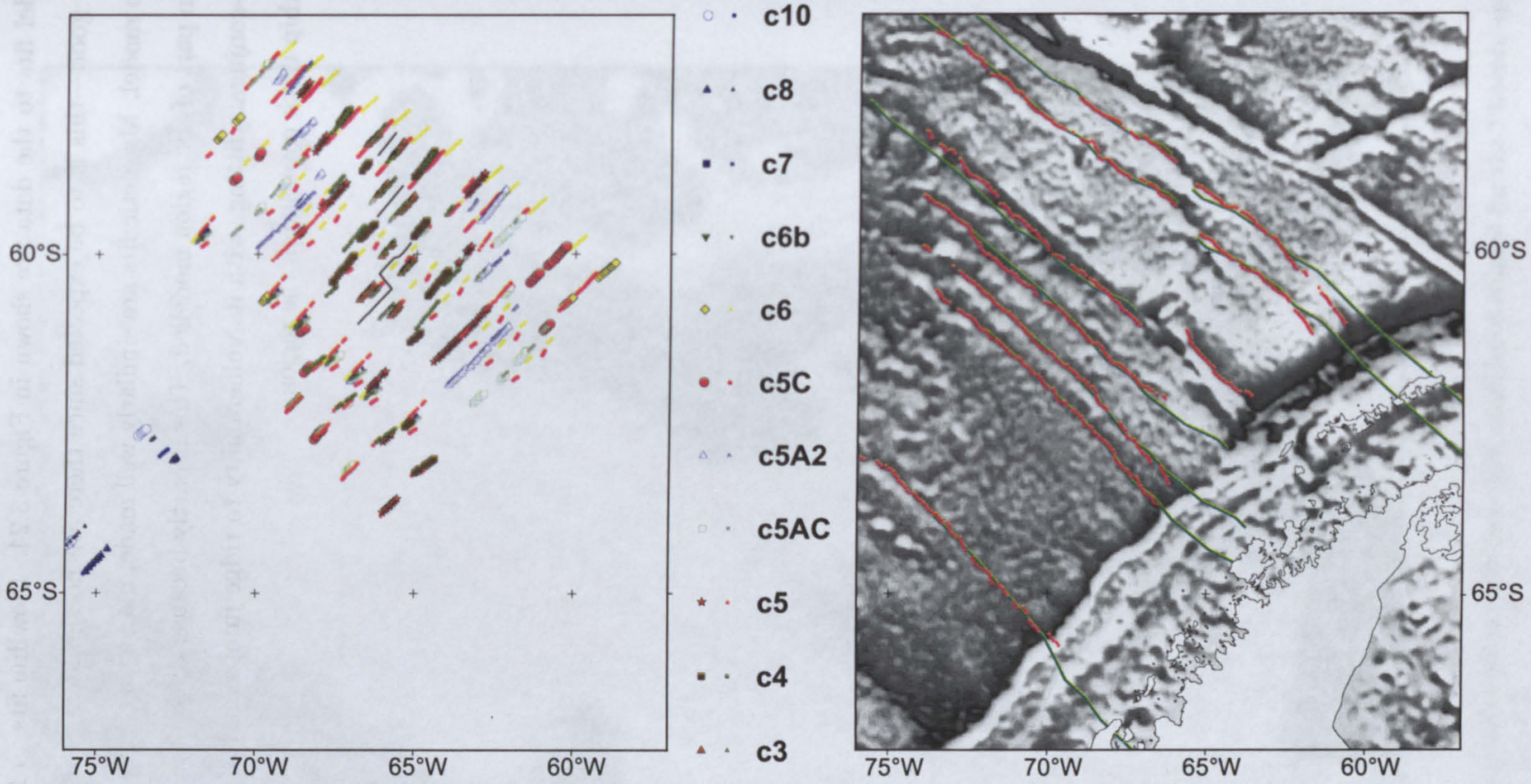

Figure 3.24: Fits of the model elements to the data used in the inversion for the Phoenix spreading system. Flowlines, right, in green are compared to fracture zone picks (red). Rotated magnetic anomalies (left, various small coloured symbols) are compared to their target great circles (orange lines and larger coloured symbols).

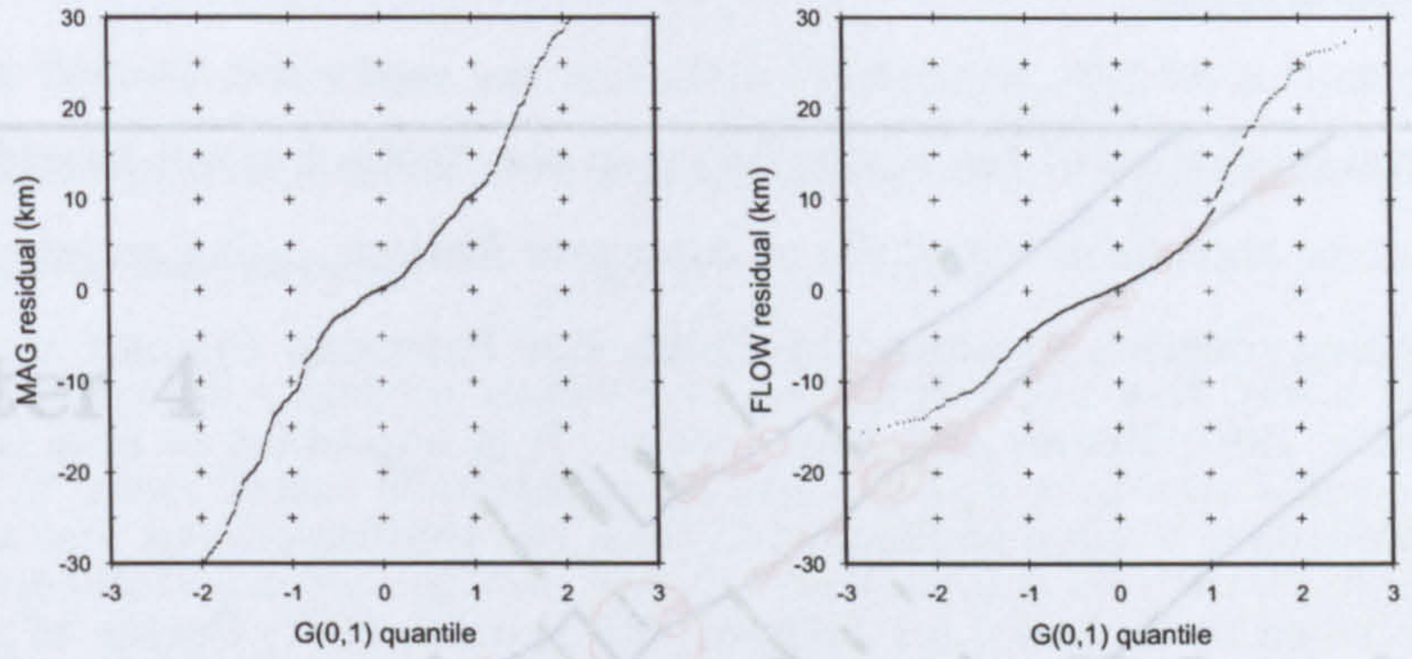

Figure 3.25: Quantile-quantile plots of residuals inverted for in the Phoenix spreading system. MAG refers to residuals from magnetic isochron picks, FLOW to those from fracture zone picks. Facetting in the magnetic isochron plot is probably due to the difference between the well-defined grid in the north of the system, and the less-well defined part in the south where ship tracks are more scarce.

Quantile-quantile plots for magnetic and fracture zone residuals are shown in Figure 3.25. Cutoff criteria, for both, of $\pm 1\sigma$ are used. Residuals for the magnetic data hint at two populations. The first population (lower gradient bar in center of plot) is the product of conjugate fitting of well-defined anomaly edges in the northern part of the Phoenix system. The second population, with the higher standard deviation, is the result of non-conjugate fitting of less-well-defined anomaly edges in the remainder of the system, where ship tracks are less closely spaced and data picked from the grid are, in effect, the same as profile data. Relative importances of the data used for the inversion are shown in Figure 3.26. Paucity of picks of C8 and C10 means that these are the most important magnetic data. Fracture zone data are the most important overall: the prominence of troughs used to pick the data inspires high confidence in them, and this extends to the solution itself.

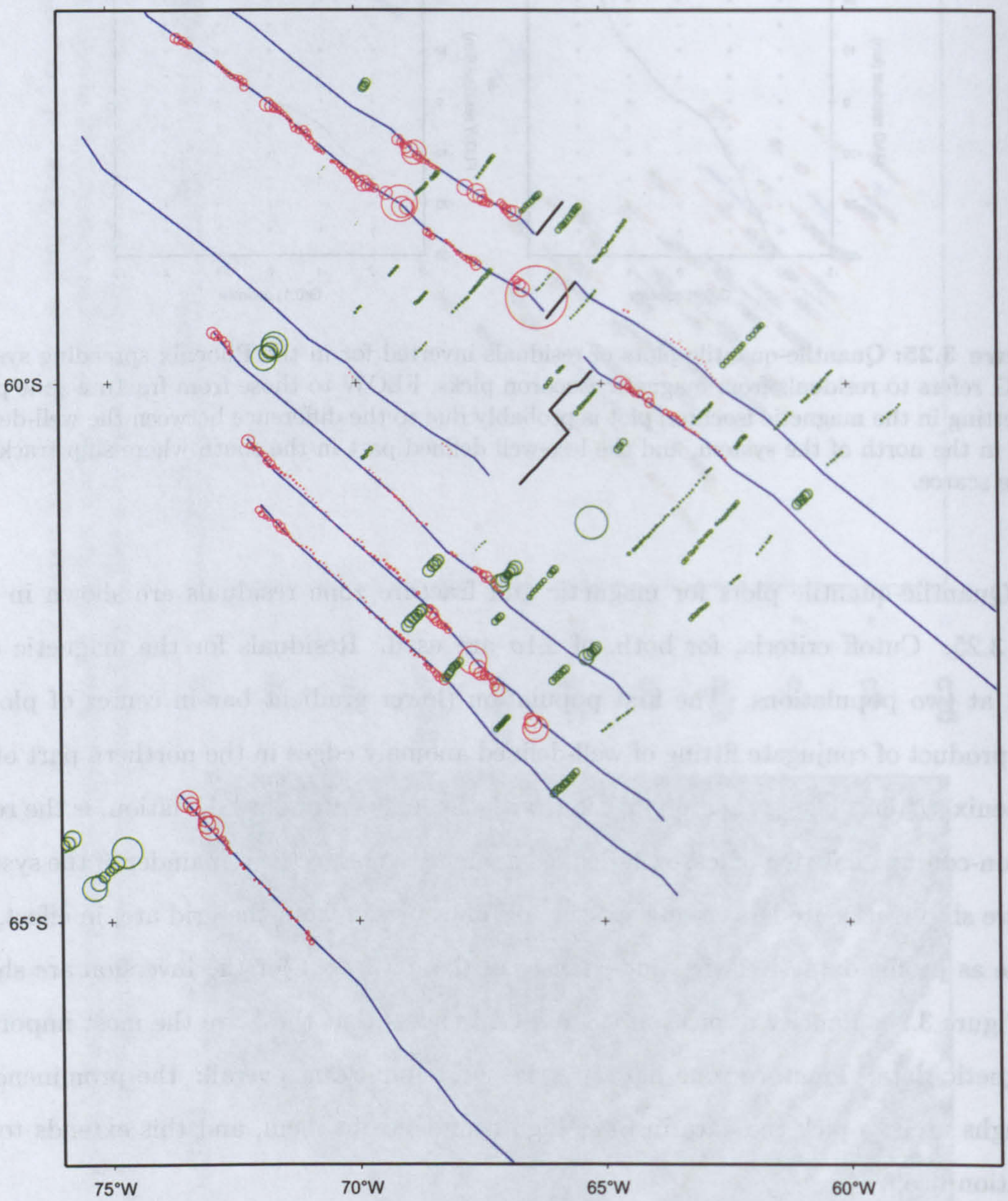

Figure 3.26: Relative importances of data in the Phoenix spreading system, to the results of the inverted for poles. Picks at the centres of larger circles are relatively more important, in proportion to the circle's size, than those in smaller circles. Red circles for fracture zone picks, green ones for magnetic isochron picks. Model flowlines are included, in blue.

Chapter 4

Reconstructions of small basins

Keywords Visual fits. Small basins. Plate circuits.

4.1 Making qualitative reconstructions

Outside the west Scotia Sea, east Scotia Sea, and the Phoenix–Antarctic regime the advantages of automated reconstruction are lost because the smaller basins of the region do not show large areas of well-identified magnetic reversal isochrons and tectonic flowlines or simply do not show enough of these features to be statistically significant. Stretching of continental crust becomes important in consideration of the opening of small basins, where the stretched regions occupy proportionally much more space. As a result, for smaller systems, only subjective, visual assessments of reconstructions can be carried out. The rotations applied to produce these reconstructions are themselves subjective and confidence regions can not be quantified for them. In this chapter reconstructions of this type will be presented of the west Scotia rift basins, North Scotia Ridge, Powell, Protector and Dove basins, and the Jane–Discovery back-arc basin (Figure 1.11 locates these features). Following this a short section will explain why I have made no attempt to reconstruct seafloor spreading in the central Scotia Sea.

4.1.1 Visual fitting

Reconstructions by closure of the minor basins in the Scotia Sea are here done by trial and error to make acceptable visual fits of conjugate features, using an interactive plate tectonic modelling program developed by Cambridge Paleomap Systems and called *AT-LAS* (Hall, 1996; 1997; Reeves and Sahu, 1999). It is important to note however that this type of modelling is more sophisticated than the traditional 'cut and move' reconstructions described in Section 1.5.1 (Barker and Burrell, 1977; Barker *et al*, 1984; for example) because it is all done on a mathematical representation of a sphere rather than on a projection. The distortion effects inherent in the use of map projections are not an issue, and the reconstructions can be described using the same systematic (Euler poles) as for major plate reconstructions. The resulting fits are presented using *GMT* (Wessell and Smith, 1991; Taylor *et al*, 1999; Frey *et al*, 2000).

4.1.2 Completing circuits

In Chapter 3 the opening of the west Scotia Sea is shown to have been strongly influenced by the relative motion between South America and the 'proto-South Sandwich–Discovery slab' in the mantle whose kinematic identity is similar to that of East Antarctica. The essence of the west Scotia Sea is that it formed the main part of a microplate circuit between the South American plate, which was mobile with respect to the mantle, and a plate seismically coupled to the proto-South Sandwich–Discovery Trench, which was more closely fixed to the mantle. With this interpretation I have a model of first-order kinematics within which context I make assessment of microplate reconstructions. The result is the first model of Scotia Sea kinematics that is complete at first and second order; that is both self consistent and consistent within the context of separation of South America from East Antarctica.

If we suspect the presence of an ocean basin, at a certain time, within a given plate circuit whose other elements are well known a reconstruction pole for the basin can be

derived from the circuit. This approach is used successfully for major plate circuits involving the Weddell Sea whose age and plate boundaries were for a long time unknown (Barker and Lawver, 1988; Livermore and Woollett, 1993; Livermore and Hunter, 1996; Nankivell, 1997a; for example).

A similar approach might be expected to be useful in the west Scotia Sea: to predict the opening of minor basins alongside spreading at the west Scotia Ridge—an approach taken, in a qualitative sense, by Hill and Barker (1980) for Protector Basin. However, aside from the real uncertainties involved in determining the ages of small basins, the distances between finite poles describing the opening of the west Scotia Sea are smaller than the 95% uncertainty ellipses for the poles themselves. So, despite confidence that the set of reconstruction poles describes the gross opening process in the west Scotia Sea, there can be little confidence in the azimuthal predictions of stage poles derived from them (Figure 4.1). There is little chance of success in trying to derive reconstruction poles from 'stage' circuits containing the Scotia Sea's short lived minor basins. Instead of this process, the assumption that minor basins complete circuits is used to assess reconstruction poles derived from visual fits. If the reconstruction pole for a basin of known age can be used to complete a plate circuit within known bounds of uncertainty then greater confidence can be applied to that rotation as part of a self consistent model. This approach is of less use when the age of the sub-basin is unknown.

4.1.3 Checking reconstructions with model flowlines

The use of model flowlines to illustrate reconstructions is familiar from Chapter 3. Barker and Lawver (1988); Livermore and Woollett (1993); Livermore and Hunter (1996) and Nankivell (1997a) all use poles from the circuit between South America, Antarctica and Africa to construct sets of flowlines for visual comparison with fracture zones. In this chapter this approach will be taken using poles derived from forward modelling in order to compare model flowlines to tectonic features expressed in the potential field anomalies of the minor basins.

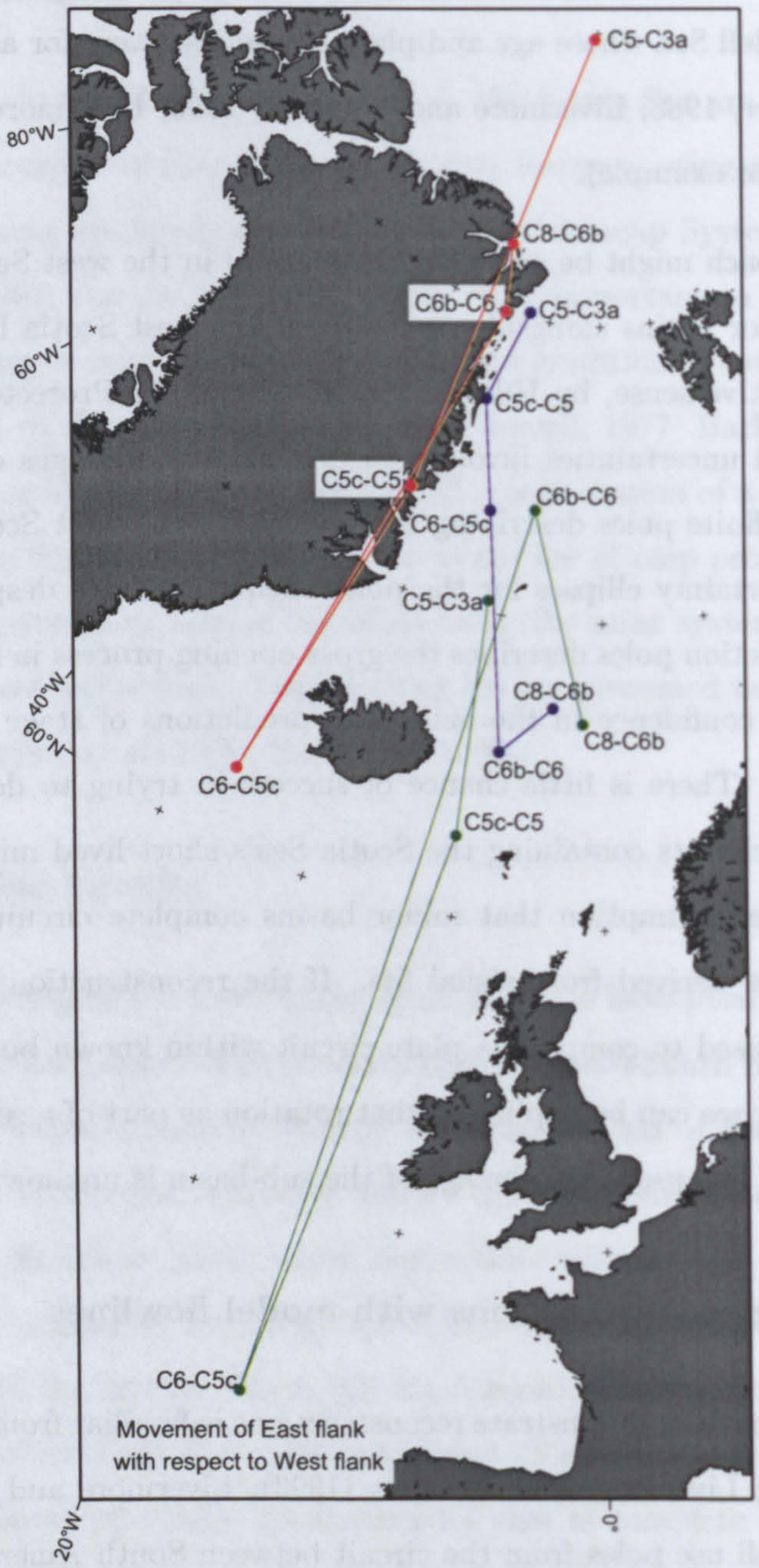

Figure 4.1: Comparison of stage poles for west Scotia Sea and South American–Antarctic spreading. Stages denoted by their start and end chrons. Red, northern west Scotia Sea; Green, southern west Scotia Sea; Blue, three plate inversion of Nankivell (1997a) for South America–Antarctica. All three sets occupy the same region, showing the strong similarity between South American–Antarctic and west Scotia relative motions. Greater uncertainty in Scotia Sea inversions results in sequences of stage poles without smooth progression: the large jumps are in the direction of greatest uncertainty. Poles predicted for opening of minor basins, by balancing these three progressions, would be fatally flawed.

4.2 Rift basins in the west Scotia Sea

4.2.1 No need for 'chaotic seafloor spreading'

Pre-C8 extension in the Drake Passage region is predicted from major plate reconstructions (Lawver *et al*, 1985; Livermore and Woollett, 1993) where Tierra del Fuego passes the tip of the Antarctic Peninsula by at least C21 ($\sim$ 48 Ma). Reconstructions at 26.55 Ma (C8o) of the west Scotia Sea show part of this as remaining separation between Tierra del Fuego–Burdwood Bank and the elevated regions of the eastern flank (Figure 4.2, Barker and Burrell (1977)). In the reconstructions of Barker and Burrell (1977) and Burrell (1983), where the Shackleton Fracture Zone is used as flowline constraint, the area of separation is of variable width along the length of the west Scotia Sea. To account for this, and for the discontinuous nature of identified C9 and C10 anomalies, they invoke an early so-called 'chaotic' episode of seafloor spreading, involving multiple ridge jumps and the asynchronous onset of rifting in an apparently random sequence of locations. Using the 'break-up' reconstruction poles (C8) from Chapter 3 instead, the region separating the eastern and western flanks is about 150 km in east–west extent all along its length (Figure 4.2). As a result I believe a simple model of stretching prior to synchronous break-up at C8o of the entire west Scotia Sea margin is preferable. In this scheme the isolated C9 and C10 identifications commute to expressions of local break-up volcanism off the eastern margin of Burdwood Bank and south of Staten Island. Seismic reflection data could provide corroborating evidence for this interpretation.

4.2.2 Reconstructing stretching

Previous reconstructions

The reconstructions of Barker *et al* (1984) and King and Barker (1988) (Section 1.5.1) show the rift basin region closed by 40 Ma. The variable sizes, shapes and positions of the reconstructed blocks suggest that the rifting episode is largely unconstrained, although

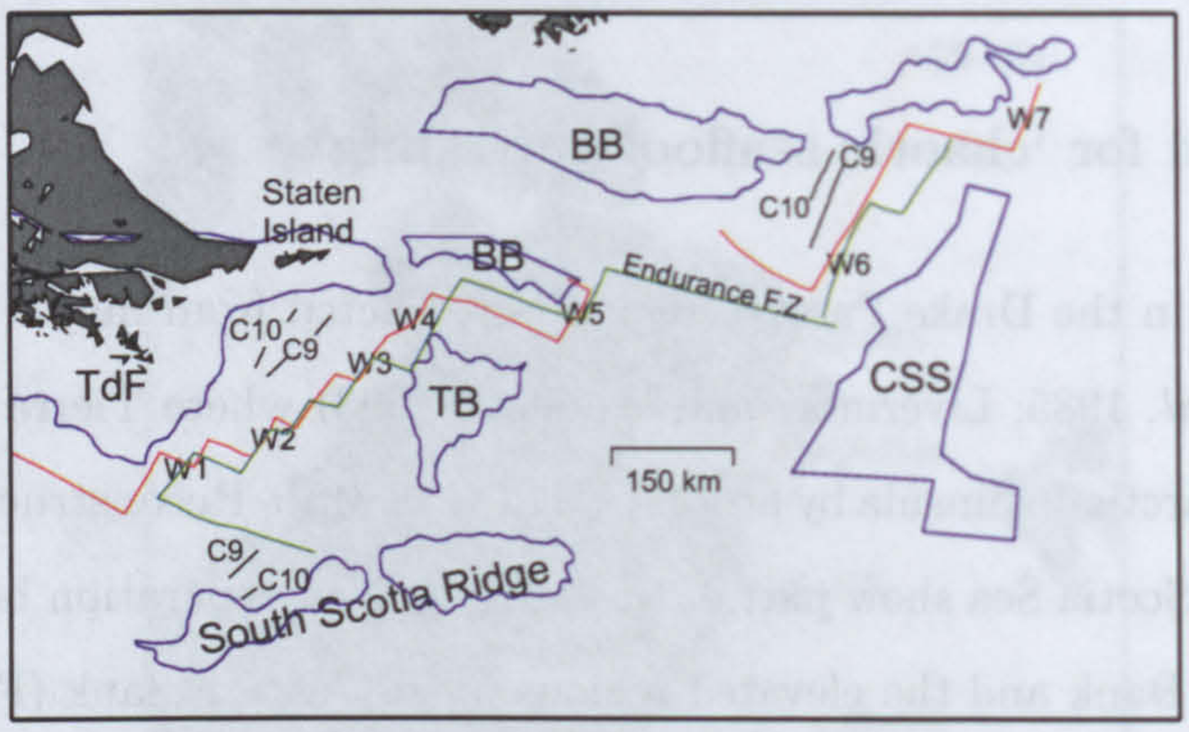

Figure 4.2: Reconstruction of west Scotia Sea at chron C8 using poles from Chapter 3. Blue: Bouguer anomaly outlines Tierra del Fuego (TdF), Burdwood Bank (BB), Terror block (TB), and a line around the province of east-striking magnetic reversal anomalies in the central Scotia Sea (CSS). Red and green lines: C8 ($\sim$ 26.5 Ma) on west and east flanks, respectively. Rift basins $\sim$ 150 km wide (approximate scale shown) are inferred on east flank (W1–W2, W4–W5), and west flank (W3, W6). Black lines: 'C9 and C10' anomalies of LaBrecque and Rabinowitz (1977); Lodolo *et al* (1998); Tectonic map of the Scotia arc, 1985, occupying the inferred rift basins.

Barker *et al* (1991) mention that further closure in the Barker *et al* (1984) reconstruction is achieved using the same rate and trajectory as the earliest seafloor spreading.

For closure of the stretched southern part of the west Scotia Sea I assume the east-northeast trending magnetic anomaly of Tierra del Fuego and the more attenuated east-northeast trending anomaly of the Terror block are conjugates. I attribute the difference in peak-to-peak amplitudes simply to the greater depth to source over the Terror block (Figure 4.3). The likely duration of a typical stretching episode, from intrusion of the first dykes to break-up is 7–15 million years (White and McKenzie, 1989). Assuming a single rotation of the west flank by 8.22°, lasting 10 million years, about a close-by reconstruction pole (36.8°N, 34.1°W) the conjugate edges of the magnetic anomalies are tightly reconstructed at 37 Ma. The C18y ($\sim$ 38.4 Ma) pole of Nankivell (1997a) (76.5°N, 1.8°E, 12.09° rotation of west flank with respect to east flank) provides a slightly less tight fit and implies a rifting episode of $\sim$ 12 million years duration. However this pole is more consistent with the 'close coupling' scenario which developed in Chapter 3.

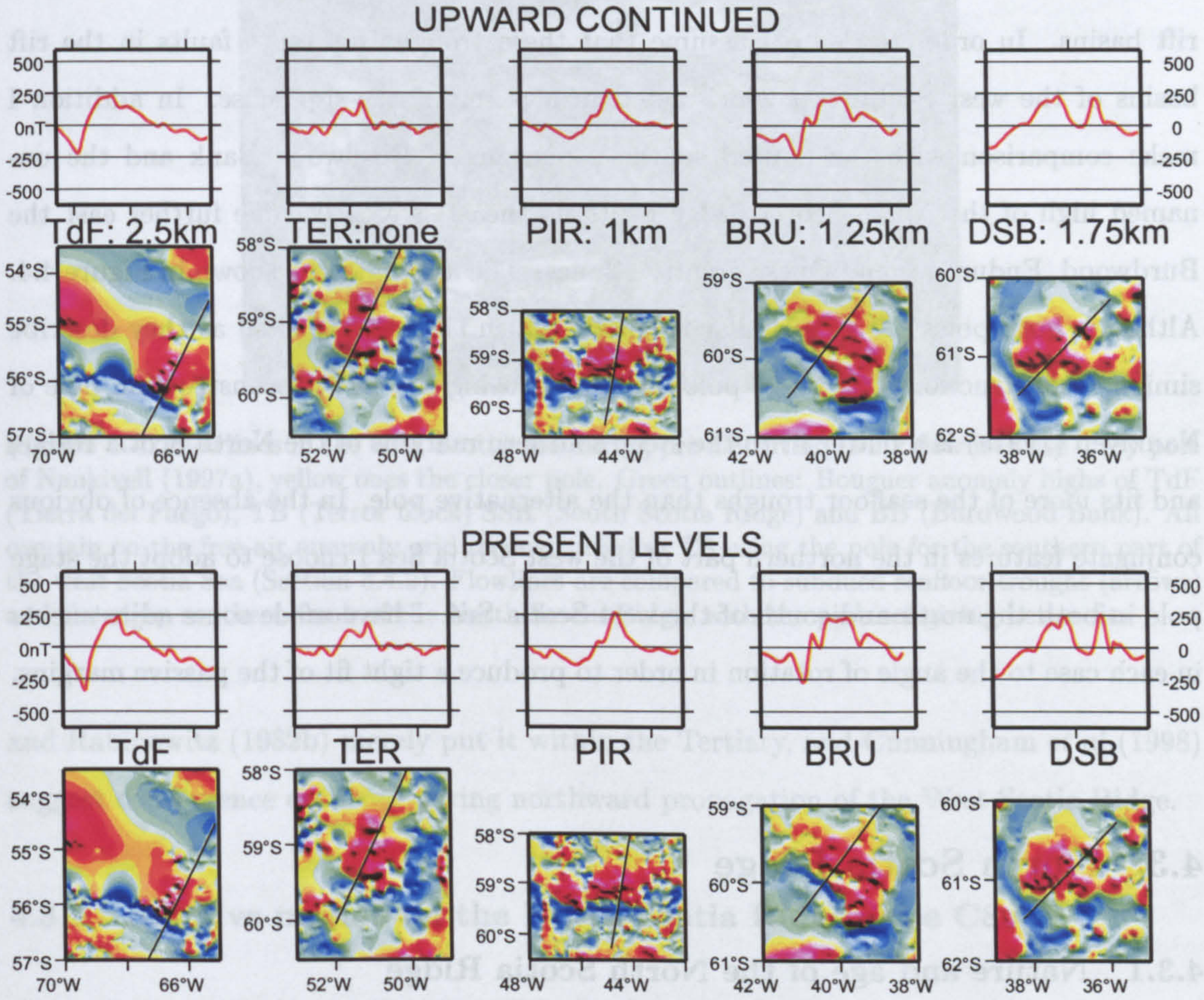

Figure 4.3: Bottom: five total field anomalies of similar width across-axis in Tierra del Fuego (TdF), the Terror block (TER), Pirie Bank (PIR), Bruce Bank (BRU) and southwestern Discovery Bank (DSB). Differing peak-to-peak amplitudes are shown by profiles over the grids along lines shown (left–right = south–north). Upward-continuation (top, distance in km) to the bathymetric level of the deepest component (Terror block) improves the likeness. Differences persist after upward-continuation—for instance anomalies over the Terror block and Pirie Bank have a more subdued negative component south of the positive peaks. These two blocks are the most subsided and it may be that processes related to extension (burial and/or intrusion) could have reduced the magnetic susceptibility of the batholith on each.

Assessment

To assess which of the alternative reconstruction poles to use I compare model flowlines about them to troughs in the free-air gravity anomaly crossing parts of the stretched rift basins. In order to do so I assume that these troughs represent faults in the rift basins of the west Scotia Sea which acted in a purely strike-slip sense. In addition I make comparison with the faulted southern margins of Burdwood Bank and the unnamed high of the North Scotia Ridge to its northeast, which become further east the Burdwood, Endurance and Quest Fracture Zones. The assessment is shown in Figure 4.4. Although both poles produce similar flowlines, which is to be expected as they describe similar reconstructions, the stage pole implied by using the C18y reconstruction pole of Nankivell (1997a) is a better fit to the steep southern margins of the North Scotia Ridge, and fits more of the seafloor troughs than the alternative pole. In the absence of obvious conjugate features in the northern part of the west Scotia Sea I choose to adopt the stage pole in both the north and south of the west Scotia Sea. I have made some adjustments in each case to the angle of rotation in order to produce a tight fit of the passive margins.

4.3 North Scotia Ridge

4.3.1 Nature and age of the North Scotia Ridge

Ludwig and Rabinowitz (1982b) use seismic reflection profiles as evidence for north-south compression of the North Scotia Ridge and subduction of the oceanic or thinned continental floor of the Falkland Trough (Ewing *et al*, 1971; Ludwig *et al*, 1978; Ludwig, 1983; Lorenzo and Mutter, 1988) beneath the Scotia Sea. In contrast Cunningham *et al* (1998) and Cunningham (1998) contend that compression, which gave rise to deformed sediment accretions on the northern side of the North Scotia Ridge buttress, may never have developed as full-blown subduction, and has mostly ceased and given way to local transpression. The timing of the onset of this convergence is even less well known, Ludwig

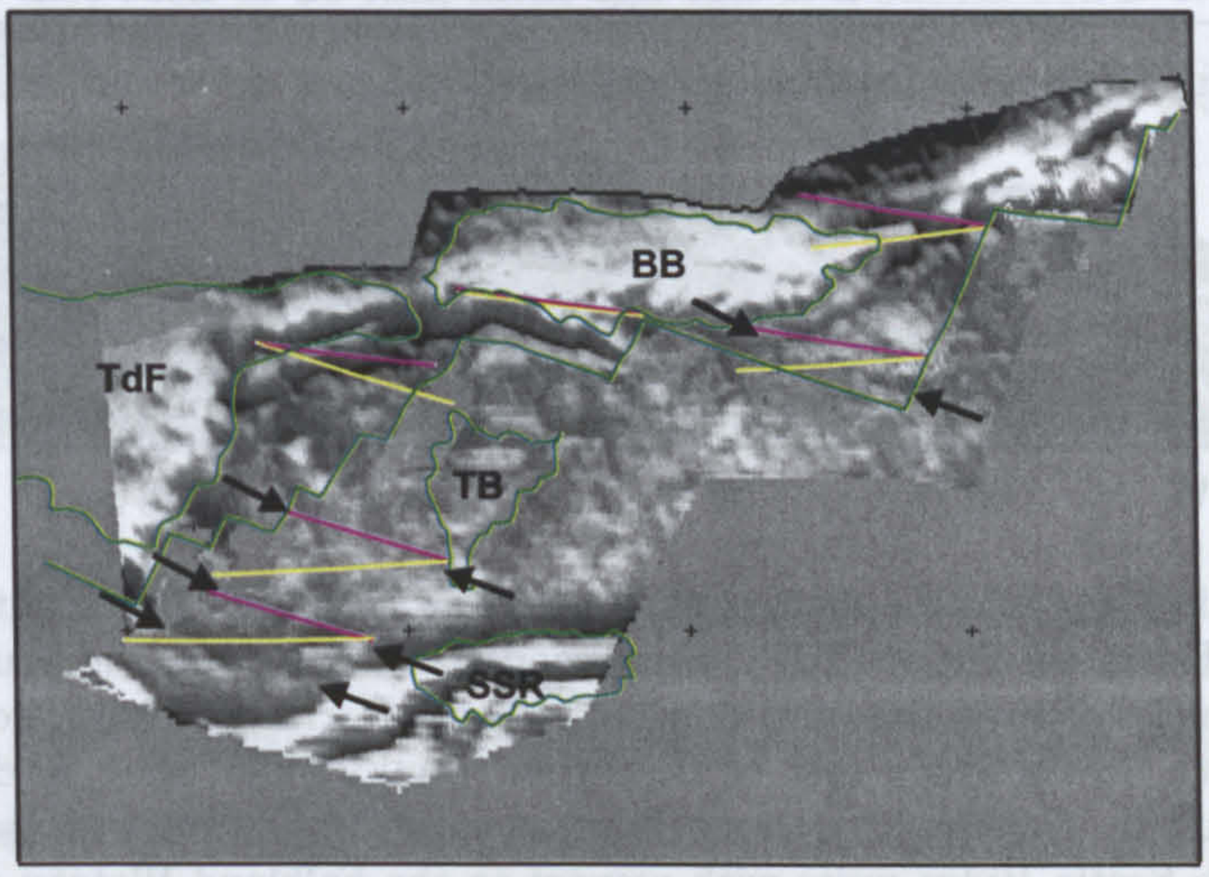

Figure 4.4: Flowlines in the west Scotia Sea during pre-C8 rifting. Pink flowlines use C18y pole of Nankivell (1997a), yellow ones the closer pole. Green outlines: Bouguer anomaly highs of TdF (Tierra del Fuego), TB (Terror block) SSR (South Scotia Ridge) and BB (Burdwood Bank). All overlain on the free-air anomaly grid reconstructed at C8 using the pole for the southern part of the west Scotia Sea (Section 3.4.2). Flowlines are compared to subdued seafloor troughs (arrows) and the steep southern flank of the North Scotia Ridge, with the pink set giving better fits.

and Rabinowitz (1982b) merely put it within the Tertiary, and Cunningham *et al* (1998) suggest convergence occurred during northward propagation of the West Scotia Ridge.

4.3.2 Relative motion on the North Scotia Ridge since C8o

Assuming that the North Scotia Ridge was the sole locus of decoupling between the South American–Antarctic and west Scotia Sea systems between C8 and C3a a flowline for relative movements on the North Scotia Ridge can be produced. A set of such flowlines is shown in Figure 4.5. The flowlines show movement of the flanks of the west Scotia Sea with respect to a fixed South American plate.

It would be unwise to place too much confidence in the detailed changes in the flowlines, because of the large instabilities in the west Scotia Sea poles with respect to the variation between them. However there is a pronounced change in the motion of the west

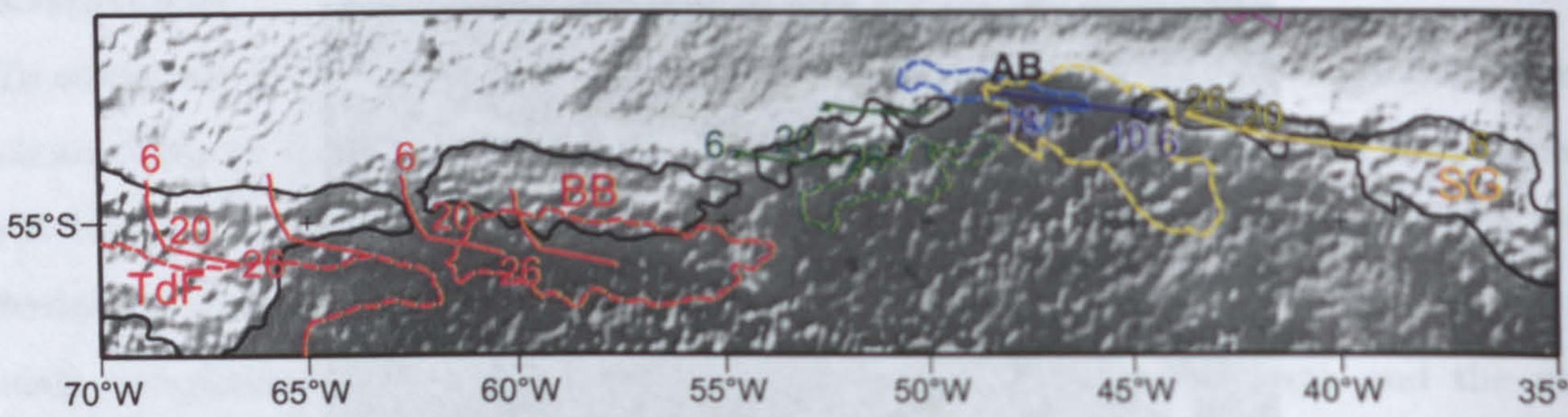

Figure 4.5: Flowlines for relative motion at North Scotia Ridge. Black outlines: present-day Bouguer highs at Tierra del Fuego (TdF), Burdwood Bank (BB) and the South Georgia microcontinent (SG). Thick coloured lines are flowlines. Red: Tierra del Fuego, southern Burdwood Bank; Green: North Scotia Ridge east of Burdwood Bank; Blue: Shag Rocks; Yellow: South Georgia microcontinent. Coloured numbers: flowline ages (Ma). Coloured dashed outlines: positions of the North Scotia Ridge units with respect to the Falkland Plateau at C8, red: Tierra del Fuego and Burdwood Bank, dark green: North Scotia Ridge, blue: Shag Rocks, yellow: South Georgia. Flowlines stop at 6 Ma, not showing modern sinistral strike-slip. AB: present location of Aurora Bank.

flank of the west Scotia Sea with respect to South America, which occurs at 20 Ma. A 20 Ma 'kinematic epoch' is evident in the reconstruction poles of the unmodified three-plate inversion of Nankivell (1997a) which have been used here, although the change is quite small. However, as shown here, when combined with the small changes in the reconstruction poles for spreading in the west Scotia Sea, which began to decelerate soon after 20 Ma, it is enough to have produced quite a pronounced alteration of the tectonic setting at the North Scotia Ridge.

On the west flank of the west Scotia Sea, relative motion between Burdwood Bank and the Falkland Plateau prior to 20 Ma is predicted to have been dextral strike-slip, fast, and occurring almost parallel to the axis of the Falkland Trough. The flowlines suggest that a more significant component of convergence is predicted further north, where the North Scotia Ridge strikes north of east, although here the West Scotia Ridge's west flank plate is subtly different. After 20 Ma and until extinction of the west Scotia Sea at 6 Ma, much slower relative movement is associated with the introduction of a significant component of convergence all along the ridge west of Aurora Bank. On the east flank, a change in

relative motion is also seen at 20 Ma, although this is a subtle bend. It implies a change from sinistral strike-slip with a minor component of extension (mild transtension), to a purer sense of strike-slip.

4.4 Protector Basin

4.4.1 Age of Protector Basin

Hill and Barker (1980) suggest that a spreading centre in Protector Basin may have been active in the post-c8 period on the grounds of postulated east–west extension in the southern part of the west Scotia Sea, needed to provide coincidence in their visual fits of C8 (Barker and Burrell, 1977). In the basin itself, which is about 200–250 km wide, a short sequence of magnetic reversals shows symmetry about a subdued central trough in free air gravity. Hill and Barker (1980) model this sequence as C5c (~ 16.7 Ma) to C5 (~ 10 Ma). This interpretation is based on a west Scotia Sea reconstruction by visual fitting which I believe to have been sufficiently flawed, because of its over-reliance on the Shackleton Fracture Zone as a tectonic flowline, to invalidate the 'circuit' closed within it. Thus only the reasonably good fit of reversal anomalies remains to commend it, and this requires adjustment to take account of a modern, more detailed, reversal timescale, such that a reasonable fit can only be achieved at spreading rates which are at least double those in the west Scotia Sea at the same time (Figure 4.6).

A seismic reflection survey crossing Protector Basin is reproduced in Figure 4.7, showing oceanic basement rocks present between 5 s and 6 s beneath a layer of sediments which reaches 1 s or more in thickness (all two-way-time). The basin's age, using the age–depth relationship of Parsons and Sclater (1977) and corrected for sedimentary loading using the scheme of Crough (1983), is determined at twelve sites across the basin (labelled a–l on Figure 4.7; Table 4.1). The ages show no progression from younger to older from the centre to the flanks of the basin, so no attempt is made to fit the data to a subsidence curve.

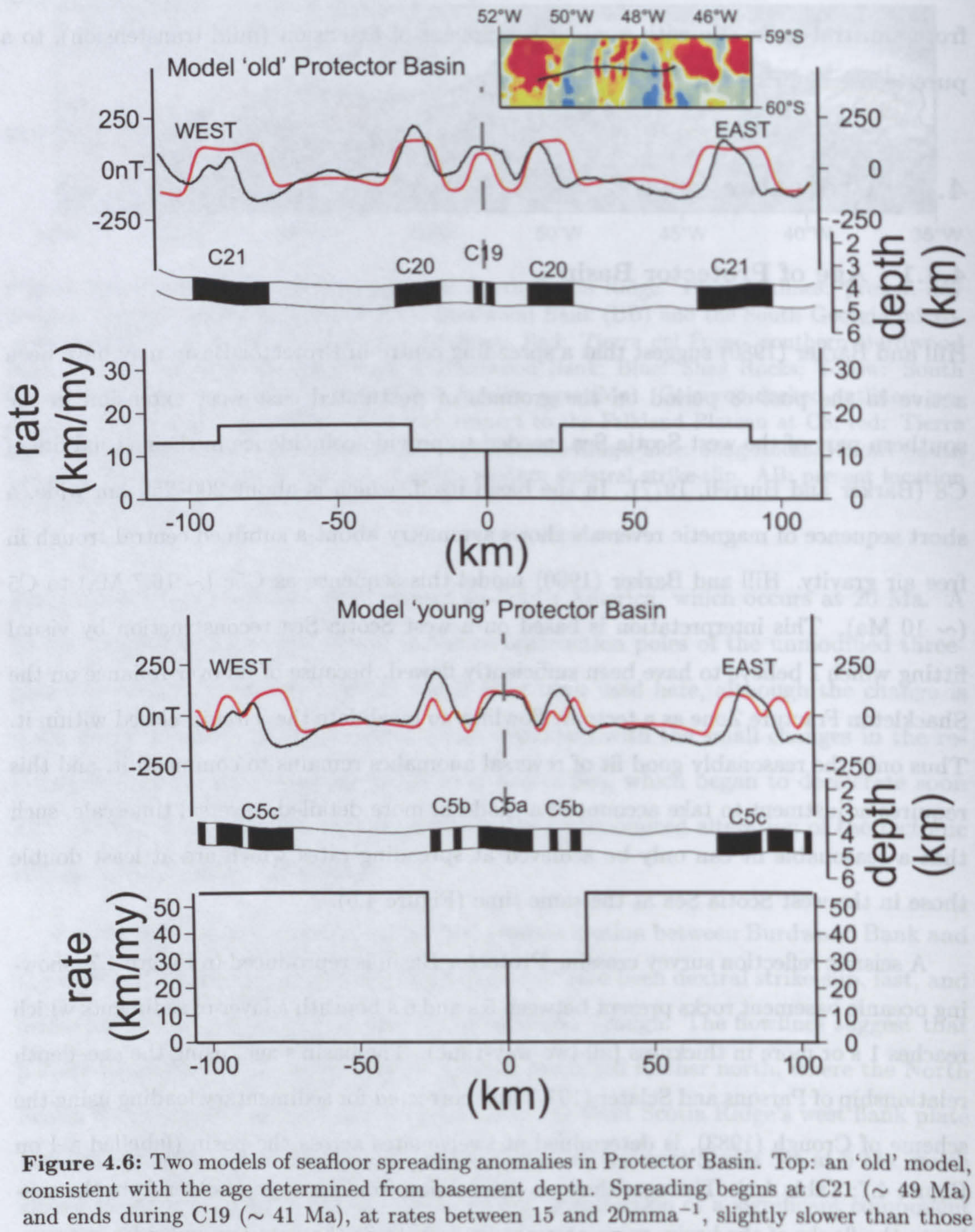

Figure 4.6: Two models of seafloor spreading anomalies in Protector Basin. Top: an 'old' model, consistent with the age determined from basement depth. Spreading begins at C21 ($\sim$ 49 Ma) and ends during C19 ($\sim$ 41 Ma), at rates between 15 and 20mma^{-1}, slightly slower than those in the west Scotia Sea models of Figures 2.16 and 2.17. Bottom: a 'young' model that falls within the bracket given by Hill and Barker (1980), re-modelled using the timescale of Cande and Kent (1995) instead of the older Lamont anomalies. To create a fit to the more detailed reversal sequence requires much faster spreading rates than in the original model. Inset shows the location of the magnetic profile.

Site	Seafloor time (ms)	Seafloor depth (m)	Sediment (ms)	Correction (m)	Corrected depth (m)	Age (Ma)
a	5180	3885	540	324	4209	25.9
b	5180	3885	1080	648	4533	36.6
c	5243	3932	1350	810	4742	44.5
d	5297	3973	1053	632	4605	39.2
e	5297	3973	729	437	4410	32.3
f	5432	4074	1080	648	4722	43.7
g	5405	4054	891	535	4589	38.7
h	5622	4217	810	486	4703	43.0
i	5216	3912	702	421	4333	29.8
j	5189	3892	864	518	4410	32.3
k	5185	3892	918	551	4443	33.4
l	5162	3872	405	243	4115	23.1

Table 4.1: Determinations of basin age from seafloor depth in Protector Basin, corrected for sedimentation. For locations see Figure 4.7. The correction used is 600 m for each two-way second of sediments.

The determined mean and median ages are close to 35 Ma and their distribution shows no significant mode. The lack of any subsidence signature, taken at face value, may be indicative of an even older basin age than that computed. Oceanic crustal ages are often not well determined from basement depth in small ocean basins, which led Burrell (1983) to reject an 'old' interpretation for Protector Basin in favour of that of Hill and Barker (1980). However, nearby Powell Basin, which has similar dimensions, obeys the age-depth relationship well (King and Barker, 1988; Eagles and Livermore, 1999; Section 4.5).

Clearly there is ambiguity regarding the age of Protector Basin, but none of the evidence presented here is inconsistent with an older Protector Basin than has been thought previously, whereas some of it is inconsistent with the younger age previously modelled. Unless the oceanic crust of the Protector Basin is unusual in some way—for instance being anomalously thin—basement depths might be admitted, at least to say that Protector Basin pre-dates the west Scotia Sea, and possibly that it does so by 10 million years or more. In fact, magnetic data recorded over the basin can be modelled by slow spreading between chrons C21 and C19 (49–41 Ma), which is consistent with the

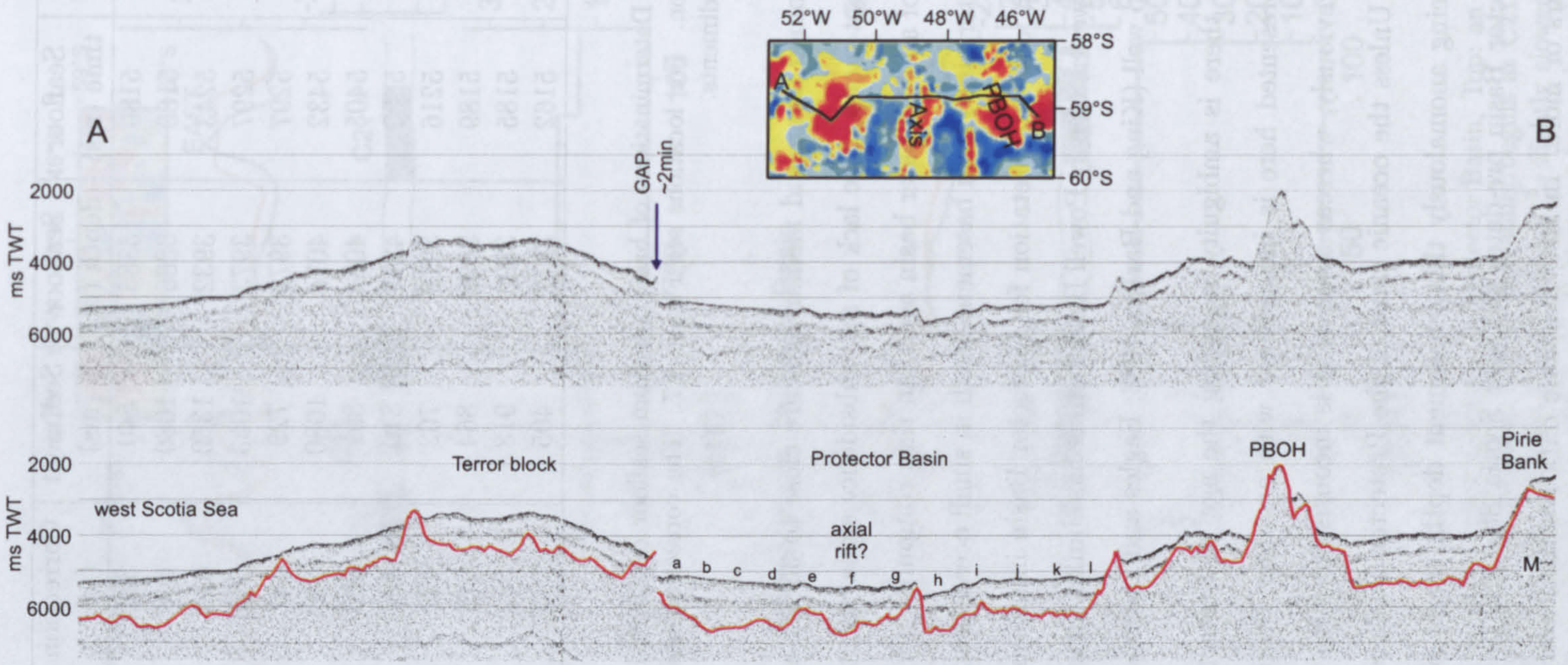

Figure 4.7: Single channel seismic reflection profile over Protector Basin, British Antarctic Survey, 1975. Data have been digitised from magnetic tape, processed to remove gaps between tapes. Automatic gain control and bandpass filtering have been applied to enhance the oceanic basement reflector below the sediments. Interpreted section (bottom) shows the basement reflector as a red line, a–l refer to the positions where basement age is determined (Table 4.1). PBOH: 'Pirie Bank Outlying High' refers to a relative high in the rift basin which was not picked from the Bouguer anomaly. M: seafloor multiple. Inset, location of profile overlaid on total field anomalies.

basement depth prediction of an 'old' Protector Basin (Figure 4.6).

I favour the older interpretation for Protector Basin given here because it does not require the basin to open at a time when it might complicate the simple, close-coupled, west Scotia Sea model developed in the previous chapter in the following ways:

1) The northern and southern parts of the west Scotia Sea were present within different microplate circuits (Chapter 3, Barker and Burrell (1977)). Protector Basin is an obvious location for an extra plate in the south but no combination of the reconstruction poles of Chapter 3, within their 95% confidence ellipses, requires extension there; instead $\sim$ 95 km of north–south *convergence* is needed to close the west Scotia Sea at C8.

2) Any reconstruction where Protector Basin opens at the same time as the west Scotia Sea implies significant transfer movement of Pirie and Bruce banks with respect to the South Scotia Ridge and the central Scotia Sea, and fluctuations in the rate of subduction beneath Bruce Bank with respect to subduction further north, to balance the acceleration of the opening basin (see Chapter 5, Figure 5.2, and Hill (1978)). I can see no compelling evidence in the form of fossil plate boundaries for any of this complexity.

Reconstruction of Protector Basin is neither necessary nor sufficient for closing the Scotia Sea at C8 in this model. Indeed its inclusion needlessly complicates matters. An earlier opening is a simpler proposition for the model Scotia Sea's development so I suggest, tentatively, an older age of $\sim$ 49–41 Ma (*i.e.* inception at C21) and call attention firstly to the (albeit disputable) evidence favouring it and secondly to the circumstances of regional reconstructions in which extra accretion is required in the Drake Passage region prior to C8 (Lawver *et al*, 1985; Livermore and Woollett, 1993). In fact Livermore and Woollett (1993) suggest this extension may have begun at C21, upon consideration of stage poles from visual fitting of Weddell Sea magnetic anomalies; this suggestion is supported by consideration of the stage poles of Nankivell (1997a) which also exit a stable period at the same time.

With the rejection of the 'young' model of Protector Basin, I suggest that the differential motion between the north and south parts of the west Scotia Sea (C8–C3a) is

instead taken up elsewhere—maybe by convergent deformation of the western Endurance Fracture Zone and Burdwood Bank.

4.4.2 Reconstructing Protector Basin

Previous reconstructions

Protector Basin is shown closed in the 20 Ma reconstruction of Barker *et al* (1984), but no elevated region is shown on its western flank. Presumably Pirie Bank has been translated westward, perpendicular to the reversal anomalies of Hill and Barker (1980).

Reconstruction criteria for Protector Basin are shown in Figure 4.8. I reconstruct Protector Basin to the start of spreading by making visual fits of the reversal anomalies within the basin. In addition, for a reconstruction at closure, I assume the linear magnetic anomaly along the southern margin of Pirie Bank is a conjugate feature to the anomaly on the Terror block. In doing so I consider a stretched Patagonian batholith to have extended through the Terror block and Pirie Bank prior to the opening of Protector Basin—possibly as recently as 49 Ma (Figure 4.3). Reconstruction poles with longitudes at or very near to 50°W, but with latitudes in the range 40°S to 90°N, produce reasonable fits for all the features. A set of short, poorly-defined, east-striking troughs is present within Protector Basin, possibly including its southern margin along the northern base of the South Scotia Ridge. These troughs may represent fracture zones, and are better fit by a model using a more remote pole. As a result a pole at 80°N, 50°W is adopted for the full development of Protector Basin. Rotations of 2.75° and 3.7° produce start-of-spreading and closure reconstructions, respectively.

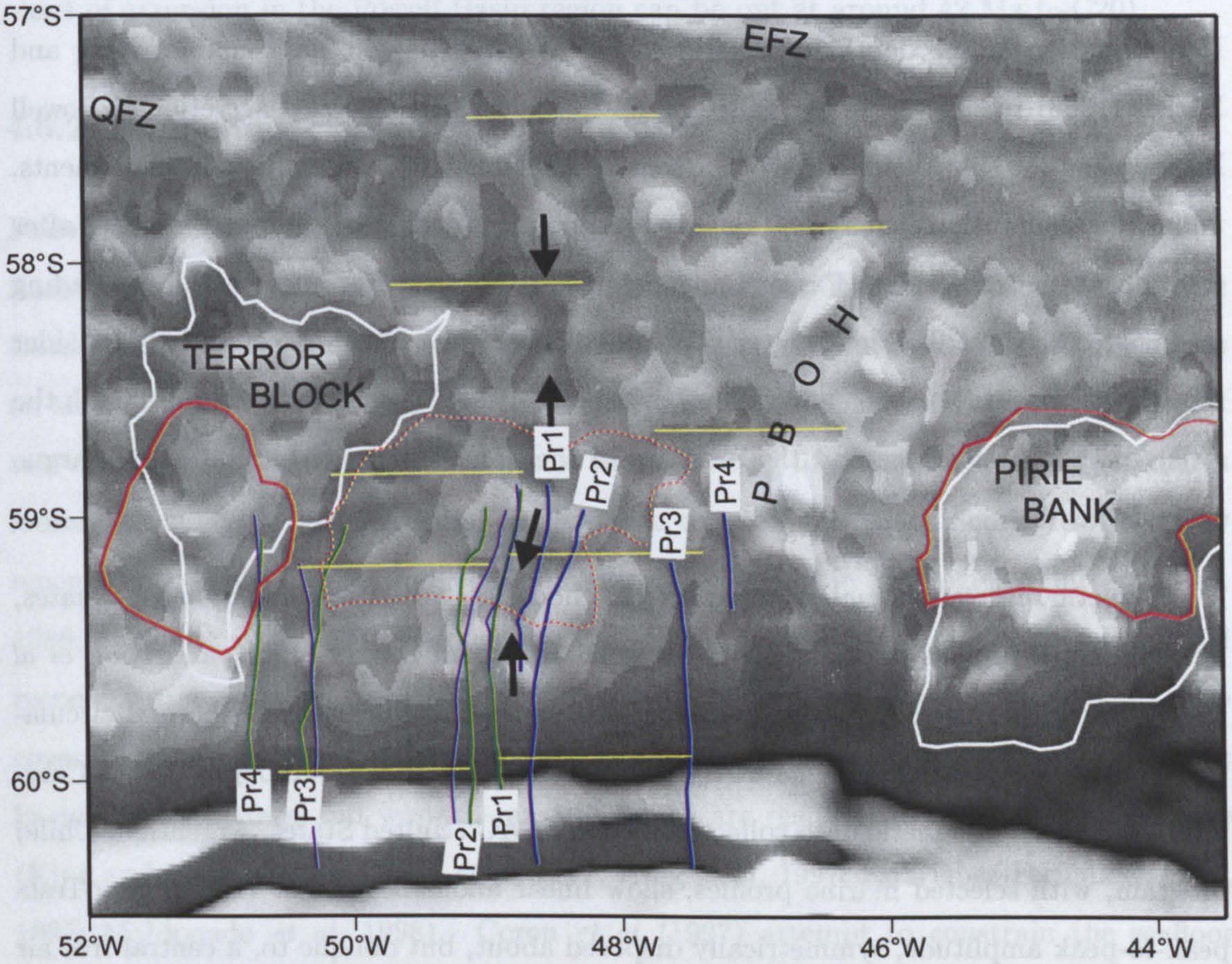

Figure 4.8: Reconstruction of Protector Basin opening, using pole given in the text. Background: modern free-air anomaly. Reversal anomalies (green and blue lines, Pr1–Pr4) are symmetrical about subdued segmented central trough (arrows). In the favoured model Pr1 = C19o, Pr2 = C20y, Pr3 = C21y and Pr4 = C21o. White outlines: Bouguer highs. Red outlines: 'batholith' anomaly; thin dark blue lines: reconstructed east flank reversal anomalies. Dashed red line: reconstructed Pirie Bank 'batholith' anomaly. Yellow lines: model flowlines. Comparable troughs are present well north of the magnetic reversals; Protector Basin spreading may have extended to Quest (QFZ) or Endurance (EFZ) fracture zone. PBOH: gravity expression of 'Pirie Bank Outlying High' from Figure 4.7.

4.5 Powell Basin

4.5.1 Age and nature of Powell Basin

Determination of the depth to oceanic basement using seismic data enables King and Barker (1988) to suggest an age range of 29–23 Ma for oceanic crust accretion in Powell Basin, using the subsidence curve of Parsons and Sclater (1977). Heat flow measurements, under the assumption that Powell Basin's oceanic crust cooled in a 'typical' manner after creation at an axial ridge (Parsons and Sclater, 1977), however suggest that spreading may have ceased at 30.5 Ma (Lawver *et al*, 1994; Howe *et al*, 1998). Most authors consider that Powell Basin formed as a back-arc basin behind the 'Discovery' trench, although the strike of the Powell ridge and the presence of the Jane–Discovery back-arc basin argue against this.

Magnetic reversal anomalies would help to choose between the different age estimates, but ship-track profiles do not show them well. King and Barker (1988) and King *et al* (1997) attribute this to a poor source due to slow cooling during hydrothermal circulation within thick axial sediments at the ridge crest (Levi and Riddihough, 1986). Carefully levelled aeromagnetic data collected by the USAC (United States, Argentina, Chile) program, with selected marine profiles, show linear anomalies, a few tens of nanoTesla peak-to-peak amplitude, symmetrically disposed about, but oblique to, a central free air gravity trough (Figures 4.9 and 4.13). High-pass filtering, to remove a long wavelength negative component of the Pacific Margin Anomaly (the USAC data do not show enough of the anomaly to allow reduction to the pole to remove the component), shows that the lineations represent polarity reversals. Profiles taken over the grid of reversals are compared with synthetics for the two age ranges suggested by basement depth and heat flow, with plausible fits achieved for each. However the older timescale predicts some minor peaks which are not evident on the grid, whereas the age–depth guided timescale (Figure 4.10) does not. So seafloor spreading in Powell Basin is put tentatively at between 32.1 (C12) and 23.3 Ma (C6c). This is broadly consistent with the intrusion of alkali

basalt dykes at 31–29 Ma on Livingston Island, South Shetland Islands, which has been suggested to be related to opening of Powell Basin (Willan and Kelley, 1999). Assuming a 10 million years-long rifting episode, which immediately proceeded to spreading, the onset of extension in the Powell Basin region can be put at around 42 Ma (~C20).

4.5.2 Modelling closure of Powell Basin

Previous reconstructions

Assuming former continuity of Pacific accretionary terranes, Dalziel and Elliott (1971) and Dalziel (1982; 1984), attempt reconstructions by restoring Mesozoic stretching lineations on the South Orkney, Elephant, and Clarence islands. Meneilly and Storey (1986) reject this on the basis of uncertain affinities of the stretching lineations, instead advocating a looser fit merely by extending the bathymetric trend of the South Scotia Ridge. Later reconstructions fit the disrupted Pacific Margin Anomaly in the region (Garrett *et al*, 1986; Suriñach *et al*, 1997; Maldonado *et al*, 1998). Garrett *et al* (1986) present a total reconstruction pole for the PMA, at 67°S, 50°W with a rotation angle of 30°. Dense coverage of Powell Basin by seismic reflection data enables interpretation of paired rift basins on its eastern and western margins which are restored in recent reconstructions (King and Barker, 1988; Coren *et al*, 1997; King *et al*, 1997; Rodriguez-Fernandez *et al*, 1997; Maldonado *et al*, 1998). Coren *et al* (1997) attempt to constrain the seafloor spreading stage of Powell Basin development using a single magnetic anomaly profile. The resulting model suggests two-stages of seafloor spreading—the latter stage accretes material to the eastern flank only (Figure 4.11). Consideration of the magnetic reversal anomalies of the grid reveals no evidence to support such a model.

Full reconstructions of the region suffer from large overlap of the South Scotia Ridge and South Orkney Microcontinent (Figure 4.12a) which has never been satisfactorily addressed. The nature and timing of seafloor spreading was, until now, uncertain due to the lack of magnetic reversal isochron control.

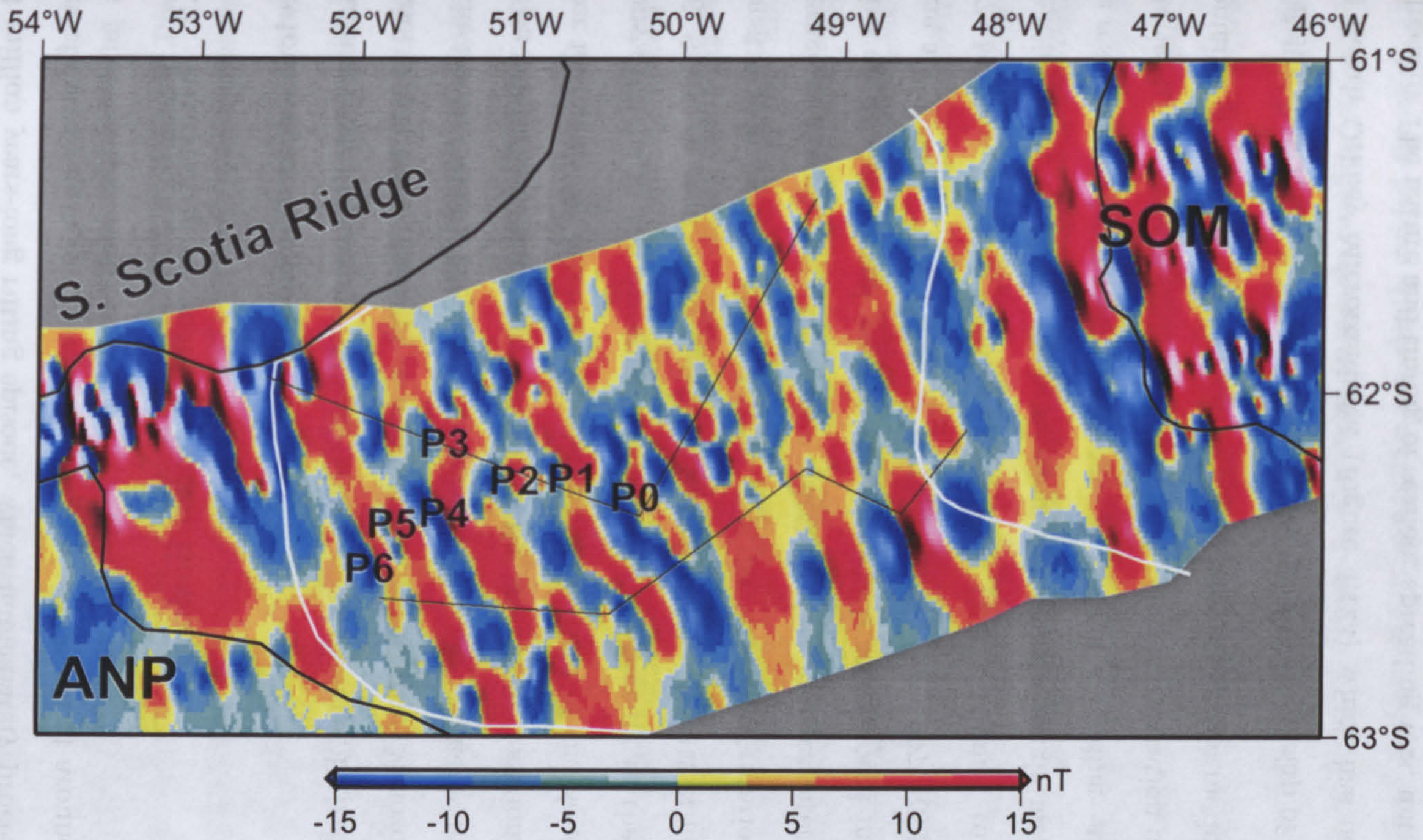

Figure 4.9: Gridded magnetic anomalies over Powell Basin recorded by nine equally-spaced USAC flights crossing the basin from southwest to northeast, produced by Peter Morris of BAS. The data are high-pass filtered to reveal low-amplitude reversal anomalies. Six anomalies (P1–P6) are present on each flank, with P0 the central anomaly. Thick black lines: Bouguer anomalies of South Orkney Microcontinent (SOM), Antarctic Peninsula (ANP) and South Scotia Ridge. White lines: seaward limit of 'extended continental crust' (King *et al*, 1997). Rotated fault blocks or volcanic flows may express the high amplitude anomalies within the extended regions. Thin black lines: profiles over grid for comparison to synthetics (Figure 4.10).

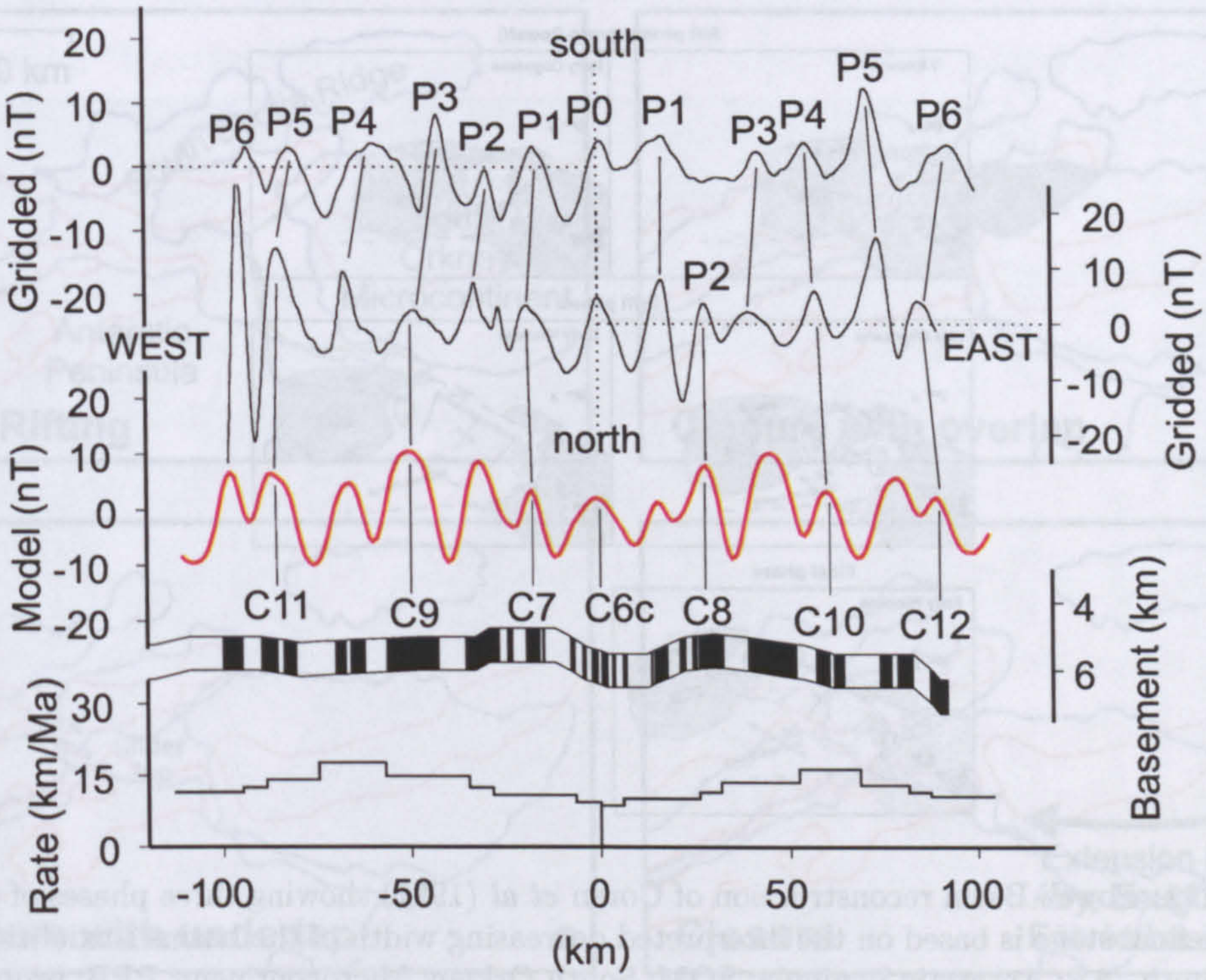

Figure 4.10: Model of seafloor spreading anomalies in Powell Basin. Synthetic seafloor spreading anomalies (red) for Powell Basin, between 32.1 Ma and 23.3 Ma, modelled using a 1 km thick layer whose upper surface is defined by seismic basement in the basin (Coren *et al*, 1997). The sequence of anomalies in Powell Basin (P0–P6), taken from the grid along the lines shown in Figure 4.9, corresponds to anomalies C6c–C12 in the timescale of Cande and Kent (1995).

Reconstruction Poles for Powell Basin

Filtered aeromagnetic data show the pattern of magnetic reversal isochrons in Powell Basin for the first time. Visual fitting of these isochrons is possible, enabling real constraint on seafloor spreading in Powell basin. Reconstruction of the marginal rift basins makes use of their seismic and free-air gravity expressions. Constraint is possible for full closure using the free-air anomaly expressions of basins within the South Orkney Microcontinent and by recreating a continuous Pacific Margin Anomaly.

At closure the older (landward) edges of the free-air anomalies are digitised for fitting

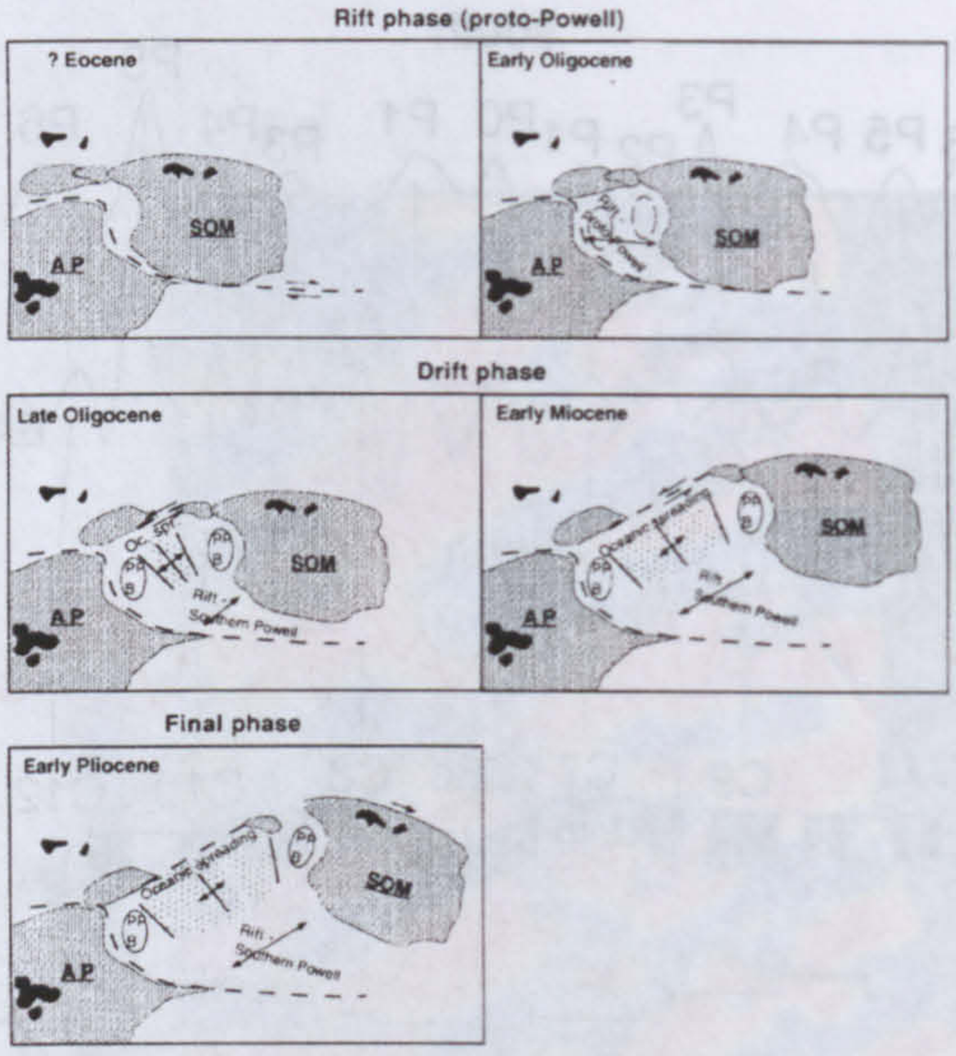

Figure 4.11: Powell Basin reconstruction of Coren *et al* (1997) showing three phases of development. The final stage is based on the interpreted decreasing width of the basins's axial ridge from north to south. AP: Antarctic Peninula; SOM: South Orkney Microcontinent; PPB: proto-Powell Basin.

by test rotations in *ATLAS*. These edges provide east–west constraint on the reconstruction. North–south constraint is supplied by the northern edge of the Pacific Margin Anomaly which strikes roughly east through the Antarctic Peninsula and South Orkney Microcontinent. Reconstruction of Powell Basin at closure is achieved by rotation of the South Orkney Microcontinent by 14.6° about a pole at 72.6°S, 37.5°W. For end-rifting reconstruction (Figure 4.12) the younger (oceanward) edges of the rift basin King *et al* (1997) are digitised and fitted. There is no obvious complexity in the reversal anomaly sequence, so a simple spreading phase seems most likely. This is described by a pole which moves the South Orkney Microcontinent from its end-rifting position to its present day position with respect to the Antarctic Peninsula: by 12.9° about a pole at 69.7°S, 38.1°W. This pole is tested by looking at the visual fits of outlines drawn around the gridded conjugate magnetic isochrons (Figure 4.13). The success of the pole in this task

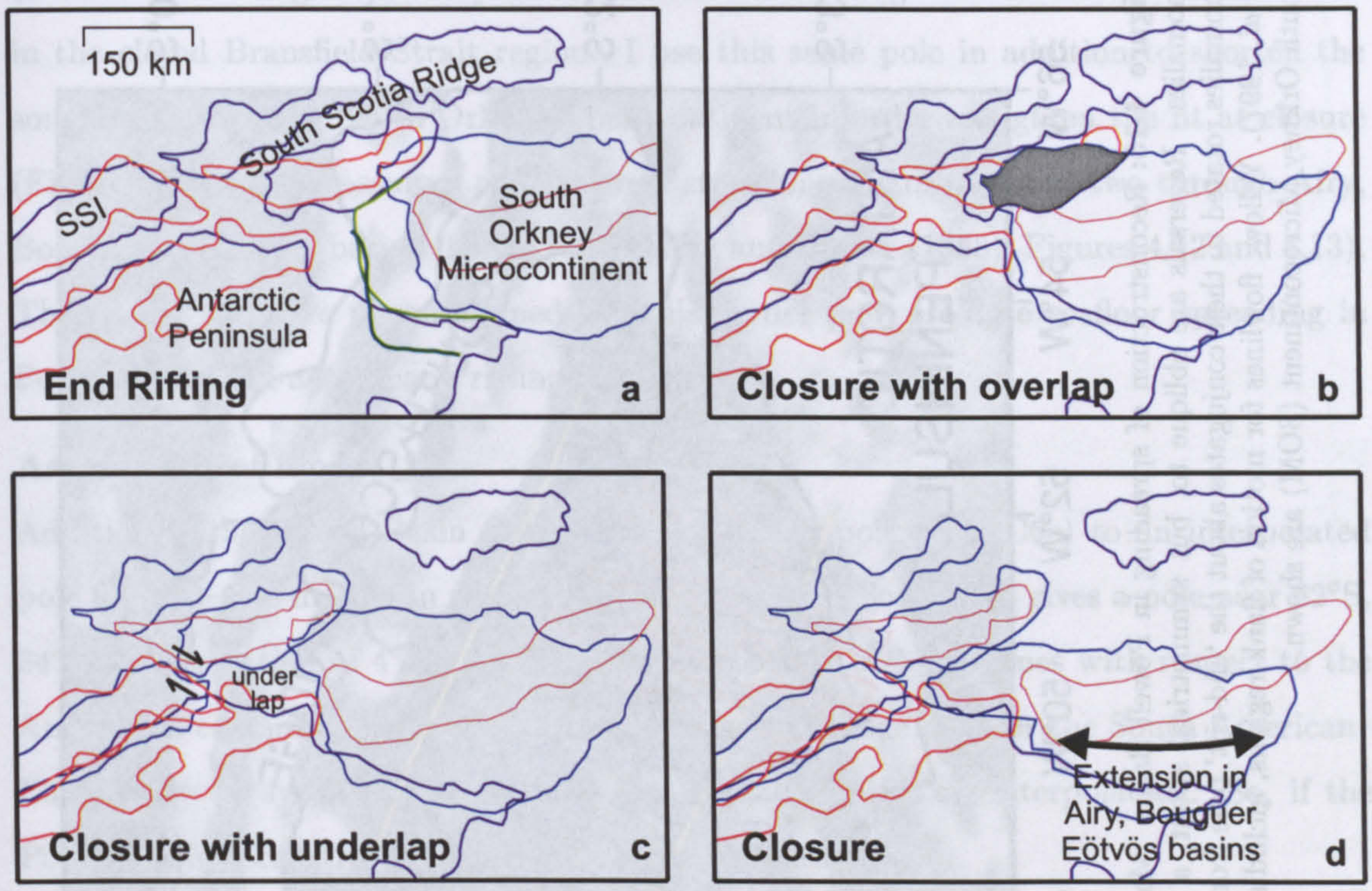

Figure 4.12: Four stages in modelling of Powell Basin. Blue outlines: Bouguer anomalies and red: parts of the Pacific Margin Anomaly. (a) end rifting reconstruction shows fit of seaward edges of 'extended continental crust' (green; King *et al* (1997)). (b) closure reconstruction by fitting Pacific Margin Anomaly. Grey: Problem overlap of South Orkney Microcontinent and South Scotia Ridge. (c) removal of overlap by aligning northern branch of Pacific Margin Anomaly in South Scotia Ridge and South Shetland Islands (closure of Bransfield Strait and inclusion of western South Scotia Ridge in Powell rifting episode). (d) further tightening of fit by including extension of southern part of South Orkney Microcontinent—Airy, Bouguer and Eötvös basins.

suggests that seafloor spreading in Powell Basin was indeed a single stage, steady affair.

To remove the overlap in the northwest of the closed Powell Basin region (Figure 4.12b) some movement of the South Scotia Ridge was long deemed necessary (Garrett *et al*, 1986; King and Barker, 1988; King *et al*, 1997). This is achieved by movement of the South Scotia Ridge along an offset, which is evident in both the Pacific Margin Anomaly and the gravity anomalies, between the South Shetland Islands and the South Scotia Ridge (Figure 4.12c). The stage pole for rifting in Powell Basin produces a good alignment

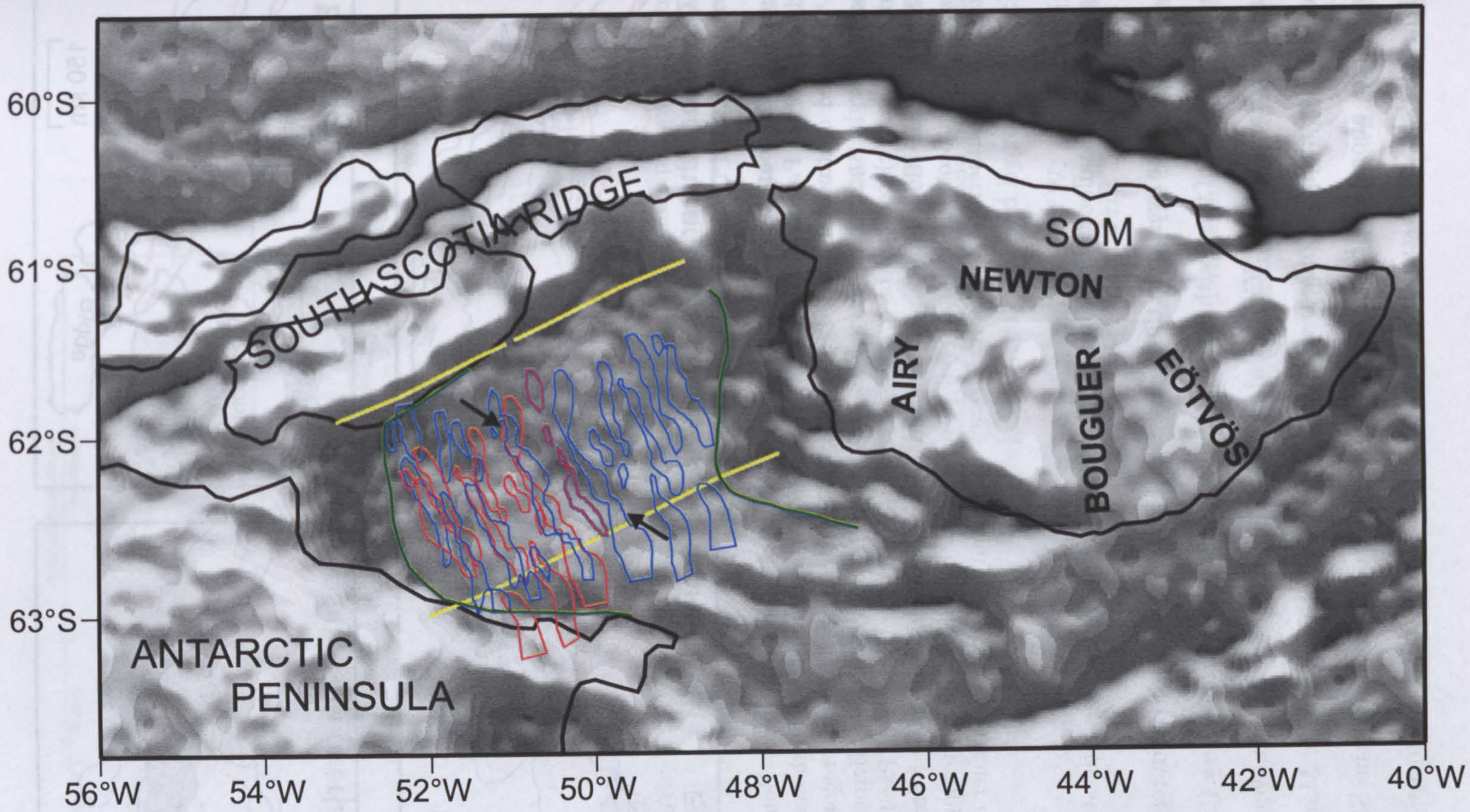

Figure 4.13: Reconstruction of spreading in Powell Basin. Magnetic reversal anomalies from the grid (blue) overlain on free-air anomalies. Reversals are oblique to, but symmetrical about, a central gravity trough (arrows). Red outlines: east-flank reversal anomalies rotated to their conjugates about the 'end-rift' pole from the text. Green: seaward edge of extended continental crust (King *et al*, 1997). Yellow: flowlines for motion of flank regions, including rifting episode. Airy, Bouguer, Eötvös and Newton basins on the South Orkney Microcontinent (SOM) are shown.

of the Pacific Margin Anomaly on the South Scotia Ridge and South Shetland Islands in the closed Bransfield Strait region. I use this same pole in addition to shorten the southern part of the South Orkney Microcontinent in order to tighten the fit at closure (Figure 4.12d). This assumes an east–west stretching factor of about two through Airy, Bouguer and Eötvös basins (King (1983); King and Barker (1988); Figures 4.12 and 4.13). The basins' ages are unconstrained—in this model they pre-date seafloor spreading in Powell Basin and accompany rifting there.

Assessment of model

Addition of the Powell Basin closure reconstruction pole (C12–C6c) to an interpolated pole for C12–C6c motion in the south part of the west Scotia Sea gives a pole near 62°S, 34°W, and rotation of 4° as a stage pole for rotation of Magallanes with respect to the Antarctic Peninsula. This bears no resemblance to a stage pole for the South American–East Antarctic system for that timescale (Nankivell (1997a), interpolated). So, if the Powell Basin reconstruction pole is correct, then either

1) the basin can not have been present in a simple circuit between South America and East Antarctica, or

2) the determinations of its age are all wrong.

As shown here, Powell Basin's age and opening seem well constrained by a variety of data, so the former case seems more reasonable. In addition to the complications to the circuit within the Scotia Sea, a reconstruction pole for relative movement between West Antarctica (which includes the Antarctic Peninsula) and East Antarctica, in opening of the Adare Trough, Ross Sea, is given for chron C13 by Cande *et al* (2000), along with a 95% confidence ellipse. Assuming this rotation was finished by C6c time (24 Ma—in fact Cande *et al* (2000) put extinction of the Adare Trough between 28 and 26 Ma), a hypothetical circuit equivalent to South American–East Antarctic relative motion could be constructed which includes both the Scotia Sea and Adare Trough regions. One simple circuit like this incorporates movement on the North Scotia Ridge (Section 4.3), the southern west Scotia Sea (Section 3.4.2), Powell Basin (this section), and the Adare

Trough (Cande *et al* (2000); Figure 4.14). The circuit can be closed using poles from this study and an Adare Trough reconstruction pole at 69°S, 43°W, having 11° rotation (East Antarctica with respect to West Antarctica). Even notwithstanding the undoubtedly large uncertainty in the Powell Basin pole, and the over-simple circuit, this pole falls just inside the southern extremity of the 95% confidence ellipse given by Cande *et al* (2000) (Figure 4.14). So extension in Powell Basin, the only reconstruction in the circuit for which no confidence ellipses have been determined, can be said to be very close to consistent with the crude circuit hypothesised here. Considering the encouraging nature of this result, and the possibility of unknown further minor movements between the Antarctic Peninsula and East Antarctica, I suggest that more confidence can be placed in the interpretation of Powell Basin as a local consequence of major plate motion (Eagles and Livermore, 1999), rather than as a back-arc basin (King and Barker, 1988). Such confidence can be equated with confidence in the circuit hypothesised for it. More work should be applied, therefore, to the characterization of plate boundaries within and between West Antarctica and East Antarctica during the Cenozoic, not least the South Scotia Ridge.

4.6 Dove Basin

4.6.1 Age of Dove Basin

There has been no published work on the age of Dove Basin, the basin intervening between Pirie and Bruce Banks, and named informally so by Hill (1978). Hill (1978) suggests, based on its depth, that Dove Basin is the site of the oldest seafloor in the Scotia Sea. Burrell (1983) merely suggests that it could have formed by back-arc extension as part of a multiphase back-arc Scotia Sea. Seismic reflection data (Figure 4.15) show basement rocks which, if they are assumed to be of oceanic crust, have a sediment-corrected depth suggesting Dove Basin was opening around 37 Ma (mean and median of determinations at a–q, Figure 4.15, Table 4.2).

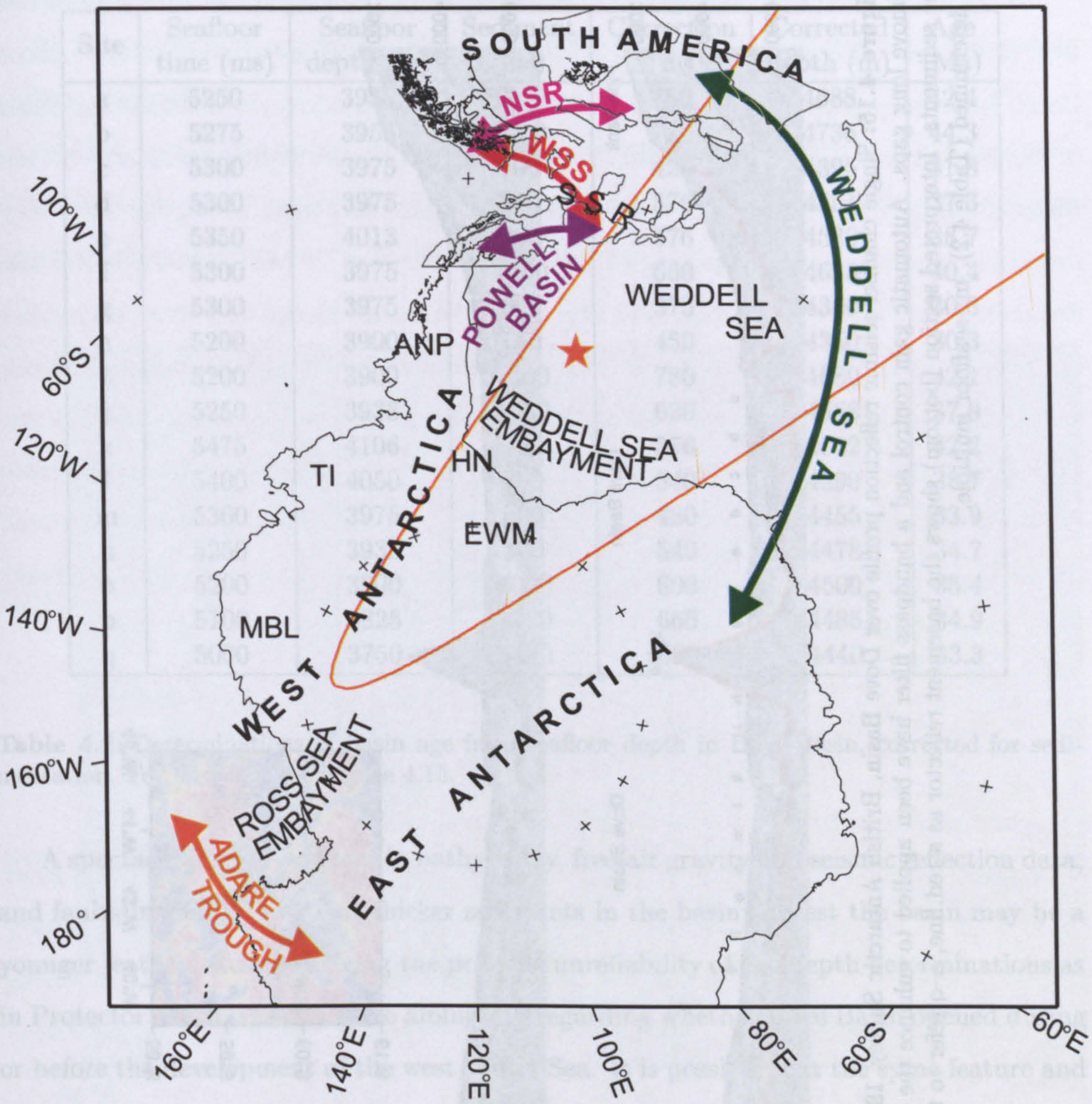

Figure 4.14: A possible South American–East Antarctic plate circuit including movement on the North Scotia Ridge (NSR), spreading in the west Scotia Sea (WSS), Powell Basin, Adare Trough, and Weddell Sea. Bouguer anomaly highs in the Scotia Sea are reconstructed to their positions at C8 relative to East Antarctica which is fixed. The circuit can be closed using poles from the text, and a reconstruction pole—at the orange star—for spreading in the Adare Trough. Compare this to the 95% confidence ellipse (orange) for East Antarctica–West Antarctica relative motion—expressed by Adare Trough spreading (orange arrow) determined by Cande *et al* (2000). Additional plate boundaries may have existed at the South Scotia Ridge (SSR) or within West Antarctica, which consists of several discrete crustal blocks: MBL, Marie Byrd Land; TI, Thurston Island; EWM, Ellsworth-Whitmore Mountains; HN, Haag Nunataks; ANP, Antarctic Peninsula.

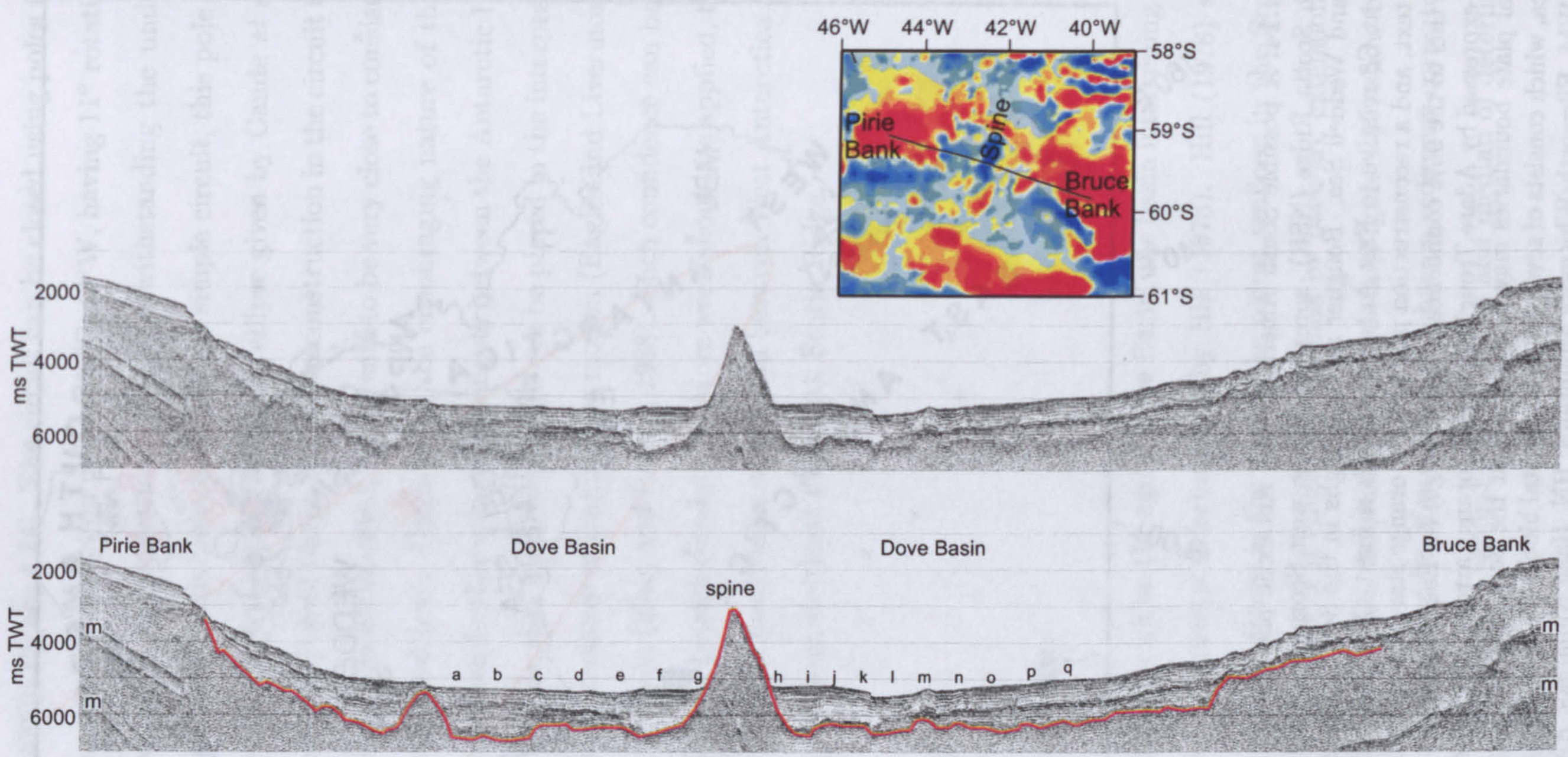

Figure 4.15: Single channel seismic reflection profile over Dove Basin, British Antarctic Survey, 1988. Data have been processed to remove long gaps. Automatic gain control and a bandpass filter have been applied to enhance the oceanic basement reflector below the sediments. Interpreted section (bottom) shows the basement reflector as a red line, a–q refer to the positions where basement age is determined (Table 4.2). m: seafloor multiple.

Site	Seafloor time (ms)	Seafloor depth (m)	Sediment (ms)	Correction (m)	Corrected depth (m)	Age (Ma)
a	5250	3938	1250	750	4688	42.4
b	5275	3956	1300	780	4736	44.3
c	5300	3975	700	420	4395	31.8
d	5300	3975	950	576	4551	37.3
e	5350	4013	950	576	4589	38.7
f	5300	3975	1100	660	4635	40.4
g	5300	3975	625	375	4350	30.3
h	5200	3900	750	450	4350	30.3
i	5200	3900	1300	780	4680	42.1
j	5250	3938	1050	630	4568	37.9
k	5475	4106	950	576	4682	42.2
l	5400	4050	900	540	4590	38.7
m	5300	3975	800	480	4455	33.9
n	5250	3938	900	540	4478	34.7
o	5200	3900	1000	600	4500	35.4
p	5100	3825	1100	660	4485	34.9
q	5000	3750	1150	690	4440	33.3

Table 4.2: Determinations of basin age from seafloor depth in Dove Basin, corrected for sedimentation. For locations see Figure 4.15.

A spectacular spine, evident in bathymetry, free-air gravity and seismic reflection data, and faults breaking the 1 s-or-thicker sediments in the basin suggest the basin may be a younger feature. Acknowledging the possible unreliability of age-depth determinations as in Protector Basin, there is some ambiguity regarding whether Dove Basin opened during or before the development of the west Scotia Sea. It is possible that the spine feature and faults could be explained by recent reactivation of an 'old' Dove Basin. The spine has a strong negative magnetization so is unlikely to be a Recent feature: similar highs, both fossils, are known from Powell Basin ($\sim$ 23 Ma) (King *et al*, 1997) and from the Phoenix Ridge ($\sim$ 3 Ma) (Livermore *et al*, 2000), and have been related to volcanism draining a magma plumbing system after spreading ceases. A very short sequence of two or three magnetic reversal anomalies are present over the basin but I consider them too poorly developed to attempt to model.

As for Protector Basin, attempts to model Dove Basin opening at the same time as the west Scotia Sea imply plate boundaries between the central Scotia Sea and northern Bruce Bank, between southern Bruce Bank and the South Scotia Ridge, and differential rates of subduction at the South Sandwich Trench, for which there is little evidence. Given these admittedly flimsy premises I opt to use the basement depth as a guide to a very tentative determination for opening of Dove Basin between 44 Ma and 30 Ma (Middle Eocene). I note that this overlaps with the age for Protector Basin, and that this implies complexity. If these ages are anywhere near appropriate then Dove Basin and its environs should have been undergoing thermal subsidence following intitial rifting during this time. Possible evidence for Eocene subsidence is given by water depth determinations for Bruce Bank (increasing in the range 800-1500m, 49–47 Ma or Middle Eocene), using planktonic foraminifers, pollen and spores collected from core samples on its southern flank (Toker *et al*, 1991; Mao and Mohr, 1995).

4.6.2 Modelling closure of Dove Basin

Previous reconstructions

No attempt is made in the reconstructions of Barker *et al* (1984) to close Dove Basin prior to 30 Ma. Dove Basin does not exist in the 40 Ma reconstruction of King and Barker (1988), where Pirie Bank is shown north of Bruce Bank, implying opening involving significant southwesterly motion of Pirie Bank with respect to Bruce Bank in the 40Ma–present period.

I close Dove Basin by visually fitting the 'Patagonian batholith' magnetic anomaly of Pirie Bank with a similar anomaly on Bruce Bank. Again it is assumed the two are conjugate features and that an unextended continuous batholith occupied the region prior to Dove Basin opening (Figure 4.3). A good fit is achieved by rotation of Pirie Bank by 1.6° about a closure reconstruction pole at 71.43°N, 2.68°E (Figure 4.16). This rotation also has the following virtues:

1) It produces a good fit of the opposing edges of Bruce and Pirie banks' Bouguer

anomalies,

2) The rotation is approximately perpendicular to the strike of magnetic lineaments in Dove Basin itself, and

3) Flowlines drawn about the pole through the basin are sub-parallel to the magnetic anomaly marking the northern limit of the basin and parallel to some trends of troughs (interpreted as fracture zones) within the basin itself.

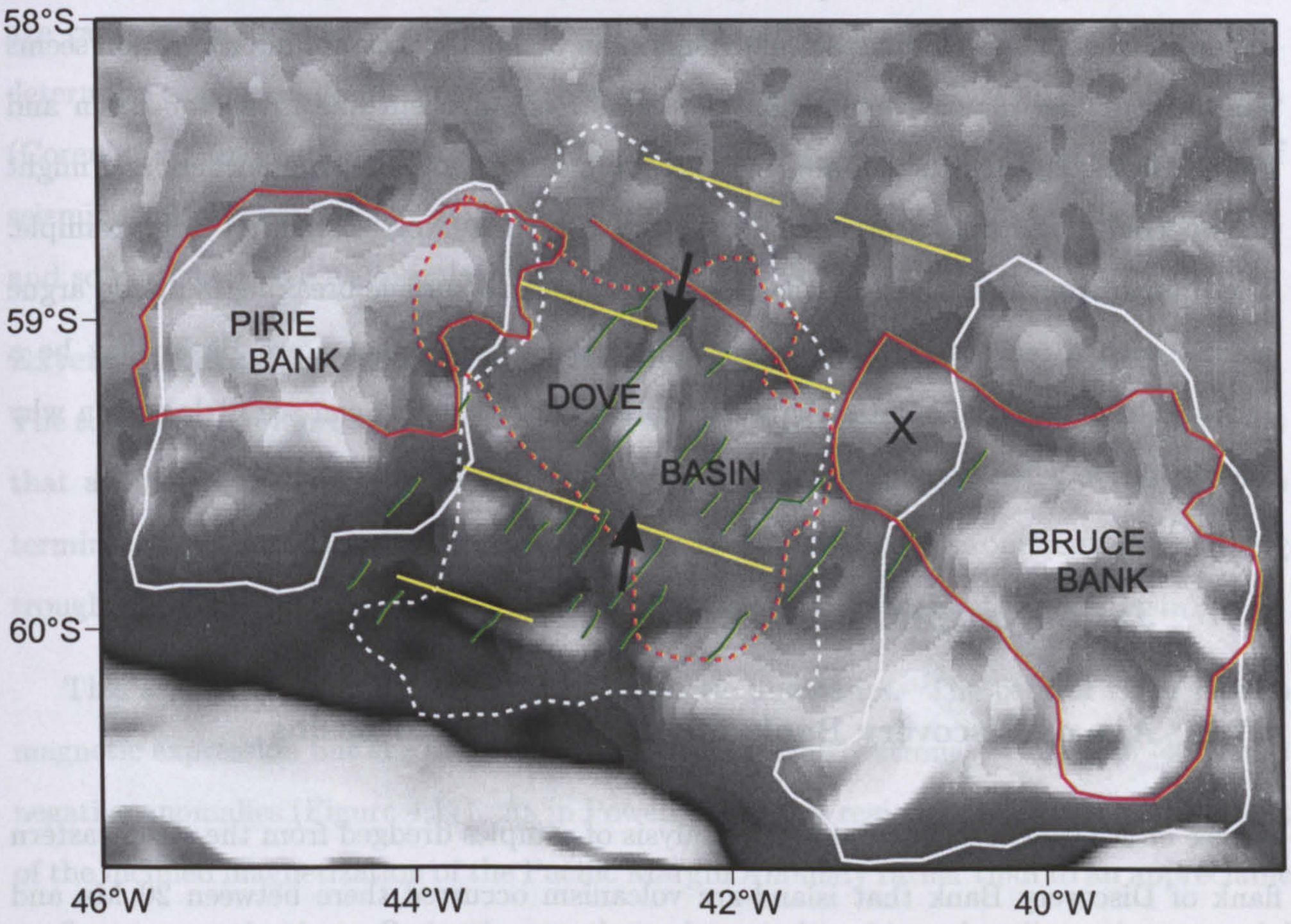

Figure 4.16: Reconstruction of Dove Basin opening. Background: free-air anomalies, showing 'spine' feature (arrows). White outlines: Bouguer anomalies; Red outlines: inferred batholith anomaly; Green lines: magnetic reversal fabric; Dashed red outline: Bruce Bank batholith anomaly rotated about the reconstruction pole; Single red line: magnetic anomaly near northern edge of Dove Basin; Dashed white outline: Bruce Bank Bouguer anomaly rotated about the reconstruction pole; Yellow lines: flowlines about the reconstruction pole. Batholith anomaly on Bruce Bank apparently continues onto the basin floor (area 'X') and may there represent volcanic rocks or rotated fault blocks in a rift basin.

If the adopted age for Dove Basin bears any resemblance to its true age, then it may represent a small, aborted ocean opening in response to relative movements between South America and the proto-South Sandwich Arc plate as a precursor to spreading in the west Scotia Sea. The closure pole is in the same part of the North Atlantic as Nankivell's 3-plate South American–Antarctic reconstruction poles and the west Scotia Sea reconstruction poles of Chapter 3, which is consistent with the notion that the relative movements responsible for its opening were closely coupled to major plate motion in the region. Given all this circumstantial evidence, an orthodox back-arc interpretation seems less likely to me than an exposition as a minor ocean basin like Protector Basin and Powell Basin. Failed rifts and aborted spreading centres are known elsewhere and might be expected in the west Scotia Sea. The Rockall trough (North Atlantic) is an example. The hints of youth provided by the magnetic spine and surface breaking faults do argue against such a reasoned interpretation, suggesting instead that Dove Basin may be a back-arc basin, and post-dates the west Scotia Sea, although I can see little reason why this should be when back-arc spreading was well established in the east Scotia Sea.

4.7 'Jane-system' subduction

4.7.1 Age of Discovery Bank and Jane Bank and basins

Barker *et al* (1982) report from K-Ar analysis of samples dredged from the steep eastern flank of Discovery Bank that island-arc volcanism occurred there between 20 Ma and 12 Ma, probably close to 16 Ma (~C5c). According to Barker *et al* (1982) the arc deactivated by collision of a segment of the South American–Antarctic Ridge with the parental subduction zone. This idea is applied by Barker *et al* (1984) for an earlier collision to the southwest which deactivated arc volcanism at Jane Bank. In these models it is necessary for the back-arc basin to have developed behind an active arc and trench. Arc deactivation time, and hence younger bounds on the duration of back-arc extension to the north and west of the Discovery and Jane Banks is determined by identification

of the reversal chrons juxtaposed with the fossil trench, a narrow bathymetric trough. This approach suggests that back-arc spreading in Jane Basin could have ceased soon after collision at C6a (Barker *et al*, 1984; $\sim$ 21Ma) or C6b (Hamilton, 1989; $\sim$ 22.5Ma), and further northeast behind Discovery Bank soon after 10 Ma (Barker and Hill, 1981; C5n1) or 5 Ma–2.5 Ma (Hamilton, 1989). In Jane Basin at least, this determination is broadly supported by age–depth and heat flow analysis, which suggests an age in the region of 32 to 25 Ma ($\sim$C12 to C7) (Lawver *et al*, 1991). Note the similarity of this age range with that determined for Powell Basin. In contrast Maldonado *et al* (1998) determine that Jane Basin opened following the deactivation of Powell Basin at 18 Ma (Coren *et al*, 1997) and persisted until 13–15 Ma. These ages are based on correlation of seismic stratigraphic units in the Powell Basin and Jane Basin, with no continuity proved, and so must be taken as speculative.

Extent of back-arc basins behind Discovery and Jane Banks

The southwestern limit of Jane Basin is not well known. Satellite free-air gravity suggests that an indistinct central ridge may continue as far west as 45°W where it appears to terminate at a north-northwest trending ridge (Figure 4.17). A prominent east-striking trough connects this high to the southern, transtensional, margin of Powell Basin.

This segmentation is less evident in magnetic anomalies. The central ridge has no magnetic expression but the basin as a whole exhibits fairly strong ($\sim$ -2000 to -4000 nT) negative anomalies (Figure 4.17). As in Powell Basin this regional low is probably a result of the inclined magnetization of the Pacific Margin Anomaly rather than to an appreciable seafloor magnetization. Reduction to the pole reveals a hint of a discontinuous axial relative high which disappears in the southwest at 62.85°S, 42.2°W and in the northeast at 61.25°S, 39.2°W. The southwestern termination is against a north-northwest trending positive high which appears to coincide with the free-air gravity ridge which crosses the basin there. To the northeast, the negative magnetic anomaly regime of Jane Basin terminates along a northwest trending line which connects the northern edges of the prominent positive magnetic highs of Bruce Bank and the Discovery Bank southern core.

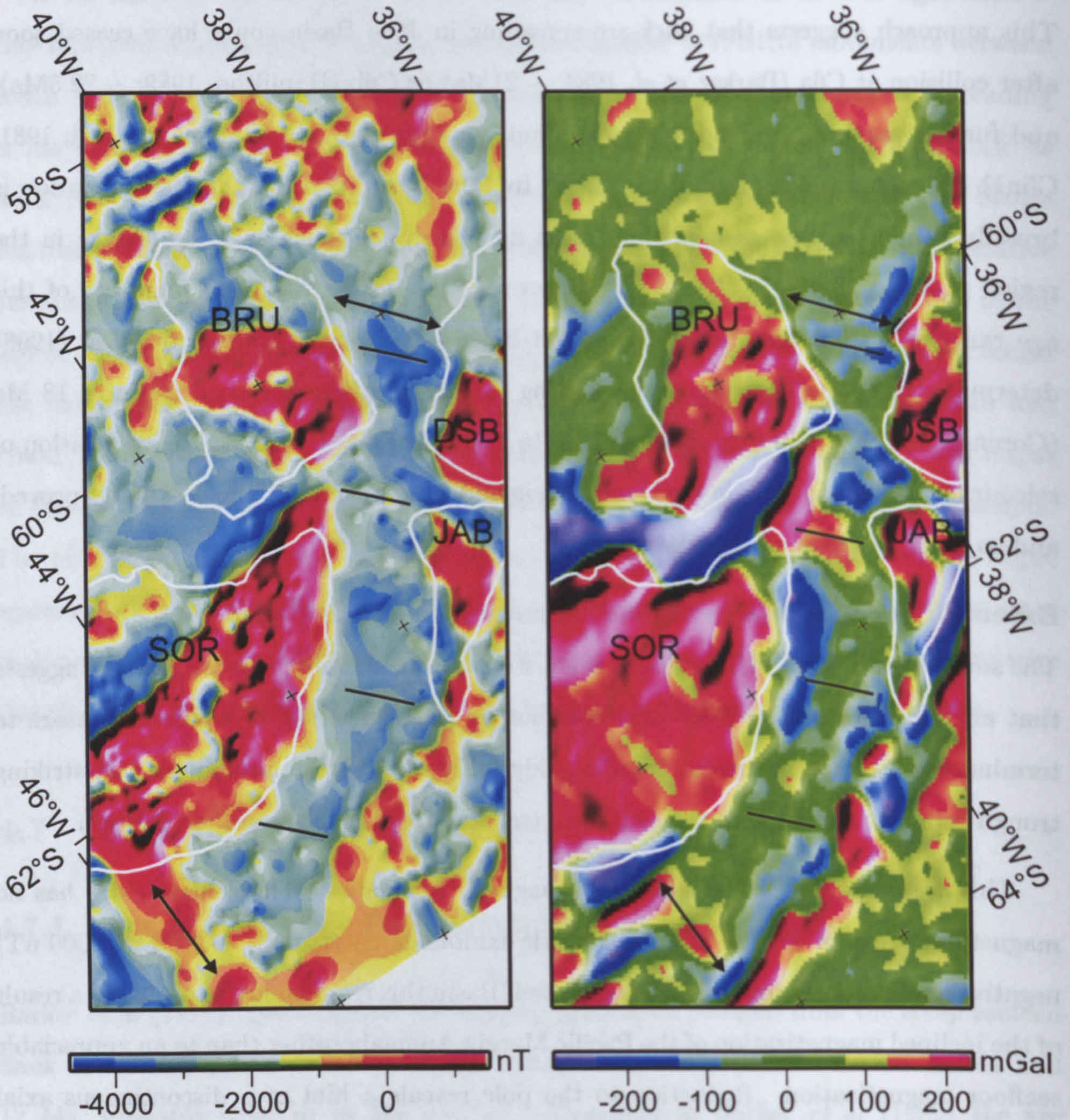

Figure 4.17: Gridded magnetic (left) and free-air gravity (right) anomalies over the Jane–Discovery back-arc basin. Reduction to the pole has been performed on the magnetic data to reveal a subdued, discontinuous, central magnetic low which coincides with a relative free-air high. White lines: Bouguer anomaly highs, SOR: South Orkney Microcontinent; BRU: Bruce Bank; DSB: Discovery Bank; JAB: Jane Bank. The central free-air ridge and magnetic relative low may terminate in the southwest at a subdued ridge and in the northeast at a subdued step, trending north and northwest respectively (arrows). Black lines are flowlines for Jane Bank about the reconstruction pole mentioned in the text, which in many cases parallel free-air anomaly lineaments. Oblique Mercator projection.

This is consistent with the idea that the magnetic signature of Jane Basin is heavily influenced by nearby strongly magnetized bodies rather than to a significant seafloor magnetization of its own. This line is marked only by a weak, diffuse relative low in the free-air gravity anomaly, so that it is not possible to say whether the basin is, or was, linked to the seafloor further north or northeast.

In the region to the north, over and east of the relative Bouguer anomaly high along 36.5°W, the magnetic grid reveals scattered short wavelength anomalies which are not all linear. Where linear trends are discernible an east-striking magnetic fabric is hinted at, which might be a continuation of the anomaly fabric of the central Scotia Sea just to the west. Some lesser north-striking anomalies tempt an interpretation involving east–west spreading in a back-arc basin ancestral to the modern east Scotia Sea. In Chapter 6 I give reasoning for why I am inclined to the former interpretation. The conclusion here is that it is probable that the Jane–Discovery back-arc basin extends only as far north as the northern edge of Bruce Bank, at ~ 59°S, and if it continues beyond there it does so to the northeast for a short distance only, as far as 59°S, 35°W.

4.7.2 Modelling closure of Discovery–Jane Basin

Previous reconstructions

In the reconstruction of Barker *et al* (1984) the Jane–Discovery basin is shown closed orthogonal to its length. King and Barker (1988) suggest that opening of Jane Basin in fact had an easterly azimuth based on the orientation and shape of its margins.

The lack of definite conjugate features to fit makes closure of the basin a difficult task. Possible seafloor flowlines suggest opening orthogonal to the trend of the basin, as has been assumed for Bransfield Strait. An opening direction similar to the present east Scotia Sea could instead be used, but there seems no compelling reason to do so when multiphase back-arc basins are known to exhibit different spreading directions (Karig, 1971). Closure orthogonal to the basin strike (using gravity ridges as flowlines for visual

fitting) is achieved by 0.7° rotation of the Jane (during 26.55–21 Ma) and Discovery (during 22.5–15 Ma) banks, with respect to the South Orkney Microcontinent, about a pole at 28.8°S, 169.6°W. Notably this rotation also aligns high amplitude magnetic anomalies on Bruce Bank and southwestern Discovery Bank. That southwestern Discovery Bank may have a continental core, of pre-Scotia arc-batholith crust, is suggested by Garrett *et al* (1986) and by Hamilton (1989). In fact Hamilton (1989) contends that much of the complex of highs in the southeastern Scotia Sea has continental basement—including Herdman Bank and Southern Thule. If such a body does exist at Discovery Bank, it completes the presence of the extended 'Patagonian batholith' body (Figure 4.3) along the entire length of the southern Scotia Sea from Tierra del Fuego to Discovery Bank, and increases the length of the west–east arm of the Patagonian orocline.

4.8 South Georgia and the central Scotia Sea in the Cenozoic

4.8.1 Dismemberment of South Georgia and Shag Rocks

The reconstruction poles of Chapter 3 predict much more extension than is seen in northernmost W6, W7, and beneath Aurora Bank, all north of latitude 55°S. A simple way to correct these imbalances is if the west Scotia Sea opens asynchronously, allowing strike-slip motions within one or both of the passive margins of the west Scotia Sea. The sense of movement would be dextral for strike-slip faults on the west flank, or sinistral on the east flank. Dextral movement on the west flank could have opened the Falkland Trough. Sinistral movements on the east flank would place the Shag Rocks block to the north of South Georgia, and internally deform the South Georgia microcontinent. I note, as did Barker (1995), an offset in the shelf of the South Georgia microcontinent along 55°S, and that elimination of this offset requires about 70 km sinistral strike-slip to have occurred. Such a restoration extends the strike of the Drygalski Fjord Complex from north of the offset to a restored Clerke Rocks offshore to the south, without the need for a change

in strike to connect the outcrops in the sense of Tanner (1982). It is impossible to say which of the strike-slip movements, west flank or east, acted to accommodate the spreading imbalance, or whether both acted. I choose to show strike-slip movement within the South Georgia block as discussed, because it provides a means by which the ancestral South Sandwich Trench need not be present immediately to the east of South Georgia (there is no evidence for subduction beneath it), yet South Georgia itself can remain on the eastern passive margin of the west Scotia Sea system—by the action of a continental transfer zone within the South Georgia microcontinent.

4.8.2 Provenance of South Georgia

Comparison of the geology of South Georgia with that of Tierra del Fuego suggests that the Rocas Verdes Basin has an analogue on the South Georgia block, where a pseudo-ophiolitic body (the Larsen Harbour Complex) crops out at the island's southeast corner (Katz, 1973; Dalziel *et al*, 1975; De Wit, 1977; Storey *et al*, 1977). The simplest reconstruction of a continuous Rocas Verdes–Larsen Harbour basin, in the absence of other such outcrops, places South Georgia immediately to the south of Burdwood Bank and is a major theme in the reconstruction work of Dalziel (Dalziel and Elliott, 1971; being its first appearance). From such a reconstruction South Georgia requires approximately 1600 km displacement to its present position, with significant north–south and east–west components, that can not be accounted for by relative motion between the Antarctic Peninsula and Tierra del Fuego along the Shackleton Fracture Zone (Cunningham *et al*, 1995). The extra east–west component is not adequately explained (Barker *et al*, 1991; Royden, 1993; Cunningham *et al*, 1995) because it needs extra back-arc extension in the Scotia Sea for which there is scant evidence. A suggested source of the north–south component is the proposed contemporaneous opening of the central Scotia Sea (Hill, 1978; Barker and Hill, 1980; Hill and Barker, 1980; 20 Ma to 6Ma). This model is attractive because it predicts changes in spreading rate in the central Scotia Sea which correlate with changes in the west Scotia Sea (Figure 4.18), and taken at face value it does seem

to place South Georgia within the heart of a reconstructed cusp *sensu* King and Barker (1988). But there are problems, just one of which is outlined below, which suggest that the simplest reconstruction of a Rocas Verdes–Larsen Harbour basin is not as easy to reproduce using seafloor spreading data as it might seem.

4.8.3 The central Scotia Sea did not open after 26Ma

Chapter 3 shows how relative motion in the west Scotia Sea strongly resembles relative motion between South America and Antarctica, and suggests the reason for the small difference is the presence at the eastern margin of the central Scotia Sea of the migrating ancestral South Sandwich Trench. In this chapter I have suggested that relative motions at the North Scotia Ridge, and opening of most of the small sub-basins of the Scotia Sea could also be consequences of this situation. In the model, as it stands, major plate motion and the local complications of a migrating trench are accounted for without the need for a large back-arc basin opening in the central Scotia Sea.

Now since the central Scotia Sea occupies most of the eastern flank of the west Scotia Sea spreading system, and is enclosed by the South Sandwich Trench and North Scotia Ridge, it is most reasonable that during the interval of spreading in the west Scotia Sea the entire central Scotia Sea should also have been closely coupled within the South American–Antarctic system. The simplest way to achieve this is for the central Scotia Sea to be a passive element in the circuit. For the central Scotia Sea instead to be actively spreading during this time, and for apparent close approximation of the South American–Antarctic circuit across it, would require

1) complete decoupling of a linked west–central–east Scotia Sea system, most simply by subduction beneath, or of, the Scotia Sea on two or three sides, and

2) an extraordinary coincidence where 'random relative motions' (Barker and Griffiths, 1972) combine to resemble the major plate motions one might expect to have seen in the region in the first place.

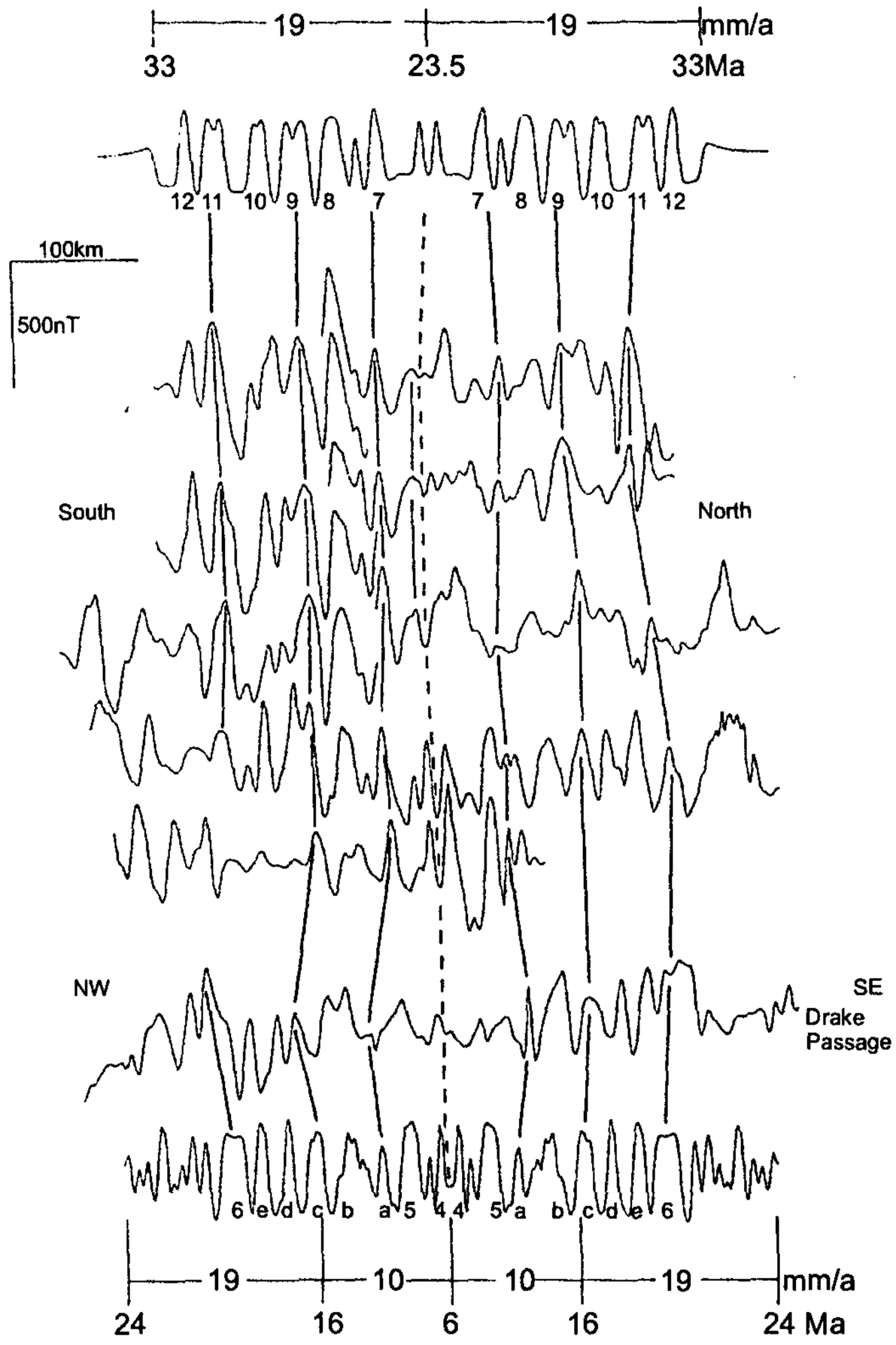

Figure 4.18: Central Scotia Sea magnetic models of Barker and Hill (1981). The models (top and bottom) are compared to recorded sequences in the central and west Scotia Seas ('Drake Passage'). The bottom, younger, model is favoured as a fit to the data.

I reaffirm that, as an alternative to the above, the scenario of close-coupling of microplates to major plates in the region is more believable. That is to say, the central Scotia Sea and South Georgia together formed the eastern passive margins to the opening west Scotia Sea and that these margins were kinematically independent in only a small way from the Antarctic plate. On these grounds a different model for the central Scotia Sea is essential. The alternative options are summarised in Chapter 6, and one new option is pursued further there. For now it is enough to say that the central Scotia Sea must be included in Scotia Sea reconstructions, as a discrete, passive fragment, at least as far back as C8.

Chapter 5

Reconstructions of the Cenozoic Scotia Sea

Keywords Cenozoic. Scotia Sea reconstruction. Scotia Sea paleo-plate boundaries.

5.1 Models of Scotia Sea plate kinematics

The main part of this chapter presents reconstructions of the total field anomaly grid and of the Bouguer anomaly grid for six chrons (C3, C5c, C6, C8, C13, C30) during the Cenozoic evolution of the Scotia Sea. Ages in millions of years before present are given for these chrons based on the reversal timescale of Cande and Kent (1995). The plate tectonic situation in each is described, and interpreted plate boundaries are presented.

The model to be presented is summarised in Figure 5.1. It is based on the reconstructions discussed in Chapter 3 and Chapter 4, and is preferred to previous reconstructions for reasons discussed in those chapters on a basin-by-basin basis. I have attempted to represent a summary of previous reconstructions in Figure 5.2 as an alternative model. To summarise, the principal differences between the two models are given below.

1) Spreading in the west Scotia Sea. In the preferred model this is reconstructed using

tectonic flowlines and magnetization reversals together. The west Scotia Sea regime is split into two parts about the Endurance Fracture Zone. In the other model I use the 'red' set of reconstruction poles from Burrell (1983; Figure 3.1) which is based on total field anomaly data and assumes the Shackleton Fracture Zone is a tectonic flowline representative of motion in the entire west Scotia Sea.

2) Movement of South Georgia and Shag Rocks. In the preferred model these blocks migrate as the eastern passive margins of the west Scotia Sea, which propagate northwards. In the other model they move entirely independently of all other elements in order to be reconstructed to the area south of Burdwood Bank at 40 Ma. The east–west component of this dispersal is greater than the amount of spreading seen in the west Scotia Sea.

3) Spreading in the central Scotia Sea. In the preferred model spreading in the central Scotia Sea precedes that in the west Scotia Sea, so that the central Scotia Sea exists as a rigid block throughout the model. In the other model the central Scotia Sea opens at the same time as the west Scotia Sea, filling the gap left by the northward component of the drift of South Georgia and the Shag Rocks block out of a cuspate reconstruction at 40 Ma. This would need subduction to the north of South Georgia and Shag Rocks, and complex migrating and jumping triple junctions connecting the central Scotia ridge to those in the west Scotia Sea and east Scotia Sea.

4) Opening of Dove Basin and Protector Basin. In the preferred model both of these basins open as failing precursors to the opening of the west Scotia Sea, maybe both somewhere in the interval between C21 ($\sim$ 49 Ma) and C8 ($\sim$ 26.5 Ma). In the other model Protector Basin opens very quickly between C5c and C5 (Hill and Barker, 1980) and Dove Basin opens immediately following extinction of the west Scotia Sea. The extra east–west accretion they represent imply strike-slip plate boundaries between them and the central Scotia Sea and South Scotia Ridge, as well as much faster trench rollback at the south end of the proto-South Sandwich Trench than at the north.

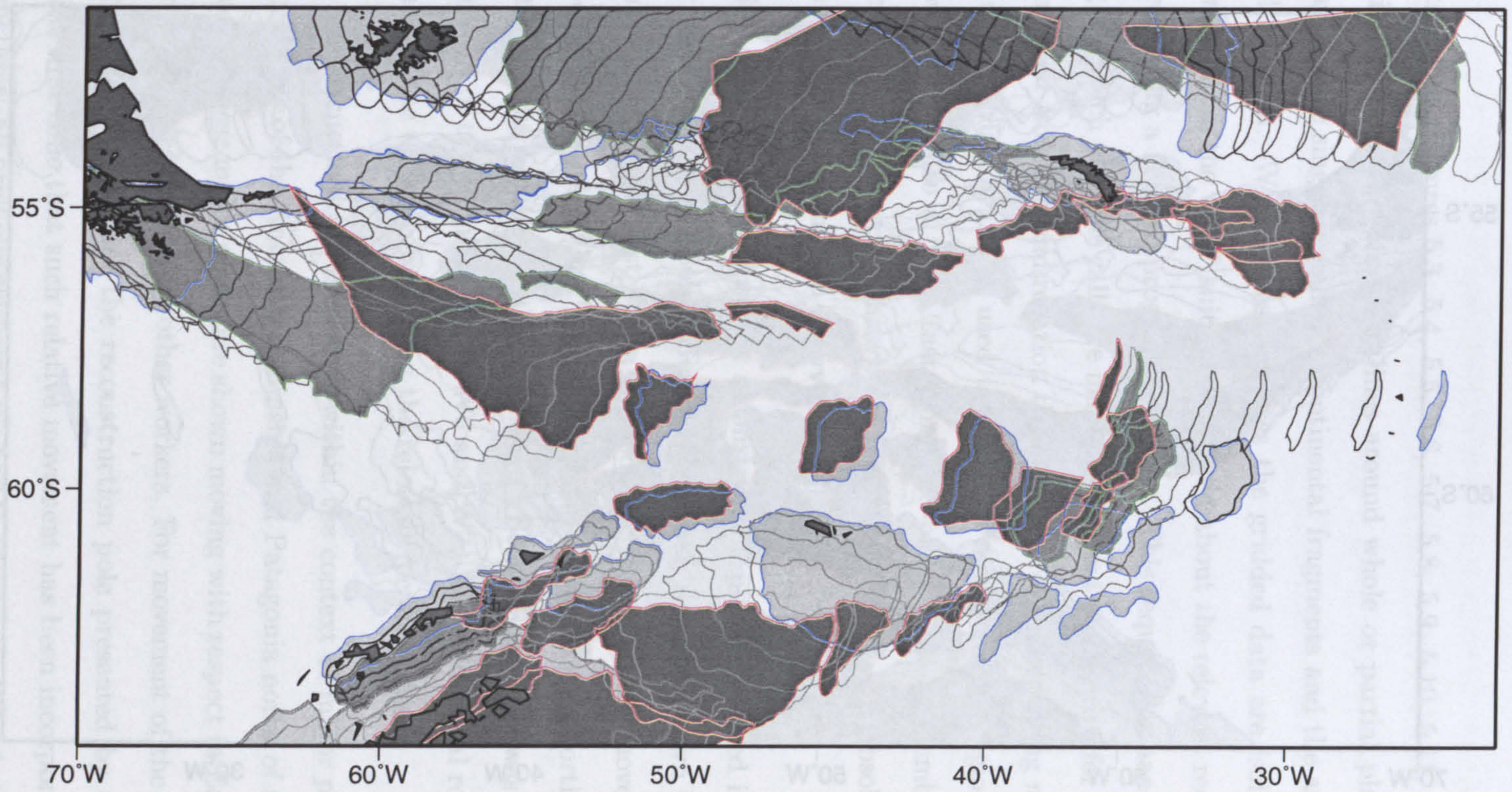

Figure 5.1: Preferred Scotia Sea kinematic model using the reconstructions given in Chapters 3 and 4. Outlines of the Bouguer anomaly highs are shown for 40 Ma, 35 Ma, 30 Ma, 27 Ma, 24 Ma, 21 Ma, 18 Ma, 15 Ma, 12 Ma, 9 Ma, 6 Ma, 3 Ma and present-day. For clarity three sets of outlines have been highlighted by coloured outlines and grey infill: 40 Ma (red outline, dark grey fill); 21 Ma (green and mid-grey); present-day (blue and light grey).

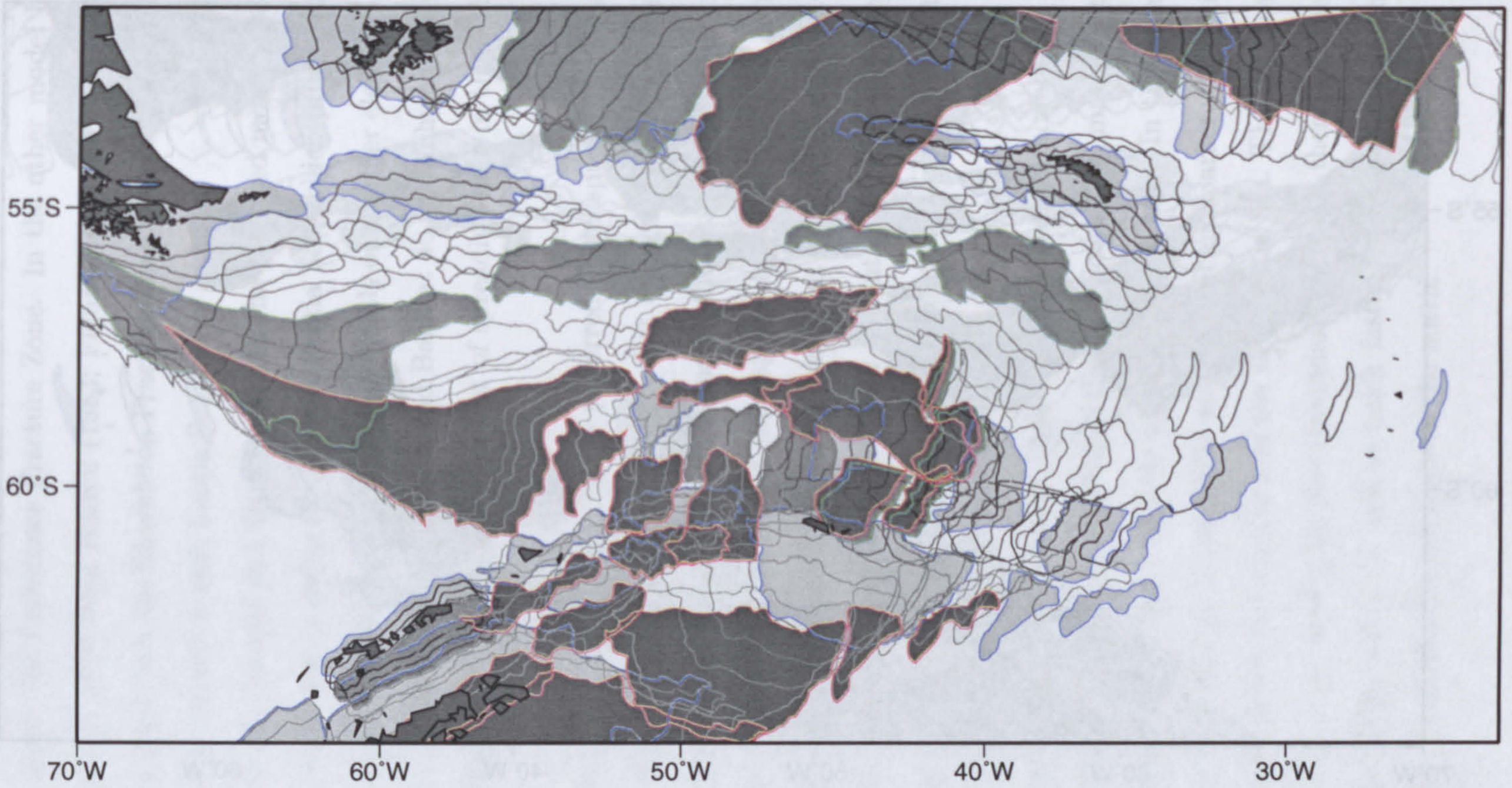

Figure 5.2: Alternative Scotia Sea kinematic model resembling a synthesis of the reconstructions given in Chapter 1. Outlines of the Bouguer anomaly highs are shown for 40 Ma, 35 Ma, 30 Ma, 27 Ma, 24 Ma, 21 Ma, 18 Ma, 15 Ma, 12 Ma, 9 Ma, 6 Ma, 3 Ma and present-day. For clarity three sets of outlines have been highlighted by coloured outlines and grey infill: 40 Ma (red outline, dark grey fill); 21 Ma (green and mid-grey); present-day (blue and light grey).

5.2 Reconstruction technique

Reconstructions (Figures 5.3, 5.4, 5.5, 5.6, 5.7, 5.8, 5.9, 5.10, 5.11, 5.12, 5.13 and 5.14) are made by drawing isochron outlines around whole or partial plates, or microplates, that may include single or multiple continental fragments and the areas of oceanic crust accreted to them. Within these outlines the gridded data are isolated, using *grdmask* and *grdmath* from the *GMT* suite, and rotated about the relevant reconstruction pole for that chron using a Fortran program: **rotator**. This sequence is handled in a shell script **rotfrag**, to which multiple calls are made in a parent shell script for each reconstruction. Following their isolation and rotation the data are re-gridded using *nearneighbor* (*GMT*) to produce a surface which is used to map the reconstructed region. All rotations are shown with respect to a fixed East Antarctic plate, and so resemble absolute motions inasmuch as East Antarctica has been relatively fixed in an absolute reference frame through much of the Cenozoic (Lawver *et al*, 1992).

Within the Scotia Sea I use the reconstruction poles presented in Chapters 3 and 4. Seafloor spreading west of South Georgia and Shag Rocks is shown beginning later than in the main part of the west Scotia Sea, so that in effect they move simply by switches of the South American–'Scotia' plate boundaries between their north and south edges at different times during the opening of the west Scotia Sea. This was done in view of the lesser amount of crustal accretion in W6 and W7. Any additional rotations used will be mentioned in the text accompanying the relevant reconstruction.

The reconstructions are presented within the context of major plate motions, shown by the positions of the Antarctic Peninsula and Patagonia north of the Magallanes fault zone. Both of these major plates are shown moving with respect to East Antarctica about reconstruction poles derived by other workers. For movement of the Antarctic Peninsula in the period C20–C8 I use the reconstruction pole presented by Cande *et al* (2000). This is the first time that such relative movement has been incorporated into Scotia Sea reconstructions: all previous workers have had to assume that the Antarctic Peninsula was

part of the East Antarctic plate throughout the Cenozoic. For the periods prior to and after this motion I assume the Peninsula was fixed with respect to East Antarctica. This assumption is not valid prior to C20, but large relative movements at least are thought to have been confined to the pre-C34 period. For movement of South America with respect to East Antarctica I use the reconstruction poles in the unmodified three-plate inversion of Nankivell (1997a).

Because the South Scotia Ridge has the characteristics of a fairly simple, recent, transtensional or strike-slip boundary (Galindo-Zaldívar *et al*, 1996) I assume, as in Section 4.3, that most of the differential motion between the west Scotia Sea systems and the relative movement of South America and Antarctica was taken up along the northern margin of the Scotia Sea: the Magallanes fault, North Scotia Ridge and Endurance Fracture Zone. As a consequence no relative plate motion between East Antarctica and the Scotia Sea plates is shown, although the proposed mechanism for spreading in the west Scotia Sea requires at least some small relative motion between them (Section 3.4.4). The sense and magnitude of any such motion could only be known in the light of detailed knowledge of the past kinematics of the lithospheric slab in the mantle below the South Sandwich Trench.

5.3 A reminder: the present day

At the present day the Scotia Sea is comprised of two plates: the Scotia plate and Sandwich plate. The Scotia plate is defined by the North Scotia Ridge (which exhibits minor sinistral transpression at its western end), the South Scotia Ridge (mild sinistral transtension and strike-slip), the East Scotia Ridge (an active back-arc spreading centre), and the Shackleton Fracture Zone (sinistral transpression) (Pelayo and Wiens, 1989). Onshore in Tierra del Fuego, the Magallanes fault zone extends the North Scotia Ridge to meet the southern Chile Trench, which is linked to the Shackleton Fracture Zone at its southeastern end.

The Sandwich plate is defined by the East Scotia Ridge and the South Sandwich Trench, which is strongly arcuate, concave on its western edge, and meets the East Scotia Ridge at its northern and southern ends. The means by which the North Scotia Ridge links through the South Georgia area with these two features to form a South American–Sandwich–Scotia triple junction is uncertain. There is similar uncertainty regarding the exact nature and path of linkage through the Discovery Bank region of the South Scotia Ridge, East Scotia Ridge, South Sandwich Fracture Zone and South Sandwich Trench which separate the Scotia and Antarctic, Scotia and Sandwich, South American and Antarctic, and Sandwich and South American plates, respectively.

A final small plate, the South Shetland microplate, is defined by the axis of stretching in Bransfield Strait and the residual subduction zone at the South Shetland trench. West of the Shackleton Fracture Zone the Phoenix ridge has been inactive since about anomaly C2a (Livermore *et al*, 2000), at which point the Phoenix plate amalgamated with the Antarctic plate.

5.4 The west Scotia Sea dies: C3a

The reconstruction of the Scotia Sea at chron C3a ($\sim$ 6 Ma) is shown in Figures 5.3 and 5.4. The east Scotia Sea is shown partly closed simply by visually fitting gridded magnetization anomalies for C3a on the east flank to those on the west, using 5.33° rotation about a pole at 83.77°S, 28.28°W. Relative movements with respect to the Antarctic plate are shown for the South American, Sandwich, and South Shetland plates. In addition the distinction, post-C3a, between a Magallanes and a Burdwood plate is retained (dashed black line), although for simplicity no relative motion is shown between the two. The West Scotia Ridge is shown at its death, so there is no relative motion between the Magallanes–Burdwood plates and a central Scotia plate. In effect a rigid Scotia plate exists. The cessation of spreading in the west Scotia Sea could have been the result of a collision on the east flank between South Georgia and the Northeast Georgia Rise (Burrell,

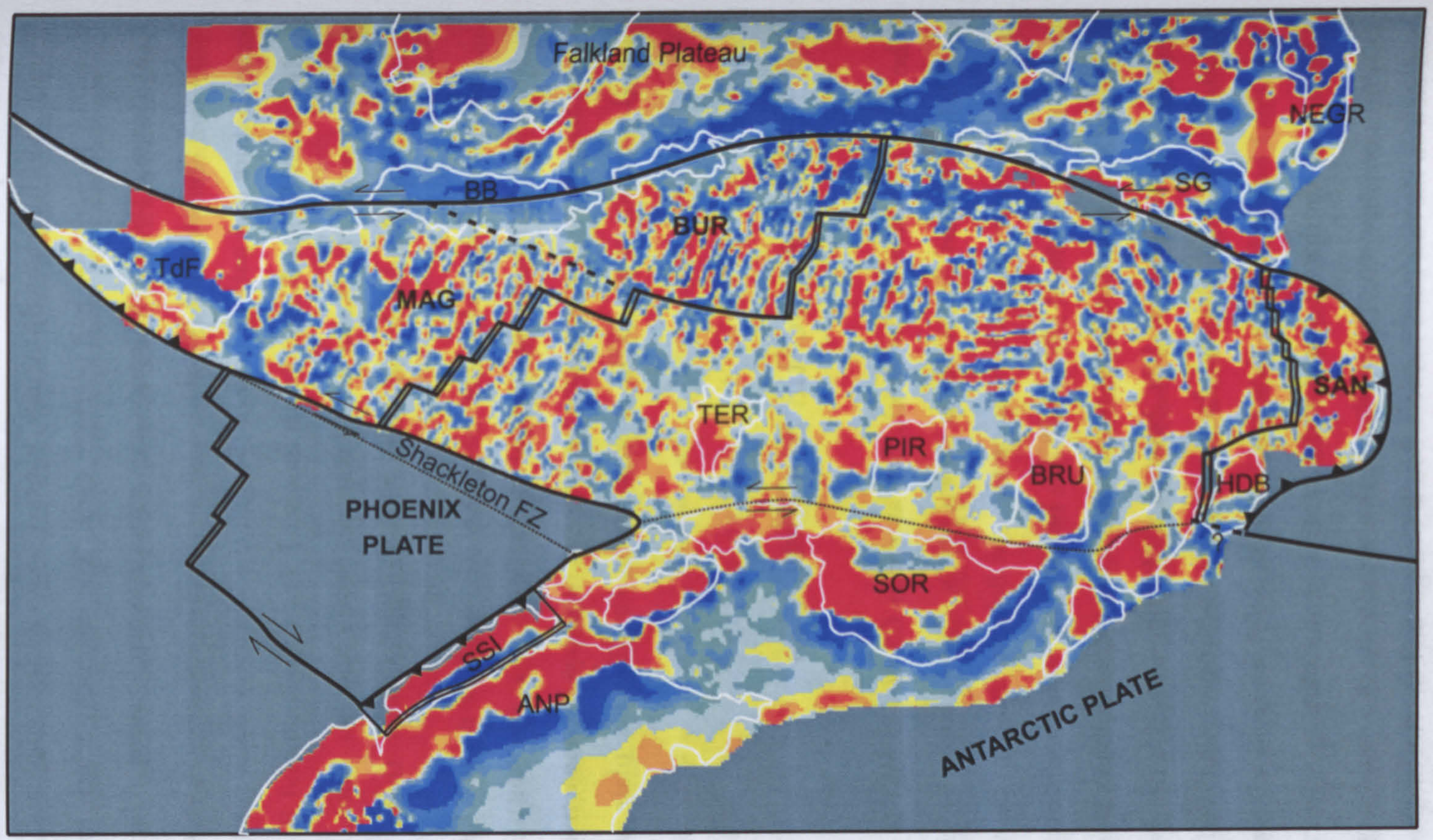

Figure 5.3: Reconstruction of the total field anomaly in the Scotia Sea at chron C3a (about 6 Ma). Bouguer anomaly outlines of thickened crustal blocks are shown in white, inferred plate boundaries by black lines. Double lines: spreading centres, toothed lines: subduction zones with teeth on overriding plate. Boundaries with significant strike-slip components of relative motion shown by half-arrows. Thick dashed line is the residual Magallanes/Burdwood plate boundary. Dotted line is a possible locus for small relative movements on the South Scotia Ridge. ANP: Antarctic Peninsula, BB: Burdwood Bank, BRU: Bruce Bank, HDB: Herdman Bank, NEGR: Northeast Georgia Rise, PIR: Pirie Bank, SOR: South Orkney Microcontinent, SG: South Georgia, SSI: South Shetland Islands, TdF: Tierra del Fuego, TER: Terror block. Bold-lettered labels denote the Magallanes (MAG), Burdwood (BUR) and Sandwich (SAN) plates. A larger version of this figure can be found inside the back cover of the thesis.

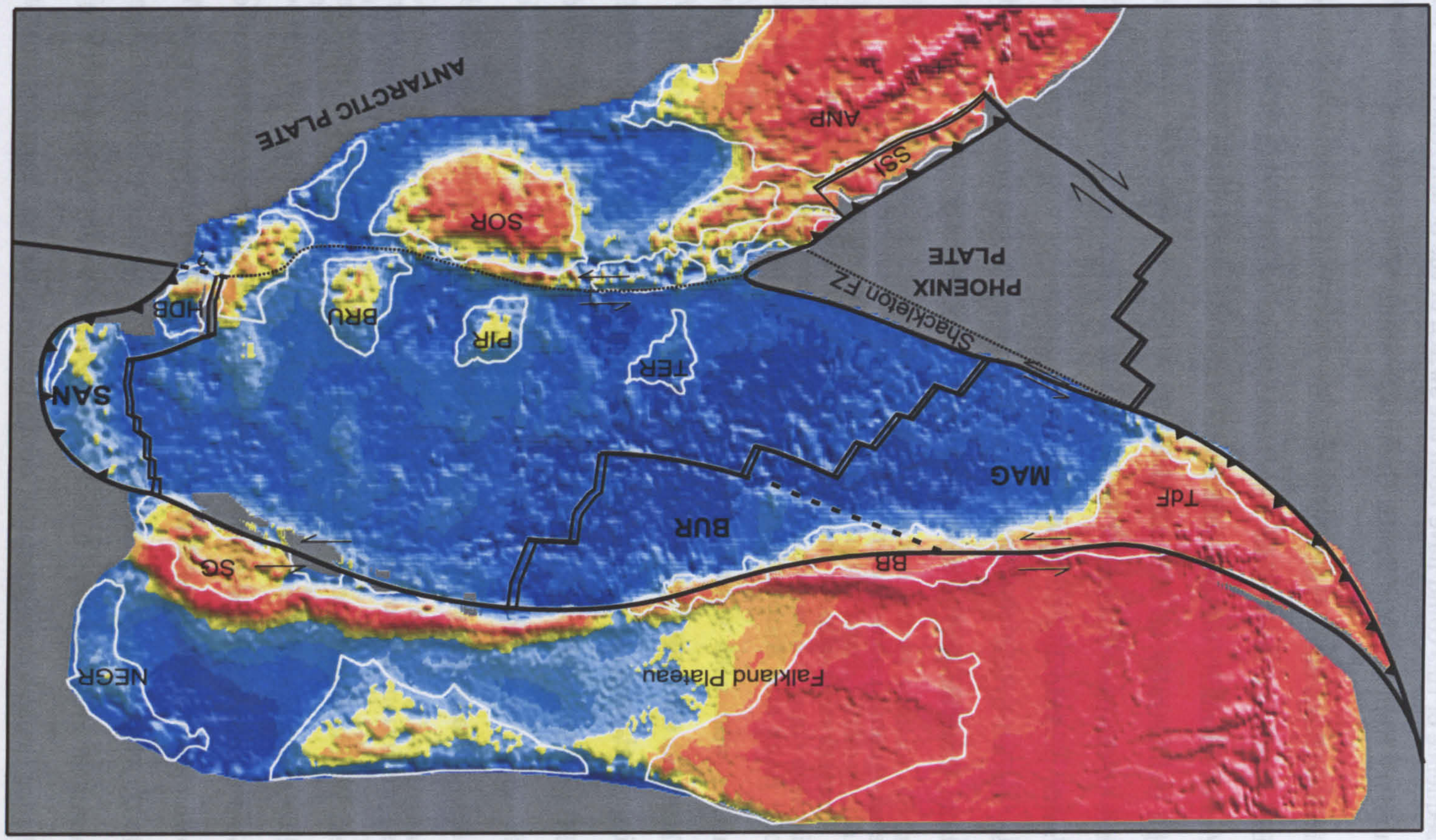

Figure 5.4: Reconstruction of the Bouguer gravity anomaly in the Scotia Sea at chron C3a. White outlines of thickened crustal blocks are shown for reference. Inferred plate boundaries are shown by black lines. Labels as for Figure 5.3. A larger version of this figure can be found inside the back cover of the thesis.

1983). One consequence of this could have been the switch of the South American–central Scotia plate boundary from north of South Georgia to south of it, as shown.

The reconstruction has a number of implications for post-C3a movements in the region. The assumption that all such movements were concentrated on the North Scotia Ridge is inadequate, as recent seismicity on the South Scotia Ridge attests. I retain the assumption because although it illustrates an extreme situation it does, nonetheless, predict many known movements in the post-C3a era. The movements implied are not great, and could be modified if some partitioning of regional stress is permitted onto the South Scotia Ridge. I suggest, guided by the generally reasonable nature of the predictions made by this reconstruction, that this partition was small until very recently.

The relative movements, post-C3a, predicted by the reconstruction are:

1) $\sim$ 65 km sinistral strike-slip on the North Scotia Ridge at the southern edges of, or within, Burdwood Bank and Aurora Bank with respect to the Falkland Plateau (about 10 mma^{-1}), further west with a small component of convergence between the Scotia (Magallanes) plate and the South American plate on the Magallanes fault zone.

2) sinistral oblique extension on the North Scotia Ridge east of Burdwood Bank ($\sim$ 54°S, 51°W) and, possibly, west of it ($\sim$ 54.2°S, 61.9°W). That is to say, at left bends on a sinistral fault.

3) sinistral oblique convergence between South Georgia and the nascent Scotia plate.

Some of these predictions are consistent with observations of recent relative movements in the Scotia Sea. Within Burdwood Bank and Aurora Bank seismicity shows relative motion dominated by sinistral strike-slip (Forsyth, 1975; Pelayo and Wiens, 1989), presently occurring at about 5 mma^{-1}. In continental Tierra del Fuego, modern sinistral strike-slip is also well known on the Magallanes fault zone (Forsyth, 1975; Pelayo and Wiens, 1989; Cunningham, 1993; Klepeis, 1994; Cunningham *et al*, 1995), where there is evidence for 25 km of displacement on an unknown timescale (Klepeis, 1994). The component of convergence implied for the southern margin of South Georgia has also been recorded by an earthquake (Pelayo and Wiens, 1989). The recent distinction between Magallanes and

Burdwood plates may be manifest as seismicity on the Endurance Fracture Zone (Forsyth, 1975).

None of the geological studies of the Magallanes fault zone provides evidence for the predicted small component of convergence in Tierra del Fuego being accommodated on the Magallanes fault zone. Recent convergence is, of course, known at the southern Chile Trench, although it is difficult to envisage how the component in question could be partitioned there. Alternatively, if convergence does, or did, happen, I suggest it may be accommodated aseismically within the Magallanes fold and thrust belt to the north of the Magallanes fault. Strain partitioning is also a possibility in the South Georgia area, where the strike-slip component of predicted oblique convergence has not been proved. It could occur on the same fault system as the known thrust solution (Pelayo and Wiens, 1989), or be partitioned elsewhere, for instance to the north of the South Georgia block. Lastly there is no evidence for or against the occurrence of oblique extension predicted in the areas east and west of Burdwood Bank.

What is observed, but not predicted by the reconstruction, however, is the small component of convergence at the western part of the North Scotia Ridge within Burdwood Bank where the South American–Scotia plate boundary exhibits mild transpression. The significance of this failure is impossible to assess in view of the following: (a) transpression is shown by just one event in the inversion of Pelayo and Wiens (1989), (b) the orientation of the plate boundary within Burdwood Bank is not known (Cunningham *et al*, 1998), (c) uncertainties in all the C3a reconstruction poles, and (d) the lack of consideration given to any relative motion on the South Scotia Ridge.

The reconstruction shows that a much smaller Sandwich plate existed at C3a. Its present-day southern part does not exist due to reconstructed closure of the basin separating Herdman Bank from Discovery Bank, for which I have used the same pole as for the Sandwich plate motion, but with just 2.33° rotation of Herdman Bank with respect to Discovery Bank. This part of the reconstruction is prompted by that of Hamilton (1989) and implies that the Sandwich–Scotia plate boundary passed to the north of Herdman

Bank at the time. Herdman Bank and Discovery Bank are interpreted as arc and fore-arc, respectively, into whose mutual boundary the East Scotia Ridge propagated after C3a.

Possibly the final cessation of the west Scotia Sea and the east–west component of regional stretching it supplied meant that the east Scotia Sea back-arc basin started spreading more coherently and quickly. Barker (1995) notes the same point, along with an increase in the rate of spreading at the East Scotia Ridge beginning at about 8 Ma.

The possibility of very young seafloor spreading in Dove Basin was suggested in Chapter 4. If it existed it would introduce a 'Dove' plate and ridge into the C3a reconstruction. However, here an interpretation where Dove Basin opens before the west Scotia Sea is favoured based on the lack of evidence for large recent relative movements between the central Scotia Sea, Bruce Bank and the South Scotia Ridge implied by the younger interpretation.

5.5 The young east Scotia Sea: C5c

The reconstruction of the Scotia Sea at chron C5c ($\sim$ 16.7 Ma) is shown in Figures 5.5 and 5.6. Four plates comprise the model Scotia Sea at C5c. The Magallanes and Burdwood plates are present on the west flank of the west Scotia Sea spreading system, opposing the central Scotia plate on the east flank. Seafloor spreading defining them is shown as only having just begun in W7, as opposed to the already mature system in W1–W6. Hence Shag Rocks and the western North Scotia Ridge are still close neighbours. This scheme is preferred to ones where (a) the entire west Scotia Sea opens synchronously at C8 and shuts down progressively from north to south, or where (b) W7 is the contemporary of W1–W6 but opens about a different pole.

The assumption that all major–micro-plate decoupling occurred at the North Scotia Ridge is retained, under which predicted motion at the North Scotia Ridge can be accounted for. Nonetheless the probability remains that some small relative movements

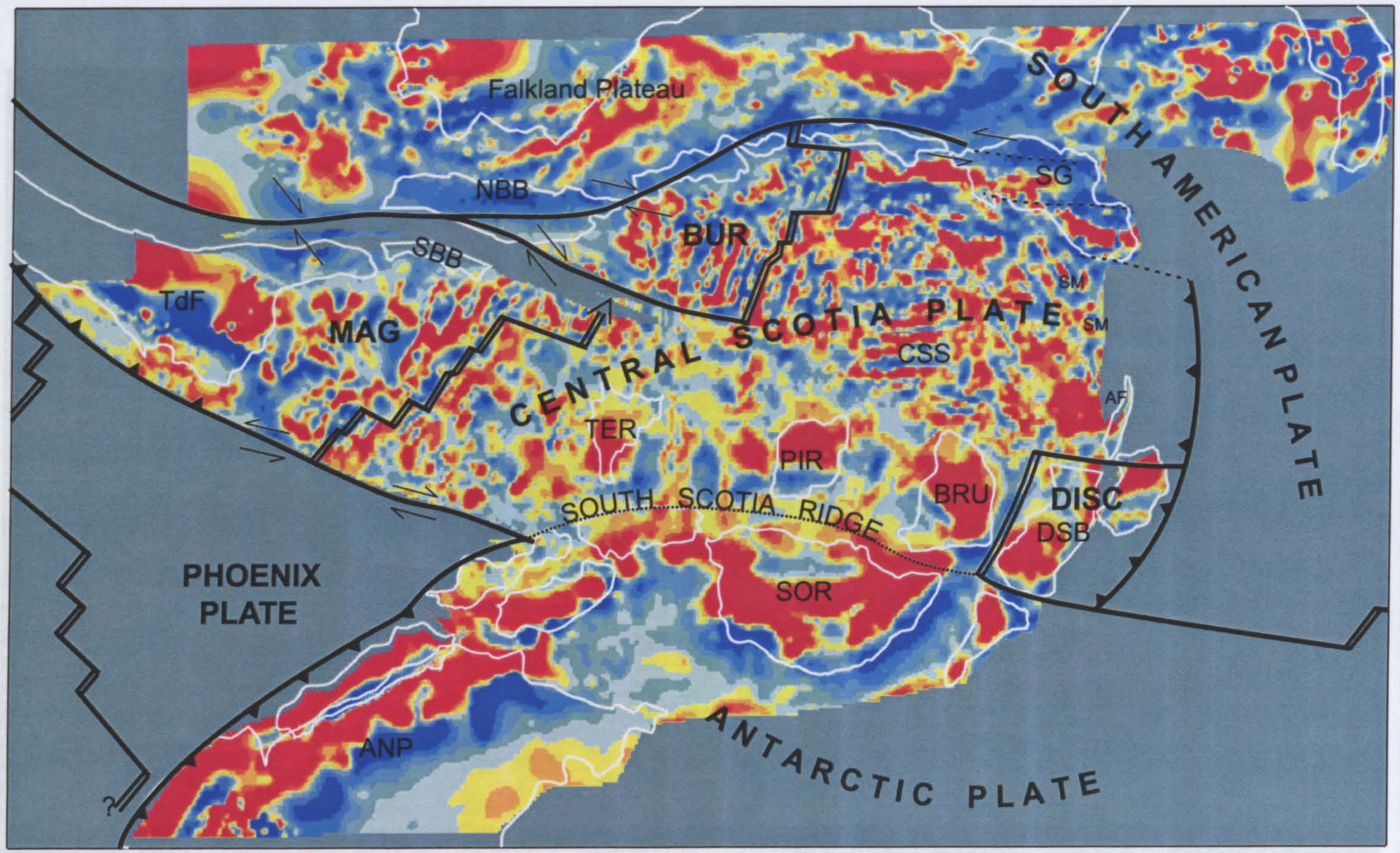

Figure 5.5: Reconstruction of the total field anomaly in the Scotia Sea at chron C5c. Ornament as for Figure 5.3. ANP: Antarctic Peninsula, BRU: Bruce Bank, CSS: central Scotia Sea, DSB: Discovery Bank, NBB: northern, accreted part of Burdwood Bank, PIR: Pirie Bank, SBB: southern buttress of Burdwood Bank, SG: South Georgia, TdF: Tierra del Fuego, TER: Terror block. AF ('arc fragment') and SM ('seamount') may show a previous location of the northern part of the proto-South Sandwich–Discovery Arc. Bold lettering for plate names, BUR: Burdwood plate, DISC: Discovery plate, MAG: Magallanes plate. A larger version of this figure can be found inside the back cover of the thesis.

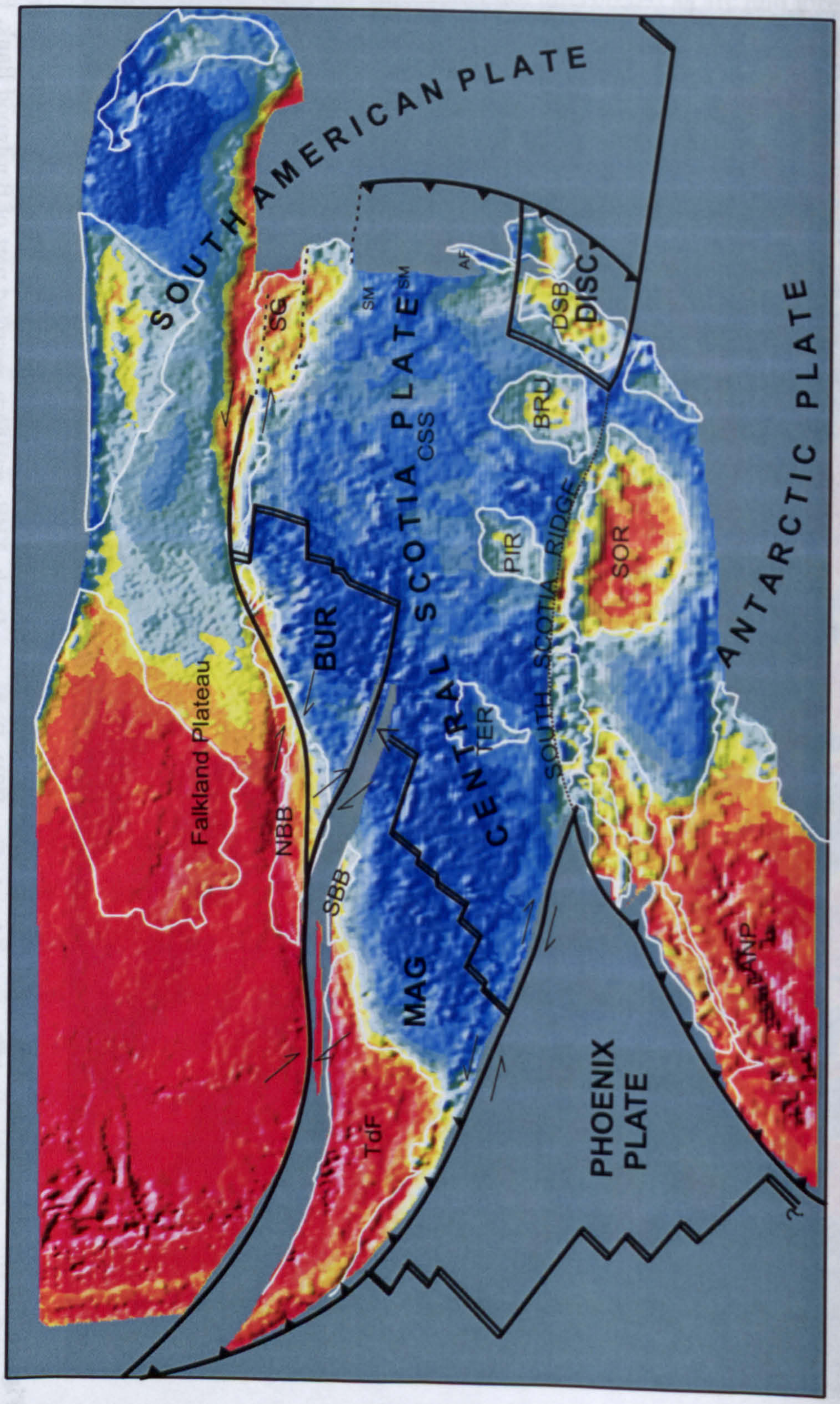

Figure 5.6: Reconstruction of the Bouguer gravity anomaly in the Scotia Sea at chron C5c. Ornament and labels as for Figure 5.5. A larger version of this figure can be found inside the back cover of the thesis.

occurred at the South Scotia Ridge, to accommodate the difference in absolute motion between the East Antarctic plate and the South Sandwich Trench and central Scotia plate above it. In view of this, a central Scotia plate is labelled despite the reconstruction showing it to be kinematically indistinct from the Antarctic plate to the south. South Georgia and Shag Rocks are part of this central Scotia plate, and I have chosen to show the South Georgia microcontinent to be acting as a continental transfer zone between the South Sandwich subduction zone and the North Scotia Ridge, in preference to a discrete junction to the northeast of the block. This provides (a) an explanation for the lack of any evidence for subduction beneath South Georgia itself, (b) a means by which South Georgia and Shag Rocks can be present on the eastern passive margin of the west Scotia Sea, and (c) a locus for strike-slip faults accommodating the northward propagation of the west Scotia ridge. The South American plate incorporates the Falkland Plateau and a tapering hook of oceanic crust south of its eastern extremity which is simultaneously being subducted at the South Sandwich Trench and created at the South American–Antarctic Ridge. This ridge is isolated from its parent margin at Tierra del Fuego, however, by the presence and rollback of the South Sandwich Trench. The result is continuing spreading in the west Scotia Sea.

The later stages of back-arc basin opening behind Discovery Bank are shown defining a Discovery plate which ceased independent motion following the deactivation of the ridge and basin at or after C5 (Barker and Hill, 1981; Hamilton, 1989). North and east of this the proto-South Sandwich Arc (the present arc is less than 4 million years old (Baker, 1978)) may have been extending as a prelude to the main phase of extension in the east Scotia Sea, or a nascent East Scotia Ridge and Sandwich plate (not shown) may already have existed. The extent of this arc at least as far north as W5 is shown by the reconstructed position of the arc fragment, out of the present South Sandwich fore-arc, which had been active well before C5c (Livermore *et al*, 1994; Barker, 1995). I show the trench as being present as far north as the southeastern extremity of the South Georgia microcontinent and note, after Barker (1995), that the seamounts presently at 56.14°S,

36.49°W and 56.78°S, 35.79°W (present coordinates) may represent arc volcanoes of a similar age which did not become entrained in the modern fore-arc further north along the trench.

In the reconstruction the South Shetland plate is not yet active: Bransfield Strait has been fully closed by rotating the South Shetland Islands with respect to the Antarctic Peninsula, by 0.80° about a pole at 61.51°N, 46.60°E.

The reconstruction implies the following movements in the C5c–C3a period:

1) Dextral strike-slip between the Magallanes and South American plates in Tierra del Fuego–Burdwood Bank, accompanied by convergence increasing in importance from west to east as the strike of the plate boundary becomes more easterly. About 60 km movement.

2) A similar type and amount of relative movement between Magallanes and Burdwood plates on the western arm of the Endurance Fracture Zone.

3) About 60 km dextral oblique convergence between the Burdwood and South American plates along the North Scotia Ridge east of Burdwood Bank and at Aurora Bank.

4) Continuing sinistral strike-slip north of South Georgia and 'continental transfer' (dashed lines) within the South Georgia microcontinent.

Convergent motion between the Magallanes and the South American plates (which was expressed also in Figure 4.5) could be manifest as the accretionary prism of the North Scotia Ridge. It has been shown that the southern edge of Burdwood Bank (*i.e* the Magallanes–South American and Magallanes–Burdwood plate boundary) is the buttress against which the prism accumulated (Cunningham, 1998; Cunningham *et al*, 1998). Further east of the buttress, convergent motion between the Magallanes and Burdwood plates may have been taken up on the 'Endurance transform fault' itself. Figure 4.5 also predicts oblique convergence on the North Scotia Ridge between the Burdwood and South American plates as far east as Aurora Bank where evidence for an accretionary prism persists (Cunningham, 1998). In the reconstructions the arrow at the northern end of the ridge segment in W5 implies its propagation accompanying convergence at the Burdwood

Bank buttress. The reality of convergence between the Magallanes and Burdwood plates is open to debate, bearing in mind the questionable nature of the inversion for Burdwood plate motion (Section 3.4.3) and the applicability of the Endurance Fracture Zone as a natural break within the west Scotia Sea system.

The prediction of Hill and Barker (1980) that seafloor spreading in Protector Basin could have started at C5c, would imply the presence of a 'Protector ridge' between a 'Terror plate' and the Magallanes plate (Figure 5.2). This interpretation is not favoured because the model of west Scotia Sea spreading used here simply does not require it. Instead I keep Protector Basin open in this reconstruction.

5.6 A change in the west Scotia Sea: C6

The reconstruction of the Scotia Sea at chron C6 ($\sim$ 20.1 Ma) is shown in Figures 5.7 and 5.8. The plate configuration is broadly similar to that at C5c except that back-arc spreading is happening behind both the Jane and Discovery arcs. The central Scotia plate is still shown to be rigidly attached to the East Antarctic plate via the South Orkney Microcontinent region and northwest Weddell Sea but, as with the foregoing reconstructions, I believe this is an oversimplification and minor motions probably did occur on the South Scotia Ridge. Seafloor spreading is shown as only having just begun in northern W6, in a similar manner as has been envisaged for W7 at C5c, so that Shag Rocks and the North Scotia Ridge at $\sim$ 50°W (present coordinates) are directly opposed, and northern South Georgia has just rifted away from the North Scotia Ridge to the south of this. A sinistral strike-slip boundary exists between the Shag Rocks block and South Georgia microcontinent. The Magallanes and Burdwood plates remain separated from the South American plate (Falkland Plateau) by the Magallanes fault and North Scotia Ridge.

Predicted relative movements for the C6–C5c period are similar to those for the C5c–C3 period, implying a 14 million year long period of stability in the west Scotia regime,

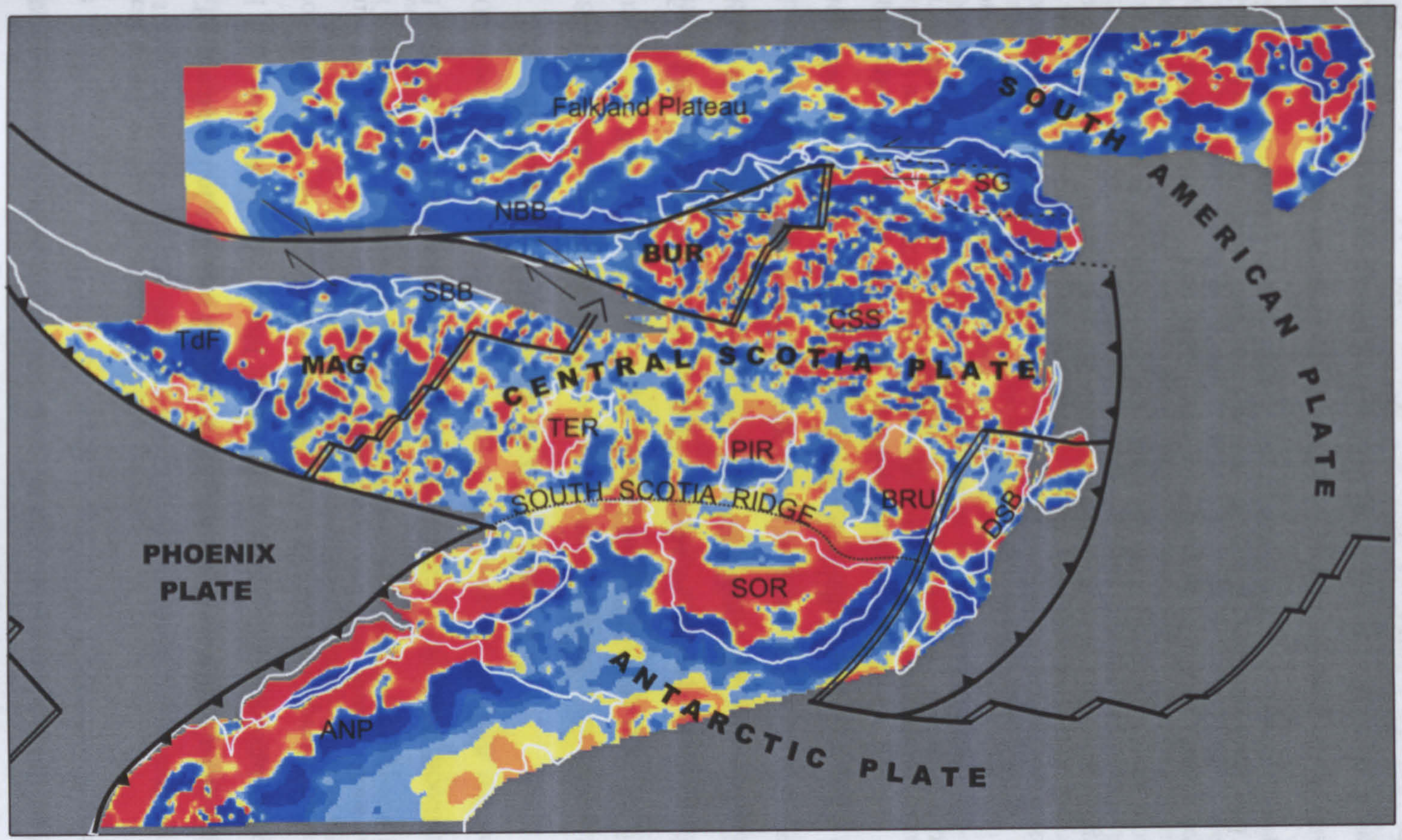

Figure 5.7: Reconstruction of the total field anomaly in the Scotia Sea at chron C6. Ornament as for Figure 5.3. Labels as for Figure 5.5. A larger version of this figure can be found inside the back cover of the thesis.

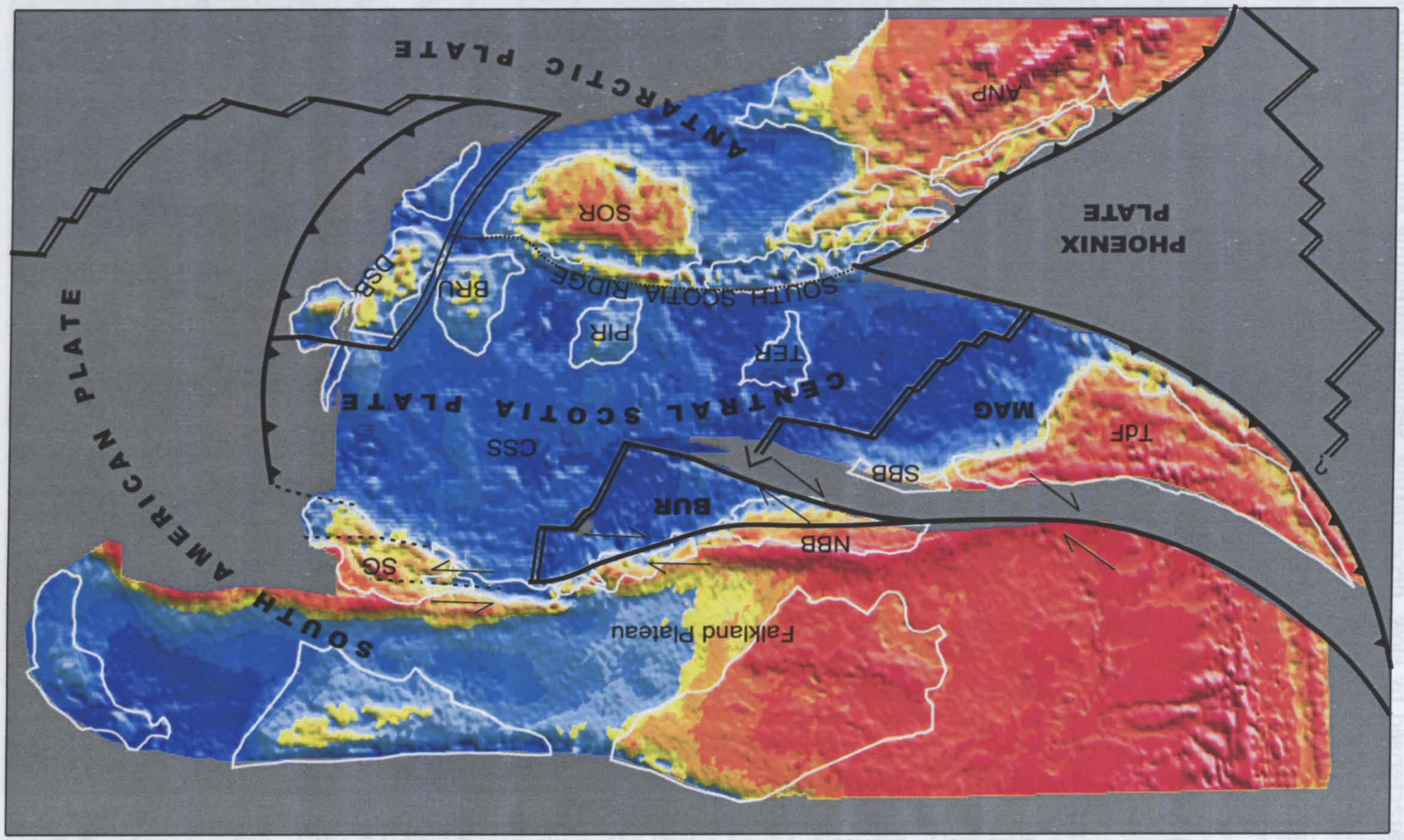

Figure 5.8: Reconstruction of the Bouguer gravity anomaly in the Scotia Sea at chron C6. Ornament and labels as for Figure 5.7. A larger version of this figure can be found inside the back cover of the thesis.

which was characterised by slow, decelerating, seafloor spreading and convergence at the northern margins of the west flank plates. This was a change, however, from what had been the situation just previously, as will be outlined in the next section.

5.7 The young west Scotia Sea: C8

The reconstruction of the Scotia Sea at chron C8 ($\sim$ 26.5 Ma) is shown in Figures 5.9 and 5.10. The West Scotia Ridge in W1–W6 is shown as just having started as a spreading centre following initial rifting. As a consequence the Magallanes, Burdwood and central Scotia plates have just come into existence and are separated from each other by the West Scotia Ridge and western arm of the Endurance Fracture Zone, and from the South American plate by the North Scotia Ridge. The South American plate includes the part of the South Georgia microcontinent north of the present-day offset in its edge at 55°S. The remainder of the microcontinent continues to act as a continental transfer zone between the central Scotia and South American plates. This has been done in order to maintain the conditions where subduction does not occur beneath South Georgia but the southern part of South Georgia can be present on the eastern passive margin of the west Scotia Sea. At this time the Antarctic Peninsula has just ceased moving as part of a separate plate to East Antarctica and spreading in Powell Basin has just begun to decline over what will be the next three million years to extinction of the Powell ridge. Back-arc basins behind Discovery and Jane banks are not yet open on the east flank of the South Orkney Microcontinent, beneath which subduction of South American seafloor is occurring.

Predicted movements between C8 and C6 are different to those following C6. On the North Scotia Ridge fast dextral strike-slip is predicted. In addition, due to the opening of Powell Basin, the northern margin of the South Orkney Microcontinent acts as a sinistral strike-slip fault with a significant convergent component. This movement would have lasted until C6c, when Powell Basin ceased opening.

As in the foregoing reconstructions kinematic coupling between the central Scotia

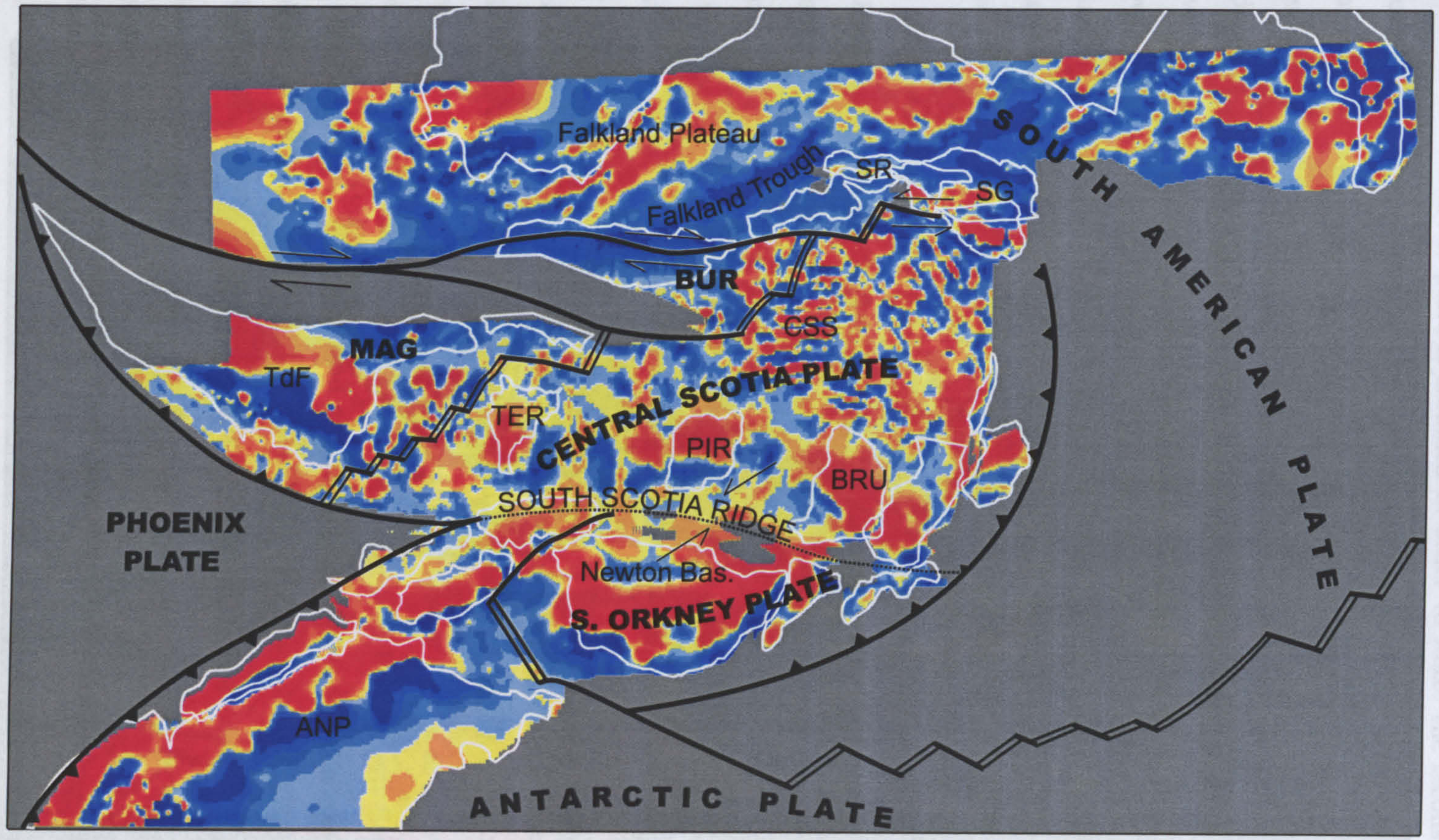

Figure 5.9: Reconstruction of the total field anomaly in the Scotia Sea at chron C8. Ornament as for Figure 5.3. ANP: Antarctic Peninsula, BRU: Bruce Bank, CSS: central Scotia Sea, Newton Bas.: Newton Basin, PIR: Pirie Bank, SG: South Georgia, SR: Shag Rocks, TdF: Tierra del Fuego, TER: Terror block. Bold lettering for plate names, BUR: Burdwood plate, MAG: Magallanes plate. A larger version of this figure can be found inside the back cover of the thesis.

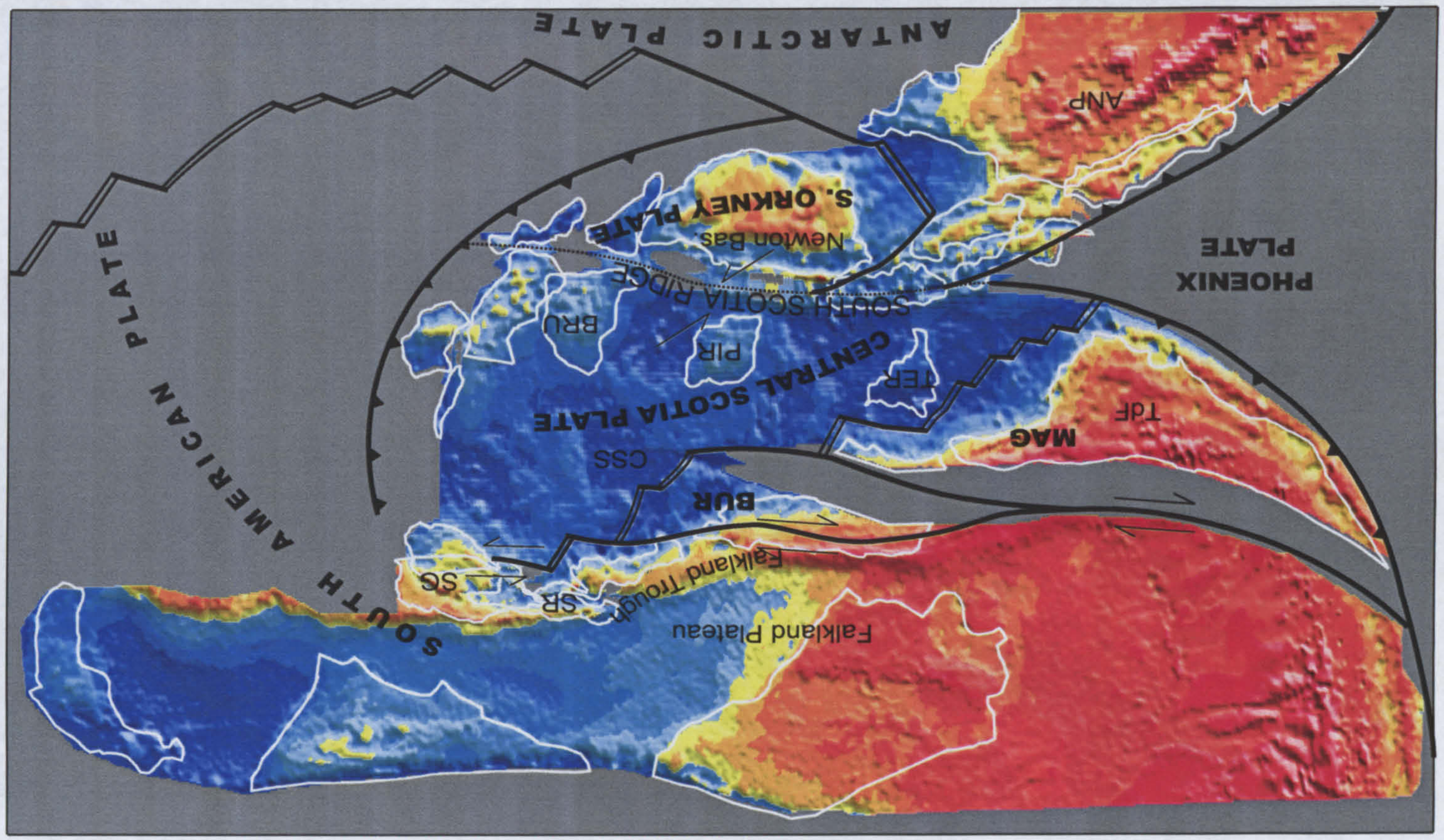

Figure 5.10: Reconstruction of the Bouguer gravity anomaly in the Scotia Sea at chron C8. Ornament and labels as for Figure 5.9. A larger version of this figure can be found inside the back cover of the thesis.

plate and the Antarctic plate is assumed in order to make the reconstruction. Here it is only via the northern Antarctic Peninsula and western South Scotia Ridge that the central Scotia plate could be connected rigidly to East Antarctica. This connection is dominated by continental crust and is so narrow that it could not really have acted in a rigid sense. Instead at this time I believe it more realistic for the central Scotia plate to have been seismically coupled to the proto-South Sandwich–Discovery Trench and moving slowly with respect to the mantle and East Antarctica. As in the previous reconstructions a small amount of relative movement at the South Scotia Ridge seems to be necessary, but is not shown because of a lack of direct knowledge of the past kinematics of the proto-South Sandwich–Discovery Trench with respect to East Antarctica.

Now possibly, as spreading in the west Scotia Sea proceeded, and with the extinction of Powell Basin and the Discovery–Jane trench the area of connection between the Magallanes and East Antarctic plates grew and relative motion along the South Scotia Ridge became more difficult to sustain. At chron C6 there were changes to seafloor spreading in the region; the direction of relative motion of South America with respect to East Antarctica changed from west-northwest to west, and the west Scotia Sea spreading centre began deceleration and underwent a minor azimuth change. In addition this time probably saw the initial stretching and rifting in the proto-South Sandwich Arc. It is difficult to assess cause and effect, but I put forward a scenario where initial rifting and spreading in the west Scotia Sea were due to the relative motion of Tierra del Fuego away from the central Scotia Sea, which was strongly coupled to the South Sandwich Trench at its eastern margin. With time and growth of the connection between the central Scotia and East Antarctic plates coupling at the trench became less strong at the expense of fast strike-slip decoupling at the North Scotia Ridge, to a point where an orthodox back-arc basin (the east Scotia Sea) developed in proximity to the trench and the North Scotia Ridge entered a compressive phase that ended with the extinction of the West Scotia Ridge. Maybe the change in motion of South America at about C6 was the event that set off such a change. Certainly after this time the spreading systems in the west Scotia

Sea and between South America and Antarctica were more closely comparable in terms of the amount of crust created.

Inception of spreading

A remaining question is: why did seafloor spreading begin at C8, and not earlier or later? Since the presence of the South Sandwich Trench appears to be instrumental in this model to the process of spreading in the west Scotia Sea, changes to subduction might be considered important in answering the question. Two possible changes which I can envisage giving rise to the need for accretion in the west Scotia Sea are:

1) Pre-C8 propagation of the trench to a point, at C8, where it isolates the South American margin south of the Falkland Plateau from spreading at the South American–Antarctic Ridge. Such propagation could have occurred either northward from the south, or in the opposite direction.

2) Ridge-crest–trench collisions in the northwest Weddell Sea, prior to and southwest of those hypothesised for Jane and Discovery Banks, deactivate the spreading centre there. A large ridge jump results, into the west Scotia Sea region behind the still-active length of the subduction zone.

Both scenarios are unproved. In the first case the history and direction of trench propagation is not well known outside of positions of presently-known dated arc fragments. In the latter case there is no reliable evidence for ridge-crest–trench collisions southwest of Jane Bank, let alone any that immediately pre-date C8.

5.8 More speculative reconstructions

Prior to chron C8 any reconstruction becomes more speculative as the rotations within the Scotia Sea are no longer based on the well-defined isochrons and azimuthal indications of features created during seafloor spreading. In particular it is difficult to demonstrate whether South American–Antarctic relative motion should have been outpaced by extension in the proto-Scotia Sea as has been done for the C8–C3a period and so the position of

Tierra del Fuego with respect to the rest of South America in the following reconstructions becomes much more speculative with increasing age.

Excess accretion in the west Scotia Sea has been attributed to the presence of the South Sandwich Trench at the eastern margin of the central Scotia Sea, isolating Tierra del Fuego from the East Antarctic plate and accretion at the South American–Antarctic Ridge. If subduction can be proved to have been active in the pre-C8 period (the occurrence of probable arc rocks dated at 29–32 Ma in the present-day South Sandwich fore-arc suggests this may be the case) then 'excess' accretion similar to that demonstrated in the west Scotia Sea might be expected to have occurred.

5.8.1 Early main extension: C13

A reconstruction for chron C13 ($\sim$ 32.1 Ma) is shown in Figures 5.11 and 5.12. The main body of the Scotia Sea is shown to consist of one kinematically distinct plate which is deforming by rifting in the future location of the West Scotia Ridge, at least as far north as the middle part of W6. South of this plate the onset of spreading in Powell Basin defines a South Orkney plate whose boundary with the plate in the Scotia Sea runs through the eastern South Scotia Ridge. The western South Scotia Ridge, which during Powell Basin rifting had remained part of the South Orkney plate is about to be abandoned to the Antarctic Peninsula by a jump of the boundary to the future Shackleton Fracture Zone. The Peninsula itself is moving as part of a West Antarctic plate with respect to East Antarctica as described by Cande *et al* (2000). The proto-South Sandwich Arc, and hence the trench, is likely to have been present at least to the north of Herdman and Bruce Banks at this time (Livermore *et al*, 1994; Barker, 1995).

Bearing in mind that the reconstruction is more speculative than those already shown, the following relative movements are tentatively predicted:

1. Extension in the northwest part of the west Scotia Sea—where it overlaps the North Scotia Ridge just east of Burdwood Bank (cross-hatched area). I have illustrated

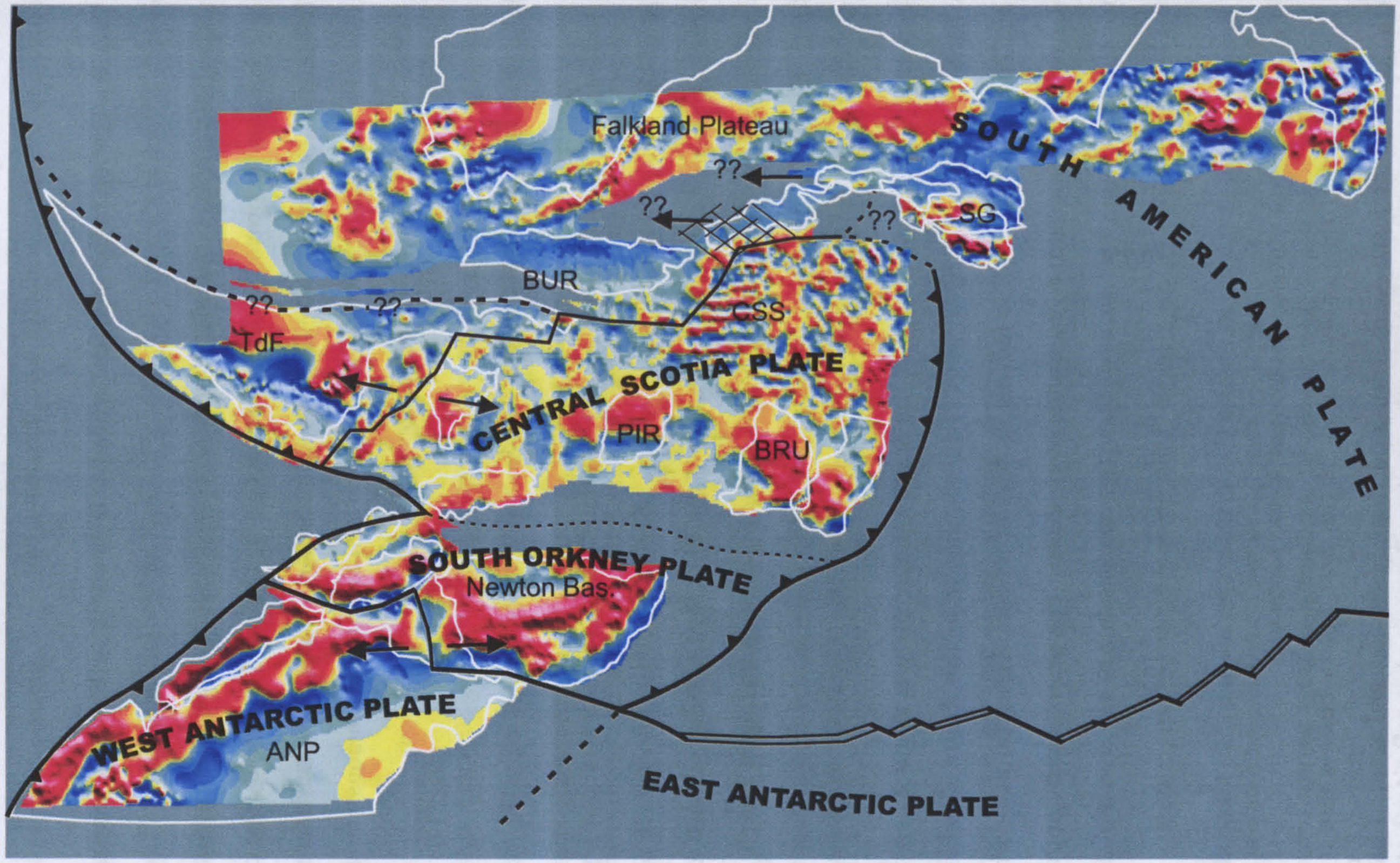

Figure 5.11: Reconstruction of the total field anomaly in the Scotia Sea at chron C13. Ornament as for Figure 5.3, except cross-hatching: area of overlap discussed in the text, arrows: sense of stretching in west Scotia and Powell rift basins. ANP: Antarctic Peninsula, BRU: Bruce Bank, BUR: Burdwood Bank, CSS: central Scotia Sea, Newton Bas.: Newton Basin, PIR: Pirie Bank, SG: South Georgia, TdF: Tierra del Fuego.

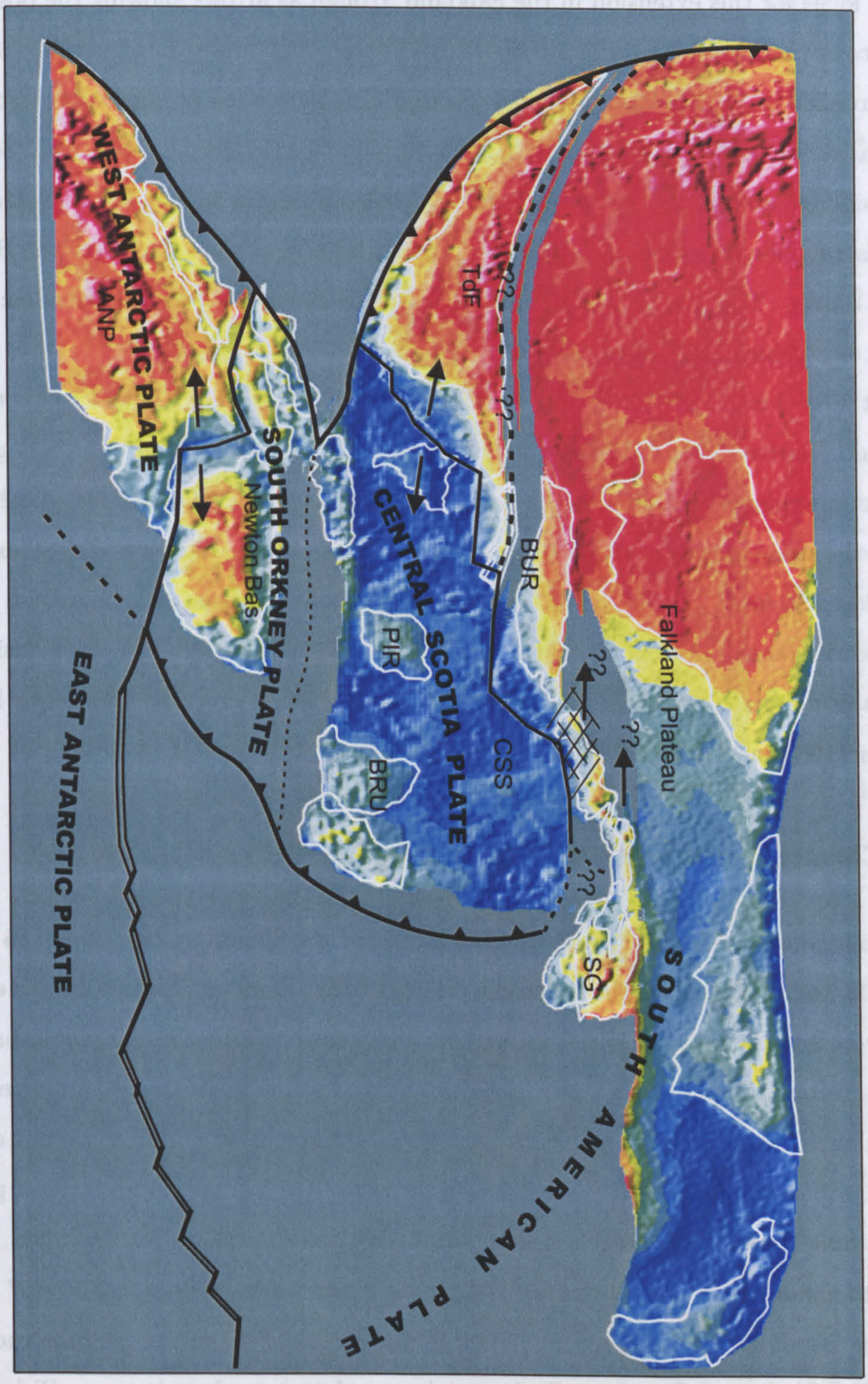

Figure 5.12: Reconstruction of the Bouguer gravity anomaly in the Scotia Sea at chron C13. Ornament and labels as for Figure 5.11.

a possible locus for this extension in the Falkland Trough as arrows showing the possible further reconstruction of the North Scotia Ridge into the Falkland Trough region (which has been masked to 2000 m bathymetry, not to the Bouguer anomaly edge as previously). An alternative scenario, invoking sinistral strike-slip faulting in the oceanic central Scotia Sea is considered less likely given the strength of oceanic lithosphere, and is not illustrated.

2. Sinistral oblique compression between the South Orkney Microcontinent and Bruce and Pirie Banks. The magnitude of this predicted movement is open to question: the prediction exists due to the use of the Adare Trough pole of Cande *et al* (2000) rather than a pole that fully closes the hypothetical circuit described in Section 4.5, in which case there would be no relative motion. When constructing this circuit no consideration was given to possible movements on the South Scotia Ridge. I note the presence of Newton basin parallel to the strike of the predicted fault, which I suggest may be interpreted as a flexural feature related to loads accumulated by the hypothetical compressional component.

3. Dextral transtension along southern margin of Powell Basin. The transtensional nature of this margin is preserved to the present-day and has been demonstrated by King and Barker (1988) and later workers.

5.8.2 Closure, prior to early failed rifts: C30

This speculative reconstruction, near the beginning of the Cenozoic, or C30 ($\sim$ 65 Ma; Figures 5.13 and 5.14), shows the situation prior to the opening and failure of two early rifts in Protector Basin and Dove Basin. The age–depth relationships in these basins are the main constraints on their ages, although in Protector Basin this is supported by magnetic reversal modelling. Both basins have been ascribed Middle to Late Eocene ages, consistent with predictions of early extension in the Drake Passage region from major plate reconstructions (Lawver *et al*, 1985; Livermore and Woollett, 1993). At this point, and maybe until the initial rifting of one or both of the small basins, say by C26 ($\sim$ 57 Ma) there is the possibility of transient land linkage for mammal dispersal. Reconstruction of both Dove Basin and Protector Basin requires a plate boundary between Pirie and

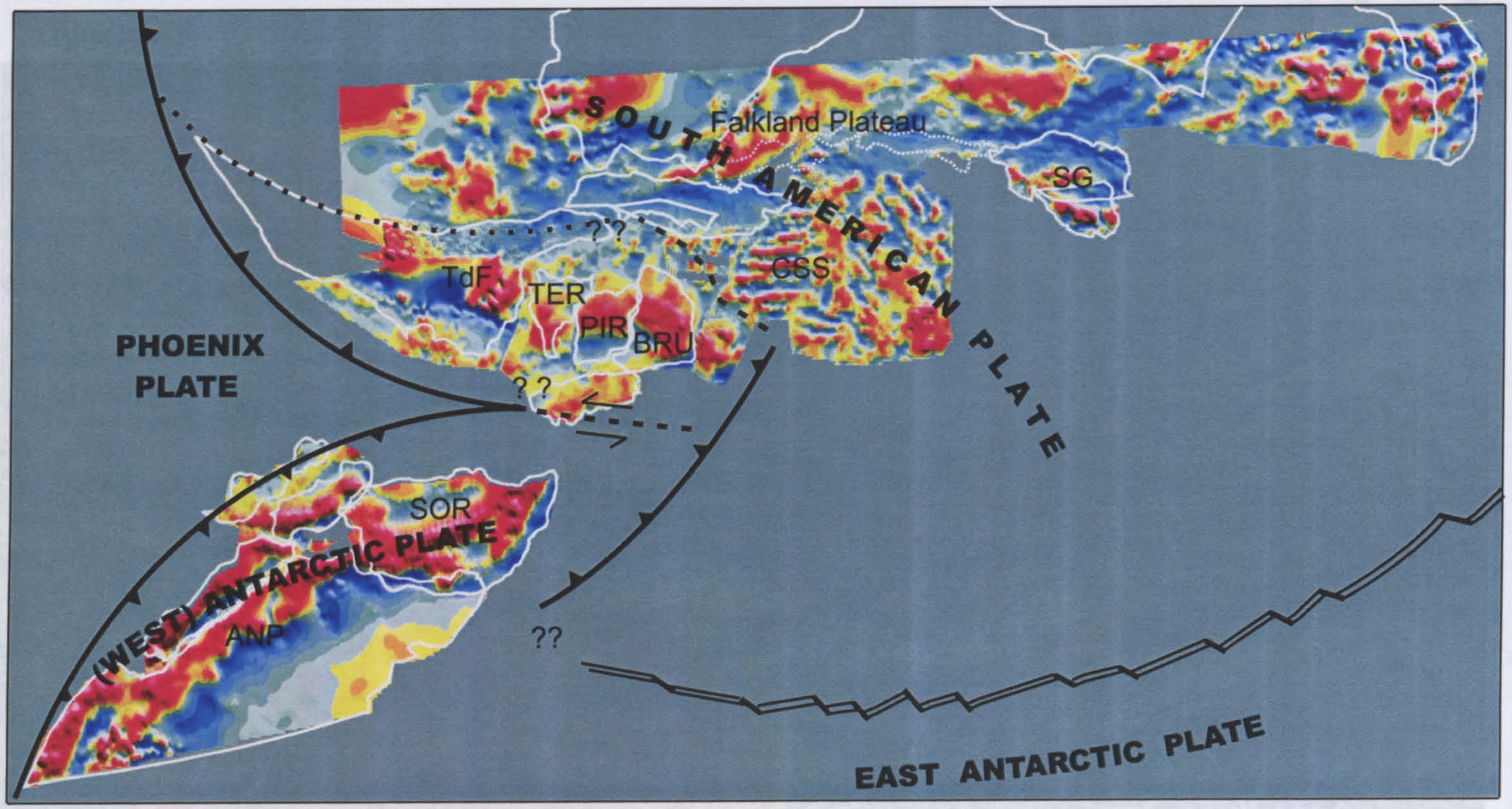

Figure 5.13: Reconstruction of the total field anomaly in the Scotia Sea at chron C30. Ornament as for Figure 5.3, except dotted white outlines: possible reconstruction of early dextral strike-slip on North Scotia Ridge. ANP: Antarctic Peninsula, BR: Bruce Bank, CSS: central Scotia Sea, PIR: Pirie Bank, SG: South Georgia, SOR: South Orkney Microcontinent, TdF: Tierra del Fuego, TER: Terror block. Note that the Powell Basin region has not been tightly reconstructed as suggested in Section 4.5.2.

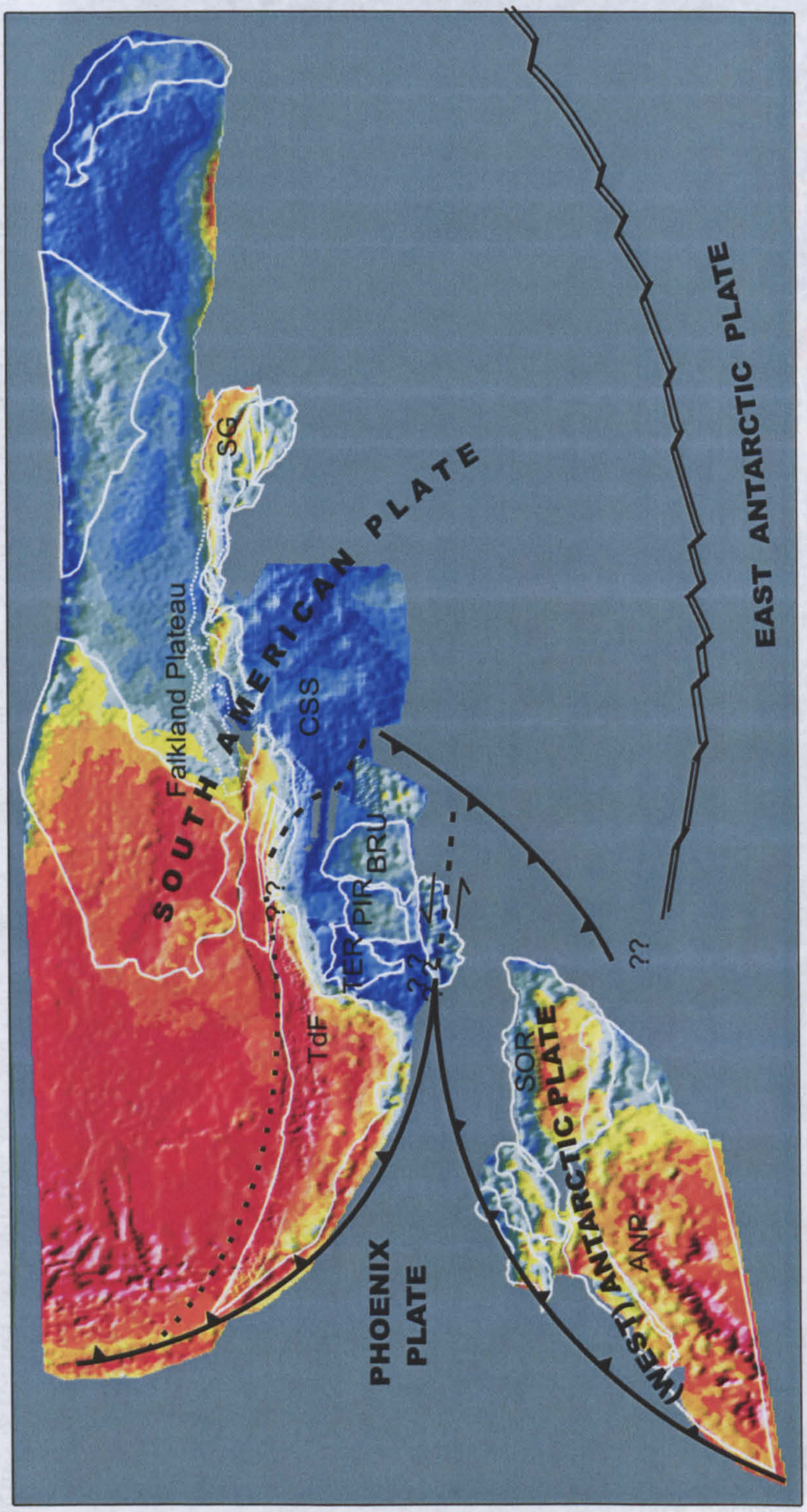

Figure 5.14: Reconstruction of the Bouguer gravity anomaly in the Scotia Sea at chron C30. Ornament and labels as for Figure 5.13.

Bruce banks and the central Scotia Sea and Antarctic plates, which I show as dotted lines at C30. I have been unable to produce any reconstruction that does not require such a boundary in some form at some stage. I assume that subduction was active at the eastern margin of the system and that, similar to the west Scotia Sea, its presence was the stimulus for spreading in Protector Basin and Dove Basin.

Chapter 6

Central Scotia Sea as conjugate to the southwest Weddell Sea

Keywords Central Scotia Sea. Weddell Sea. Thermal rejuvenation.

6.1 Introduction

The reconstructions of Chapter 5 show that it is entirely possible for the province of east-striking magnetic reversal anomalies of the central Scotia Sea to exist as a discrete, passive, element within the Scotia Sea during its growth, as suggested in Section 4.8.3. They also show that at chron C8, the South Georgia microcontinent was juxtaposed with the elevated portion of the North Scotia Ridge just east of Burdwood Bank (Figures 5.9 and 5.10). It seems unlikely that strike-slip movements preceding this time could have moved South Georgia around the southeast corner of Burdwood Bank from a position further west, as any preceding movement would have been likely to have been associated with initial rifting in the west Scotia Sea, as shown in the more speculative reconstructions at C13 and before. The only remaining undoubted oceanic crust in juxtaposition with South Georgia is in the central Scotia Sea. Understanding the central Scotia Sea is

important in determining whether South Georgia might have originated elsewhere in the pre-C8 period.

That seafloor spreading has created the central Scotia Sea seems inescapable, on the grounds of the depth of seafloor, the depth and character of seismic basement, and the very well developed linear magnetic reversal anomalies. However the anomaly sequence shows no strong symmetry, there is no median ridge feature and fracture zones are not obvious as free-air anomaly troughs as they are in the neighbouring west Scotia Sea. As a result, the nature and timing of this spreading has been the subject of much speculation:

1) The central Scotia Sea formed as a back-arc basin behind the proto-South Sandwich–Discovery Trench in the period 20–6 Ma (Hill and Barker, 1980)

2) The central Scotia Sea formed as a back-arc basin behind the proto-South Sandwich–Discovery Trench in the period 33-23.5 Ma (Hill and Barker, 1980)

3) The central Scotia Sea formed behind the proto-South Sandwich–Discovery Trench as a back-arc basin with no definite locus of accretion (Livermore *et al*, 1994; Hamburger and Isacks, 1988)

4) The central Scotia Sea formed by Mesozoic back-arc spreading behind the ancestor to the Chile Trench as an extension to the Rocas Verdes basin (De Wit, 1977)

5) The central Scotia Sea is a fragment of older normal oceanic crust trapped during growth of the Scotia Sea (Livermore *et al*, 1994) like the Celebes Sea (southeast Asia) (Silver and Rangin, 1991; Nichols and Hall, 1999), the Bering Sea (Cooper *et al*, 1976; 1992), or (possibly) the Caribbean plate (Malfait and Dinkelman (1972); Pindell (1985); Ross and Scotese (1988), but see Meschede and Frisch (1998) for an alternative view).

Section 4.8 shows that spreading in the central Scotia Sea, whatever its origin, is kinematically unlikely to have taken place during the period 26.55–6 Ma while the west Scotia Sea was active, because there is no evidence for the subduction that would be needed to accommodate it. Interpretations (1) and (2) are therefore rejected. Now, given that no subduction of central Scotia Sea floor has occurred beneath the North Scotia Ridge or South Scotia Ridge, and if the central Scotia Sea formed by back-arc spreading at any

time, the lack of symmetry in its reversal sequence requires that the locus of accretion must have been non-stationary. However the lack of any ridge-like features (Figure 6.1) or numerous seamounts suggests that the province contains *no* fossil accretionary centres. Moreover the long, well-developed, east-striking anomalies (Figure 6.2) are not compatible with multiple loci. On these grounds I reject interpretation (3). Interpretation (4) is elegant except that it too does not explain the anomalies' asymmetry, nor the lack of a median ridge. In addition I can see no evidence for the gradual eastwards widening of the back-arc basin from Tierra del Fuego that De Wit (1977) requires. In summary so far, then, an autochthonous central Scotia Sea is not compatible with the evidence.

Interpretation (5), an allochthonous central Scotia Sea, seems the most attractive as a trapped fragment need not bear any fossil ridge if it represents just one limb of a system, and can be present in a purely passive sense: there is no need to explain its accretion *in situ*. It is this possibility that I explore in this chapter.

6.2 Provenance of an allochthon

So, if the central Scotia Sea is an allochthon, representing only one limb of a pre-C8 system, where can it have come from? Where is the other limb? The Scotia Sea is surrounded by regions of oceanic crust which pre-date it. To the west the Phoenix–Antarctic regime had been active since the Mid-Cretaceous. To the northeast, oceanic crust forms by opening of the Atlantic Ocean in response to separation of South America from Africa, and has done since $\sim$ 130 Ma. To the southeast, the Weddell Sea formed by separation of South America from East Antarctica between the mid Mesozoic (maybe 165 Ma, Livermore and Hunter (1996)) and about 20 Ma.

Trapping crust of the Phoenix plate within the Scotia Sea seems impossible since it would have to pass through the undoubtedly closed Tierra del Fuego–Antarctic Peninsula connection in order to be positioned on the east flank of the nascent west Scotia Sea

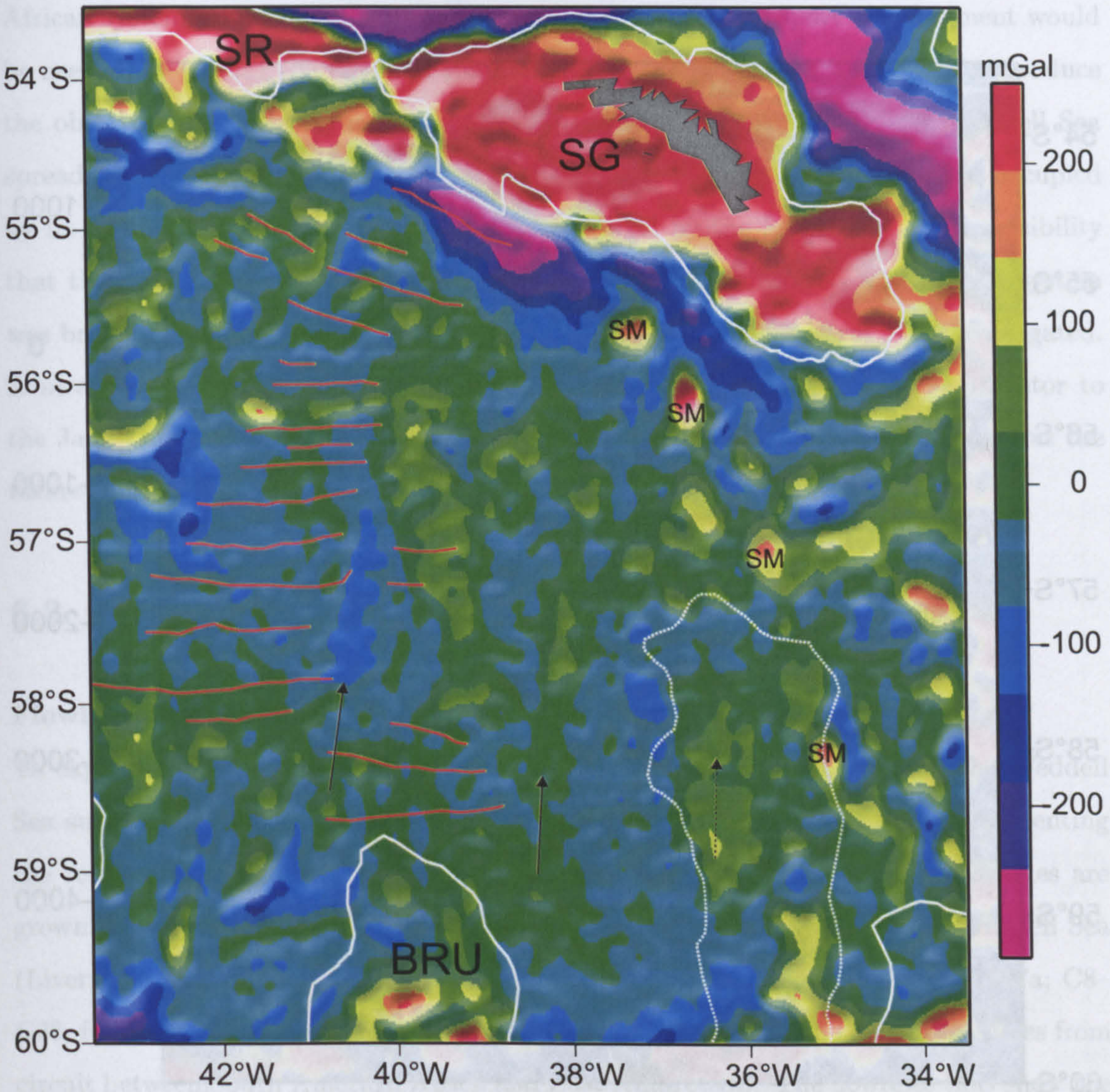

Figure 6.1: Gridded free-air gravity anomalies over the central Scotia Sea. White outlines: Bouguer anomalies, SG: South Georgia, SR: Shag Rocks, BRU: Bruce Bank. Dotted white outline: relative Bouguer anomaly high extending north from Discovery Bank, this feature and a line of seamounts (SM) may mark the location of the proto-South Sandwich Arc. Red lines: central Scotia Sea magnetic reversal anomalies. Absence of prominent ridge features or seamounts suggests no accretionary locus for these anomalies is preserved. Short-wavelength rectilinear fabric parallel and perpendicular to the reversal anomalies (black arrows) may represent the original fabric of seafloor spreading, overprinted by later anomalies like the prominent north–northwest anomaly north of Bruce Bank.

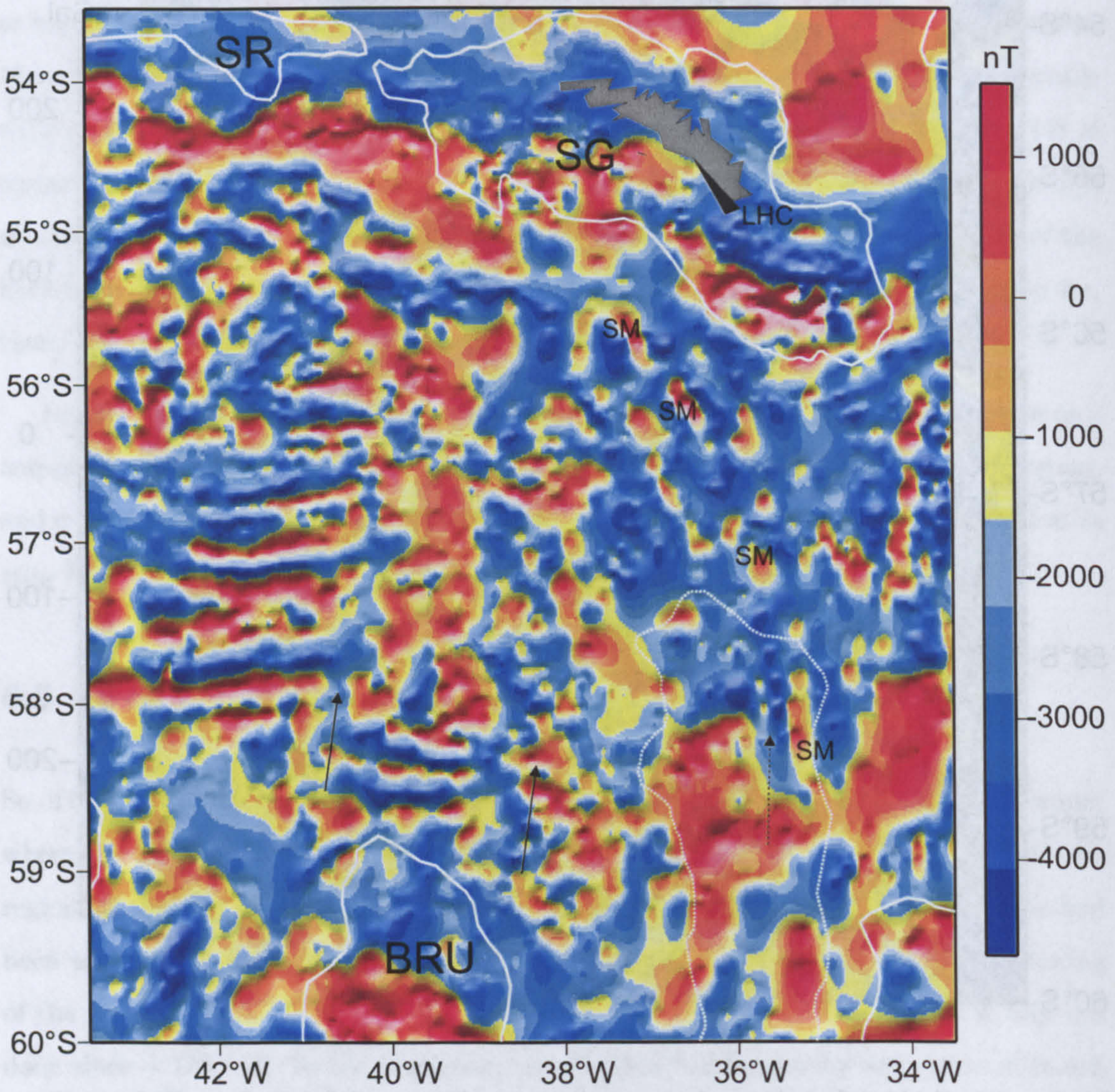

Figure 6.2: Gridded magnetic anomalies over the central Scotia Sea, reduced to the pole. White outlines: Bouguer anomaly highs as Figure 6.1. East-striking anomalies are well developed in the west of the region, and just north and east of Bruce Bank. The offsets between these regions (arrows) correspond to short-wavelength ridges and troughs in the free air anomaly which may represent the original spreading fabric of the system. LHC: Larsen Harbour Complex (the pseudo-ophiolite suite on South Georgia). SM: seamounts.

system as its passive margin. Likewise, trapping lithosphere of the South American–African system would be difficult as substantial southerly transport of a fragment would be needed, by-passing the Falkland Plateau *en route*, as well as a 90° rotation to produce the observed strike of magnetic anomalies in the central Scotia Sea. The Weddell Sea spreading system is the most likely origin of a fragment, as the region once occupied by its northern (South American) limb is now filled by the Scotia Sea. The possibility that the Scotia Sea may entrain parts of the northern limb to the Weddell Sea system was briefly mentioned by LaBrecque and Barker (1981), but has never been investigated. A means by which part of this limb could have escaped subduction at the ancestor to the Jane–Discovery trench is the principal kinematic obstacle to its emplacement as the future central Scotia Sea.

6.3 Trajectory and Fitting

Flowline modelling

To explore the possibility further that a fragment of the northern limb of the Weddell Sea survives in the central Scotia Sea I construct a set of model flowlines representing the relative motion of South America and Antarctica since closure. The flowlines are grown outwards from seed points on well-defined isochrons in the northern Weddell Sea (Livermore and Woollett, 1993) using the reconstruction poles of Nankivell (1997a; C8–C33, full joint inversion) and Livermore and Hunter (1996; C33–FIT, model B, poles from circuit between South America, Africa and East Antarctica). The flowlines thus show the predicted trajectories of fracture zones on both the Antarctic and South American limbs of the Weddell Sea system between 165 Ma (the 'FIT' pole of Livermore and Hunter (1996)) and 26.55 Ma (a C8o pole interpolated from the unmodified 3-plate inversion set of poles of Nankivell (1997a)). To build the flowlines I assume that

(1) the west Scotia Sea represents all South American–Antarctic accretion west of the proto-South Sandwich–Discovery Trench after C8, and

Chron	Age (Ma)	Latitude	Longitude	Angle
Nankivell (1997), unmodified 3-plate inversion				
C8	25.82	0.00	0.00	0.00
C13	33.06	71.76	15.45	2.48
C18	38.43	75.60	27.42	4.46
C20	42.54	76.06	41.94	6.08
C21	46.26	77.20	42.54	7.16
C30	65.58	73.80	82.42	15.27
C32	71.07	72.89	72.70	16.62
C33	73.62	73.00	73.04	17.92
C33r	79.08	72.90	76.40	20.56
C34	83.00	72.71	77.68	22.41
Livermore and Hunter (1996), model B				
E	93.00	71.7	71.2	25.78
M0	118.70	68.1	95.4	41.67
M2	122.64	67.4	91.7	41.39
M4	126.46	66.7	88.3	41.18
M10N	131.65	64.4	84.4	40.96
M21	149.65	58.8	87.7	41.07
FIT	165.00	52.3	90.7	41.71

Table 6.1: Finite poles used to produce the model flowlines of Figure 6.3; these are the poles of Nankivell (1997a) and Livermore and Hunter (1996), with the C8 pole of Nankivell (1997a) removed in consideration of the growth of the west Scotia Sea behind the South Sandwich Trench. Note that Nankivell (1997a) uses the younger end of C8, for which no adjustment has been made, and that Livermore and Hunter (1996) use the reversal timescale of Kent and Gradstein (1986).

(2) The spreading centre at C8 was $\sim$ 30 km wide. Table 6.1 shows the set of poles used.

The model flowlines are shown in Figure 6.3. The lengths of flowlines crossing the west Scotia Sea aged between 93 Ma and M10 ($\sim$ 130 Ma) have a northerly trend and are enclosed by the Scotia Arc. Older portions of the flowlines towards M21 ($\sim$ 150 Ma) show a northeasterly trend which is locally included within the Scotia Arc. Assuming the 'Weddell ridge' trended approximately normal to its transform faults a model set of 'Weddell' reversal anomalies stranded in the central Scotia Sea should, therefore, mainly strike east or southeast in its northern part. Figure 6.2 shows the magnetic reversal

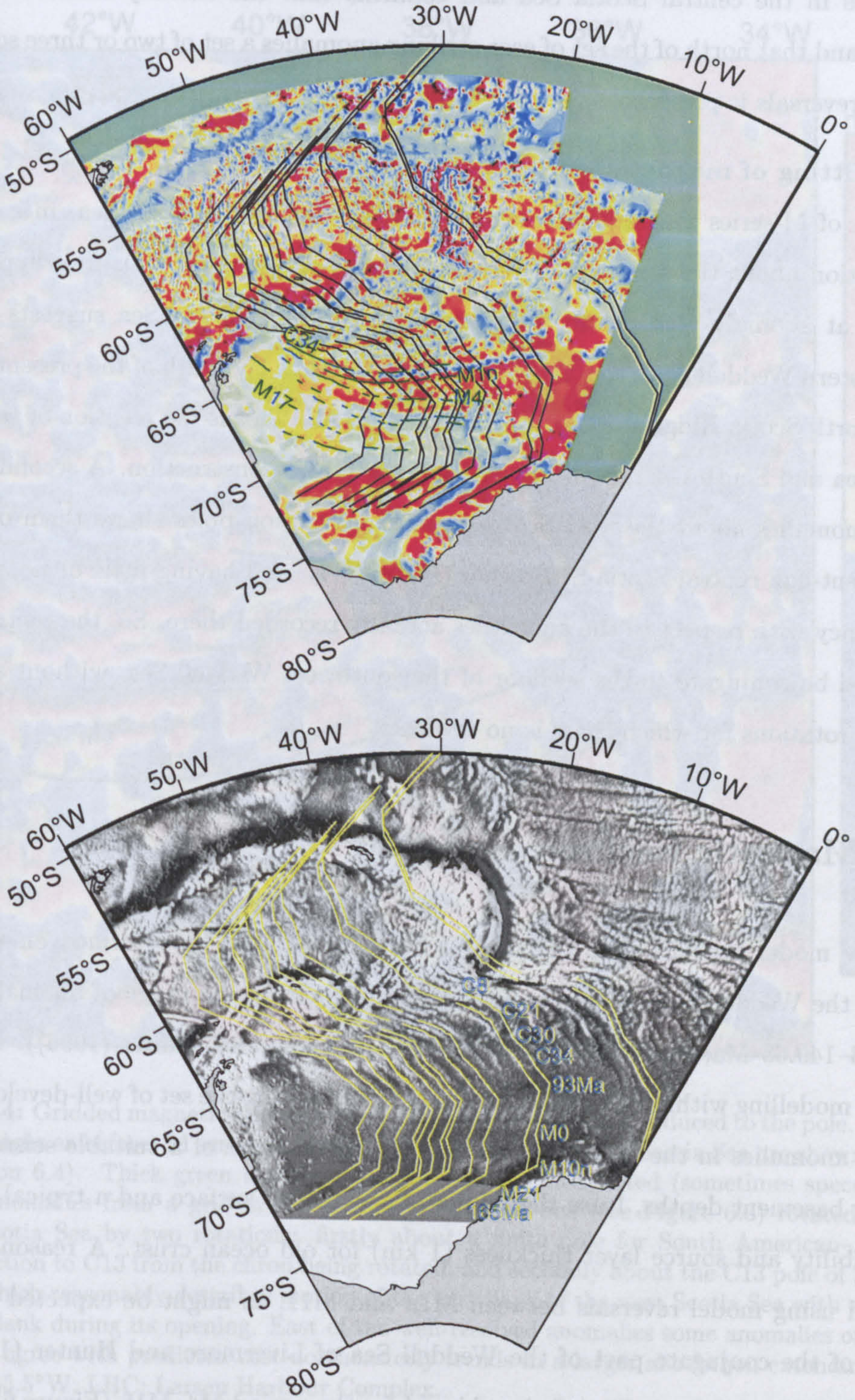

Figure 6.3: Model flowlines for spreading in the Weddell Sea between 165 Ma and C8. Bottom: flowlines (yellow) overlain on free-air anomalies, flowpoints are labelled by their age or chron. Top: flowlines (black) overlain on total field anomalies. Green lines identify some anomalies on the grid in the Weddell Sea, which are used in Figure 6.4, chron numbers labelled in green.

anomalies in the central Scotia Sea and confirms that the easterly strike is certainly evident, and that north of the set of east-striking anomalies a set of two or three southeast-striking reversals is present.

Visual fitting of magnetic isochrons

Rotation of M-series magnetic reversal anomalies from the Weddell Sea, in a forwards construction about the same set of reconstruction poles (Figure 6.3), to a hypothetical position at anomaly C13 before the opening of the west Scotia Sea suggests that the southwestern Weddell Sea's conjugate seafloor at the time lay south of the present position of the North Scotia Ridge and east of Burdwood Bank. This is the position of the central Scotia Sea and South Georgia in Figure 5.11, the C13 reconstruction. A second rotation of the anomalies about the west Scotia Sea reconstruction poles shows them occupying the present-day central Scotia Sea region (Figure 6.4), and having little or no azimuthal discrepancy with respect to the anomalies actually recorded there. So, the central Scotia Sea could be conjugate to the seafloor of the southwest Weddell Sea, without appealing to extra rotations for which there is no evidence.

6.4 Magnetic isochron modelling

The new model predicts that the central Scotia Sea could have formed on the north flank of the Weddell ridge by spreading somewhere within the range of anomalies 'E' to M21 (93–149.65 Ma; Cande and Kent (1995); Livermore and Hunter (1996)). I perform reversal modelling within this period for ship tracks crossing the set of well-developed east-striking anomalies in the central Scotia Sea. In the absence of a suitable seismic profile showing basement depths, I use the modern bathymetric surface and a typical magnetic susceptibility and source layer thickness (1 km) for old ocean crust. A reasonable fit is achieved using model reversals between M1n and M11, as might be expected using the models of the conjugate part of the Weddell Sea of Livermore and Hunter (1996) as a guide. However a more striking fit is achieved for the period M4–M16 (Figure 6.5), which

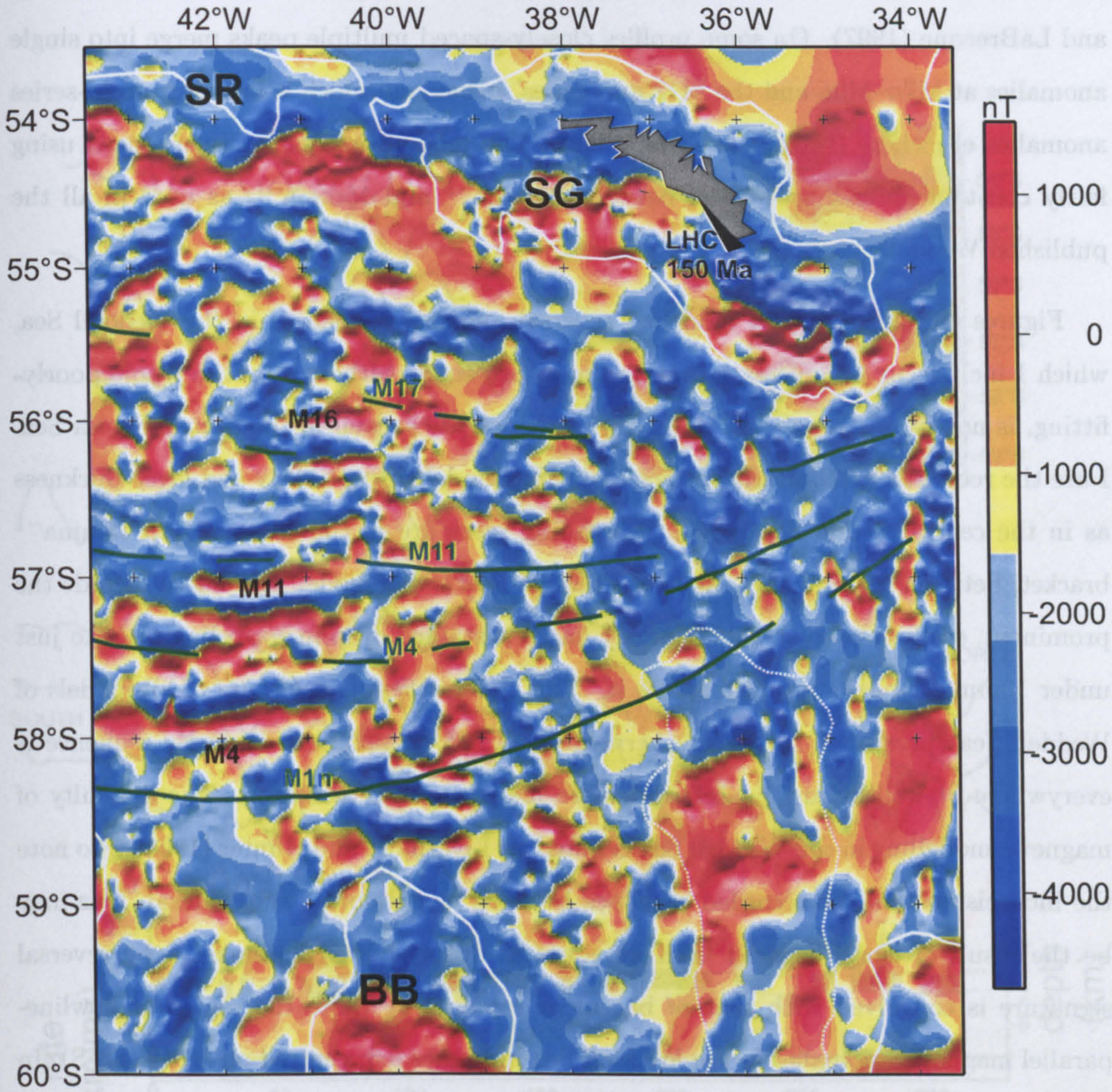

Figure 6.4: Gridded magnetic anomalies over the central Scotia Sea, reduced to the pole. Bouguer anomaly highs as before. M series anomalies identified in the central Scotia Sea are shown in black (see Section 6.4). Thick green lines and annotations are interpreted (sometimes speculatively) reversal anomalies from a grid in the southwest Weddell Sea (see Figure 6.3) rotated into the central Scotia Sea by two rotations: firstly about a finite pole for South American–Antarctic reconstruction to C13 from the chron being rotated, and secondly about the C13 pole of Nankivell (1997a) which reasonably describes motion of the east flank of the west Scotia Sea with respect to the west flank during its opening. East of the well-resolved anomalies some anomalies of the grid appear to agree with predicted east-northeasterly trends in a larger allochthon extending maybe as far as 35.5°W. LHC: Larsen Harbour Complex.

is similar to the modelled Weddell Sea sequences of LaBrecque *et al* (1989) and Ghidella and LaBrecque (1997). On some profiles closely-spaced multiple peaks merge into single anomalies at M7n–M9n and the M12 anomalies, behaviour which is known from M-series anomalies elsewhere (Nakanishi *et al*, 1992). The modelled sequence is produced using fairly constant spreading rates of between 20mma^{-1} and 15mma^{-1}, as used in all the published Weddell Sea models.

Figures 6.6 and 6.7 show modelled reversal anomaly sequences in the Weddell Sea, which I include to demonstrate that the sequence there, although on the whole poorly-fitting, is not inconsistent with the sequence which fits so well in the central Scotia Sea. I use the recorded bathymetric surface and same model susceptibility and layer thickness as in the central Scotia Sea model. Spreading rates are in the 20mma^{-1} to 15mma^{-1} bracket, between M4 and M16, as in the central Scotia Sea model. All tracks include the prominent, easily modelled, C34 anomaly and a sustained drop in spreading rates to just under 10mma^{-1} beginning just before it. This deceleration is a feature of all models of Weddell Sea spreading. In the southern Weddell Sea no magnetic anomaly sequence is everywhere fit well by any model, and these models are no exception. The difficulty of magnetic modelling in the Weddell Sea is noted by Livermore and Hunter (1996) who note the inconsistency of the recorded sequence between neighbouring ship tracks. This may be the result of closely spaced fracture zones in deeply-buried basement—the reversal signature is convolved with that of basement topography (note the region of flowline-parallel magnetic anomalies in the Weddell Sea in Figure 6.3, centred on 50°W, 68°S). In addition non-flowline ship passage is likely to be important and anomalous skewness may have an effect. With this difficulty I have only found it possible to produce fits to the recorded sequences which are consistent locally with a model guided by the central Scotia Sea sequence. In particular reversals M11n–M14 are often well reproduced. Livermore and Hunter (1996) note that on some profiles in the southernmost part of the Weddell Sea the modelled anomalies' amplitudes exceed those actually recorded. I also see this on the same profiles with my model parameters which is unsurprising as I use the bathymetric

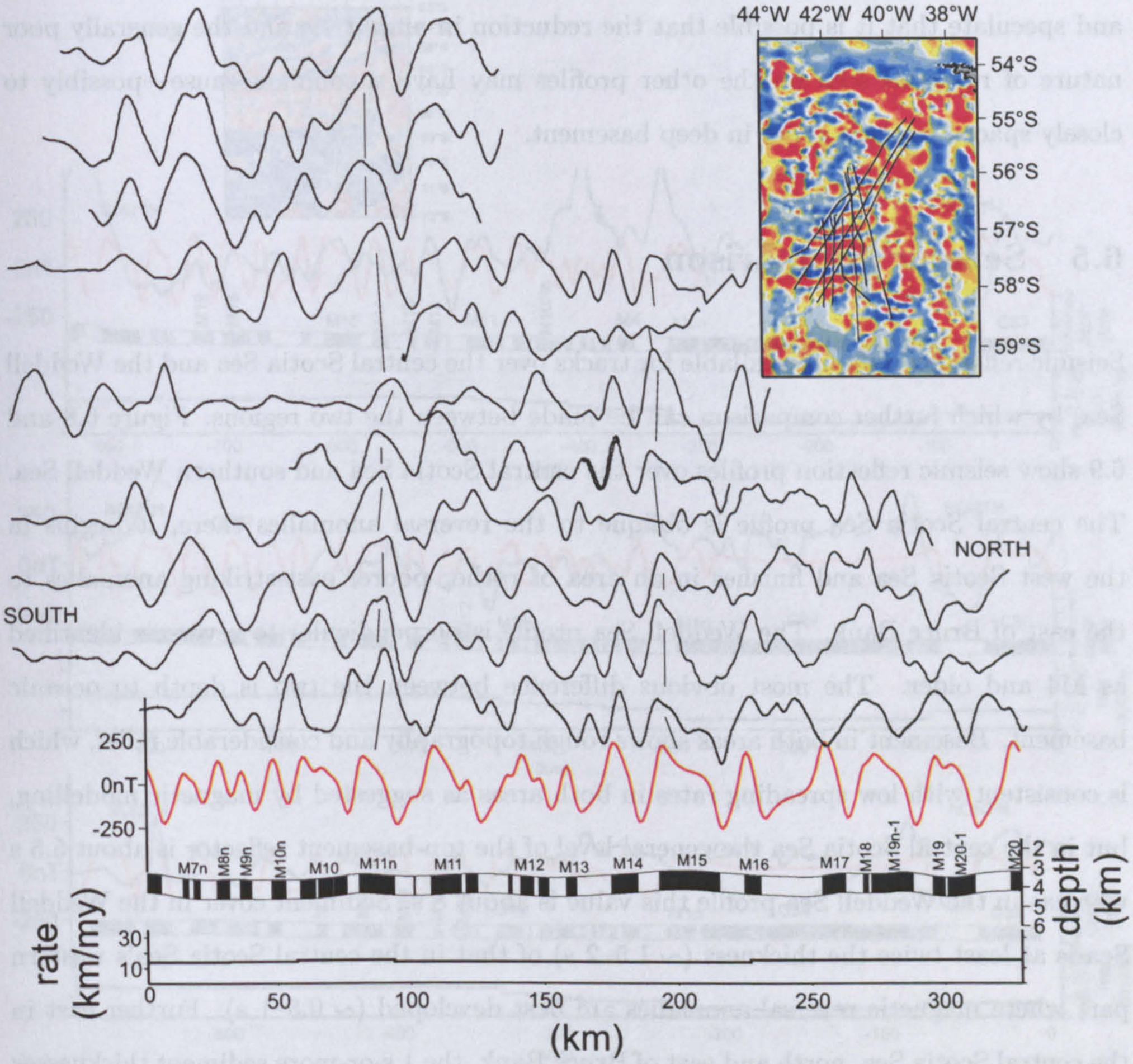

Figure 6.5: Mesozoic model seafloor spreading in the central Scotia Sea (red) compared to ship track sequences crossing the east-striking anomaly province (black). Inset shows the locations of the ship tracks. In the two best-fitting long profiles anomalies between M4 and M20 (~ 125–149 Ma) are identifiable. Compare with the Cenozoic models in Figure 4.18.

surface instead of seismic basement to represent the top of layer 2. However not all of the difference is likely to be attributable to the choice of upper surface for the source layer. I note that on the best fitting profiles the amplitude difference is least evident and speculate that it is possible that the reduction in amplitude and the generally poor nature of reversals seen on the other profiles may have a common cause—possibly to closely spaced fracture zones in deep basement.

6.5 Seismic comparison

Seismic reflection data are available for tracks over the central Scotia Sea and the Weddell Sea, by which further comparison can be made between the two regions. Figure 6.8 and 6.9 show seismic reflection profiles over the central Scotia Sea and southern Weddell Sea. The central Scotia Sea profile is oblique to the reversal anomalies there, it begins in the west Scotia Sea and finishes in an area of rather poorer east-striking anomalies to the east of Bruce Bank. The Weddell Sea profile is perpendicular to reversals identified as M4 and older. The most obvious difference between the two is depth to oceanic basement. Basement in both areas shows rough topography and considerable relief, which is consistent with low spreading rates in both areas as suggested by magnetic modelling, but in the central Scotia Sea the general level of the top-basement reflector is about 5.5 s whereas in the Weddell Sea profile this value is about 8 s. Sediment cover in the Weddell Sea is at least twice the thickness ($\sim$ 1.5–2 s) of that in the central Scotia Sea's western part where magnetic reversal anomalies are best developed ($\sim$ 0.5–1 s). Further east in the central Scotia Sea, north and east of Bruce Bank, the 1 s-or-more sediment thicknesses are more comparable to those in the Weddell Sea profile, but still less thick. In both areas the sediment pile is characterised by parallel reflectors onlapping basement highs. In the central Scotia Sea, however, the seafloor reflector is not at all smooth as it is in the Weddell Sea, and the crenulations of the surface appear to be present throughout the sediment pile. This character dies out further east, into a region which is less well characterised

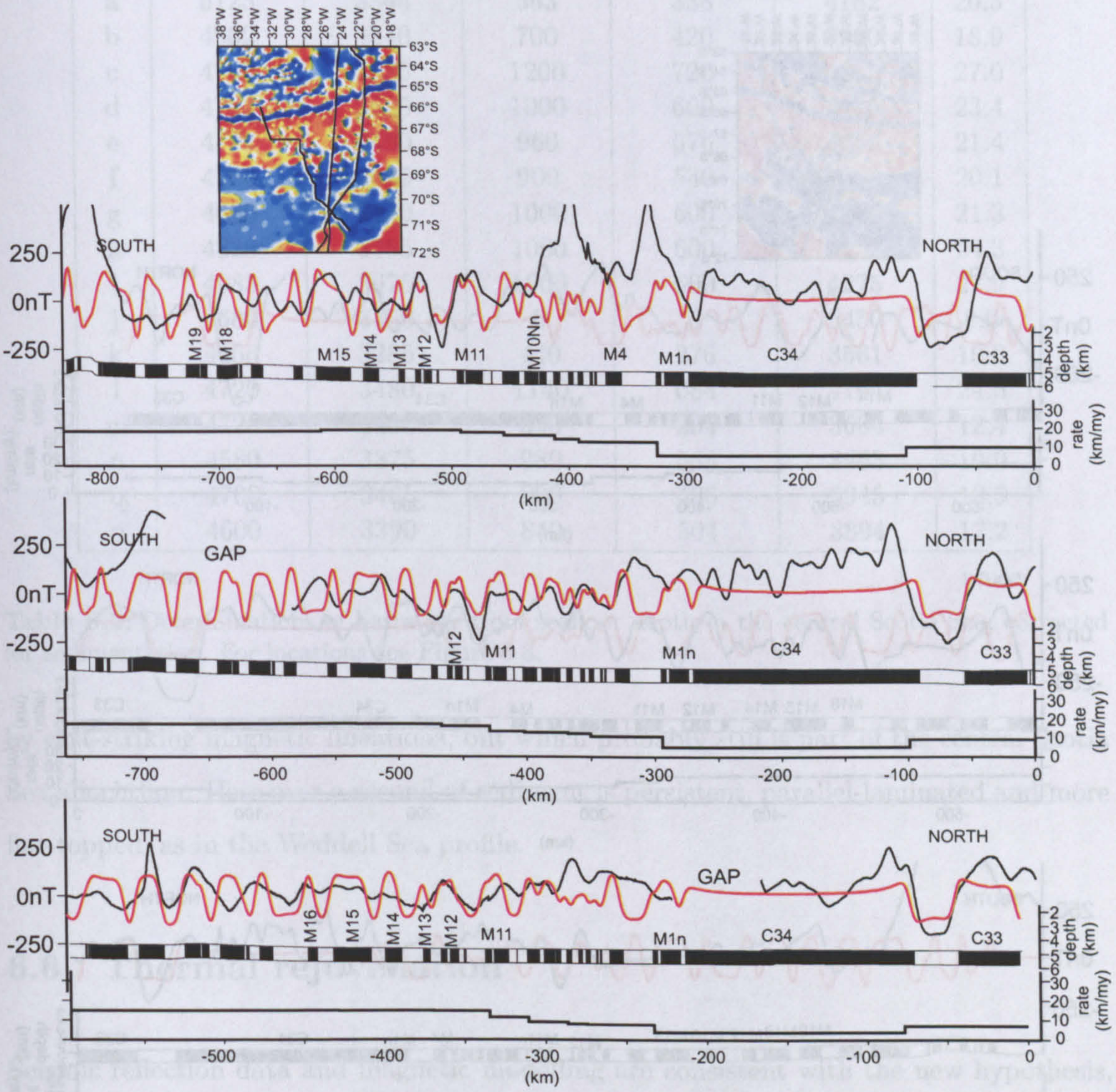

Figure 6.6: Mesozoic model seafloor spreading in the Weddell Sea (red) compared to ship track sequences (black). These sequences and those of Figure 6.7 are not exhaustive, but are representative: some fit well, others not so well. Overall, as for all published Weddell Sea magnetic reversal models, the fits are poor. Features common to all, however, are good fits for C33–C34 and M11–M12, which makes these models consistent with that in Figure 6.5.

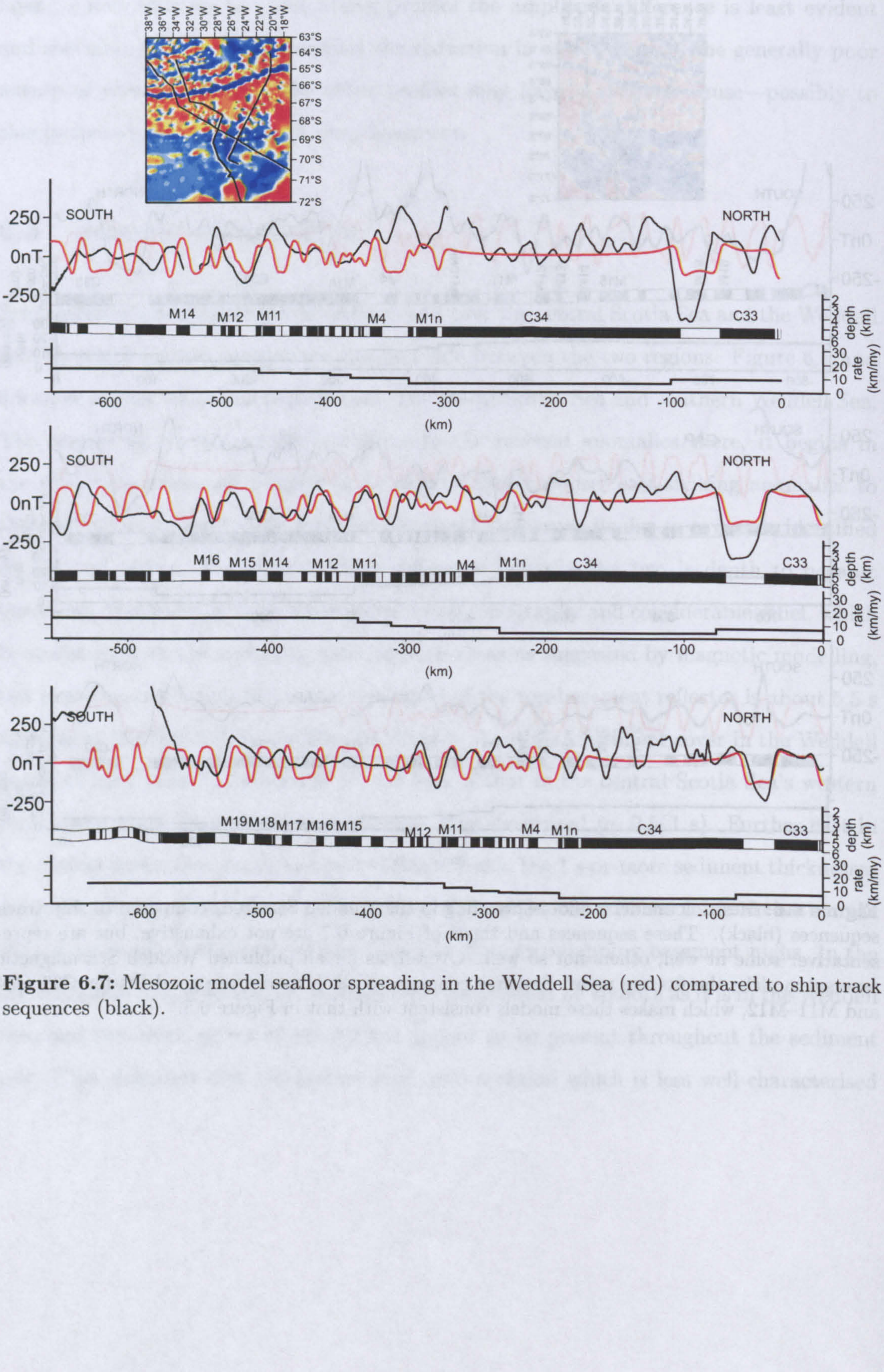

Figure 6.7: Mesozoic model seafloor spreading in the Weddell Sea (red) compared to ship track sequences (black).

Site	Seafloor time (ms)	Seafloor depth (m)	Sediment (ms)	Correction (m)	Corrected depth (m)	Age (Ma)
a	5125	3844	563	338	4182	20.3
b	4802	3540	700	420	3960	18.9
c	4782	3525	1200	720	4255	27.0
d	4782	3525	1000	600	4125	23.4
e	4721	3480	960	576	4056	21.4
f	4700	3465	900	540	4005	20.1
g	4680	3450	1000	600	4050	21.3
h	4820	3555	1000	600	4155	24.3
i	4985	3675	1000	600	4275	27.9
j	4680	3450	0	0	3450	8.0
k	4456	3285	440	276	3561	10.0
l	4720	3480	1140	684	4164	24.5
m	4720	3480	340	204	3684	12.4
n	4580	3375	980	588	3963	19.0
o	4700	3465	800	480	3945	18.5
p	4600	3390	840	504	3894	17.2

Table 6.2: Determinations of basin age from seafloor depth in the central Scotia Sea, corrected for sedimentation. For locations see Figure 6.8.

by east-striking magnetic lineations, but which probably still is part of the central Scotia Sea allochthon. Here over a second of sediment is persistent, parallel-laminated and more flat-topped, as in the Weddell Sea profile.

6.6 Thermal rejuvenation

Seismic reflection data and magnetic modelling are consistent with the new hypothesis, except for the following points:

1. Magnetic anomalies in the central Scotia Sea are more than twice the amplitude of those in the Weddell Sea.

2. Basement depth in the central Scotia Sea is about 2.5 seconds two-way-time sooner than expected, or about 2 km too shallow, as is the seafloor itself.

3. The central Scotia Sea is not as heavily sedimented as crust of a similar age in the

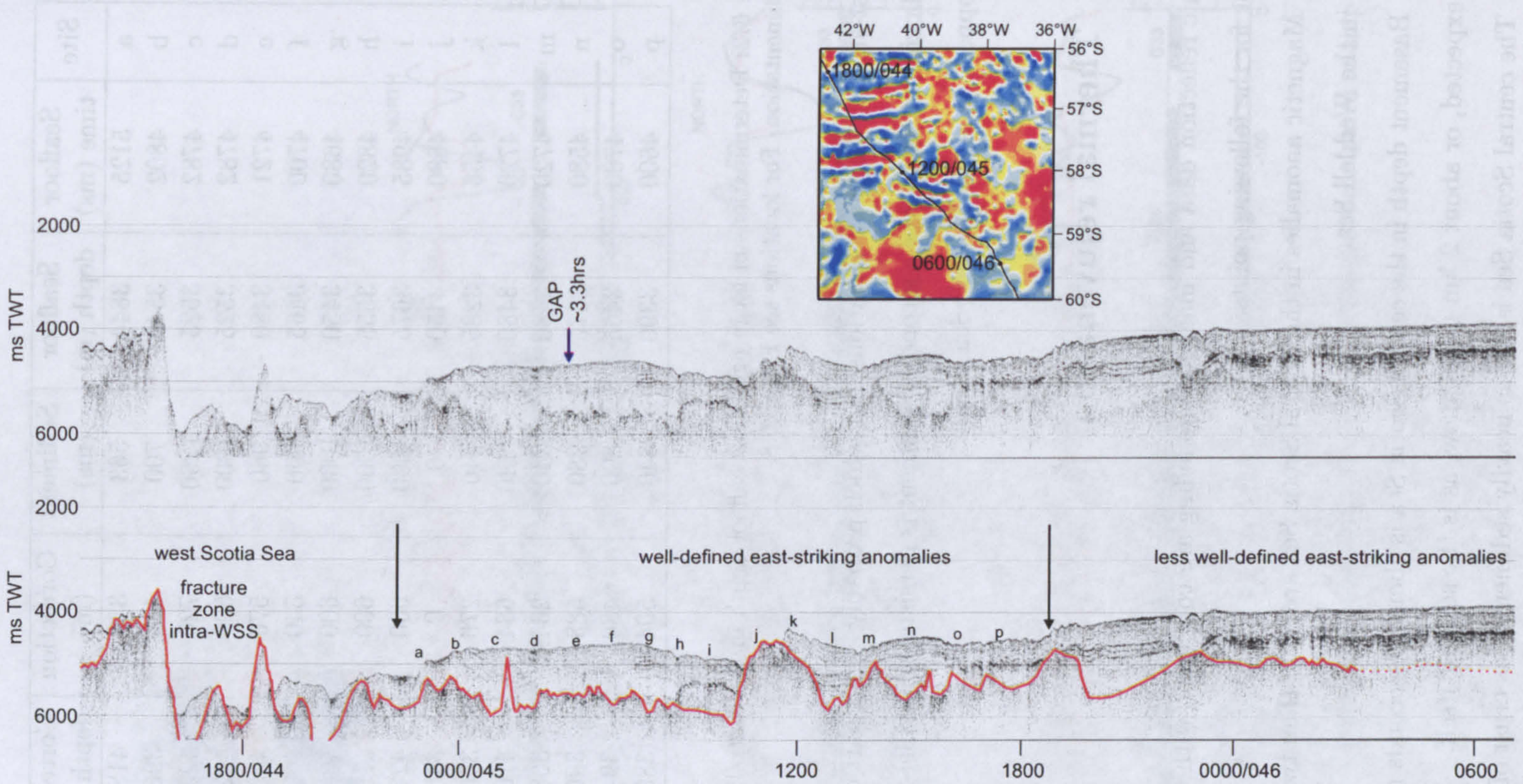

Figure 6.8: Single channel seismic reflection profile over the central Scotia Sea, British Antarctic Survey, 1988. The points of passage into and out of the region of prominent east-striking reversal anomalies are shown by black arrows. Data have been processed to remove long gaps, the position of one very long gap is shown. Automatic gain control and a bandpass filter have been applied to enhance the oceanic basement reflector below the sediments. Interpreted section (bottom) shows the basement reflector as a red line, a–p refer to the positions where basement age is determined (Table 6.2).

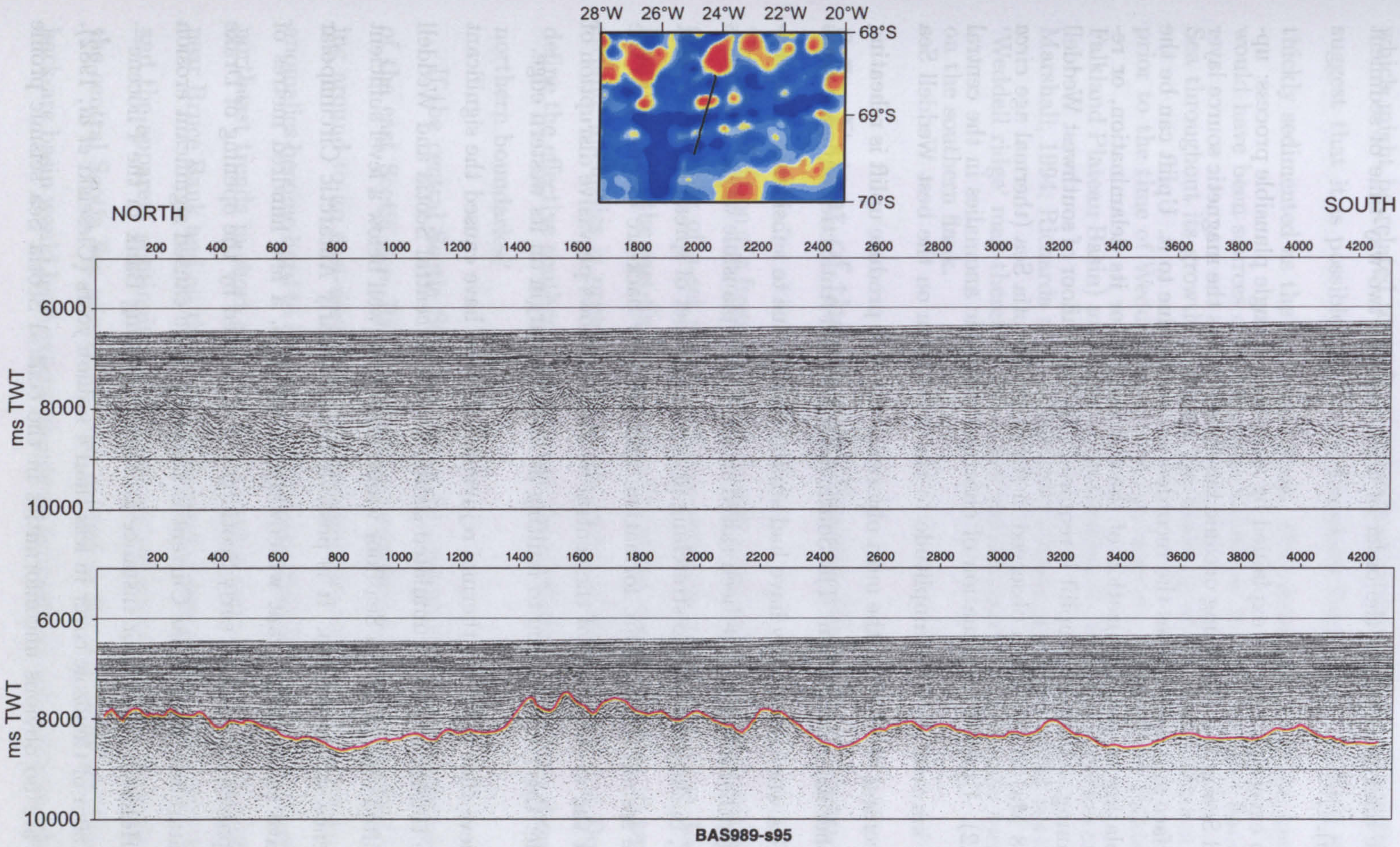

Figure 6.9: Single channel seismic reflection profile over a region of the Weddell Sea crossing 'anomaly T' of Livermore and Hunter (1996) (late Cretaceous), British Antarctic Survey, 1999. This line is perpendicular to spreading anomalies and shorter than the central Scotia Sea profile, approximating in length the section between points d and j in Figure 6.8. Automatic gain control and a bandpass filter have been applied to enhance the oceanic basement reflector below the sediments. Interpreted section (bottom) shows the basement reflector as a red line. Sediments in this section are 0.5–1 s thicker, on average, than those of the western part of the central Scotia Sea.

Weddell Sea, the discrepancy is of the order of 0.5–1 seconds two-way-time of sediment (about 0.5–1 km).

The first two exceptions can be explained by appeal to a single plausible process: uplift of the central Scotia Sea. Uplifting oceanic basement brings the magnetic source layer closer to the surface and so amplifies the recorded anomalies due to it. Uplift can be the result of underplating or serpentinization of the lithosphere, or its delamination, or reheating and thinning. About 2 km uplift is required to bring seafloor of southwest Weddell Sea age (150–118 Ma) to the depth observed in the central Scotia Sea (thermal age *circa* 19 Ma, Table 6.2). Upward continuation of observed magnetic anomalies in the central Scotia Sea by 2 km reduces their amplitude to the levels seen on the best Weddell Sea profiles. In the central Scotia Sea, the most obvious process to produce uplift is reheating and thinning—thermal rejuvenation. The South American and Antarctic conjugate areas of the Weddell Sea would originally have had similar depths due to subsidence. The central Scotia Sea geotherm could have been raised in one of two plausible ways. The first is crustal thinning, in the west, due to stretching prior to the onset of spreading in the west Scotia Sea. The second is island arc formation, and possibly back-arc extension to the east. I note that the western part of the central Scotia Sea shows pervasive disruption of the sediment pile: this could be due to faulting at a rifted margin on its western edge.

I do not believe that uplift by thermal rejuvenation could have caused the significant difference in the thicknesses of accumulated sediments in the central Scotia and Weddell Seas, as the uplifted central Scotia Sea floor would have been well below a level sufficient for it to experience strong erosion. It is possible that the early Antarctic Circumpolar Current may have caused significant winnowing of, perhaps, a few hundred metres of sediment, as it passed through an early Scotia gateway created by the opening of Drake Passage: the Antarctic Circumpolar Current is known to have caused significant erosion (Berggren and Hollister, 1977), for instance at Maurice Ewing Bank in the Pliocene—removing over 150m of Cenozoic cover in less than 4 million years (Cieselski *et al*, 1982). However, there are no obvious unconformities in the central Scotia Sea seismic profile

which might be related to such an episode of erosion. As an alternative explanation, I suggest that it is possible the South American flank of the Weddell Sea was never as thickly sedimented as the Antarctic flank. East Antarctica and the Antarctic Peninsula would have been sources of voluminous sediments to the Antarctic flank of the Weddell Sea throughout its growth, enabling the build up of the thick sediment pile seen. Even prior to the time of Weddell Sea break-up, however, much of the Falkland Plateau (the Falkland Plateau Basin) may have been significantly subsided (Lorenzo and Mutter, 1988; Marshall, 1994; Richards *et al*, 1996) and sedimentary influx to the northern flank of the 'Weddell ridge' may therefore have been significantly less, and more localised, than that on the southern flank.

6.7 Extent of the central Scotia Sea allochthon

The identification of a fragment of much older crust in the central Scotia Sea relies strongly on the presence of a set of east-striking magnetic anomalies there, having its western boundary with the east-flank C8 anomalies of the west Scotia Sea. A smaller set of east-striking anomalies is present just to the north of Bruce Bank and Dove Basin, which define the effective southern boundary of the allochthon. But what about its eastern and northern boundaries?

If the central Scotia Sea extends as far east as the westernmost reversal anomalies of the east Scotia Sea, its east-striking anomalies might be expected to be seen curving around to an east-northeasterly direction further east (Figure 6.4). Linear reversal anomalies become hard to identify east of the central Scotia Sea, but there is a hint of east-northeast trends in short anomalies to the east and north of the area of good anomalies near Bruce Bank and on the Bouguer anomaly relative high along 36.5°W. On this basis, and the apparent continuity of sedimentary reflectors through the region, I believe that the central Scotia Sea allochthon may extend as far east as 36°W. The Jane–Discovery back-arc basin would have extended only as far north as the northern edge of Bruce Bank

does, and the Bouguer anomaly relative high along 36.5°W could be representative of arc material constructed on a Mesozoic basement of central Scotia Sea crust, possibly with more sporadic expression as seamounts further north (Figure 6.1).

The present northern boundary to the central Scotia Sea spreading anomalies is the free-air gravity low immediately south of the South Georgia microcontinent. The west Scotia Sea reconstructions of Chapter 5 suggest that strike-slip deformation on the North Scotia Ridge was located within, or north of, South Georgia during most of its growth. Despite the 70 km offset between the northern and southern parts of the South Georgia microcontinent along 55°S with which differential amounts of opening of the west Scotia Sea have been accommodated, it seems that the northern boundary to the central Scotia Sea system is the South Georgia microcontinent and possibly the Shag Rocks block. The northern boundary would represent the conjugate passive margin to that in the Weddell Sea. In such an interpretation the free air anomaly low just south of South Georgia could represent thick sediments in a rift basin of late Jurassic age. One might expect to see tectonic inversion of originally-extensional features in it consistent with it having since been: (i) involved in the Rocas Verdes Basin inversion event, (ii) the locus of strike-slip deformation of the South Georgia microcontinent ($\sim$ 26–6 Ma) and, (iii) the locus of latter-day limited underthrusting of Scotia Sea floor beneath the microcontinent (post 6 Ma, Pelayo and Wiens (1989)). I know of no seismic reflection survey which shows the contents of the basin to test this prediction. Whatever the contents of the basin, this new interpretation of the central Scotia Sea and its northern margin represents a different, and new, opportunity to study the initial break-up of the Weddell Sea region, previous attempts at which have been hampered by sea ice cover in the Weddell Sea.

6.8 Mesozoic Reconstruction of the Weddell Sea

Assuming South Georgia and the central Scotia Sea together represent the conjugate passive margin and seafloor to the southwestern Weddell Sea, a reconstruction at closure of

the Weddell Sea is shown in Figure 6.10. South Georgia is situated in a gap in the reconstruction of Livermore and Hunter (1996) between the Falkland Plateau and the Dronning Maud Land–Berkner Island coast. The southeastern margin of the South Georgia microcontinental block extends the implied strike-slip boundary between Maurice Ewing Bank and Dronning Maud Land as far as the present-day bend in the coast at $\sim 30°$W, 72.5°S. This positioning is consistent with the provenance, from the southeast and southwest, of volcaniclastic turbidites of the Cumberland Bay Formation of South Georgia (Macdonald and Tanner, 1983; Macdonald *et al*, 1987). Furthermore I note the geological similarities between South Georgia and Maurice Ewing Bank: both exhibit a Phanerozoic sequence of Lower/Middle Jurassic to Cretaceous rocks followed by depositional hiatuses, suggesting a common Phanerozoic history.

The Rocas Verdes–Larsen Harbour Basin and proto-Weddell Sea

The reconstruction suggests that a long but not very wide Rocas Verdes–Larsen Harbour Basin could have existed at the time of onset of spreading in the southern Weddell Sea, which may have been near to 165 Ma if it opened initially as part of a South American–African–Antarctic plate circuit (Livermore and Hunter, 1996). Stretching associated with this basin may have given rise to the widespread 'Serie Tobifera' volcanism. The Rocas Verdes pseudo-ophiolites are almost continuous, but very thin across axis, through Tierra del Fuego. A similar body is present on the South Georgia microcontinent as a 'Larsen Harbour basin'. No intervening occurrences of pseudo-ophiolitic bodies are known, but the reconstruction suggests that they might be found on the northern Terror block, Pirie, Bruce and possibly Discovery bank blocks: in the hinterland of the reconstructed Patagonian batholith anomaly. More speculatively, I note that the Orion anomaly, a magnetic anomaly at the continent–ocean boundary in the southern Weddell Sea which has been interpreted as representative of break-up volcanism (Kristoffersen and Haugland, 1986; LaBrecque *et al*, 1986), continues the trend of the Patagonian batholith body, and may also mark a continuation of it in pre-165 Ma times, linking the Discovery Bank part of the body to that speculated at the southern margin of the South Georgia block.

The Larsen Harbour Complex is dated at 150 Ma by Mukasa and Dalziel (1996). This determination is an ^{40}Ar-^{39}Ar plateau date on a granite which cuts the complex, but which is cut by some of its dykes. The oldest identifiable seafloor spreading anomaly in the central Scotia Sea (from the model in Section 6.4) is M20 ($\sim$ 149 Ma). The ages are consistent with the Larsen Harbour Complex being representative of oceanic crust which was originally continuous with that in the central Scotia Sea. An implication of this is that the Larsen Harbour Complex does not represent the floor of a back-arc basin but instead the very earliest oceanic crust formed in separation of South America from East Antarctica. This is consistent with geochemical analyses of the complex which conclude the Larsen Harbour basin did not form in relation to a subduction zone but instead by the action of a Gulf of California-type propagating ridge (Alabaster and Storey, 1990).

Interpreted proto-Rocas Verdes Basin magmatism in Patagonia and Tierra del Fuego ('Serie Tobifera') is dated at 164 Ma by Mukasa and Dalziel (1996) whereas the Sarmiento Complex (basin floor) itself has been dated at 137–142 Ma (Stern *et al*, 1992). Assuming a simply-linked Larsen Harbour–Rocas Verdes Basin these dates imply that the basin may have propagated from southeast to northwest (Dalziel, 1992; Mukasa and Dalziel, 1996) and furthermore that the entire Rocas Verdes Basin was not a back-arc basin in the strict sense of forming in response to subduction dynamics. The alternative presented here, a propagating oceanic rift like the modern Gulf of California, is consistent with this idea of propagation as well. Such a simple picture is complicated however when considering how the basins might have evolved from an initial setting like that shown in the reconstruction. Specifically, why should the Larsen Harbour part of the basin have proceeded to more orthodox mid-oceanic spreading (whence it produced the central Scotia Sea) when the Rocas Verdes part certainly did not?

Inversion of the Rocas Verdes Basin in Tierra del Fuego is thought to have occurred at about 100 Ma based on a cooling age for the Beagle granite suite rocks in the Rocas Verdes Basin floor (Mukasa and Dalziel, 1996) and similar ages for uplift of the Larsen Harbour Complex (Macdonald *et al*, 1987). This occurs during a gradual change in

seafloor spreading in the Weddell Sea which culminates in a situation with almost a reversal of the earliest sense of opening, and coincides with global spreading rate changes. Inversion of the 'Larsen Harbour Basin', at least, and possibly the Rocas Verdes Basin, might therefore represent the response of a passive margin to changes in the direction of spreading in its ocean, rather than to collision of a volcanic island arc with a continental active margin.

6.9 Preservation of the allochthon

In Chapter 4 it was mentioned that the principal kinematic obstacle to dispersal of a central Scotia Sea allochthon is subduction at the ancestral Discovery–Jane trench. The history of subduction at the trench is not well known prior to its collision with the South American–Antarctic Ridge and shutdown. Its date of inception is simply not known.

Figure 6.11 is a sequence of reconstructions through the Mesozoic, made using the same set of reconstruction poles used for the flowlines in section 6.3 which shows the dispersal of the future central Scotia Sea out of the Weddell Sea. The possibility of internal deformation of the Antarctic Peninsula and its position relative to South America and East Antarctica is not well known at the early stages. The earliest motion of South American crust away from East Antarctica is directed northeast, and implies dextral strike-slip motion at the boundary between the Dronning Maud Land–Berkner Island Coast and Maurice Ewing Bank–South Georgia. This persists between roughly 165 Ma and 140 Ma. Later motion, until about 100 Ma, is predominantly north–south and creates the earliest-identifiable parts of the Weddell Sea and the central Scotia Sea. The position of the Antarctic Peninsula during this time is only partly known, using paleomagnetic poles, but it seems likely to have been present to the west of the region of crust created (summary in DiVenere *et al* (1996)). The mutual boundary may have been a passive margin or a strike-slip fault. The latest stage of motion is directed predominantly west-northwest (although changes have occurred) and continues to the present day. Its earliest stages

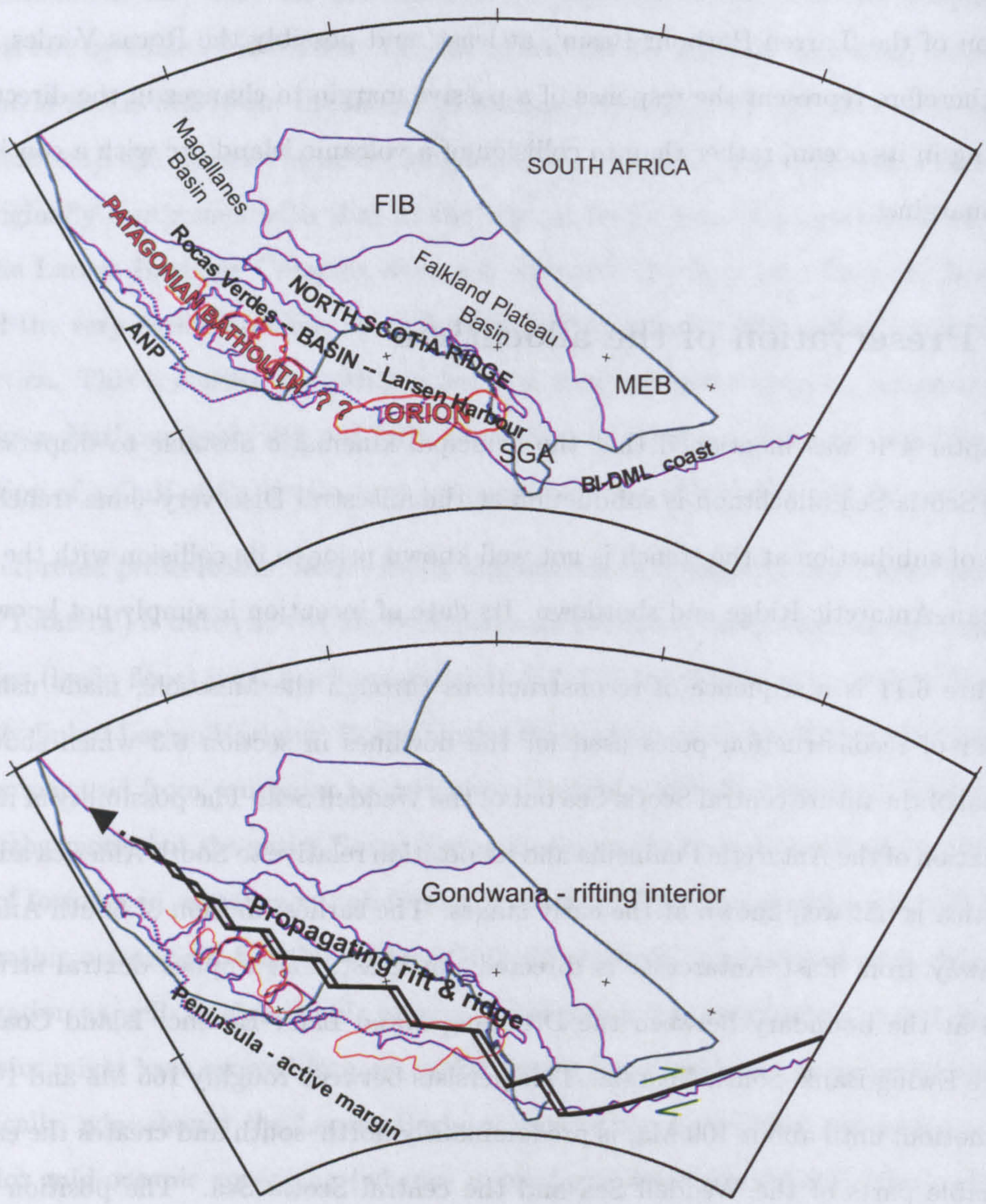

Figure 6.10: A reconstruction of the earliest stage in the growth of the Weddell Sea (165 Ma). The position of the Antarctic Peninsula (dotted blue line) is schematic only, based on the 175 Ma reconstruction in DiVenere *et al* (1996). Top: main features discussed in the text, FIB: Falkland Islands block, MEB: Maurice Ewing Bank, ANP: Antarctic Peninsula, SGA: South Georgia, BI–DML coast: Berkner Island–Dronning-Maud Land coast. Bottom: interpretation as a true ocean basin propagating into a back-arc region rather than a back-arc basin.

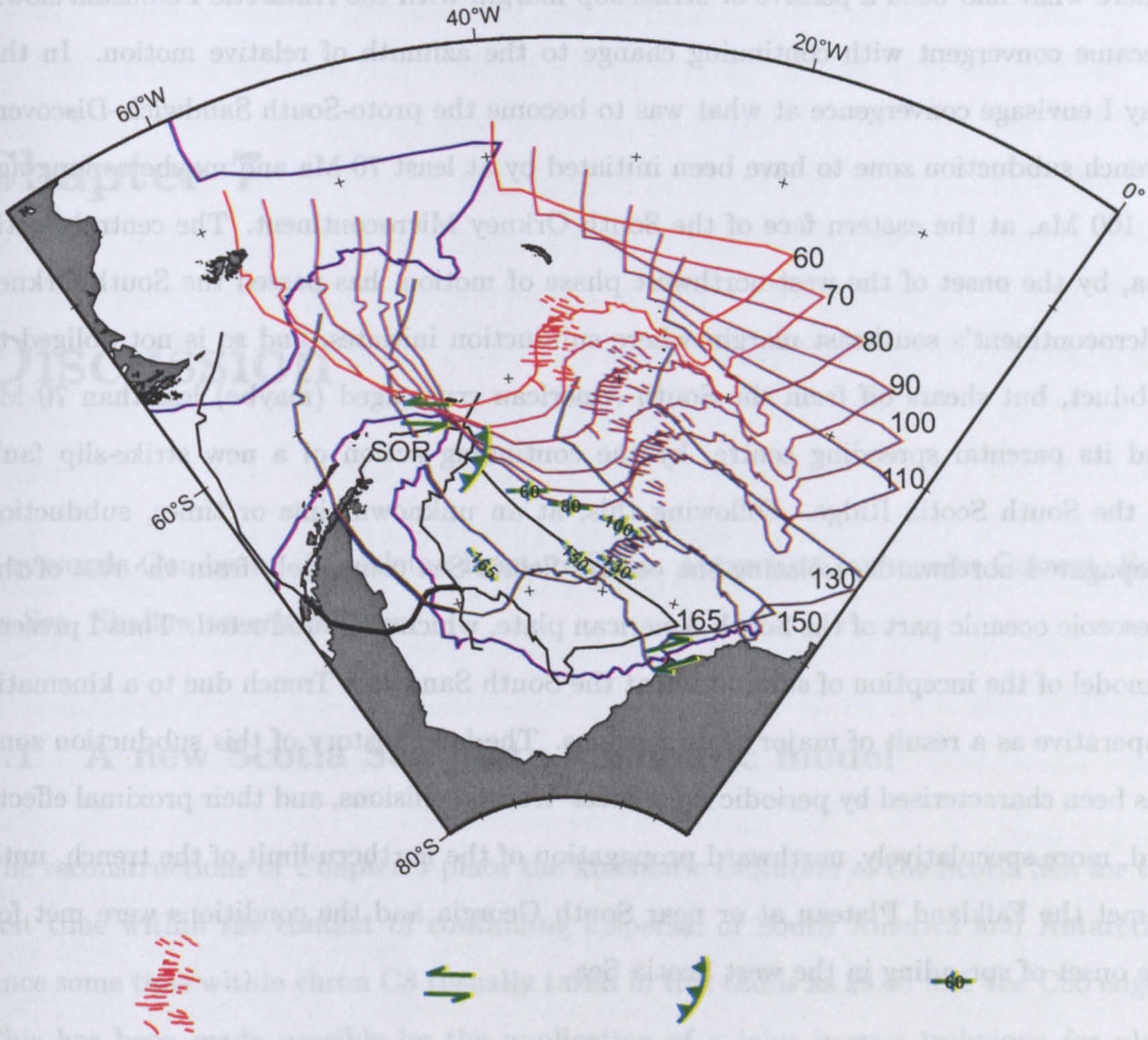

Figure 6.11: A sequence of reconstructions of the growth of the Weddell Sea through the Mesozoic, showing how the central Scotia Sea survived subduction at the proto-South Sandwich–Discovery Trench. Reconstructions made using the poles of Nankivell (1997a) and Livermore and Hunter (1996). SOR: South Orkney Microcontinent. Blue lines: present-day outlines of Antarctic Peninsula, South America and East Antarctica. Black outline: pre-Adare Trough spreading position of Antarctic Peninsula. Brown–red outlines: successively younger reconstructions of South America (ages in Ma, at northeast tip of Falkland Plateau). Thickened lines show overlap regions between South America and the Antarctic Peninsula, which ceases by 110Ma.

are a slow rotation of the Magallanes region about the South Orkney Microcontinent, where what had been a passive or strike-slip margin with the Antarctic Peninsula slowly became convergent with continuing change to the azimuth of relative motion. In this way I envisage convergence at what was to become the proto-South Sandwich–Discovery Trench subduction zone to have been initiated by at least 70 Ma and maybe as long ago as 100 Ma, at the eastern face of the South Orkney Microcontinent. The central Scotia Sea, by the onset of the west-northwest phase of motion, has passed the South Orkney Microcontinent's southeast margin where subduction initiates, and so is not obliged to subduct, but shears off from the South American crust aged (maybe) less than 70 Ma and its parental spreading centre, by the continuing action of a new strike-slip fault at the South Scotia Ridge. Following this, at an unknown time or times, subduction propagated northwards, isolating the central Scotia Sea completely from the rest of the Mesozoic oceanic part of the South American plate, which was subducted. Thus I present a model of the inception of subduction at the South Sandwich Trench due to a kinematic imperative as a result of major plate motions. The later history of this subduction zone has been characterised by periodic ridge-crest–trench collisions, and their proximal effects and, more speculatively, northward propagation of the northern limit of the trench, until it met the Falkland Plateau at or near South Georgia and the conditions were met for the onset of spreading in the west Scotia Sea.

Chapter 7

Discussion

Keywords Gondwana. Shackleton Fracture Zone. Antarctic Circumpolar Current. Scotia Sea. Shallow mantle outflow.

7.1 A new Scotia Sea plate kinematic model

The reconstructions of Chapter 5 place the kinematic evolution of the Scotia Sea for the first time within the context of continuing dispersal of South America and Antarctica since some time within chron C8 (usually taken in this thesis as 26.55 Ma; the C8o edge). This has been made possible by the application of a joint inverse technique for plate tectonic reconstruction of the west Scotia Sea, which has enabled interpretations to be made of its development as a small oceanic basin—opening in response to plate motions which were a close approximation to those between South America and East Antarctica between chrons C8 and C3a. The spreading phase of this opening has been the main tectonic event in the late Cenozoic evolution of the Scotia Sea, in the light of which it has been possible to postulate that minor basins in the region represent (i) failed rifts and oceanic precursors to this spreading (the west Scotia rift, Protector, Powell and Dove basins), and (ii) back-arc basins opening behind subduction zones to the east of its eastern

margin (Jane–Discovery basin and the east Scotia Sea).

In addition to the quantified reconstructions, more speculative reconstructions showing the development of deep-water parts of the Scotia Sea region from the latest Jurassic are presented. An explanation of this development as a special consequence of both the onset of subduction and of the capture of an oceanic crustal unit from the north flank of the ancestral South American–Antarctic Ridge (in effect simultaneously creating and fixing to the mantle a new plate with a passive margin opposing that at Tierra del Fuego) is put forward. This new plate later became dispersed as an allochthon by the opening of the west Scotia Sea. The allochthon hypothesis is attractive because it makes modelling the whole Scotia Sea as a reasonably simple plate tectonic system, rather than as a multi-phase back-arc basin, quite straightforward. In addition if the allochthon really does represent conjugate crust to the southwest Weddell Sea, it has important implications for studies of break-up in the Weddell Sea, and of Gondwana as a whole, as I have tried to suggest by simple means in Chapter 6. As such, this hypothesis regarding the central Scotia Sea is the most important tectonic result presented in this thesis.

Future work

The new view of Scotia Sea tectonics afforded by this work suggests a wide range of new studies might be fruitful. In particular, the allochthon hypothesis might be tested simply and effectively by dredging of exposed oceanic basement in the central Scotia Sea, or by deep-sea drilling. The history of subduction at the eastern margin of the Scotia Sea is critical to the capture, preservation, and dispersal of the hypothetical allochthon, yet little is known about it. There is no solid evidence supporting hypotheses regarding the initiation in space and time of this subduction, such as those presented in this thesis, or that given by Barker *et al* (1991). Neither is there any strong or complete evidence for the subsequent evolution of the subduction zone by its propagation or by ridge-crest–trench collision. The southeastern extremities of Jane Bank, to the south of the transtensional southern margin of Powell Basin, and the isolated seamounts south of South Georgia (Section 5.5) represent possible subduction-related features which have

not yet been investigated to these ends.

More briefly, kinematic explanations for the opening of the Protector, Dove and Powell Basins are presented for the first time here. If the Scotia Sea model is taken to be correct these basins represent an unusual situation where a region of continental crust had been experiencing more or less continuous extension over a period of at least 30 million years, as the tips of South America and the Antarctic Peninsula separated. Unfortunately the former two basins suffer with uncertainties in the determined ages of their floors. These difficulties might be overcome by sediment drilling or dredging to determine the ages of the basins' contents, either directly or via ties to seismic reflection images.

7.2 Tectonics of the Shackleton Fracture Zone

The Shackleton Fracture Zone has been an important issue throughout much of this thesis in considerations of the west Scotia Sea spreading system. Perhaps the most important difference between the reconstructions made here of that system, and all those which precede it, is the assumption that the the Shackleton Fracture Zone is not a reliable tectonic flowline for the opening of the west Scotia Sea. A close look at the Shackleton Fracture Zone shows that unlike the other tectonic flowlines picked, it does not consist of a simple linear trough. Figure 7.1 shows three representations of the Shackleton Fracture Zone. The top two are perspective views of an oblique Mercator projection of satellite free-air gravity and ships' bathymetry which show a compound ridge–trough feature and its, first order, *en echelon*, segmentation. The form of the Shackleton Fracture Zone is asymmetrical about the axis of the southern spreading segment in the west Scotia Sea, having both greater relief and elevation on the Elephant Island side than on the Tierra del Fuego side. This kind of segmentation, into transverse ridges rotated from the gross trend of the offset, is characteristic of transpressional offsets in the oceanic realm: the Clipperton (Pacific), Romanche (Atlantic), and Zabargad (Red Sea) transforms being examples (Marshak *et al*, 1992; Bonatti *et al*, 1994; Bonatti, 1996; Pockalny, 1997), in the latter

cases uplift appears to have been enough to have produced emergence. Oceanic transpression has also been shown for areas outside active offsets, at the Tiburon, Barracuda and Researcher ridges in the western equatorial Atlantic (Müller and Smith, 1993), where relative plate motions between South and North America and Africa and Eurasia, respectively, have been subtly different, leading to minor relative movements between North and South America. This situation is broadly similar to that envisaged for the ancient Shackleton Fracture Zone, where relative plate movements between the Phoenix, Magallanes and central Scotia plates have had only a minor cross-axial component. Transpression is the present condition on the Shackleton Fracture Zone (Pelayo and Wiens, 1989), and appears to have been so in the past (Maldonado *et al*, 2000; Figure 7.2).

The Shackleton Fracture Zone is also an important element in the considerations of the Antarctic Circumpolar Current and paleoclimate of Barker and Burrell (1977; 1982). These workers consider the bathymetric highs of the Shackleton Fracture Zone extending oceanward from Tierra del Fuego and from Elephant Island to represent continental crust which subsided slowly following the initial opening of the west Scotia Sea, remaining a significant barrier to deep-water passage (because of their overlap) until 23.5 ± 2.5 Ma. Burrell (1983) reports a dredge haul of 'quartz-rich cataclasite' from the flank of the Shackleton Fracture Zone (location unspecified) and suggests this may be supporting evidence for the continental nature of the ridges, having rejected the possibility of the haul containing glacial drop stones. However, 'continental' lithologies are known from other, undoubtedly oceanic, fracture zones (Honnorez *et al*, 1994), possibly representing pods entrained there since break-up, and are not representative of the bulk composition of the fracture zone. Furthermore, the ridges are shown in Figure 7.1 not always to be physically connected to the continental fragments of Tierra del Fuego and Elephant Island (although the latter is in bathymetric, but not free-air gravity, continuity). Finally an 'old' continental ridge at the Shackleton Fracture Zone might reasonably be expected to show a significant magnetic anomaly which is different to the surrounding pattern of oceanic polarity reversals. The bottom part of Figure 7.1 is a grid of total field anomalies over the

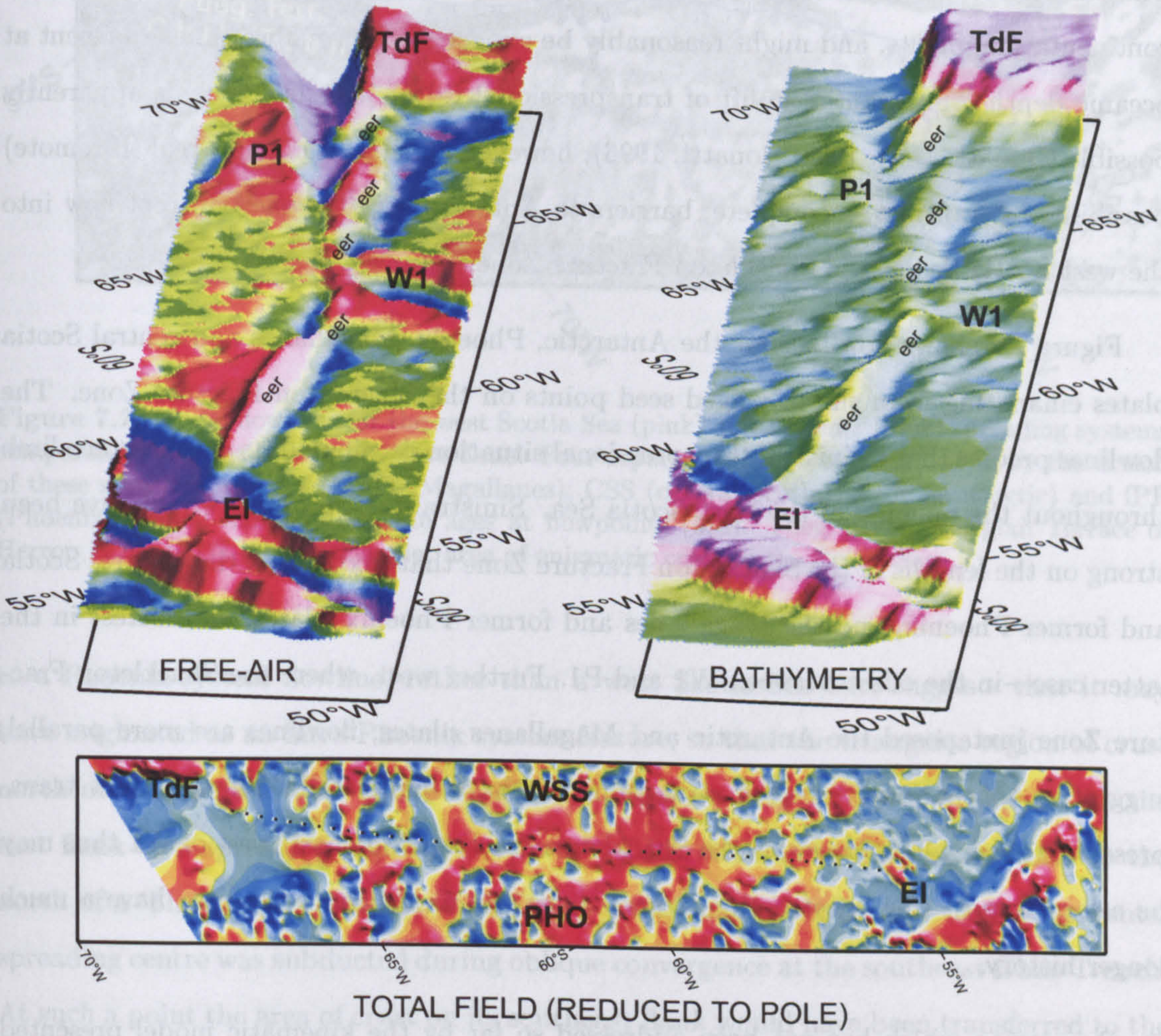

Figure 7.1: The Shackleton Fracture Zone in free-air gravity, bathymetry and total field anomaly (reduced to the pole). eer: *en echelon* ridge (label on north slope), EI: Elephant Island, TdF: Tierra del Fuego, W1: southern spreading segment in the west Scotia Sea (WSS), P1: northern spreading segment on the Phoenix Ridge, former Phoenix plate (PHO).

same area as the two perspective views above it, and shows clearly that the Shackleton Fracture Zone has very little magnetic expression of its own, and is only discernible by virtue of its offsets of the west Scotia Sea and Phoenix plate reversal anomalies. The elevated ridges, therefore, are most unlikely to represent, in their entirety, subsided continental fragments, and might reasonably be expected to have always been present at oceanic depths. Substantial uplift of transpressional ridges, to emergence, is apparently possible (Bonatti *et al*, 1994; Bonatti, 1996), however, so there remains a real (if remote) possibility of transient, incomplete, barriers to Antarctic Circumpolar Current flow into the west Scotia Sea at the Shackleton Fracture Zone.

Figure 7.2 shows flowlines for the Antarctic, Phoenix, Magallanes and central Scotia plates emanating from suitably-aged seed points on the Shackleton Fracture Zone. The flowlines predict that a sinistral transpressional situation dominated its southeastern limb throughout the opening of the west Scotia Sea. Sinistral transpression would have been strong on the lengths of the Shackleton Fracture Zone that juxtaposed the Central Scotia and former Phoenix, and the Magallanes and former Phoenix Plates, and fastest in the latter case—in the offset between W1 and P1. Further west, where the Shackleton Fracture Zone juxtaposed the Antarctic and Magallanes plates, flowlines are more parallel, suggesting that a purer sense of strike-slip may have dominated. The apparent transpressional ridge which expresses the Shackleton Fracture Zone northwest of W1 thus may be a largely post-C3a construction, whereas the one to the southeast may have a much longer history.

One region which has not been addressed so far by the kinematic model presented in this thesis is the triangular region to the north of the Shackleton Fracture Zone and northwest of Elephant Island (shown in Figure 7.2, in green). If this triangle formed by accretion at the West Scotia Ridge, as suggested by Lodolo *et al* (1998), then some explanation is needed for the lack of a western flank. Here I put forward an alternative view.

The closer gross similarity of the trend and curvature of the Shackleton Fracture Zone

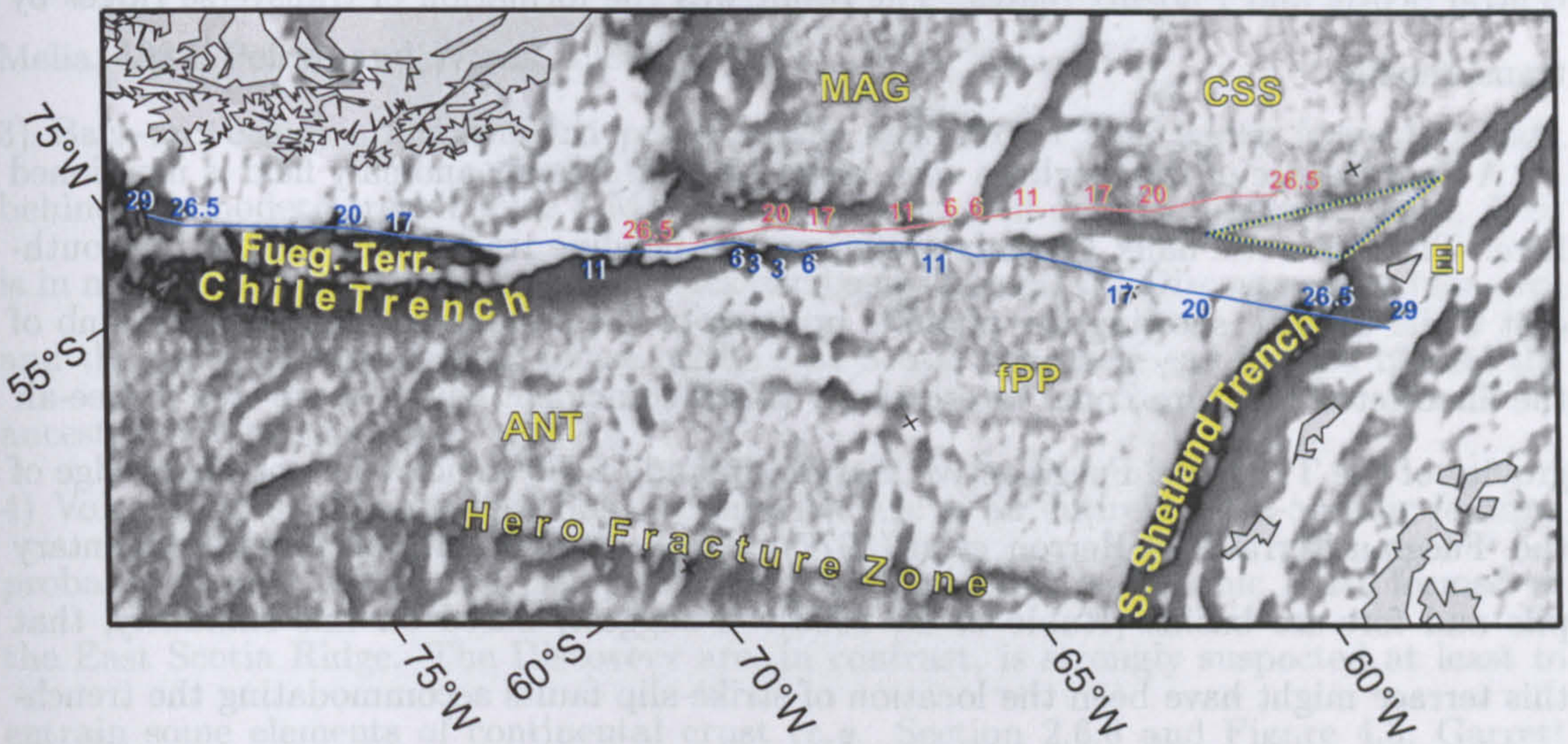

Figure 7.2: Model flowlines for the west Scotia Sea (pink) and Phoenix (blue) spreading systems compared to the Shackleton Fracture Zone. Four separate plates were accreted to by the action of these spreading centres: MAG (Magallanes); CSS (central Scotia); ANT (Antarctic) and fPP (Phoenix). Small numbers indicate ages at flowpoints (Ma). Fueg. Terr.: Fuegian Terrace of Herron *et al* (1977). Green triangle: area of enigmatic crust in the Scotia Sea.

to a Phoenix-system flowline, rather than a west Scotia Sea one, suggests that it may have originated as an intra-Phoenix system feature, so that the triangular region of crust north of the South Scotia Ridge–Shackleton Fracture Zone intersection formed on the east flank of a spreading segment northwest of P1, within the Phoenix system, to the north of a 'Shackleton transform fault'. It is a reasonable assumption that the parental spreading centre was subducted during oblique convergence at the southeast Chile Trench. At such a point the area of crust on its southeast flank would have been transferred to the Antarctic plate, or possibly the central Scotia plate, but in either case the net result would be the cessation of subduction at the South Shetland Trench beneath Elephant Island, as the central Scotia plate was kinematically similar to the Antarctic plate. Continuing relative motion between the Antarctic and Phoenix plates would have become focused on the southwestern flank of the Shackleton Fracture Zone rather than its (now subducted) parental transform fault. Relative movement on its northeastern flank was between the

central Scotia and Phoenix plates. The result was the formation of transverse ridges by transpression.

A final feature of the flowlines with respect to the free-air anomaly field is mentioned here. The Antarctic-flank Phoenix-system model flowline tracks back behind the south-east Chile Trench, showing the possible position of the subducted northwestern limb of the Shackleton Fracture Zone. Interestingly this is coincident with a sharp step in free-air gravity of the Tierra del Fuego active margin, inland of the trench (the northeast edge of the 'Fuegian Terrace' of Herron *et al* (1977)) which bears a thick accreted sedimentary pile and fore-arc basins (Rubio *et al*, 2000). I suggest, based on this similarity, that this terrace might have been the location of strike-slip faults accommodating the trench-parallel component of the very oblique convergence at this part of the Chile Trench during the time when the Phoenix Ridge was active. Such an interpretation is given as one of two alternative views of the back wall of the fore-arc basin on the terrace by Rubio *et al* (2000), based on seismic and gravity evidence. The trench-normal component would have been very much smaller and characterised by very slow subduction or convergence within the sediment-filled trough to the south of the terrace.

7.3 Pacific–Atlantic mantle outflow

The modern South Sandwich Trench shows a number of differences from its predecessor, which I have been referring to as the proto-South Sandwich–Discovery Trench:

1) Planform. The reconstructions of Chapter 5 show the new subduction zone to be strongly arcuate, as opposed to the more linear older trench parallel to the Jane and Discovery Banks, and the 'Endurance Collision Zone' to its southwest.

2) Rollback. The new model for the opening of the west Scotia Sea requires that rollback of the old trench was rather slow as it was responsible for the creation of 150–200 km more crust at the West Scotia Ridge than at the South American–Antarctic Ridge—over the period C8–C3a (about 20 million years) this rollback would be of the order 10 mma^{-1},

which is less than one fifth of the rate of rollback of the modern trench (Carlson and Melia, 1984; Pelayo and Wiens, 1989).

3) Back-arc basins. The modern phase of the east Scotia Sea, which formed quickly behind the modern trench since 8 Ma, is a large, very well-defined, back-arc basin. This is in marked contrast to the narrower back-arc basins behind the Discovery and Jane arcs and the early, slow-spreading, phase of the east Scotia Sea itself—all formed behind the ancestral subduction zone.

4) Volcanic arcs. The modern South Sandwich Arc is an entirely intra-oceanic feature, probably formed within the last 4 million years and built on oceanic crust formed at the East Scotia Ridge. The Discovery arc, in contrast, is strongly suspected at least to entrain some elements of continental crust (*e.g.* Section 2.6.6 and Figure 4.3, Garrett *et al* (1986); Hamilton (1989)), and may even be built on continental basement.

The transition from the old subduction regime to the new may have begun in the kinematic changes which happened at chron C6 ($\sim$ 20 Ma), as outlined in Chapters 3, 4 and 5. At this time the first signs of back-arc spreading to the north of Discovery Bank are seen, apparently at the expense of the spreading rate at the West Scotia Ridge. But why the reorganisation, especially why the counter-intuitive increase in the rate of trench rollback that occurred later? A very speculative reasoning can be related to the possibility of asthenospheric outflow through the Scotia Sea, from the sub-Pacific asthenosphere to the sub-Atlantic. This outflow has been related to the shrinking of the Pacific basin and simultaneous growth of the Atlantic basin by Alvarez (1982). In this hypothesis the oceanic asthenosphere, which occurs at very shallow depths, is obliged not to flow beneath thick (maybe 600 km deep) continental lithospheric 'keels' and/or the subducted slab 'curtains' at their margins, but takes place instead around their edges through shallow mantle gateways. Such gateways, allowing the shrinking sub-Pacific asthenosphere to augment the growing sub-Atlantic asthenosphere, are present beneath the largely oceanic Caribbean and Scotia seas. A test of this hypothesis, using shear-wave splitting results to demonstrate seismic anisotropy in aligned mantle minerals, by Russo and Silver (1994)

is consistent with asthenospheric flow parallel to the subducted slab at the Chile Trench, and with an eastward bend in this flow north of Venezuela, possibly indicating a shallow mantle outflow beneath the Caribbean plate, as predicted. Perhaps due to a lack of suitably-placed seismic observatories, no similar result is available for the Scotia Sea. The results of Russo and Silver (1994) do not ubiquitously show seismic anisotropy and as such, also, are by no means unequivocal. So shallow mantle outflow in the Scotia Sea remains an interesting, but unproved, hypothesis.

Accepting the mantle return flow hypothesis, however, provides a reason for the unexpected increase in the rate of trench rollback at the eastern margin of the modern Scotia Sea with respect to that in earlier times. With the possibility that the trench tip propagated northward from an initiation south of the South Orkney Microcontinent, (as suggested by the northward propagation of the onset of spreading at the West Scotia Ridge), and with ongoing descent of the slab, it is possible that, at some stage—maybe near chron C6, the subducted slab had reached a situation where it entirely closed off the eastern end of the oceanic Scotia Sea to shallow outflow. At the northern tip of the subduction zone the slab 'curtain' was juxtaposed with thickened continental lithosphere of the Falkland Plateau, and at its southern end it was juxtaposed with the thickened continental lithosphere of the Antarctic Peninsula at the South Orkney Microcontinent. The slab at this point was blocking a hydrostatic gradient between the Pacific and Atlantic asthenosphere, and could have been compelled to move, like a sail, within it. I note that the rate of rollback of the modern South Sandwich Trench (~ 55 mma^{-1}) is close to the calculated rate of asthenospheric outflow (~ 40 mma^{-1}) through the gateways postulated by Alvarez (1982). The faster rollback of the new trench is consistent with the change in back-arc basin character from small confined basins to a large, open ocean, basin. Drag on the northern and southern edges of this 'sail', where it is juxtaposed with thickened continental lithosphere, could explain the strongly-arcuate shape of the modern trench. What is not explained by such speculation, however, is why trench rollback might still be so fast at the modern day, when apparently the slab should no longer be blocking the

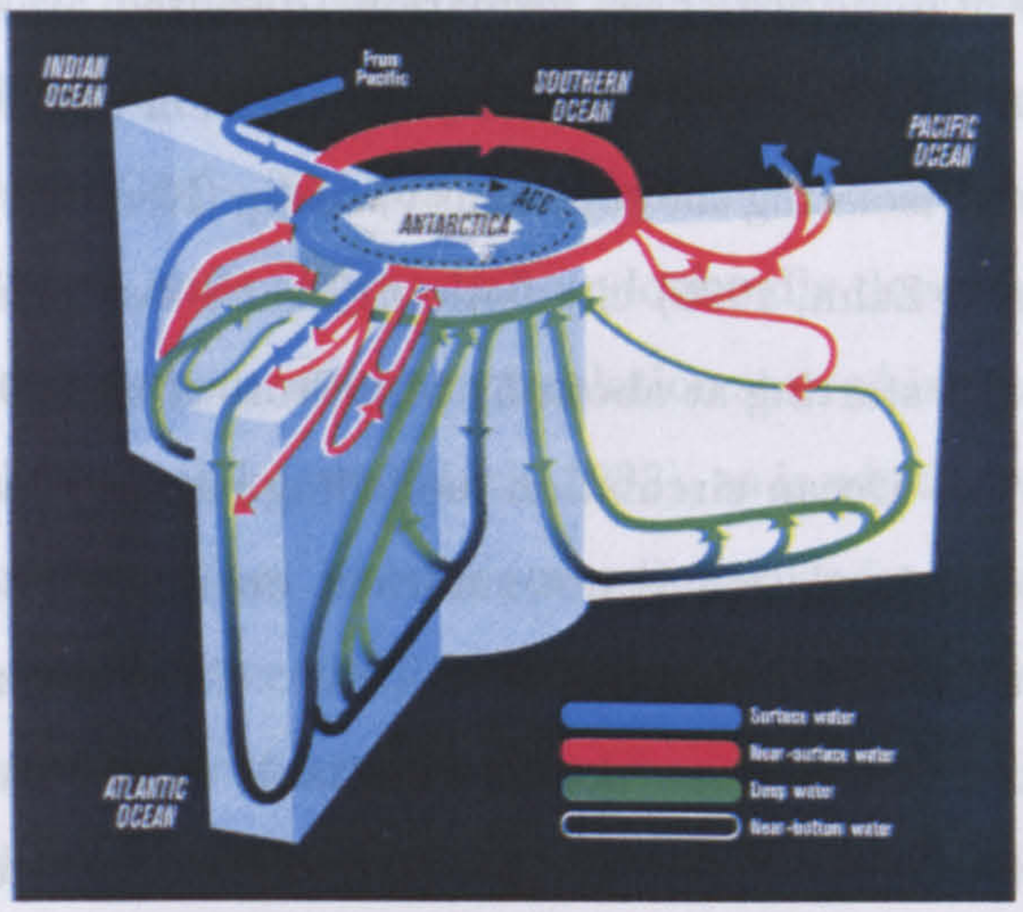

Figure 7.3: World ocean circulation showing the central importance of the Antarctic Circumpolar Current as a link between deep waters of the meridional oceans. From Cromwell (20 May, 2000).

'Scotia gateway': new paths having developed to the north of the east and west Scotia Seas by their opening.

7.4 Paleoclimatic implications

The Antarctic Circumpolar Current is the dominant feature of Southern Ocean circulation and the largest current system in the world ocean. It transports 100–140 $\times 10^6 \mathrm{m}^3/\mathrm{s}$ of sea water in the west–east direction, and passes through the axial region of the west Scotia Sea (Grose *et al*, 1995; Orsi *et al*, 1995), exiting via deep water gaps in the North Scotia Ridge. It is of great importance in ocean circulation because it forms the sole substantial link between the deep meridional oceans (Figure 7.3), and thus is the primary conduit for chemical and biological admixture between them. Nutrient-rich water upwelling at the Antarctic Convergence (the current's northern front) is the principal seat of production of biogenic silica in the world ocean.

It has been suggested that the Antarctic Circumpolar Current was solely responsible

for the inception of Antarctic ice sheet formation (disputed by some workers to have happened over the Eocene–Oligocene boundary (Shackleton and Kennett, 1975; Zachos *et al*, 1992)) by thermally isolating the continent via deep (Kennett, 1977) or intermediate water (Diester-Haass and Zahn, 1996) circulation. That substantial cooling did occur is well established, probably starting at about 53 Ma (Stott *et al*, 1990; Stott and Kennett, 1990; Zachos *et al*, 1994). Ocean circulation modelling results however suggest that the inception of circumpolar circulation is not sufficient on its own to achieve the cooling effect needed for glaciation (Mikolajewicz *et al*, 1993). The same modelling results also suggest that circumpolar currents are not an inevitable consequence of the creation of polar seaways, but develop instead if equatorial circulation is restricted, and thermohaline circulation develops (Warren, 1983; Gordon, 1986). However it started, the Antarctic Circumpolar Current and thermohaline circulation are both intimately linked with the evolution of the glacial pattern of the later-Cenozoic Earth (Berggren and Hollister, 1977).

The current itself is manifest in the entire water column and is strongly affected by seafloor topography which has been linked to the banded structure of the current's mass (Gordon *et al*, 1978; Hofmann, 1985; Rattray Jr, 1985; Nowlin and Klinck, 1986). The post-40 Ma pattern of global circulation is characterised by strong currents at the seafloor, a change from the preceding situation where tranquil, warm bottom waters saw widespread deposition (Berggren and Hollister, 1977). In the Scotia Sea the Antarctic Circumpolar Current is strong at the seafloor, sometimes strong enough to cause significant erosion (Cieselski *et al*, 1982). Deposition occurs only locally by interactions with seafloor topography, typically forming large 'mudwaves' (Barker and Burrell, 1977; Howe *et al*, 1998; Pudsey and Howe, 1998). A speculative link between ridge crest collisions at the 'Discovery Trench' and acceleration of the Antarctic Circumpolar Current is suggested by Rack (1993).

A necessary prerequisite to the inception of the Antarctic Circumpolar Current is an ocean pathway for it to flow within. True Antarctic Circumpolar Current flow includes near-bottom water and so requires the pathway to be in seaways of oceanic depths. The

final two barriers to such a seaway were south of Australia at Tasmania, and the west Scotia Sea. A Tasmanian gateway was established by 40 Ma (Lawver *et al*, 1992), with the west Scotia Sea opening at C8 ($\sim$ 26.5 Ma) long considered to be the final barrier (Barker and Burrell, 1977; 1982). A wide seaway had undoubtedly developed by 20 Ma (Lawver *et al*, 1992) but whether, or when, vigorous circulation started in the aftermath of opening of the west Scotia Sea is not well known (Rack, 1993), as is whether this was preceded by a less-vigorous mid-water circulation. Shorter spreading episodes in the time between 60 Ma and 25 Ma, in the Protector, Dove and Powell Basins have been hypothesised and tested in Chapter 4, and shown in reconstructions in Chapter 5. In the case of the Protector and Dove basins the hypotheses are very vulnerable ones. Furthermore, whether these basins, being so small, and almost inevitably therefore confined, could have been available as conduits for a precursor circumpolar current is open to question, but the possibility remains that a shallow or medium-depth Drake Passage seaway could have existed prior to 26.55 Ma.

The possibility of the existence of such a seaway is not a new idea: Lawver and Gahagan (1998) suggest that spreading in Powell Basin might have provided opportunity for current flow since about 35 Ma. I note from the reconstructions of Chapter 5 that the presence of an active strike-slip northern margin to this basin, which may also have had a compressional component, could have presented a transient barrier to passage through the basin from west to east. Further north however, subsided Terror, Pirie and Bruce Bank bodies may have existed since as long ago as the Middle Eocene ($\sim$ 50 Ma), allowing any current body passage through to the central Scotia Sea allochthon and beyond. Alongside the uncertainty regarding the age of subsidence of these blocks, which results from uncertainty in the age of Protector and Dove basins, there is similar uncertainty regarding the width of any mid-water depth gap at the northwestern South Scotia Ridge, north of Elephant Island. This uncertainty comes directly from the uncertainties in the reconstruction poles for East Antarctica–West Antarctica (Cande *et al*, 2000), in those for South America–Antarctica (Nankivell, 1997a) and from uncertainty in the relative

movement between the Magallanes and South American plates prior to C8 (Section 5.8). Within all this uncertainty, it is possible that a gap may have existed for current flow into the future west Scotia Sea, if it existed as subsided continental crust as suggested in Chapter 5. A final unknown is the possibility of outward flow, either across the Falkland Plateau or directly eastwards. The existence or otherwise, and extent, of subduction to the east of the central Scotia plate and its potential to place volcanic island arc material as a barrier to eastward progress of any current that had entered the region is not well known. Added to all this the uncertainty regarding the timing of the onset of thermohaline circulation means that very little can be said beyond that it is possible that a mid-water seaway could have existed since as long ago perhaps as 50 Ma. I note that this date is similar to that put forward by Stott *et al* (1990); Stott and Kennett (1990) and Zachos *et al* (1994) for the onset of cooling leading to the glaciation of Antarctica.

Appendix A

Inversion technique of Nankivell (1997a)

A.1 Joint inversion technique of Nankivell (1997a)

In this appendix further description of Nankivell's (1997) joint inversion technique is given to augment what was presented in Chapter 3. For a full treatment, however, the reader is referred to Nankivell (1997a) and Nankivell (1997b).

A.1.1 Rotations and spherical geometry

Notation

A 3-vector is described by its three components. Throughout this thesis a 3-vector has been given as a lower-case bold character so that

$$\mathbf{x} = \begin{bmatrix} x_1 \\ x_2 \\ x_3 \end{bmatrix}. \tag{A.1}$$

A 3×3 matrix is denoted by an upper-case bold character so that

$$\mathbf{A} = \begin{bmatrix} A_{11} & A_{12} & A_{13} \\ A_{21} & A_{22} & A_{23} \\ A_{31} & A_{32} & A_{33} \end{bmatrix}. \tag{A.2}$$

Coordinate system

One use of 3-vectors is in a Cartesian coordinate system for positions on spheres. The familiar latitude-longitude system describes the position of a point on a sphere with respect to a grid wrapped around it. A 3-vector describes the position of the same point with respect to the centre of the sphere, by use of three axes originating at it. A point, $\mathbf{p}$, at latitude, longitude (λ, ϕ) is given by the 3-vector

$$\mathbf{p} = \begin{bmatrix} p_1 \\ p_2 \\ p_3 \end{bmatrix} = \begin{bmatrix} \cos(\lambda)\cos(\phi) \\ \cos(\lambda)\sin(\phi) \\ \sin(\phi) \end{bmatrix}, \tag{A.3}$$

and

$$\lambda = \sin^{-1}(p_3), \qquad \phi = \tan^{-1}\left(\frac{p_2}{p_1}\right). \tag{A.4}$$

Vector products

The dot product of two vectors, $\mathbf{a}$ and $\mathbf{b}$ is defined as

$$\mathbf{a}.\mathbf{b} = a_i b_i = |\mathbf{a}||\mathbf{b}|\cos(\theta), \tag{A.5}$$

where θ is the angle between the vectors. When the vectors are unit vectors on a sphere, the dot product can be used to yield the distance, along a great circle, between the points they describe.

The cross product of two vectors is

$$\mathbf{c} = \mathbf{a} \wedge \mathbf{b} = \begin{bmatrix} a_2 b_3 - a_3 b_2 \\ a_3 b_1 - a_1 b_3 \\ a_1 b_2 - a_2 b_1 \end{bmatrix}, \tag{A.6}$$

and its magnitude

$$|\mathbf{c}| = |\mathbf{a}||\mathbf{b}|\sin(\theta). \tag{A.7}$$

Now **c** is perpendicular to both **a** and **b**, forming a right-handed set, so that (with unit vectors on a sphere) the cross product can be used to find a pole to the great circle in whose plane both **a** and **b** reside.

Rotations on a sphere

The method of rotation used in this thesis, and in that of Nankivell (1997a), uses Euler poles. The rotation pole is a point on the sphere which is joined to the centre of the sphere to form an axis about which a rotation of a given number of degrees occurs. The rotation can be described using a 3×3 matrix operating on a 3-vector. A rotation, which is positive in a right-handed sense (*i.e.* anticlockwise), of θ degrees about an axis defined by point **p** is given by

$$\mathbf{R} = \begin{bmatrix} p_1p_1(1-\cos(\theta)) + \cos(\theta) & p_1p_2(1-\cos(\theta)) - p_3\sin(\theta) & p_1p_3(1-\cos(\theta)) + p_2\sin(\theta) \\ p_2p_1(1-\cos(\theta)) + p_3\sin(\theta) & p_2p_2(1-\cos(\theta)) + \cos(\theta) & p_2p_3(1-\cos(\theta)) - p_1\sin(\theta) \\ p_3p_1(1-\cos(\theta)) - p_2\sin(\theta) & p_3p_2(1-\cos(\theta)) + p_1\sin(\theta) & p_3p_3(1-\cos(\theta)) + \cos(\theta) \end{bmatrix} \tag{A.8}$$

This can be derived from three elementary rotation matrices **A**, **B** and **E** which are rotations for λ, ϕ and θ so that $\mathbf{R} = (\mathbf{BA})^\top \mathbf{E}(\mathbf{BA})$ (Shaw, 1987).

Rotating point **x** by $(\mathbf{p}, \theta)$ or (λ, ϕ, θ) to point **y** is given by

$$\mathbf{y} = \mathbf{Rx}. \tag{A.9}$$

Summation

For summation of rotations, that is to say, rotating **x** about **R** to **y** and then about **S** to **z**:

$$\begin{aligned} \mathbf{z} &= \mathbf{Sy} \\ &= \mathbf{S(Rx)} \\ &= \mathbf{(SR)x} \\ &= \mathbf{Tx}, \end{aligned} \tag{A.10}$$

where $\mathbf{T} = \mathbf{SR}$ is a single matrix to rotate **x** to **z**, not necessarily via **y**.

A.1.2 Partial derivatives

The inversion method takes partial derivatives of each of the residuals with respect to small alterations, or perturbations, to the Euler pole parameters (λ,ϕ,θ).

For magnetic isochron residuals, rotation of pick **d** about stage pole **S** to point **r** is given by

$$\mathbf{r} = \mathbf{S}\mathbf{d}. \tag{A.11}$$

The target great circle's pole, **g**, is used to define the misfit: the angular displacement of **r** from **g**, minus ninety degrees:

$$\varepsilon = \cos^{-1}(\mathbf{r}.\mathbf{g}) - \frac{\pi}{2}. \tag{A.12}$$

Given the derivative of $\cos^{-1}$ and differentiating A.12, applying the chain rule, we have

$$\frac{\partial \varepsilon}{\partial p^\gamma} = \left(\frac{-1}{1-(\mathbf{r}.\mathbf{g})^2}\right)\frac{\partial(\mathbf{r}.\mathbf{g})}{\partial p^\gamma}. \tag{A.13}$$

Since **g** is constant, and given (from A.11) that

$$\frac{\partial \mathbf{r}}{\partial p^\gamma} = \left[\frac{\partial \mathbf{S}}{\partial p^\gamma}\right]\mathbf{d}, \tag{A.14}$$

then

$$\frac{\partial \varepsilon}{\partial p^\gamma} = \left(\frac{-1}{1-(\mathbf{r}.\mathbf{g})^2}\right)\mathbf{g}.\left[\frac{\partial \mathbf{S}}{\partial p^\gamma}\right]\mathbf{d}. \tag{A.15}$$

The determination of partial derivatives of the type $\frac{\partial \mathbf{S}}{\partial p^\gamma}$ is given in Appendix A of Nankivell (1997a).

Fracture zone residuals are measured great circle displacements from the flowline, grown out from a zero-age seed, $\mathbf{f}_0$. The finite rotation for chron τ is $\mathbf{F}^\tau(\lambda^\tau, \phi^\tau, \theta^\tau)$, and the flowpoint on the rotating plate at chron τ is

$$\mathbf{f}_\tau = \mathbf{F}^{\frac{\tau}{2}}\mathbf{f}_0, \text{ or} \tag{A.16}$$

$$\mathbf{f}_\tau = \mathbf{F}^{-\frac{\tau}{2}}\mathbf{f}_0, \tag{A.17}$$

depending on which is the reference plate and where $\mathbf{F}^{\frac{\tau}{2}}$ is a rotation of $(\lambda^\tau, \phi^\tau, \frac{\theta^\tau}{2})$ and $\mathbf{F}^{-\frac{\tau}{2}}$ is a rotation of $(\lambda^\tau, \phi^\tau, \frac{-\theta^\tau}{2})$.

With flowpoints and finite poles thus constructed a stage pole $\mathbf{S}^{ab}$ describing motion between flowpoints at chrons 'a' and 'b' is given by

$$\mathbf{S}^{ab} = \mathbf{F}^{\frac{b}{2}}\mathbf{F}^{-\frac{a}{2}} \tag{A.18}$$

such that

$$\mathbf{f}_b = \mathbf{F}^{\frac{b}{2}}\mathbf{f}_0 = \mathbf{F}^{\frac{b}{2}}\mathbf{F}^{-\frac{a}{2}}\mathbf{f}_a = \mathbf{S}^{ab}\mathbf{f}_a. \tag{A.19}$$

$\mathbf{S}^{ab}$ can provide the stage pole vector $\mathbf{s}$, and the flowline between $\mathbf{f}_a$ and $\mathbf{f}_b$ is a constant angle θ from $\mathbf{s}$ so that

$$\cos^{-1}(\mathbf{p}.\mathbf{s}) = \cos^{-1}(\mathbf{f}_a.\mathbf{s}) = \cos^{-1}(\mathbf{f}_b.\mathbf{s}) = \theta. \tag{A.20}$$

The residual for pick $\mathbf{d}$, the angular distance between a small circle containing $\mathbf{d}$ and the flowline segment itself is

$$\begin{aligned} \varepsilon &= \cos^{-1}(\mathbf{f}_a.\mathbf{s}) - \cos^{-1}(\mathbf{d}.\mathbf{s}) \\ &= \cos^{-1}(\mathbf{f}_b.\mathbf{s}) - \cos^{-1}(\mathbf{d}.\mathbf{s}). \end{aligned} \tag{A.21}$$

Given the derivative of $\cos^{-1}$ the partial derivative of ε for a perturbation to the pole parameter p^γ is:

$$\begin{aligned} \frac{\partial\varepsilon}{\partial p^\gamma} &= \left(\frac{-1}{1-(\mathbf{f}_a.\mathbf{s})^2}\right)\frac{\partial(\mathbf{f}_a.\mathbf{s})}{\partial p^\gamma} - \left(\frac{-1}{1-(\mathbf{d}.\mathbf{s})^2}\right)\frac{\partial(\mathbf{d}.\mathbf{s})}{\partial p^\gamma} \\ &= \left(\frac{-1}{1-(\mathbf{f}_b.\mathbf{s})^2}\right)\frac{\partial(\mathbf{f}_b.\mathbf{s})}{\partial p^\gamma} - \left(\frac{-1}{1-(\mathbf{d}.\mathbf{s})^2}\right)\frac{\partial(\mathbf{d}.\mathbf{s})}{\partial p^\gamma}. \end{aligned} \tag{A.22}$$

Parameters of finite pole $\mathbf{F}^a$ do not affect point $\mathbf{f}_b$, and vice versa, so

$$\frac{\partial\varepsilon}{\partial p^\gamma} = \begin{cases} \left(\frac{-1}{1-(\mathbf{f}_a.\mathbf{s})^2}\right)\mathbf{f}_a\left[\frac{\partial\mathbf{s}}{\partial p^\gamma}\right] - \left(\frac{-1}{1-(\mathbf{d}.\mathbf{s})^2}\right)\mathbf{d}.\left[\frac{\partial\mathbf{s}}{\partial p^\gamma}\right] & p^\gamma \in \{\lambda^b, \phi^b, \theta^b\} \\ \left(\frac{-1}{1-(\mathbf{f}_b.\mathbf{s})^2}\right)\mathbf{f}_b\left[\frac{\partial\mathbf{s}}{\partial p^\gamma}\right] - \left(\frac{-1}{1-(\mathbf{d}.\mathbf{s})^2}\right)\mathbf{d}.\left[\frac{\partial\mathbf{s}}{\partial p^\gamma}\right] & p^\gamma \in \{\lambda^a, \phi^a, \theta^a\}. \end{cases} \tag{A.23}$$

The partial derivative of a stage pole vector with respect to a pole-parameter perturbation, of the type $\frac{\partial\mathbf{s}}{\partial p^\gamma}$, is given in Appendix A of Nankivell (1997a).

Transform fault residuals are defined as the angular distance between the small circle about the current pole $\mathbf{p}^1$ containing the rotated pick and the best fit small circle to the set of picks. For the i^{th} transform fault pick $\mathbf{t}_i$ the residual is given by

$$\varepsilon_i = \theta - \cos^{-1}(\mathbf{p}^1.\mathbf{t}_i), \tag{A.24}$$

where θ is the angle describing the distance of the best fit small circle from the current pole.

For this residual the partial derivative, with respect to a perturbation to pole parameter, p^γ, is given by

$$\begin{aligned}
\frac{\partial \varepsilon_i}{\partial p^\gamma} &= \frac{\partial \theta}{\partial p^\gamma} - \frac{\partial}{\partial p^\gamma}\cos^{-1}(\mathbf{p}^1.\mathbf{t}_i) \\
&= \frac{1}{n}\frac{\partial}{\partial p^\gamma}\left(\sum_{i=1}^{n}\cos^{-1}(\mathbf{p}^1.\mathbf{t}_i)\right) - \left(\frac{-1}{1-(\mathbf{p}^1\mathbf{t}_i)^2}\right)\frac{\partial(\mathbf{p}^1\mathbf{t}_i)}{\partial p^\gamma} \\
&= \left\{\sum_{i=1}^{n}\left(\frac{-1}{1-(\mathbf{p}^1\mathbf{t}_i)^2}\right)\left[\frac{\partial \mathbf{p}^1}{\partial p^\gamma}\right].\mathbf{t}_i\right\} - \left(\frac{-1}{1-(\mathbf{p}^1\mathbf{t}_i)^2}\right)\left[\frac{\partial \mathbf{p}^1}{\partial p^\gamma}\right].\mathbf{t}_i
\end{aligned} \tag{A.25}$$

where the summation term describes the best-fit small circle to the set of n picks in the set $t = \{t_1 \ldots, t_i \ldots, t_n\}$. The partial derivative $\frac{\partial \mathbf{p}^1}{\partial p^\gamma}$ is determined in Nankivell (1997a), appendix A.

A.1.3 Least squares and inversion

A matrix of partial derivatives for all residuals with respect to all model pole parameters enables a least squares inversion procedure to determine changes to the model for minimising the whole set of residuals. The model parameters inverted for are a set of l finite rotation poles each consisting of (λ, ϕ, θ). That is, $n = 3l$ parameters, in a set $p = \{p_1 \ldots, p_\mathrm{j} \ldots, p_{3\mathrm{l}}\}$. The total set of residuals, from magnetic, transform fracture zone and transform fault data, will all equal zero for a perfect description of the observed data. So for the i^{th} residual, $\varepsilon_i(\mathbf{p})$, in the hypothetical set $\mathbf{p}^*$, with the 'perfect' set of parameters:

$$\varepsilon_i(\mathbf{p}^*) = 0. \tag{A.26}$$

Each residual generated by any imperfect pole parameter set $\mathbf{p}$ has a partial derivative relating how a perturbation to the next pole parameter, ∂p_j, effects a change in that residual. Assuming the set of poles, $\mathbf{p}$, is close to the perfect set $\mathbf{p}^*$, then

$$\varepsilon_i(\mathbf{p}^*) - \varepsilon_i(\mathbf{p}) \approx \sum_j \frac{\partial \varepsilon_i}{\partial p_j}(p_j^* - p_j). \tag{A.27}$$

Following this, by defining the difference between the j^{th} parameter in each set as

$$\Delta p_j = p_j^* - p_j, \tag{A.28}$$

and applying equation (A.26), we have

$$\varepsilon_i(\mathbf{p}) \approx -\sum_j \Delta p_j \frac{\partial \varepsilon_i}{\partial p_j}. \tag{A.29}$$

Normalisation of partial derivatives for all three data sets; magnetics (mag), transform fracture zones (fz) and transform faults (tf), is done by dividing each by its set's standard deviation: $\sigma^{\text{mag}}, \sigma^{\text{fz}}$ or σ^{tf}. Normalised matrices of partial derivatives are thus constructed;

$$\hat{\mathbf{A}}_{ij}^{\text{mag}} = \frac{1}{\sigma^{\text{mag}}} \frac{\partial {\varepsilon_i}^{\text{mag}}}{\partial p_j}, \qquad \hat{\mathbf{A}}_{ij}^{\text{fz}} = \frac{1}{\sigma^{\text{fz}}} \frac{\partial {\varepsilon_i}^{\text{fz}}}{\partial p_j}, \qquad \hat{\mathbf{A}}_{ij}^{\text{tf}} = \frac{1}{\sigma^{\text{tf}}} \frac{\partial {\varepsilon_i}^{\text{tf}}}{\partial p_j}. \tag{A.30}$$

Similarly, vectors containing normalised residuals are;

$$\hat{\mathbf{b}}_i^{\text{mag}} = -\frac{1}{\sigma^{\text{mag}}} {\varepsilon_i}^{\text{mag}}, \qquad \hat{\mathbf{b}}_i^{\text{fz}} = -\frac{1}{\sigma^{\text{fz}}} {\varepsilon_i}^{\text{fz}}, \qquad \hat{\mathbf{b}}_i^{\text{tf}} = -\frac{1}{\sigma^{\text{tf}}} {\varepsilon_i}^{\text{tf}}. \tag{A.31}$$

These combine in a single matrix, dimension mn, of partial derivatives and a single vector, length m, of residuals, respectively:

$$\hat{\mathbf{A}} = \begin{bmatrix} \hat{\mathbf{A}}^{\text{mag}} \\ \hat{\mathbf{A}}^{\text{fz}} \\ \hat{\mathbf{A}}^{\text{tf}} \end{bmatrix}, \qquad \hat{\mathbf{b}} = \begin{bmatrix} \hat{\mathbf{b}}^{\text{mag}} \\ \hat{\mathbf{b}}^{\text{fz}} \\ \hat{\mathbf{b}}^{\text{tf}} \end{bmatrix}. \tag{A.32}$$

From equation (A.29) we have the matrix equation which can be inverted:

$$\hat{\mathbf{A}} \Delta \mathbf{p} = \hat{\mathbf{b}}. \tag{A.33}$$

After additional weighting using a weighting matrix $\mathbf{W}$ to mitigate the effects of poor quality data (see next Section):

$$\mathbf{A} = \mathbf{W}\hat{\mathbf{A}}, \qquad \mathbf{b} = \mathbf{W}\hat{\mathbf{b}} \tag{A.34}$$

or more simply, as the weighting matrix is diagonal, and $\mathbf{W}_{ii} = w_i$,

$$\mathbf{A}_{ij} = w_i\hat{\mathbf{A}}_{ij}, \qquad \mathbf{b}_i = w_i\hat{\mathbf{b}}_i, \tag{A.35}$$

the matrix equation reads

$$\mathbf{A}\Delta\mathbf{p} = \mathbf{b}. \tag{A.36}$$

This is solved iteratively, using a least squares method with a provision for damping (NAG, 1985; Paige and Saunders, 1982), for sets of adjustments to pole parameters, $\Delta\mathbf{p}$, until a minimised stable parameter set has been found.

A.1.4 Data weighting

In addition to normalisation, extra weighting is applied to mitigate the effects of 'bad' data. Crude bias can be applied using factors $\beta^{\mathrm{mag}}, \beta^{\mathrm{fz}}$ and β^{tf}. Weighting proper is applied according to some of the properties and uses of the data as follows.

For isochron-groups of magnetic picks four factors determine the weight: i) w_{ng}, the number of great circles to which the group rotates, ii) w_e, the root mean square residual of all picks defining and rotating to the target great circle, iii) w_{np}, related to the number of picks n_c defining the target great circle,

$$w_{np} = \begin{cases} 2 & n_c = 2 \\ 1 & n_c \geqslant 3 \end{cases}$$

iv) w_r, related to the type of fitting (conjugate fitting is preferred)

$$w_r = \begin{cases} 1 & \text{target conjugate anomaly} \\ 1.5 & \text{target axial anomaly} \\ 2 & \text{target independent anomaly.} \end{cases}$$

Weights less than a standard deviation, σ^{mag}, are given unit weighting and those greater a normalised weight. Each magnetic isochron datum's total weight, including biasing, is given by:

$$W = \begin{cases} \beta^{\text{mag}} & \text{when } (w_{ng} \times w_e \times w_{np} \times w_r) \leqslant \sigma^{\text{mag}} \\ \frac{\sigma^{\text{mag}} \times \beta^{\text{mag}}}{w_{ng} \times w_e \times w_{np} \times w_r} & \text{when } (w_{ng} \times w_e \times w_{np} \times w_r) > \sigma^{\text{mag}}. \end{cases}$$

The best fracture zone or transform fault data are those with the best fit to synthetic flowlines. Given a fracture zone or transform fault (a fault feature 'ff') with root mean square error w_e, biasing factor β and overall standard deviation σ^{ff} the data from each pick are weighted according to:

$$W = \begin{cases} \beta^{\text{ff}} & \text{when } w_e \leqslant \sigma^{\text{ff}} \\ \frac{\sigma^{\text{ff}} \times \beta^{\text{ff}}}{\xi} & \text{when } w_e > \sigma^{\text{ff}}. \end{cases}$$

Appendix B

Fourier techniques for potential field anomaly grids

B.1 The Fourier transform

The Fourier transform ($\mathcal{F}$) of a function F is

$$F(\mathbf{k}) = \mathcal{F}\left(f\left(x\right)\right) = \int_{-\infty}^{\infty}\int_{-\infty}^{\infty} f\left(\mathbf{x}\right) e^{-i2\pi\mathbf{k}.\mathbf{x}} d^2\mathbf{x}, \tag{B.1}$$

in which $\mathbf{x}$ is the coordinate (x, y) and $\mathbf{k}$ is the horizontal wavenumber vector (k_x, k_y).

B.2 Terrain correction technique

The technique used for terrain correction of the simple Bouguer anomaly is that of Parker (1995; 1996). The correction is evaluated by integration of columnar mass elements within the survey area:

$$\frac{g_{\text{terr}}(\mathbf{r})}{\mathsf{G}\rho} = \int_D d^2\mathbf{s}\left(\frac{1}{|\mathbf{s}-\mathbf{r}|} - \frac{1}{\left[\left(h(\mathbf{s})-h(\mathbf{r})\right)^2 + |\mathbf{s}-\mathbf{r}|^2\right]^{\frac{1}{2}}}\right), \tag{B.2}$$

where $\mathbf{r}$ is the observation locality, $\mathbf{s}$ is the locality of the attracting column and $h(\mathbf{r})$ and $h(\mathbf{s})$ describe the observation surface and the bathymetric surface at each, respectively. The domain D is split in two: $D_<$ inside a cylinder centred on the observation point and $D_>$ outside (Figure B.1). $D_<$ is evaluated numerically and $D_>$ using a wavenumber domain approach, which follows. A binomial expansion of equation B.2 describes the bathymetric surface as a series in powers of $\frac{1}{|\mathbf{s}-\mathbf{r}|}$, so that:

$$\frac{g_{\text{terr}_>}(\mathbf{r})}{\mathsf{G}\rho} = \int_{D_>} d^2\mathbf{s} \sum_{n=1}^{\infty} C_n \frac{(h(\mathbf{s}) - h(\mathbf{r}))^{2n}}{|\mathbf{s}-\mathbf{r}|^{2n+1}}, \tag{B.3}$$

where $C_1 = \frac{1}{2}, C_2 = -\frac{3}{8}, C_3 = \frac{5}{16} \cdots$.

The expanded equation is itself subjected to a binomial expansion, of its numerators, in order to express it as a series of convolutions (denoted by $*$):

$$\begin{aligned}
\frac{g_{\text{terr}_>}(\mathbf{r})}{\mathsf{G}\rho} &= \int_{D_>} d^2\mathbf{s} \sum_{n=1}^{\infty} C_n \sum_{m=0}^{2n} (-1)^m C_{2n,m} \frac{h(\mathbf{s})^m h(\mathbf{r})^{2n-m}}{|\mathbf{s}-\mathbf{r}|^{2n+1}}, \\
&= \sum_{n=1}^{\infty} C_n \sum_{m=0}^{2n} (-1)^m C_{2n,m} h(\mathbf{r})^{2n-m} \times \int_{D_>} d^2\mathbf{s} \frac{h(\mathbf{s})^m}{|\mathbf{s}-\mathbf{r}|^{2n+1}}, \\
&= \sum_{n=1}^{\infty} C_n \sum_{m=0}^{2n} (-1)^m C_{2n,m} h(\mathbf{r})^{2n-m} \left(L_n * h^m\right)(\mathbf{r}),
\end{aligned} \tag{B.4}$$

where $C_{n,k}$ denotes the binomial coefficient $n!/(n-k)!k!$ and for which, with a the radius of $D_<$

$$L_n(\mathbf{s}) = \begin{cases} |\mathbf{s}|^{-2n-1}, & |\mathbf{s}| > a \\ 0, & \text{otherwise.} \end{cases}$$

Convolution in the space domain is equivalent to multiplication in the wavenumber domain to which equation B.4 is transformed, where it can be solved quickly. The method is complicated by approximations to widen the validity of the expansion and to speed computation. Its further derivation will not be described here. Reported inherent inaccuracy (due to truncation of the binomial series) is small, decreasing with water depth to the order of 10^{-3}mGal at oceanic depths. The largest errors are in the flat earth assumption and the uncertainties of the input bathymetric grid. The flat earth assumption results in

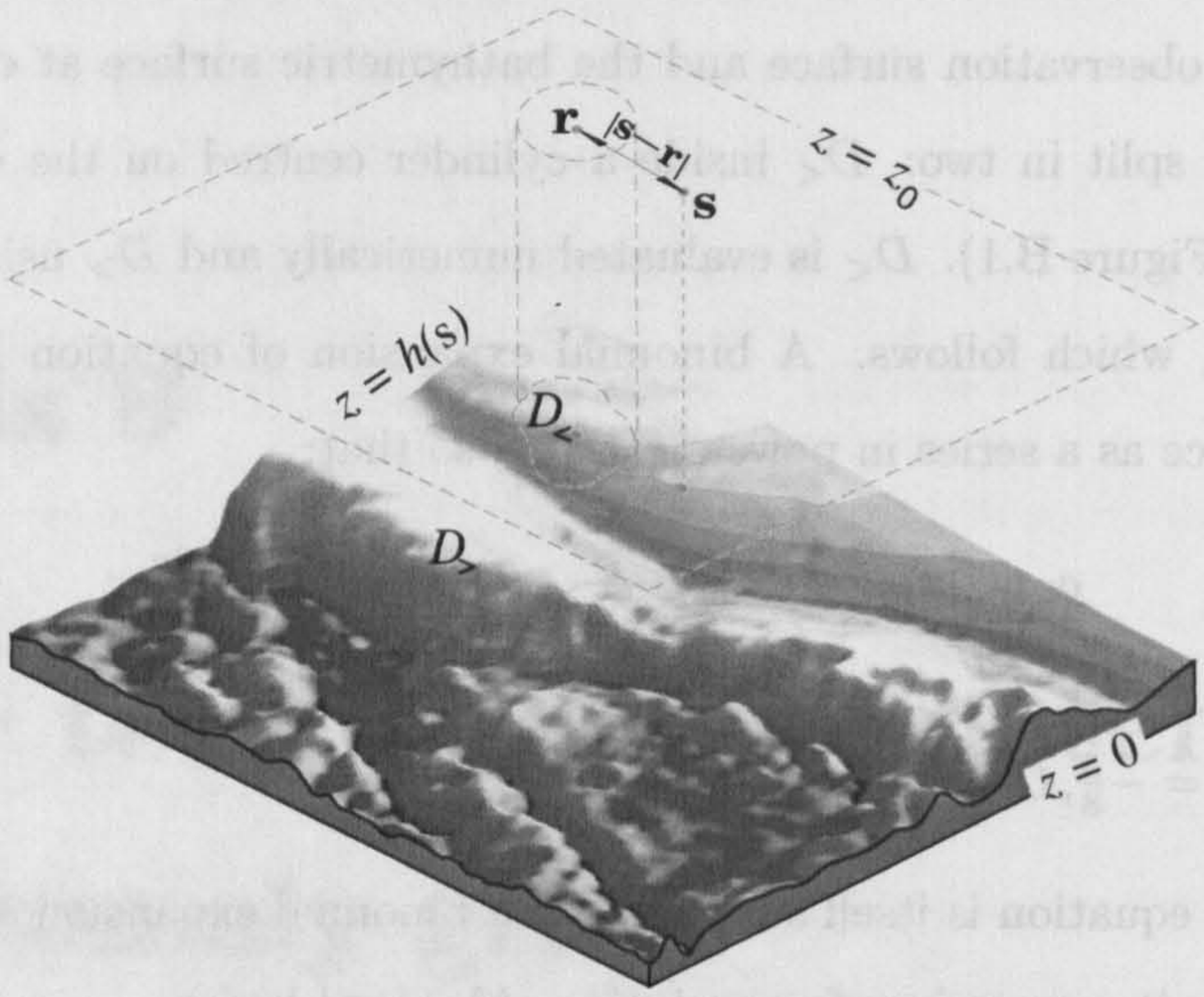

Figure B.1: Fourier technique for evaluating terrain corrections. For the observation point **r** the attraction of columns at all points **s** is summed by the integral equation B.2. Within a cylinder centred on **r** ($D_<$), the integral is evaluated numerically, outside ($D_>$) use is made of the fast Fourier transform.

inaccuracy at long wavelengths (Dahlen, 1982; $\geqslant$ 1000 km), which are of little importance to the use intended here. Implementation of the technique uses a set of *Matlab* scripts supplied by R.L. Parker.

B.3 Reduction to the pole

The following treatment is that of Blakely (1995). A model three dimensional distribution of magnetization $M(x, y, z)$ is located entirely below the observation plane z_0. The anomaly function must be harmonic so the distribution is defined as zero outside a finite region horizontally smaller than the survey. Assuming a constant direction of magnetization within the distribution, the Fourier transform of the total field anomaly is:

$$\mathcal{F}(\Delta T) = 2\pi C_{\mathrm{m}} \Theta_{\mathrm{m}} \Theta_{\mathrm{f}} |k| e^{|k| z_0} \int_{z_0}^{\infty} e^{-|k| z'} \mathcal{F}[M\,(z')] dz'. \tag{B.5}$$

$\mathcal{F}[M\,(z')]$ is the Fourier transform of the magnetization on a horizontal slice through the body at z'. C_{m} is a constant of proportionality, for SI units $C_{\mathrm{m}} = \frac{\mu_0}{4\pi}$ where μ_0 is the magnetic permeability of free space. Θ_{m} and Θ_{f} are defined in terms of unit vectors of magnetization ($\hat{\mathbf{m}} = (\hat{m}_x + \hat{m}_y + \hat{m}_z)$) and ambient field (($\hat{\mathbf{f}} = (\hat{f}_x + \hat{f}_y + \hat{f}_z)$), respectively:

$$\begin{aligned} \Theta_{\mathrm{m}} &= \hat{m}_z + i\frac{\hat{m}_x k_x + \hat{m}_y k_y}{|k|}, \\ \Theta_{\mathrm{f}} &= \hat{f}_z + i\frac{\hat{f}_x k_x + \hat{f}_y k_y}{|k|}. \end{aligned} \tag{B.6}$$

The shape of the model can be included in the integral term of equation B.5 as it too has an effect on the phase of the anomaly. The remaining source of phase (the one we want to be rid of) is the inclination of $\hat{\mathbf{m}}$ and $\hat{\mathbf{f}}$. For reduction to the pole these inclinations are vertical, *i.e.* $\hat{\mathbf{m}}' = \hat{\mathbf{f}}' = (0, 0, 1)$, and the transformed anomaly can be written:

$$\mathcal{F}(\Delta T_{\mathrm{r}}) = 2\pi C_{\mathrm{m}} \Theta'_{\mathrm{m}} \Theta'_{\mathrm{f}} |k| e^{|k| z_0} \int_{z_0}^{\infty} e^{-|k| z'} \mathcal{F}[M\,(z')] dz'. \tag{B.7}$$

Here Θ'_{m} and Θ'_{f} can be similarly defined as in equations B.6 except in terms of $\hat{\mathbf{m}}'$ and $\hat{\mathbf{f}}'$. It is obvious that $\Theta'_{\mathrm{m}} = \Theta'_{\mathrm{f}} = 1$.

Finally, combining equations B.5 and B.7, and eliminating common factors gives:

$$\mathcal{F}(\Delta T_{\mathrm{r}}) = \mathcal{F}(\psi_{\mathrm{r}}) \mathcal{F}(\Delta T), \tag{B.8}$$

where the reduction to the pole operator:

$$\mathcal{F}(\psi_{\mathrm{r}}) = \frac{1}{\Theta_{\mathrm{m}} \Theta_{\mathrm{f}}} = \frac{|k|^2}{a_1 k_x^2 + a_2 k_y^2 + a_3 k_x k_y + i|k|\,(b_1 k_x + b_2 k_y)}, \quad |k| \neq 0 \tag{B.9}$$

$$\begin{aligned} a_1 &= \hat{m}_z \hat{f}_z - \hat{m}_x \hat{f}_x, & b_1 &= \hat{m}_x \hat{f}_z + \hat{m}_z \hat{f}_x, \\ a_2 &= \hat{m}_z \hat{f}_z - \hat{m}_y \hat{f}_y, & b_2 &= \hat{m}_y \hat{f}_z + \hat{m}_z \hat{f}_y, \\ a_3 &= -\hat{m}_y \hat{f}_x - \hat{m}_x \hat{f}_y. \end{aligned}$$

Near the equator this operator supplies an unreasonably large amplitude to a narrow part of the transformed anomaly's spectrum and gives rise to unwanted artifacts. Techniques have been developed to deal with this problem (Bott and Ingles, 1972; Leu, 1981;

Hansen and Pawlowski, 1989; for example), but because of the high southerly latitude of the Scotia Sea (inclination $\sim -55°$) this instability was not an issue of concern in this study.

B.4 Seafloor Magnetization

The inverse technique for modelling seafloor magnetization was invented by Parker and Huestis (1974) and extended by Macdonald *et al* (1980). The following treatment is taken from those papers. The magnetic anomaly due to a given model magnetization (M), in the wavenumber domain, is given by

$$\mathcal{F}[T(\mathbf{r})] = \frac{1}{2}\mu_0 e^{(-|\mathbf{k}|z_0)}\left(1 - e^{(-|\mathbf{k}|h_0)}\right) V(\mathbf{k}) \cdot \sum_{n=0}^{\infty} \frac{|\mathbf{k}|^n}{n!}\mathcal{F}[M(\mathbf{r})h(\mathbf{r})^n], \tag{B.10}$$

((Parker, 1973)) where h_0 is the thickness of the model layer, $\mathbf{k}$ is the horizontal wavenumber vector, z_0 is a reference plane above the bathymetric surface $h(\mathrm{r})$ and

$$V(\mathbf{k}) = \hat{\mathbf{f}} \cdot (i\hat{\mathbf{k}}, \hat{\mathbf{z}})\hat{\mathbf{m}} \cdot (i\hat{\mathbf{k}}, \hat{\mathbf{z}}), \tag{B.11}$$

(Macdonald *et al*, 1980). $\hat{\mathbf{z}}$ is a unit vector in the vertical direction. As before $\hat{\mathbf{m}}$ is a unit vector in the magnetization of the source.

Equation B.10 is rearranged to express the Fourier transform of M as

$$\mathcal{F}[M(\mathbf{r})] = \frac{\mathcal{F}[T(\mathbf{r})]e^{(|\mathbf{k}|z_0)}}{\frac{1}{2}\mu_0\left(1 - e^{(-|\mathbf{k}|h_0)}\right)V(\mathbf{k})} - \sum_{n=1}^{\infty} \frac{|\mathbf{k}|^n}{n!}\mathcal{F}[M(\mathbf{r})h(\mathbf{r})^n]. \tag{B.12}$$

This is solved iteratively by first guessing M in equation B.12, Fourier transforming it for a new M, and by then replacing this in the equation and calculating a new M. This process continues until M does not change, or the series diverges and the inversion fails.

The operation is difficult to implement with stability. Short wavelengths in the total field anomaly are prone to contamination by noise. Transforming data from an upper observation plane (the sea surface) to inform a model (the seafloor) below amplifies the noise, and this is the source of the method's instability. Because of this some degree of

low pass filtering of M is necessary prior to inversion. Obviously the filter which is least destructive of seafloor spreading anomalies, which are typically a few to tens of kilometres in width, is most desirable. Further problems arise when non-oceanic crust is represented in the input data. The source model is inappropriate for many anomalies and may fail to adopt distributions of magnetization which can produce them. This is especially so with high amplitude anomalies in very shallow or very deep water. With such areas a dummy bathymetric surface is used to allow the inversion to converge, and the offending region removed afterwards.

Bibliography

Adie, R.J. 1952. The position of the Falkland Islands in a reconstruction of Gondwanaland. *Geological Magazine*, **89**, 401–410.

Alabaster, T. and Storey, B.C. 1990. Modified Gulf of California model for South Georgia, north Scotia Ridge, and implications for the Rocas Verdes back-arc basin, southern Andes. *Geology*, **18**, 497–500.

Alvarez, W. 1982. Geological evidence for the geographical pattern of mantle return flow and the driving mechanism of plate tectonics. *Journal of Geophysical Research*, **87**, 6697–6710.

Arctowski, H. 1895. Observations sur l'interet qui presente l'exploration geologique des Terres Australes. *Bulletin de la Société Géologique de France*, series 3, **23**, 589–591.

Baker, P.E. 1978. The South Sandwich Islands II. Petrology and geochemistry. *BAS Scientific Report*, **93**.

Baranov, V. and Naudy, H. 1964. Numerical calculation of the formula of reduction to the magnetic pole. *Geophysics*, **29**, 67–79.

Barazangi, M. and Dorman, J. 1969. World seismicity maps compiled from ESSA, Coast and Geodetic Survey, epicenter data, 1961-1967. *Bulletin of the Seismological Society of America*, **59**, 369–380.

Barber, P.L., Barker, P.F., and Pankhurst, R.J. 1991. Dredged rocks from Powell Basin

and the South Orkney Microcontinent. In Thomson, M.R.A., Crame, J.A., and Thomson, J.W., editors, *Geological Evolution of Antarctica. Proceedings V International Conference, Antarctic Earth Sciences*, pages 361–367. Cambridge University Press, Cambridge.

Barker, P.F. 1970. Plate tectonics of the Scotia Sea region. *Nature*, **228**, 1293–1296.

Barker, P.F. 1972. A spreading centre in the east Scotia Sea. *Earth and Planetary Science Letters*, **15**, 123–132.

Barker, P.F. 1979. The history of ridge-crest offset at the Falklands - Agulhas Fracture Zone from a small-circle geophysical profile. *Geophysical Journal of the Royal Astronomical Society*, **59**, 131–145.

Barker, P.F. 1982. The Cenozoic subduction history of the Pacific margin of the Antarctic Peninsula: ridge crest-trench interactions. *Journal of the Geological Society of London*, **139**, 787–801.

Barker, P.F. 1995. Tectonic framework of the East Scotia Sea. In Taylor, B., editor, *Backarc basins: tectonics and magmatism*, pages 281–314. Plenum Press, New York.

Barker, P.F. 1999. Evidence for a volcanic rifted margin and oceanic crustal structure for the Falkland Plateau Basin. *Journal of the Geological Society of London*, **156**, 889–900.

Barker, P.F., Barber, P.L., and King, E.C. 1984. An early Miocene ridge crest–trench collision on the South Scotia Ridge near 36°W. *Tectonophysics*, **102**, 315–332.

Barker, P.F. and Burrell, J. 1977. The opening of Drake Passage. *Marine Geology*, **25**, 15–34.

Barker, P.F. and Burrell, J. 1982. The influence upon Southern Ocean circulation, sedimentation and climate of the opening of Drake Passage. In Craddock, C., editor, *Antarctic Geoscience*, pages 377–385. University of Wisconsin Press, Madison.

Barker, P.F., Dalziel, I.W.D., and Shipboard Scientific Party. 1977. Site 330. *Initial reports, Deep Sea Drilling Program*, **36**, 207–227.

Barker, P.F., Dalziel, I.W.D., and Storey, B.C. 1991. Tectonic development of the Scotia Arc region. In Tingey, R.J., editor, *Antarctic Geology*, pages 215–248. Oxford University Press, Oxford.

Barker, P.F. and Griffiths, D.H. 1972. The evolution of the Scotia Ridge and Scotia Sea. *Philosophical Transactions of the Royal Society, London*, A271, 151–183.

Barker, P.F. and Hill, I.A. 1980. Asymmetric spreading in back-arc basins. *Nature*, **285**, 652–654.

Barker, P.F. and Hill, I.A. 1981. Back-arc extension in the Scotia Sea. *Philosophical Transactions of the Royal Society, London*, **A300**, 249–262.

Barker, P.F., Hill, I.A., Weaver, S.D., and Pankhurst, R.J. 1982. The origin of the eastern South Scotia Ridge as an intraoceanic island arc. In Craddock, C., editor, *Antarctic Geoscience*, pages 203–211. University of Wisconsin Press, Madison.

Barker, P.F. and Jahn, R.A. 1980. A marine geophysical reconnaisance of the Weddell Sea. *Geophysical Journal of the Royal Astronomical Society*, **63**, 271–283.

Barker, P.F. and Lawver, L.A. 1988. South American–Antarctic plate motion over the past 50Myr, and the evolution of the South American–Antarctic ridge. *Geophysical Journal*, **94**, 377–386.

Barker, P.F. and Lonsdale, M.J. 1991. A multichannel seismic profile across the Weddell Sea margin of the Antarctic Peninsula: regional tectonic implications. In Thomson, M.R.A., Crame, J.A., and Thomson, J.W., editors, *Geological Evolution of Antarctica. Proceedings V International Conference, Antarctic Earth Sciences*, pages 237–241. Cambridge University Press, Cambridge.

Barrow, J. Sir. 1830-1. Account of the Island of Deception, one of the New Shetland Isles. *Journal of the Royal Geographical Society*, **1**, 62–66.

Berggren, A. and Hollister, C.D. 1977. Plate tectonics and paleocirculation—commotion in the ocean. *Tectonophysics*, **38**, 11–48.

Bergh, H.W. 1977. Mesozoic seafloor off Dronning-Maud land. *Nature*, **269**, 686–687.

Beu, A.G., Griffin, M., and Maxwell, P.A. 1997. Opening of Drake Passage gateway and Late Miocene to Pleistocene cooling reflected in Southern Ocean molluscan dispersal: evidence from New Zealand and Argentina. *Tectonophysics*, **281**, 83–97.

Bhattacharyya, B.K. 1965. Two dimensional harmonic analysis as a tool for magnetic interpretation. *Geophysics*, **30**, 829–857.

Biddle, K.T., Uliana, M.A., Mitchum, R.M., Fitzgerald, M.G., and Wright, R.C. 1986. The stratigraphic and structural evolution of the central and eastern Magallanes basin, southern South America. In Allen, P.A. and Homewood, P., editors, *Foreland Basins*, number **8** in Special Publication, pages 41–61. International Association of Sedimentologists.

Bishop, I., Styles, P., Ernsley, S.J., and Ferguson, N.S. 1997. The detection of cavities using the microgravity method: case histories from mining and karstic environments. In McCann, D., Eddleton, M., Fenning, P.J., and Reeves, G.M., editors, *Modern Geophysics in Engineering Geology*, number **12** in Special Publication, pages 155–168. Geological Society of London.

Blakely, R. 1995. *Potential theory in gravity and magnetic applications.* Cambridge University Press, Cambridge.

Boillot, G., Beslier, M.-O., Krawczyk, C.M., Rappin, D., and Reston, T.J. 1995. The formation of passive margins: Constraints from the crustal structure and segmentation of the deep Galicia margin, Spain. In Scrutton, R.A., editor, *The tectonics, sedimentation and palaeoceanography of the North Atlantic region*, number **90** in Special Publication, pages 71–91. Geological Society of London.

Bonatti, E. 1996. Anomalous opening of the Equatorial Atlantic due to an equatorial mantle thermal minimum. *Earth and Planetary Science Letters*, **143**, 147–160.

Bonatti, E., Ligi, M., Gasperini, L., Peyve, A., Raznitsin, Y., and Chen, Y.J. 1994.

Transform migration and vertical tectonics at the Romanche fracture zone, equatorial Atlantic. *Journal of Geophysical Research*, **99**, 21779–21802.

Bott, M.H.P. and Ingles, A. 1972. Matrix methods for joint interpretation of two-dimensional gravity and magnetic anomalies with application to the Iceland–Faeroe Ridge. *Geophysical Journal of the Royal Astronomical Society*, **30**, 55–67.

Bowin, C. 1983. Depth of principal mass anomalies contributing to the earth's geoidal undulations and gravity anomalies. *Marine Geology*, **7**, 61–100.

Bratt, S.R. and Purdy, G.M. 1984. Structure and variability of oceanic crust on the flanks of the East Pacific Rise between 11° and 13°N. *Journal of Geophysical Research*, **89**, 6111–6125.

Briggs, I.C. 1974. Machine contouring using minimum curvature. *Geophysics*, **39**, 39–48.

Brodie, J. and White, N. 1994. Sedimentary basin inversion caused by igneous underplating. *Geology*, **22**, 147–150.

Bruhn, R.L. and Dalziel, I.W.D. 1977. Destruction of the early Cretaceous marginal basin in the Andes of Tierra del Fuego. In Talwani, M. and Pitman, W.G., editors, *Island arcs, deep sea trenches and back-arc basins*, pages 395–405. AGU, Washington DC.

Brun, J.P. and Beslier, M.-O. 1996. Mantle exhumation at passive margins. *Earth and Planetary Science Letters*, **142**, 161–173.

Bullard, E., Everett, J.E., and Smith, A.G. 1965. The fit of continents around the Atlantic. In Blackett, P.M.S., Bullard, E., and Runcorn, S.K., editors, *A symposium on continental drift*, volume **A258**, pages 41–51. Philosophical Transactions of the Royal Society, London.

Burrell, J. 1983. *The evolution of Drake Passage.* PhD thesis, University of Birmingham.

Cande, S.C. 1976. A palaeomagnetic pole from Late Cretaceous marine magnetic anomalies in the Pacific. *Geophysical Journal of the Royal Astronomical Society*, **44**, 547–566.

Cande, S.C. and Kent, D.V. 1995. Revised calibration of the geomagnetic polarity time scale for the late Cretaceous and Cenozoic. *Journal of Geophysical Research*, **100**, 6093–6095.

Cande, S.C., LaBrecque, J.L., and Haxby, W.F. 1988. Plate kinematics of the South Atlantic: Chron 34 to present. *Journal of Geophysical Research*, **93**, 13479–13492.

Cande, S.C., Stock, J.M., Müller, R.D., and Ishihara, T. 2000. Cenozoic motion between East and West Antarctica. *Nature*, **404**, 145–150.

Carey, S.W. 1958. A tectonic approach to continental drift. In Carey, S.W., editor, *Continental Drift: A Symposium*, pages 178–355. University of Tasmania Press, Hobart.

Carlson, R.L. and Melia, P.J. 1984. Subduction hinge migration. *Tectonophysics*, **102**, 399–411.

Carrigan, C.R. and Gubbins, D. 1979. The source of the Earth's magnetic field. *Scientific American*, **240**, 92–101.

Case, J.A., Woodburne, M.O., and Chaney, D.S. 1988. A new genus of polypoloid marsupial from Antarctica. In *Geology and Paleontology of Seymour Island, Antarctic Peninsula*, volume **169** of *Memoir*, pages 505–521. Geological Society of America, Boulder, Colorado.

Chang, T. 1987. On the statistical properties of estimated rotations. *Journal of Geophysical Research*, **92**, 6319–6329.

Chapin, D.A. 1996. A deterministic approach toward isostatic gravity residuals—A case study from South America. *Geophysics*, **61**, 1022–1033.

Chase, C.G. 1978. Extension behind island arcs and motions relative to hot spots. *Journal of Geophysical Research*, **83**, 5385–5387.

Cheney, R.E., Douglas, B.C., Agreen, R.W., Miller, L., Porter, D.L., and Doyle, N.S. 1987. *Geosat altimeter geophysical data record user handbook.* NOAA Technical Memorandum NOS NGS-46. US Department of Commerce, Rockville, Maryland, USA.

Cheney, R.E., Doyle, N.S., Douglas, B.C., Agreen, R.W., Miller, L., Timmerman, E.L., and McAdoo, D.C. 1991. *The complete Geosat altimeter GDR handbook.* NOAA Manual NOS NGS-7. US Department of Commerce, Rockville, Maryland, USA.

Chovitz, B.H. 1981. Modern geodetic earth reference models. *EOS, Transactions AGU*, **62**, 65–67.

Christensen, U. 1985. Thermal evolution models for the Earth. *Journal of Geophysical Research*, **90**, 2995–3008.

Cieselski, P.F., Ledbetter, M.T., and Ellwood, B.B. 1982. The development of Antarctic glaciation and the Neogene paleoenvironment of the Maurice Ewing Bank. *Marine Geology*, **46**, 1–51.

Coffin, M.F. and Eldholm, O. 1992. Volcanism and continental break-up: a global compilation of large igneous provinces. In Storey, B.C., Alabaster, T., and Pankhurst, R.J., editors, *Magmatism and the Causes of Continental Break-up*, number **68** in Special Publication, pages 17–30. Geological Society of London.

Cooper, A.K., Marlow, M.S., and Scholl, D.W. 1976. Mesozoic magnetic lineations in the Bering Sea marginal basin. *Journal of Geophysical Research*, **81**, 1916–1934.

Cooper, A.K., Marlow, M.S., Scholl, D.W., and Stevenson, A.J. 1992. Evidence for Cenozoic crustal extension in the Bering Sea region. *Tectonics*, **11**, 719–731.

Coren, F., Ceccone, G., Lodolo, E., Zanolla, C., Zitellini, N., Bonazzi, C., and Centonze, J. 1997. Morphology, seismic structure and tectonic development of the Powell Basin, Antarctica. *Journal of the Geological Society of London*, **154**, 849–862.

Cox, A. and Doell, R.R. 1962. Magnetic properties of the basalt in Hole EM7, Mohole project. *Journal of Geophysical Research*, **67**, 3997–4004.

Cox, A., Doell, R.R., and Dalrymple, G.B. 1963. Geomagnetic polarity epochs and Pleistocene geochronometry. *Nature*, **198**, 1049–1051.

Cox, K.G. 1980. A model for flood basalt vulcanism. *Journal of Petrology*, **21**, 629–650.

Creer, K.M. 1965. Palaeomagnetic data from the Gondwanic continents. In Blackett, P.M.S., Bullard, E., and Runcorn, S.K., editors, *A symposium on continental drift*, volume **A258**, pages 27–40. Philosophical Transactions of the Royal Society, London.

Cromwell, D. 20 May, 2000. Ocean circulation. *New Scientist, Inside Science*, **130**, 1–4.

Crough, S.T. 1983. The correction for sediment loading on the seafloor. *Journal of Geophysical Research*, **88**, 6449–6454.

Cunningham, A.P. 1998. *Geophysical investigations of the North Scotia Ridge.* PhD thesis, University of London.

Cunningham, A.P., Barker, P.F., and Tomlinson, J.S. 1998. Tectonics and sedimentary environment of the North Scotia Ridge region revealed by side-scan sonar. *Journal of the Geological Society of London*, **155**, 941–956.

Cunningham, W.D. 1993. Strike slip faults in the southernmost Andes and the development of the Patagonian orocline. *Tectonics*, **12**, 169–186.

Cunningham, W.D., Dalziel, I.W.D., Lee, T.Y., and Lawver, L.A. 1995. Southernmost south America - Antarctic Peninsula relative plate motions since 84 Ma: implications for the tectonic evolution of the Scotia Arc region. *Journal of Geophysical Research*, **100**, 8257–8266.

Dahlen, F.A. 1982. Isostatic geoid anomalies on a sphere. *Journal of Geophysical Research*, **87**, 3943–3948.

Dalziel, I.W.D. 1982. The early (pre-Middle Jurassic) history of the Scotia Arc region: A review and progress report. In Craddock, C., editor, *Antarctic Geoscience*, pages 111–126. University of Wisconsin Press, Madison.

Dalziel, I.W.D. 1983. The evolution of the Scotia Arc: a review. In Oliver, R.L., James, P.R., and Jago, J.B., editors, *Antarctic Earth Science, Proceedings IV International Symposium on Antarctic Earth Sciences*, pages 283–288. Australian Academy of Sciences, Canberra.

Dalziel, I.W.D. 1984. Tectonic evolution of a fore-arc terrane, southern Scotia Ridge, Antarctica. *Geological Society of America, Special Publication*, **200**, 1–32.

Dalziel, I.W.D. 1992. Antarctica: A tale of two supercontinents? *Annual Review of Earth and Planetary Sciences*, **20**, 501–526.

Dalziel, I.W.D., DeWit, M.J., and Palmer, K.F. 1974. Fossil marginal basin in the southern Andes. *Nature*, **250**, 291–294.

Dalziel, I.W.D., Dott Jr, R.H., Winn Jr, R.D., and Bruhn, R.L. 1975. Tectonic relations of South Georgia island to the southernmost Andes. *Bulletin of the Geological Society of America*, **86**, 1034–1040.

Dalziel, I.W.D. and Elliott, D.H. 1971. Evolution of the Scotia Arc. *Nature*, **233**, 246–251.

Dalziel, I.W.D. and Elliott, D.H. 1973. The Scotia Arc and Antarctic margin. In Nairn, A.E.M. and Stehli, D.H., editors, *The Ocean Basins and Margins, 1, the South Atlantic*, pages 171–245. Plenum Press, New York.

Dalziel, I.W.D. and Elliott, D.H. 1982. West Antarctica: problem child of Gondwanaland. *Tectonics*, **1**, 3–19.

Dalziel, I.W.D. and Grunow, A.M. 1992. Late Gondwanide tectonic rotations within Gondwanaland. *Tectonics*, **11**, 603–606.

De Wit, M.J. 1977. The evolution of the Scotia Arc as a key to the reconstruction of southwestern Gondwanaland. *Tectonophysics*, **37**, 53–81.

De Wit, M.J., Dutch, S., Kligfield, R., Allen, R., and Stern, C. 1977. Deformation, serpentinization and emplacement of a dunite complex, Gibbs Island, South Shetland Islands: possible fracture zone tectonics. *Journal of Geology*, **85**, 745–762.

Dean, S.M., Minshull, T.A., Whitmarsh, R.B., and Louden, K.E. 2000. Deep structure of the ocean–continent transition in the southern Iberia Abyssal Plain from seismic refraction profiles: The IAM-9 transect at 40°20'N. *Journal of Geophysical Research*, **105**, 5859–5885.

Dewey, J.F. 1980. Episodicity, sequence and style at convergent plate boundaries. In Strangeway, D.W., editor, *The Continental Crust and Its Mineral Deposits*, volume **20**, pages 553–573. Geological Association of Canada, Special Paper.

Diester-Haass, L. and Zahn, R. 1996. Eocene-Oligocene transition in the Southern Ocean: history of water mass circulation and biological productivity. *Geology*, **24**, 163–166.

Dietz, R.S. 1961. Continental and ocean basin evolution by spreading of the sea floor. *Nature*, **190**, 854–857.

Diraison, M., Cobbold, P.R., Gapais, D., Rossello, E.A., and Le Corre, C. 2000. Cenozoic crustal thickening, wrenching and rifting in the foothills of the southernmost Andes. *Tectonophysics*, **316**, 91–119.

DiVenere, V., Kent, D.V., and Dalziel, I.W.D. 1995. Early Cretaceous paleomagnetic results from Marie Byrd Land, West Antarctica: implications for the Weddellia collage of crustal blocks. *Journal of Geophysical Research*, **100**, 8133–8151.

DiVenere, V., Kent, D.V., and Dalziel, I.W.D. 1996. Summary of palaeomagnetic results from West Antarctica: implications for the tectonic evolution of the Pacific margin of Gondwana during the Mesozoic. In Storey, B.C., King, E.C., and Livermore, R.A., editors, *Weddell Sea tectonics and Gondwana break-up*, number **108** in Special Publication, pages 31–43. Geological Society of London.

Dobrin, M.B. and Savit, C.H. 1988. *Introduction to Geophysical Prospecting*. McGraw Hill, 4th edition.

Dott, Jr, R.H., Winn, Jr, R.D., and Smith, C.H.L. 1982. Relationship of Late Mesozoic and Early Cenozoic sedimentation to the tectonic evolution of the southernmost Andes and Scotia Arc. In Craddock, C., editor, *Antarctic Geoscience*, pages 193–202. University of Wisconsin Press, Madison.

du Plessis, A. 1977. Seafloor spreading south of the Agulhas Fracture Zone. *Nature*, **270**, 719–721.

du Toit, A.L. 1937. *Our wandering continents.* Oliver and Boyd, Edinburgh.

Eagles, G. and Livermore, R.A. 1999. Opening history of Powell Basin, Antarctic Peninsula. In *Abstracts*, page A.315. International Union of Geodesy and Geophysics, Birmingham (also manuscript submitted to *Marine Geology*), 1999.

Elsasser, W.M. 1956a. Background of the geomagnetic dynamo theory. *Journal of Geophysical Research*, **61**, 340–347.

Elsasser, W.M. 1956b. Hydromagnetic dynamo theory. *Reviews of Modern Physics*, **28**, 135–163.

Engebretson, D.C., Cox, A., and Gordon, R.G. 1984. Relative motions between oceanic plates of the Pacific Ocean. *Journal of Geophysical Research*, **89**, 10291–10310.

Ewing, J.I., Ludwig, W.J., Ewing, M., and Eittreim, S.L. 1971. Structure of the Scotia Sea and Falkland Plateau. *Journal of Geophysical Research*, **76**, 7118–7137.

Fairhead, J.D., Green, C.M., Maus, S., and Woollett, R. 1998. Highest resolution satellite gravity data. *GETECH News*, Special Issue, 1–4.

Forsyth, D.W. 1975. Fault plane solutions and tectonics of the south Atlantic and Scotia Sea. *Journal of Geophysical Research*, **80**, 1429–1443.

Forsyth, D.W. and Uyeda, S. 1975. On the relative importance of the driving forces of plate motion. *Geophysical Journal of the Royal Astronomical Society*, **43**, 163–200.

Fowler, C.M.R. 1990. *The Solid Earth.* Cambridge University Press, Cambridge.

Frey, F.A., Coffin, M.F., Wallace, P.F., Weis, D., Zhao, X., Wise Jr., S.W., Wähnert, V., Teagle, D.A.H., Saccocia, P.J., Reusch, D.N., Pringle, M.S., Nicolaysen, K.E., Neal, C.R., Müller, R.D., Moore, C.L., Mahoney, J.J., Keszthelyi, L., Inokuchi, H., Duncan, R.A., Delius, H., Damuth, J.E., Damasceno, D., Coxall, H.K., Borre, M.K., Boehm, F., Barling, J., Arndt, N.T., and Antretter, M. 2000. Origin and evolution of a submarine large igneous province: the Kerguelen Plateau and Broken Ridge, southern Indian Ocean. *Earth and Planetary Science Letters*, **176**, 73–89.

Galindo-Zaldívar, J., Jabaloy, A., Maldonado, A., and Sanz de Galdeano, C. 1996. Continental fragmentation along the South Scotia Ridge transcurrent plate boundary (NE Antarctic Peninsula). *Tectonophysics*, **258**, 275–301.

Garrett, S.W., Renner, R.G.B., Jones, J.A., and McGibbon, K.J. 1986. Continental magnetic anomalies and the evolution of the Scotia Arc. *Earth and Planetary Science Letters*, **81**, 273–281.

Ghidella, M.E. and LaBrecque, J.L. 1997. The Jurassic conjugate margins of the Weddell Sea: considerations based on magnetic, gravity and paleobathymetry data. In Ricci, C.A., editor, *The Antarctic region: geological evolution and processes. Proceedings VII International Symposium, Antarctic Earth Sciences*, pages 441–451. Terra Antartica Publications, Siena.

Gibert, D., Courtillot, V., and Olivet, J.-L. 1989. Seasat altimetry and the south Atlantic geoid 2. Short wavelength undulations. *Journal of Geophysical Research*, **94**, 5545–5559.

Gordon, A. 1986. Interocean exchange of thermocline water. *Journal of Geophysical Research*, **91**, 5037–5046.

Gordon, A.L., Molinelli, E., and Baker, T. 1978. Large-scale relative dynamic topography of the Southern Oceans. *Journal of Geophysical Research*, **83**, 3023–3032.

Greenway, M.E. 1972. Geology of the Falkland Islands. *British Antarctic Survey Scientific Report*, **76**.

Grose, T.J., Johnson, J.A., and Bigg, G.R. 1995. A comparison between FRAM (Fine Resolution Antarctic Model) results and observations in the Drake Passage. *Deep Sea Research*, **42**, 365–388.

Grunow, A.M., Dalziel, I.W.D., Harrison, T.M., and Heizler, M.T. 1992. Structural geology and geochronology of subduction complexes along the margin of Gondwanaland: New data from the Antarctic Peninsula and southernmost Andes. *Bulletin of the Geological Society of America*, **104**, 1497–1514.

Grunow, A.M., Dalziel, I.W.D., and Kent, D.V. 1987. Ellsworth-Whitmore Mountains crustal block, western Antarctica, New Paleomagnetic results and their tectonic significance. In McKenzie, G.D., editor, *Gondwana Six: Stratigraphy, Sedimentology and Palaeontology*, pages 161–171. AGU, Washington.

Grunow, A.M., Kent, D.V., and Dalziel, I.W.D. 1991. New paleomagnetic data from Thurston Island: Implications for the tectonics of West Antarctica and Weddell Sea opening. *Journal of Geophysical Research*, **96**, 17935–17954.

Gubbins, D. 1987. Mechanism for geomagnetic polarity reversals. *Nature*, **326**, 167–169.

Hall, R. 1996. Reconstructing Cenozoic SE Asia. In Hall, R. and Blundell, D.J., editors, *Tectonic evolution of Southeast Asia*, number **106** in Special Publication, pages 153–184. Geological Society of London.

Hall, R. 1997. Cenozoic plate reconstructions of SE Asia. In Fraser, A., Matthews, S.J., and Murphy, R.W., editors, *Petroleum geology of SE Asia*, number **126** in Special Publication, pages 11–23. Geological Society of London.

Hamburger, M.W. and Isacks, B.L. 1988. Diffuse back-arc deformation in the southwestern Pacific. *Nature*, **332**, 599–604.

Hamilton, I.W. 1989. *Geophysical investigation of subduction related processes in the Scotia Sea.* PhD thesis, University of Birmingham.

Hansen, R.O. and Pawlowski, R.S. 1989. Reduction to the pole at low latitudes by Wiener filtering. *Geophysics*, **54**, 1607–1613.

Hartley, R., Watts, A.B., and Fairhead, J.D. 1996. Isostasy of Africa. *Earth and Planetary Science Letters*, **137**, 1–18.

Hawkes, D.D. 1962. The structure of the Scotia Arc. *Geological Magazine*, **99**, 85–91.

Haxby, W.F. 1988. Organisation of oblique sea floor spreading into discrete, uniformly spaced ridge segments: evidence from Geosat altimeter data in the Weddell Sea. *EOS, Transactions AGU*, **69**, 1155.

Haxby, W.F., Karner, G.D., LaBrecque, J.L., and Weissel, J.K. 1983. Digital images of combined oceanic and continental data sets and their use in tectonic studies. *EOS, Transactions AGU*, **64**, 995–1004.

Haxby, W.F. and Weissel, J.K. 1986. Evidence for small-scale mantle convection from Seasat altimeter data. *Journal of Geophysical Research*, **91**, 3507–3520.

Heezen, B.C. 1959. Paleomagnetics, continental displacements and the origin of submarine topography. *International Ocean Congress*, **1**, 26–28.

Heezen, B.C. 1960. The rift in the ocean floor. *Scientific American*, **203**, 98–110.

Heezen, B.C. 1962. The Deep-Sea-Floor. In Runcorn, S.K., editor, *Continental Drift*, pages 235–268. Academic Press, New York.

Heezen, B.C., Tharp, M., and Ewing, M. 1959. The floors of the oceans, 1, The North Atlantic. *Geological Society of America Special Paper*, **68**, 1–122.

Hellinger, S.J. 1981. The uncertainties of finite rotations in plate tectonics. *Journal of Geophysical Research*, **86**, 9312–9318.

Herron, E.M., Bruhn, R., Winslow, M., and Chuaqui, L. 1977. Post Miocene tectonics of the margin of southern Chile. In Talwani, M. and Pitman, W.G., editors, *Island arcs, deep sea trenches and back-arc basins*, pages 273–284. AGU, Washington DC.

Hess, H.H. 1962. History of ocean basins. In *Petrologic Studies: A Volume in Honor of A.F. Buddington*, pages 599–620. Geological Society of America.

Hilgen, F.J. 1991. Astronomical calibration of Gauss to Matuyama sapropels in the Mediterranean and implication for the Geomagnetic Polarity Time Scale. *Earth and Planetary Science Letters*, **104**, 226–244.

Hill, I.A. 1978. *A marine geophysical study of the crustal structure and evolution of the central Scotia Sea, South Atlantic.* PhD thesis, University of Birmingham.

Hill, I.A. and Barker, P.F. 1980. Evidence for Miocene back-arc spreading in the central Scotia Sea. *Geophysical Journal of the Royal Astronomical Society*, **63**, 427–440.

Hill, M.N. 1957. Recent geophysical exploration of the ocean floor. *Physics and Chemistry of the Earth*, **2**, 129–163.

Hofmann, E.E. 1985. The large-scale horizontal structure of the Antarctic Circumpolar Current from FGGE drifters. *Journal of Geophysical Research*, **90C**, 7087–7097.

Holmes, A. 1928. Radioactivity and continental drift. *Geological Magazine*, **65**, 236–238.

Honnorez, J., Villeneuve, M., and Mascle, J. 1994. Old continent-derived metasedimentary rocks in the equatorial Atlantic: An acoustic basement outcrop along the fossil trace of the Romanche transform fault at 6°30'W. *Marine Geology*, **117**, 237–251.

Howe, J.A., Livermore, R.A., and Maldonado, A. 1998. Mudwave activity and current-controlled sedimentation in Powell Basin, northern Weddell Sea, Antarctica. *Marine Geology*, **149**, 229–241.

Hsui, A.T. and Toksöz, M.N. 1981. Back-arc spreading: trench migration, continental pull or induced convection? *Tectonophysics*, **74**, 89–98.

Isacks, B., Oliver, J., and Sykes, L.R. 1968. Seismology and the new global tectonics. *Journal of Geophysical Research*, **73**, 5855–5899.

Johnson, R.H. 1971. Reduction of discrepancies at crossing points in geophysical surveys. *Journal of Geophysical Research*, **76**, 4892–4896.

Jurdy, D.M. and Stefanick, M. 1983. Flow models for back-arc spreading. *Tectonophysics*, **99**, 191–206.

Jurdy, D.M. and Stefanick, M. 1987. Errors in plate rotations as described by covariance matrices and their combination in reconstructions. *Journal of Geophysical Research*, **92**, 6310–6318.

Karig, D.E. 1971. Origin and development of marginal basins in the western Pacific. *Journal of Geophysical Research*, **76**, 2542–2561.

Karig, D.E. 1974. Evolution of arc systems in the western Pacific. *Annual Reviews of Earth and Planetary Science*, **2**, 51–75.

Katz, H.R. 1973. Contrasts in tectonic evolution of orogenic belts in the southwest Pacific. *Journal of the Royal Society of New Zealand*, **3**, 333–362.

Kearey, P. and Vine, F.J. 1996. *Global Tectonics.* Blackwell Science, UK, 2nd edition.

Kennett, J.P. 1977. Cenozoic evolution of Antarctic glaciation, the circum-Antarctic ocean and their impact on global paleoceanography. *Journal of Geophysical Research*, **82**, 3843–3860.

Kent, D.V. and Gradstein, F.M. 1986. A Jurassic to recent chronology. In Vogt, P.R. and Tucholke, B.E., editors, *The Western North Atlantic Region*, volume M, The Geology of North America, pages 45–50. Geological Society of America.

Kent, G.M., Singh, S.C., Harding, A.J., Sinha, M.C., Orcutt, J.A., Barton, P.J., White, R.S., Bazin, S., Hobbs, R.W., Tong, C.H., and Pye, J.W. 2000. Evidence from three-dimensional seismic reflectivity images for enhanced melt supply beneath mid-ocean-ridge discontinuities. *Nature*, **406**, 614–618.

King, E.C. 1983. *The tectonic history of the South Orkney microcontinental block.* PhD thesis, University of Birmingham.

King, E.C. and Barker, P.F. 1988. The margins of the South Orkney Microcontinent. *Journal of the Geological Society of London*, **145**, 317–331.

King, E.C., Leitchenkov, G., Galindo-Zaldívar, J., Maldonado, A., and Lodolo, E. 1997. Crustal structure and sedimentation in Powell basin. In Barker, P.F. and Cooper, A.K., editors, *Geology and Seismic Stratigraphy of the Antarctic Margin Part 2, Antarctic Research Series*, volume **71**, pages 75–93. AGU, Washington DC.

Kirby, J.F. and Featherstone, W.E. 1999. Terrain correcting Australian gravity observations using the national digital elevation model and the fast Fourier transform. *Australian Journal of Earth Sciences*, **46**, 555–562.

Kirkwood, B.H., Royer, J.-Y., Chang, T.C., and Gordon, R.G. 1999. Statistical tools for estimating and combining plate rotations and their uncertainties. *Geophysical Journal International*, **137**, 408–428.

Klepeis, K.A. 1994. The Magallanes and Deseado fault zones: major segments of the south American - Scotia transform plate boundary in southernmost south America, Tierra del Fuego. *Journal of Geophysical Research*, **99**, 22001–22014.

Klepeis, K.A. and Austin Jr, J.A. 1997. Contrasting styles of superposed deformation in the southernmost Andes. *Tectonics*, **16**, 755–776.

Klepeis, K.A. and Lawver, L.A. 1996. Tectonics of the Antarctic-Scotia plate boundary near Elephant and Clarence Islands, West Antarctica. *Journal of Geophysical Research*, **101**, 20211–20231.

Kristoffersen, Y. and Haugland, V.C. 1986. Geophysical evidence for the East Antarctic plate boundary in the Weddell Sea. *Nature*, **322**, 538–541.

LaBrecque, J.L. and Barker, P. 1981. The age of the Weddell Basin. *Nature*, **290**, 489–492.

LaBrecque, J.L., Cande, S., Bell, R., Raymond, C., Brozena, J., Keller, M., Parra, J.C., and Yanez, G. 1986. Aerogeophysical survey yields new data in the Weddell Sea. *Antarctic Journal*, **21**, 69–70.

LaBrecque, J.L *et al.* 1989. USAC aerosurvey results for the Weddell Basin, Part 1. In *28th International Geological Congress*. IUGG, Washington D.C.

LaBrecque, J.L. and Rabinowitz, P.D. 1977. Magnetic anomalies bordering the continental margin of Argentina.

Langel, R.A. 1992. International geomagnetic reference field: the sixth generation. *Journal of Geomagnetism and Geoelectricity*, **44**, 679–707.

Larsen, H.C., Saunders, A.D., Clift, P.D., and Shipboard Scientific Party. 1994. Introduction: breakup of the southeast Greenland margin and the formation of the Irminger Basin: background and scientific objectives. *Initial reports, Ocean Drilling Program*, **152**, 5–16.

Larson, R.L. and Ladd, J.W. 1973. Evidence for the opening of the South Atlantic in the Early Cretaceous. *Nature*, **246**, 209–212.

Larter, R.D. and Barker, P.F. 1991. Effects of ridge crest-trench interaction on Antarctic–Phoenix spreading: forces on a young subducting plate. *Journal of Geophysical Research*, **96**, 19583–19607.

Lawver, L.A., Della Vedova, B., and Von Herzen, R.P. 1991. Heat flow in Jane Basin, Northwest Weddell Sea. *Journal of Geophysical Research*, **96**, 2019–2038.

Lawver, L.A. and Dick, H.J.B. 1983. The American–Antarctic Ridge. *Journal of Geophysical Research*, **88**, 8193–8202.

Lawver, L.A. and Gahagan, L.M. 1998. Opening of Drake Passage and its impact on Cenozoic ocean circulation. In Crowley, T.J. and Burke, K.C., editors, *Tectonic Boundary Conditions for Climate Reconstructions*, pages 212–223. Oxford University Press, New York Oxford.

Lawver, L.A., Gahagan, L.M., and Coffin, M.F. 1992. The development of paleoseaways around Antarctica. In *The Antarctic Paleoenvironment: a perspective on global change*, Antarctic Research Series, pages 7–30. AGU.

Lawver, L.A. and Hawkins, J.W. 1978. Diffuse magnetic anomalies in marginal basins: their possible tectonic and petrologic significance. *Tectonophysics*, **45**, 323–339.

Lawver, L.A., Keller, R.A., Fisk, M.R., and Strelin, J.A. 1995. Bransfield Strait, Antarctic Peninsula active extension behind a dead arc. In Taylor, B., editor, *Backarc basins: tectonics and magmatism*, pages 315–342. Plenum Press, New York.

Lawver, L.A., Sclater, J.G., and Meinke, L. 1985. Mesozoic and Cenozoic reconstructions of the south Atlantic. *Tectonophysics*, **114**, 233–254.

Lawver, L.A., Williams, T., and Sloan, B. 1994. Seismic stratigraphy and heat flow of Powell Basin. *Terra Antartica*, **1**, 309–310.

Le Pichon, X., Francheteau, J., and Bonnin, J. 1973. Plate tectonics. *Developments in geotectonics*, **6**.

Leat, P.T., Scarrow, J.H., and Millar, I.L. 1995. On the Antarctic Peninsula batholith. *Geological Magazine*, **132**, 399–412.

Leu, L.-K. 1981. Use of reduction-to-equator process for magnetic data interpretation. In *Fifty-First Annual International Meeting*, page 445. Society of Exploration Geophysicists.

Levi, S. and Riddihough, R. 1986. Why are marine magnetic anomalies suppressed over sedimented spreading centres? *Geology*, **14**, 651–654.

Livermore, R.A., Balanyá, J.C., Maldonado, A., Martínez, J.M., Rodríguez-Fernández, J., Sanz de Galdeano, C., Galindo Zaldívar, J., Jabaloy, A., Barnolas, A., Somoza, L., Hernández-Molina, J., Suriñach, E., and Viseras, C. 2000. Autopsy on a dead spreading center: The Phoenix Ridge, Drake Passage, Antarctica. *Geology*, **28**, 607–610.

Livermore, R.A., Cunningham, A.P., Vanneste, L.E., and Larter, R.D. 1997. Subduction influence on magma supply at the East Scotia Ridge. *Earth and Planetary Science Letters*, **150**, 261–275.

Livermore, R.A. and Hunter, R.J. 1996. Mesozoic seafloor spreading in the southern Weddell Sea. In Storey, B.C., King, E.C., and Livermore, R.A., editors, *Weddell Sea tectonics and Gondwana break-up*, number **108** in Special Publication, pages 227–241. Geological Society of London.

Livermore, R.A., McAdoo, D., and Marks, K. 1994. Scotia Sea tectonics from high-resolution satellite gravity. *Earth and Planetary Science Letters*, **123**, 255–268.

Livermore, R.A. and Woollett, R.W. 1993. Seafloor spreading in the Weddell Sea and southwest Atlantic since the Late Cretaceous. *Earth and Planetary Science Letters*, **117**, 475–495.

Lodolo, E., Coren, F., Schreider, A.A., and Ceccone, G. 1998. Geophysical evidence of a relict oceanic crust in the southwestern Scotia Sea. *Marine Geophysical Researches*, **19**, 439–450.

Loper, D.E. 1985. A simple model of whole mantle convection. *Journal of Geophysical Research*, **90**, 1809–1836.

Lorenzo, J.M. and Mutter, J.C. 1988. Seismic stratigraphy and tectonic evolution of the Malvinas/Falkland Plateau. *Revista Brasileira de Geociencias*, **18**, 191–200.

Ludwig, W.J. 1983. Geologic framework of the Falkland Plateau. *Initial reports, Deep Sea Drilling Program*, **71**, 281–292.

Ludwig, W.J., Ewing, J.I., and Ewing, M. 1968. Structure of Argentine continental margin. *American Association of Petroleum Geologists Bulletin*, **52**, 2337–2368.

Ludwig, W.J. and Rabinowitz, P.D. 1982a. Seismic stratigraphy and structure of Falkland Plateau. *American Association of Petroleum Geologists Bulletin*, **64**, 742.

Ludwig, W.J. and Rabinowitz, P.D. 1982b. The collision complex of the North Scotia Ridge. *Journal of Geophysical Research*, **87**, 3731–3740.

Ludwig, W.J., Windisch, C.C., Houtz, R.E., and Ewing, J.I. 1978. Structure of Falkland Plateau and offshore Tierra del Fuego, Argentina. In Watkins, J.S., Montadert, L., and Dickerson, P.W., editors, *Geological and geophysical investigations of continental margins*, pages 125–137. American Association of Petroleum Geologists, Memoir **29**, Tulsa, Oklahoma.

Macdonald, D.I.M., Storey, B.C., and Thomson, J.W. 1987. South Georgia. Sheet 1, 1:250000, Geological map and supplementary text, BAS, Cambridge.

Macdonald, D.I.M. and Tanner, P.W.G. 1983. Sediment dispersal patterns in part of a deformed Mesozoic back-arc basin on South Georgia. *Journal of Sedimentary Petrology*, **53**, 83–104.

Macdonald, K.C., Miller, S.P., Huestis, S.P., and Speiss, F.N. 1980. Three-dimensional modelling of a magnetic reversal boundary from inversion of deep-tow measurements. *Journal of Geophysical Research*, **85**, 3670–3680.

Macfadyen, W.A. 1933. Fossil foraminifera from the Burdwood Bank and their geological significance. *'Discovery' Reports*, **7**, 1–16.

Maldonado, A., Aldaya, F., Carlos Balanya, J., Galindo-Zaldívar, J., Livermore, R.A., Monsene, F.M., Rodriguez-Fernandez, J., Roussanov, M., Sanz de Galdeano, C., Suriñach, E., and Viseras, C. 1993. Tectonics and paleoceanography in the northern sector of the Antarctic Peninsula: preliminary results of HESANT 1992/93 cruise with the BIO Hesperides. *Scientia Marina*, **57**, 79–89.

Maldonado, A., Barnolas, J.C. Balanyá A., Galindo-Zaldívar, J., Hernández, J., Jabaloy, A., Livermore, R., Martínez-Martínez, J.M., Rodríguez-Fernández, J., Sanz de Galdeano, C., Suriñach, L. Somoza E., and Viseras, C. 2000. Tectonics of an extinct ridge–transform intersection, Drake Passage (Antarctica). *Marine Geophysical Researches*, **21**, 43–68.

Maldonado, A., Zitellini, N., Leitchenkov, G., Balanyá, J.C., Coren, F., Galindo-Zaldívar, J., Lodolo, E., Jabaloy, A., Zanolla, C., Rodríguez-Fernández, J., and Vinnikovskaya, O. 1998. Small ocean basin development along the Scotia–Antarctica plate boundary and in the northern Weddell Sea. *Tectonophysics*, **296**, 371–402.

Malfait, B.T. and Dinkelman, M.G. 1972. Circum-Caribbean tectonic and igneous activity and the evolution of the Caribbean plate. *Bulletin of the Geological Society of America*, **83**, 251–272.

Mao, S. and Mohr, B.A.R. 1995. Middle Eocene dinocysts from Bruce Bank (Scotia Sea, Antarctica) and their paleoenvironmental and paleogeographic implications. *Review of Palaeobotany and Palynology*, **86**, 235–263.

Marks, K.M., McAdoo, D.C., and Sandwell, D.T. 1991. Geosat GM data reveal new details of ocean floor. *EOS, Transactions AGU*, **72**, 145–149.

Marshak, S., Bonatti, E., Brueckner, H., and Paulsen, T. 1992. Fracture zone tectonics at Zabargad Island, Red Sea (Egypt). *Tectonophysics*, **216**, 379–385.

Marshall, J.E.A. 1994. The Falkland Islands: a key element in Gondwana paleogeography. *Tectonics*, **13**, 499–514.

Martin, A.K. 1986. Microplates in Antarctica. *Nature*, **319**, 100–101.

Martin, A.K., Goodlad, S.W., Hartnady, C.J.H., and du Plessis, A. 1982. Cretaceous palaeopositions of the Falkland Plateau relative to Southern Africa using Mesozoic seafloor spreading anomalies. *Geophysical Journal of the Royal Astronomical Society*, **71**, 567–579.

Martínez, F., Fryer, P., Baker, N.A., and Yamazaki, T. 1995. Evolution of backarc rifting: Mariana Trough, 20°–24°N. *Journal of Geophysical Research*, **100**, 3807–3827.

Maslanyj, M.P. and Storey, B.C. 1990. Regional aeromagnetic anomalies in Ellsworth Land: crustal structure and Mesozoic microplate boundaries within West Antarctica. *Tectonics*, **9**, 1515–1532.

Mason, R.G. and Raff, A.D. 1961. Magnetic survey off the west coast of North America, 32°N latitude to 42°N latitude. *Bulletin of the Geological Society of America*, **72**, 1259–1266.

Matthews, D.H. 1959. Aspects of the geology of the Scotia Arc. *Geological Magazine*, **96**, 425–441.

McAdoo, D.C. and Marks, K.M. 1992. Gravity fields of the southern ocean from Geosat data. *Journal of Geophysical Research*, **97**, 3247–3260.

McKenzie, D. 1984. A possible mechanism for epeirogenic uplift. *Nature*, **307**, 616–618.

McKenzie, D.P. and Morgan, W.J. 1969. Evolution of triple junctions. *Nature*, **224**, 125–133.

McKenzie, D.P. and Parker, R.L. 1967. The north Pacific: an example of tectonics on a sphere. *Nature*, **216**, 1276–1280.

McKenzie, D.P. and Sclater, J.G. 1971. The evolution of the Indian Ocean since the late Cretaceous. *Geophysical Journal of the Royal Astronomical Society*, **24**, 437–528.

McKenzie, D.P., Watts, A., Parsons, B., and Roufosse, M. 1980. Planform of mantle convection beneath the Pacific Ocean. *Nature*, **288**, 442–446.

Menard, H.W. 1955. Deformation of the Northeastern Pacific Basin and West Coast of North America. *Bulletin of the Geological Society of America*, **66**, 1149–1198.

Menard, H.W. 1978. Fragmentation of the Farallon plate by pivoting subduction. *Journal of Geology*, **86**, 99–110.

Meneilly, A.W. and Storey, B.C. 1986. Ductile thrusting within subduction complex rocks on Signy Island, South Orkney Islands. *Journal of Structural Geology*, **8**, 457–472.

Meschede, M. and Frisch, W. 1998. A plate tectonic model for the Mesozoic and Early Cenozoic history of the Caribbean plate. *Tectonophysics*, **296**, 269–291.

Mikolajewicz, U., Maier-Reimer, E., Crowley, T.J., and Kim, K.-Y. 1993. Effect of Drake and Panamanian gateways on the circulation of an ocean model. *Paleoceanography*, **8**, 409–426.

Minster, J.B., Jordan, T.H., Molnar, P., and Haines, E. 1974. Numerical modelling of instantaneous plate tectonics. *Geophysical Journal of the Royal Astronomical Society*, **36**, 541–576.

Mitchell, C., Taylor, G.K., Cox, K.G., and Shaw, J. 1986. Are the Falkland Islands a rotated microplate? *Nature*, **319**, 131–134.

Morgan, W.J. 1968. Rises, trenches, great faults and crustal blocks. *Journal of Geophysical Research*, **73**, 1959–1982.

Mukasa, S.B. and Dalziel, I.W.D. 1996. Southernmost Andes and South Georgia island, North Scotia Ridge: zircon U–Pb and Muscovite $^{40}Ar/^{39}Ar$ age constraints on tectonic evolution of Southwestern Gondwanaland. *Journal of South American Earth Sciences*, **9**, 349–365.

Müller, R.D., Sandwell, D.T., Tucholke, B.E., Sclater, J.G., and Shaw, P.R. 1991. Depth to basement and geoid expression of the Kane Fracture Zone: a comparison. *Marine Geophysical Researches*, **13**, 105–129.

Müller, R.D. and Smith, W.H.F. 1993. Deformation of the Oceanic Crust Between the North American and South American Plates. *Journal of Geophysical Research*, **98**, 8275–8291.

Mussett, A.E. and Taylor, G.K. 1994. ^{40}Ar–^{39}Ar ages for dykes from the Falkland Islands with implications for the break-up of southern Gondwanaland. *Journal of the Geological Society of London*, **151**, 79–81.

NAG. 1985. *F04QAF - NAG Fortran library routine document.* Numerical Algorithms Group.

Nakanishi, M., Tamaki, K., and Kobayashi, K. 1992. Magnetic anomaly lineations from Late Jurassic to Early Cretaceous in the west-central Pacific Ocean. *Geophysical Journal International*, **109**, 701–719.

Nankivell, A.P. 1997a. *Tectonic evolution of the Southern Ocean between Antarctica, South America and Africa over the last 84Ma.* PhD thesis, University of Oxford.

Nankivell, A.P. 1997b. User notes: Inversion suite for 2 and 3-plate reconstructions. Unpublished user manual.

Nichols, G. and Hall, R. 1999. History of the Celebes Sea Basin based on its stratigraphic and sedimentological record. *Journal of Asian Earth Sciences*, **17**, 47–59.

Nishimura, C., Wilson, D.S., and Hey, R.H. 1984. Pole of rotation analysis of present-day Juan de Fuca plate motion. *Journal of Geophysical Research*, **89**, 10283–10290.

Nowlin, W.D. and Klinck, J.M. 1986. The physics of the Antarctic Circumpolar Current. *Reviews of Geophysics, Space Physics*, **24**, 469–491.

Nürnberg, D. and Müller, R.D. 1991. The tectonic evolution of the south Atlantic from late Jurassic to present. *Tectonophysics*, **191**, 27–53.

ODP Leg 149 Shipboard Scientific Party. 1993. ODP drills the West Iberia rifted margin. *EOS, Transactions AGU*, **74**, 454–455.

Orsi, A.H., Whitworth III, T., and Nowlin Jr, W.D. 1995. On the meridional extent and fronts of the Antarctic Circumpolar Current. *Deep Sea Research*, **42**, 641–673.

Oxburgh, E.R. and Turcotte, D.L. 1968. Mid-ocean ridges and geothermal distribution during mantle convection. *Journal of Geophysical Research*, **73**, 2643–2661.

Packham, G.H. and Falvey, D.A. 1971. An hypothesis for the formation of marginal seas in the Western Pacific. *Tectonophysics*, **11**, 79–110.

Paige, C.C. and Saunders, M.A. 1982. LSQR: An algorithm for sparse linear equations and sparse least-squares. In *ACM Trans. Math. Software*, volume 8, pages 43–71. ACM.

Parker, R.L. 1973. The rapid calculation of potential anomalies. *Geophysical Journal of the Royal Astronomical Society*, **31**, 447–455.

Parker, R.L. 1995. Improved Fourier terrain correction, part I. *Geophysics*, **60**, 1007–1017.

Parker, R.L. 1996. Improved Fourier terrain correction, part II. *Geophysics*, **61**, 365–372.

Parker, R.L. and Huestis, S.P. 1974. The inversion of magnetic anomalies in the presence of topography. *Journal of Geophysical Research*, **79**, 1587–1593.

Parsons, B. and Sclater, J.G. 1977. An analysis of the variation of ocean floor bathymetry and heat flow with age. *Journal of Geophysical Research*, **82**, 803–827.

Patriat, P., Segoufin, J., Goslin, J., and Beuzart, P. 1985. Relative positions of Africa and Antarctica in the Upper Cretaceous: evidence for non-stationary behaviour of fracture zones. *Earth and Planetary Science Letters*, **75**, 204–214.

Pedersen, L.B. 1989. Relations between horizontal and vertical gradients of potential fields. *Geophysics*, **54**, 662–663.

Pelayo, A.M. and Wiens, D.A. 1989. Seismotectonics and relative plate motions in the Scotia Sea region. *Journal of Geophysical Research*, **94**, 7293–7320.

Pickup, S.L.B., Whitmarsh, R.B., Fowler, C.M.R., and Reston, T.J. 1996. Insight into the nature of the ocean–continent transition off West Iberia from a deep multichannel seismic reflection profile. *Geology*, **24**, 1079–1082.

Pilger, R.H. 1978. A method for finite plate reconstructions, with applications to Pacific-Nazca plate evolution. *Geophysical Research Letters*, **5**, 469–472.

Pindell, J. 1985. Alleghenian reconstruction and the subsequent evolution of the gulf of mexico, bahamas and proto-caribbean sea. *Tectonics*, **3**, 133–156.

Pittion, J.-L. and Gouadain, J. 1992. Source rocks and oil generation in the Austral Basin. In *Proceedings, Thirteenth World Petroleum Congress*, pages 113–120, Buenos Aires.

Platt, N.H. and Philip, P.R. 1995. Structure of the southern Falkland Islands continental shelf: initial results from new seismic data. *Marine and Petroleum Geology*, **12**, 759–771.

Plouff, D. 1977. Preliminary documentation for a FORTRAN program to compute gravity terrain corrections based on topography digitized on a geographic grid. Open file report 77-535, U.S. Geological Survey.

Pockalny, R.A. 1997. Evidence of transpression along the Clipperton Transform: Implications for processes of plate boundary reorganisation. *Earth and Planetary Science Letters*, **146**, 449–464.

Pudsey, C.J. and Howe, J.A. 1998. Quaternary history of the Antarctic Circumpolar Current: evidence from the Scotia Sea. *Marine Geology*, **148**, 83–112.

Rabinowitz, P.D. 1976. Geophysical study of the continental margin of southern Africa. *Bulletin of the Geological Society of America*, **87**, 1643–1653.

Rabinowitz, P.D. and LaBrecque, J. 1979. The Mesozoic South Atlantic Ocean and evolution of its continental margin. *Journal of Geophysical Research*, **84**, 5973–6002.

Rabinowitz, P.D. and LaBrecque, J.L. 1977. The isostatic residual gravity anomaly: key to the ocean-continent boundary at passive continental margins. *Earth and Planetary Science Letters*, **35**, 145–150.

Rack, F.R. 1993. A geologic perspective on the Miocene evolution of the Antarctic Circumpolar Current system. *Tectonophysics*, **222**, 397–415.

Raff, A.D. and Mason, R.G. 1961. Magnetic survey off the west coast of North America, 40°N latitude to 52°N latitude. *Bulletin of the Geological Society of America*, **72**, 1267–1270.

Raitt, R.W. 1963. The crustal rocks. In Hill, M.N., editor, *The sea*, volume **3**, pages 85–102. Interscience, New York.

Rapp, R.H. 1983. The determination of geoid undulations and gravity anomalies from Seasat altimeter data. *Journal of Geophysical Research*, **88**, 1552–1562.

Rattray Jr, M. 1985. The effect of bathymetry on the deep flow in Drake Passage. *Deep Sea Research*, **32**, 127–147.

Reeves, C. and Sahu, B.K. 1999. Computer animation of Gondwana dispersal and the history of igneous extrusion in the Indian Ocean. In *Abstracts*, page A.113. International Union of Geodesy and Geophysics, Birmingham, 1999.

Richards, P.C., Gatliff, R.W., Quinn, M.F., Williamson, J.P., and Fannin, N.G.T. 1996. The geological evolution of the Falkland Islands continental shelf. In Storey, B.C., King, E.C., and Livermore, R.A., editors, *Weddell Sea tectonics and Gondwana breakup*, number **108** in Special Publication, pages 105–128. Geological Society of London.

Richardson, R.M. and Cole, G.L. 1991. Plate reconstruction uncertainties using empirical probability density functions. *Journal of Geophysical Research*, **96**, 10391–10400.

Richter, F.M. 1973. Dynamical models for sea floor spreading. *Reviews of Geophysics and Space Physics*, **11**, 223–287.

Rodriguez-Fernandez, J., Balanya, J.C., Galindo-Zaldívar, J., and Maldonado, A. 1997. Tectonic evolution and growth patterns of a restricted ocean basin: the Powell Basin (Northeastern Antarctic Peninsula). *Geodinamica Acta*, **10**, 159–174.

Roest, W.R., Arkani-Hamed, J., and Verhoef, J. 1992. The seafloor spreading rate dependence of the anomalous skewness of marine magnetic anomalies. *Geophysical Journal International*, **109**, 653–669.

Ross, M.I. and Scotese, C.R. 1988. A hierarchical tectonic model of the gulf of mexico and caribbean region. *Tectonophysics*, **155**, 139–168.

Royden, L.H. 1993. Evolution of retreating subduction boundaries formed during continental collision. *Tectonics*, **12**, 629–638.

Rubio, E., Torré, M., Vera, E., and Díaz, A. 2000. Crustal structure of the southernmost Chilean margin from seismic and gravity data. *Tectonophysics*, **323**, 39–60.

Runcorn, S.K. 1959. Rock magnetism. *Science*, **129**, 1002–1011.

Russo, R.M. and Silver, P.G. 1994. Trench-parallel flow beneath the Nazca Plate from seismic anisotropy. *Science*, **263**, 1105–1111.

Sandwell, D.T. 1984. A detailed view of the South Pacific geoid from satellite altimetry. *Journal of Geophysical Research*, **89**, 1089–1104.

Sandwell, D.T. 1987. Biharmonic spline interpolation of GEOS-3 and SEASAT altimeter data. *Geophysical Research Letters*, **14**, 139–142.

Sandwell, D.T. 1992. Antarctic marine gravity field from high-density satellite altimetry. *Geophysical Journal International*, **109**, 437–448.

Sandwell, D.T. and McAdoo, D.C. 1988. Marine gravity of the southern ocean and Antarctic margin from Geosat. *Journal of Geophysical Research*, **93**, 10389–10396.

Schouten, H. and White, R.S. 1980. Zero-offset fracture zones. *Geology*, **8**, 175–179.

Shackleton, N.J., Berger, A., and Peltier, W.R. 1990. An alternative astronomical calibration of the Lower Pleistocene time scale based on ODP Site 677. *Transactions, Royal Society of Edinburgh*, **81**, 251–261.

Shackleton, N.J. and Kennett, J.P. 1975. Paleotemperature history of the Cenozoic and the initiation of Antarctic glaciation: Oxygen and carbon isotope analyses in DSDP sites 277, 279 and 281. In Kennett, J.P. and Houtz, R.E. *et al*, editors, *Initial Report of the Deep Sea Drilling Project*, volume **29**, pages 743–755. U.S. Government Printing Office, Washington D.C.

Shaw, P.R. 1987. Investigations of relative plate motions in the South Atlantic using Seasat altimeter data. *Journal of Geophysical Research*, **92**, 9363–9375.

Shaw, P.R. and Cande, S.C. 1990. High-resolution inversion for south Atlantic plate kinematics using joint altimeter and magnetic anomaly data. *Journal of Geophysical Research*, **95**, 2625–2644.

Silver, E.A. and Rangin, C. 1991. Development of the Celebes Basin in the context of western Pacific marginal basin history. *Proceedings of the Ocean Drilling Program*, **124**, 39–49.

Simpson, E.S.W., Sclater, J.G., Parsons, B., Norton, I., and Meinke, L. 1979. Mesozoic magnetic lineations in the Mozambique Basin. *Earth and Planetary Science Letters*, **43**, 260–264.

Simpson, P. and Griffiths, D.H. 1982. The structure of the South Georgia continental block. In Craddock, C., editor, *Antarctic Geoscience*, pages 185–191. University of Wisconsin Press, Madison.

Simpson, R.W., Jachens, R.C., Blakely, R.J., and Saltus, R.W. 1986. A new isostatic residual gravity map of the counterminous United States with a discussion on the significance of isostatic residual anomalies. *Journal of Geophysical Research*, **91**, 8348–8372.

Smellie, J.L. and Clarkson, P.D. 1975. Evidence for pre-Jurassic subduction in western Antarctica. *Nature*, **258**, 701–702.

Smith, A.G. and Hallam, A. 1970. The fit of the southern continents. *Nature*, **225**, 139–144.

Smith, D.K., Tivey, M.A., Schouten, H., and Cann, J.R. 1999. Locating the spreading axis along 80 km of the Mid-Atlantic Ridge south of the Atlantis Transform. *Journal of Geophysical Research*, **104**, 7599–7612.

Smith, W.H.F. 1993. On the accuracy of digital bathymetric data. *Journal of Geophysical Research*, **98**, 9591–9603.

Smith, W.H.F. and Sandwell, D.T. 1994. Bathymetric prediction from dense satellite altimetry and sparse shipboard bathymetry. *Journal of Geophysical Research*, **99**, 21803–21824.

Smith, W.H.F. and Sandwell, D.T. 1995. Marine gravity field from declassified Geosat and ERS-1 altimetry. *EOS, Transactions AGU*, **76**, 156.

Smith, W.H.F. and Wessell, P. 1990. Gridding with continuous curvature splines in tension. *Geophysics*, **55**, 293–305.

Spielman, J.B. and Ponce, D.A. 1984. Handtc, a Fortran program to calculate inner-zone terrain corrections. Open file report 84-777, U.S. Geological Survey.

Stern, C.R., Mukasa, S.B., and Fuenzalida, R. 1992. Age and petrogenesis of the Sarmiento ophiolite complex of southern Chile. *Journal of South American Earth Sciences*, **6**, 97–104.

Stock, J.M. and Molnar, P. 1983. Some geometrical aspects of uncertainties in combined plate reconstructions. *Geology*, **11**, 697–701.

Storey, B.C. 1983. The geology of South Georgia: V. Drygalski Fjord Complex. *British Antarctic Survey Scientific Report*, **107**, 88pp.

Storey, B.C. and Macdonald, D.I.M. 1984. Processes of formation and filling of a Mesozoic back-arc basin on the island of South Georgia. In Kokelaar, B.P. and Howells, M.F., editors, *Marginal basin geology*, number **16** in Special Publication, pages 207–218. Geological Society of London.

Storey, B.C. and Mair, B.F. 1982. The composite floor of the Cretaceous back-arc basin of South Georgia. *Journal of the Geological Society of London*, **139**, 729–737.

Storey, B.C., Mair, B.F., and Bell, C.M. 1977. The occurrence of Mesozoic oceanic floor and ancient continental crust on South Georgia. *Geological Magazine*, **114**, 203–208.

Stott, L. and Kennett, J.P. 1990. Cenozoic planktonic foraminifers and Antarctic Paleogene biostratigraphy, Sites 689–690. In Barker, P.F. and Kennett, J.P., *et al*, editors, *Proceedings of the Ocean Drilling Project, Science Results*, volume **113**, pages 549–569. Ocean Drilling Program, College Station, Texas.

Stott, L., Kennett, J.P., Shackleton, N.J., and Corfield, R.M. 1990. The evolution of Antarctic surface waters during the Paleogene, inferences from the stable isotopic composition of planktonic foraminifera. In Barker, P.F. and Kennett, J.P., *et al*, editors, *Proceedings of the Ocean Drilling Project, Science Results*, volume **113**, pages 849–864. Ocean Drilling Program, College Station, Texas.

Suárez, M. and Pettigrew, T.H. 1976. An Upper Mesozoic island-arc–back-arc system in the southern Andes and South Georgia. *Geological Magazine*, **113**, 305–328.

Suess, E. 1909. *Das Antlitz der Erde.* Freytag, Leipzig. 3 volumes.

Suriñach, E., Galindo-Zaldívar, J., Maldonado, A., and Livermore, R.A. 1997. Large amplitude magnetic anomalies in the northern sector of the Powell Basin, NE Antarctic Peninsula. *Marine Geophysical Researches*, **19**, 65–80.

Swain, C.J. 1976. A FORTRAN IV program for interpolating irregularly spaced data using the difference equations for minimum curvature. *Computers and Geosciences*, **1**, 231–240.

Sykes, L.R. 1967. Mechanism of earthquakes and nature of faulting on the mid-ocean ridges. *Journal of Geophysical Research*, **72**, 2131–2153.

Talwani, M., Le Pichon, X., and Heirtzler, J.R. 1965. East Pacific Rise: The magnetic pattern and the fracture zones. *Science*, **150**, 1109–1115.

Tamaki, K. 1985. Two modes of back-arc spreading. *Geology*, **13**, 475–478.

Tanner, P.W.G. 1982. Geologic evolution of South Georgia. In Craddock, C., editor, *Antarctic Geoscience*, pages 167–176. University of Wisconsin Press, Madison.

Tanner, P.W.G. and Macdonald, D.I.M. 1982. Models for the deposition and simple shear deformation of a turbidite sequence in the South Georgia portion of the southern Andes back-arc basin. *Journal of the Geological Society of London*, **139**, 739–654.

Taylor, B., Goodliffe, A.M., and Martinez, F. 1999. How continents break up: insights from Papua New Guinea. *Journal of Geophysical Research*, **104**, 7497–7512.

Taylor, F.B. 1910. Bearing of the Tertiary mountain belt on the origin of the Earth's plan. *Bulletin of the Geological Society of America*, **21**, 179–226.

Taylor, G.K. and Shaw, J. 1989. The Falkland Islands: new palaeomagnetic data and their origin as a displaced terrane from southern Africa. In Hillhouse, J.W., editor, *Deep structure and past kinematics of displaced terranes*, volume **50** of *Geophysical Monograph*, pages 59–72. American Geophysical Union. IUGG Volume 5.

Tectonic map of the Scotia arc 1:3000000 BAS (Misc) 3. British Antarctic Survey, Cambridge. 1985.

Toker, V., Barker, P.F., and Wise Jr, S.W. 1991. Middle Eocene carbonate-bearing marine sediments from Bruce Bank off northern Antarctic Peninsula. In Thomson, M.R.A., Crame, J.A., and Thomson, J.W., editors, *Geological Evolution of Antarctica. Proceedings V International Conference, Antarctic Earth Sciences*, pages 639–644. Cambridge University Press, Cambridge.

Trehu, A.M. 1975. Depth versus (age)$^{1/2}$: a perspective on mid ocean ridges. *Earth and Planetary Science Letters*, **27**, 287–304.

Trouw, R.A.J., Passchier, C.W., Valeriano, C.M., Simões, L.S.A., Paciullo, F.V.P., and Ribeiro, A. 2000. Deformational evolution of a Cretaceous subduction complex: Elephant Island, South Shetland Islands, Antarctica. *Tectonophysics*, **319**, 93–110.

Trouw, R.A.J., Ribeiro, A., and Paciullo, F.V.P. 1991. Structural and metamorphic evolution of the Elephant Island group and Smith Island, South Shetland Islands. In Thomson, M.R.A., Crame, J.A., and Thomson, J.W., editors, *Geological Evolution of Antarctica. Proceedings V International Conference, Antarctic Earth Sciences*, pages 423–428. Cambridge University Press, Cambridge.

Tunnicliffe, V., McArthur, A.G., and McHugh, D. 1998. A biogeographical perspective of the deep-sea hydrothermal vent fauna. *Advances in Marine Biology*, **34**, 353–442.

Tyrrell, G.W. 1945. Report on rocks from West Antarctica and the Scotia Arc. *'Discovery' Reports*, **23**, 37–102.

Vine, F.J. 1966. Spreading of the ocean floor: New evidence. *Science*, **154**, 1405–1415.

Vine, F.J. and Matthews, D.H. 1963. Magnetic anomalies over oceanic ridges. *Nature*, **199**, 947–949.

Vogt, P.R., Schneider, E.D., and Johnson, G.L. 1969. The crust and upper mantle beneath the sea. *Geophysical Monograph*, **13**, 556–617.

Warren, B.A. 1983. Why is no deep water formed in the North Pacific? *Journal of Marine Research*, **41**, 327–347.

Wegener, A. 1924. *The origin of continents and oceans.* Methuen, London. Translation of *Die enstehung der kontinente und ozeane*, 1915, and reprints.

Wessell, P. and Smith, W.H.F. 1991. Free software helps map and display data. *EOS, Transactions AGU*, **72**, pp. 441, 445–446.

White, R.S. and McKenzie, D. 1989. Magmatism at rift zones: the generation of volcanic continental margins and flood basalts. *Journal of Geophysical Research*, **94**, 7685–7729.

Whitmarsh, R.B. and Miles, P.R. 1995. Models of the development of the West Iberia rifted continental margin at 40°30'N deduced from surface and deep-tow magnetic anomalies. *Journal of Geophysical Research*, **100**, 3789–3806.

Whitmarsh, R.B., Pinheiro, L.M., Miles, P.R., Recq, M., and Sibuet, J.-C. 1993. Thin crust at the western Iberia ocean–continent transition and ophiolites. *Tectonics*, **12**, 1230–1239.

Willan, R.C.R. and Kelley, S.P. 1999. Mafic dike swarms in the South Shetland Islands volcanic arc: Unravelling multiepisodic magmatism related to subduction and continental rifting. *Journal of Geophysical Research*, **104**, 23051–23068.

Wilson, D.S. 1993. Confidence intervals for motion and deformation of the Juan de Fuca plate. *Journal of Geophysical Research*, **98**, 16053–16071.

Wilson, J.T. 1965. A new class of faults and their bearing on continental drift. *Nature*, **207**, 343–347.

Wilson, J.T. 1966. Are the structures of the Caribbean and Scotia Arc regions analagous to ice rafting? *Earth and Planetary Science Letters*, **1**, 335–338.

Woodburne, M.O. and Zinsmeister, W.J. 1982. Fossil land mammal from Antarctica. *Science*, **218**, 284–286.

Zachos, J.C., Breza, J.R., and Wise, S.W. 1992. Early Oligocene ice-sheet expansion on Antarctica: Stable isotope and sedimentological evidence from Kerguelen Plateau, southern Indian Ocean. *Geology*, **20**, 569–573.

Zachos, J.C., Stott, L.D., and Lohmann, K.C. 1994. Evolution of early Cenozoic marine temperatures. *Paleoceanography*, **9**, 353–387.

Index